Order Number 9020943

Analysis of synthetic polymers by near-infrared spectroscopy

Miller, Charles Edward, Ph.D.

University of Washington, 1989

U·M·I
300 N. Zeeb Rd.
Ann Arbor, MI 48106

Analysis of Synthetic Polymers by Near-infrared Spectroscopy

by Charles Edward Miller

A dissertation submitted in partial fulfillment
of the requirements for the degree of

Doctor of Philosophy

University of Washington

1989

Approved by B E Eichinger
(Chairperson of Supervisory Committee)
Bruce R. Kowalski
James B. Callis

Program Authorized
to Offer Degree Chemistry

Date 12/11/89

Doctoral Dissertation

In presenting this dissertation in partial fulfillment of the requirements for the Doctoral degree at the University of Washington, I agree that the Library shall make its copies freely available for inspection. I further agree that extensive copying of this dissertation is allowable only for scholarly purposes, consistent with "fair use" as prescribed in the U.S. Copyright Law. Requests for copying or reproduction of this dissertation may be referred to University Microfilms, 300 North Zeeb Road, Ann Arbor, Michigan 48106, to whom the author has granted "the right to reproduce and sell (a) copies of the manuscript in microfilm and/or (b) printed copies of the manuscript made from microfilm."

Signature 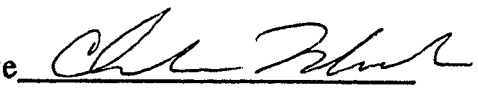

Date 12/11/89

University of Washington

Abstract

Analysis of Synthetic Polymers by Near-infrared Spectroscopy

by Charles Edward Miller

Chairman of Supervisory Committee: Professor Bruce E. Eichinger
Department of Chemistry

As the role of polymeric materials in industry broadens, it becomes increasingly important to provide rapid quality evaluation of these materials. Existing quality evaluation methods, such as physical testing, FT-IR spectroscopy, Differential Scanning Calorimetry, and X-ray scattering, cannot be used for rapid quality evaluation, because they require substantial sample preparation and long analysis times, and are usually destructive. In contrast, near-infrared (NIR) spectroscopy requires minimal sample preparation and is not destructive. Therefore, NIR spectroscopy can be used for rapid analysis of polymers, if it is periodically calibrated with a reference analytical method.

The success of NIR methods depends on the ability of NIR spectroscopy to determine important compositional and structural properties of polymers. Earlier NIR analyses have demonstrated successful determinations of a few properties, but these studies were very limited in scope, and did not utilize newly-developed NIR instrumentation and multivariate calibration techniques. In this

work, the ability of NIR spectroscopy to determine several important compositional and structural properties of polymers is demonstrated, with the aid of multivariate calibration methods. Results indicate that NIR spectroscopy can determine composition in styrene-butadiene copolymers, Reaction Injection Molded (RIM) polyurethanes, polyurethane foams, and EPDM terpolymers, microstructure of poly(butadiene) and styrene-butadiene copolymers, crystallinity in poly(ethylene terephthalate) and Ethylene-Propylene-Diene (EPDM) terpolymers, phase separation in RIM polyurethanes, and adsorption of poly(octadecyl methacrylate) to alumina. Other effects, such as π-π interactions and sequencing effects in polymers, can also be detected by NIR spectroscopy.

Table of Contents

Page

Page

Page

Page

List of Figures

Number *Page*

Number *Page*

List of Tables

Acknowledgements

The author gratefully acknowledges Prof. B. E. Eichinger, for his guidance during this research, and Dr. David E. Honigs, for improving my understanding of near-infrared spectroscopy. Essential guidance with multivariate analysis was provided by the Laboratory for Chemometrics (Prof. B. R. Kowalski, M. B. Seasholtz, Randy Pell, Dr. Tormod Naes and Dr. David Haaland). Other discussions with Dr. Bradley J. Tenge, Prof. J. B. Callis, Prof. R.O. Watts, Dr. Ed Johnson, and Dr. P.G. Edelman were very useful. The author also thanks Dr. Bradley J. Tenge, M.B. Seasholtz, D.D. Archibald, and Mike DeGrandpre for editorial comments of this dissertation.

The author thanks the University of Washington Chemistry Department, The Goodyear Tire and Rubber Company, ICI Polyurethanes and the Center for Process Analytical Chemistry for financial support of this work. The research project with Goodyear was coordinated by Dr. Thomas W. Gurley and James G. Hermiller, and received support from several employees in the Goodyear research laboratories (Lori Cianchetti, Dr. Adel Halasa, Dennis Romain, Dr. J. Visintainer, Dr. R.N. Thudium, Dr. B. Duh, Kevin Westgate, Dr. Don Brown and R. Oblath). Specific acknowledgements go to Lori Cianchetti, who performed many NMR analyses for the work in Chapters 3 and 4, and Dr. R.N. Thudium, who performed X-ray crystallinity determinations for the work in Chapter 5.

The ICI project was coordinated by Dr. William W. Brand. Support with Reaction Injection Molding experiments was provided by Dr. Jim Yavorsky, Dr. Rafael Camargo, Kevin Woolson and John Boone. Physical testing of the polyurethane samples used in this work was done by Donna Boody and Len Finnerty. Discussions with Dr. A. Hurst, Dr. Al Flint and Stewart Smith were also useful.

The author also acknowledges co-workers of some of the projects discussed in this work: Dr. Tyze-Kuan Yin (Chapter 2), Dr. Peter G. Edelman and Prof. Buddy D. Ratner (Chapter 6), Douglas D. Archibald, Dr. M. Myrick and Dr. M. Angel (Appendix A), and Dr. Tormod Naes (Appendix B).

Moral support from the authors parents, Warren and Rose Marie Miller, and from the author's graduate student colleagues, especially Dr. Bradley J. Tenge, was necessary for completion of this dissertation.

Chapter 1

Introduction

1.1 Rationale for this study

The development of polymeric materials has had a great impact on a wide range of applications (1). These applications include food and beverage containers, tires, insulation, automotive exteriors, packaging materials, human-implantable devices, and membranes. In addition, polymeric materials are currently replacing metal and ceramic materials for many applications (2). The development of new polymer applications and increased demand for current polymer applications are expected to cause a large increase in the production of polymers. As polymer production increases, the demand for rapid and reliable quality evaluation of these materials also increases. Rapid quality evaluation enables the characterization of fast polymer production processes and can improve the quality control of slower processes.

Several analytical methods can accurately determine physical, chemical and structural properties of polymers for quality control purposes. Spectroscopic methods, such as infrared (3-7), NMR (6-8), and Raman spectroscopy (6,7), can determine compositional and structural properties of polymers. Thermal analysis (9) and chromatography (10) can also provide compositional and structural information. Rheological methods (11), such as dynamic mechanical

analysis, determine several different physical properties. All of these methods provide useful information that can be used to assess the "quality" of a polymeric material. Unfortunately, these methods also require substantial sample preparation, are labor-intensive, and are usually destructive. In a situation where rapid quality control is necessary, these methods cannot provide timely results.

One approach to the problem of rapid quality control is the use of a correlative analytical method. In this approach, a faster analytical method is trained by a reference analytical method to determine an important property of a material. If the faster method provides sufficient information to determine the property, it can be used for rapid quality analysis.

Near-infrared (NIR) spectroscopy has long been used as a correlative method in the agricultural industry (12-17). The weakness of NIR absorbance bands enables rapid analysis of relatively unprepared materials. NIR transmission spectroscopy can be used to analyze bulk materials up to several centimeters thick. In addition, powdery and fibrous materials can be directly analyzed by NIR diffuse reflectance spectroscopy. Recent developments in NIR instrumentation have resulted in the production of commercial instruments that are capable of rapid process analysis.

Despite the sampling ease of NIR spectroscopy, the determination of properties by NIR spectroscopy can be difficult. This difficulty is caused in part by the broadness and high overlap of individual bands in NIR spectra. Fortunately, multivariate modeling

methods, such as Multiple Linear Regression (MLR) (18) Partial Least Squares (PLS) (19-23), Classical Least Squares (CLS) (19,24,25), and Principal Component Regression (PCR) (21,23), can provide accurate correlations of NIR spectroscopy to reference analytical methods, because the entire spectrum is used for analysis.

The combination of NIR spectroscopy and multivariate modeling has been used for rapid analysis of agricultural materials (12), and can also be used for rapid analysis of polymeric materials. However, NIR polymer analysis methods can be successful only if NIR spectroscopy contains sufficient information to determine important properties of polymers. Earlier analyses (26-42) have demonstrated the ability of NIR spectroscopy to determine several properties of polymers. However, most of these analyses only suggested the feasibility of NIR methods, and did not demonstrate accurate quantitations of polymer properties. In addition, new developments in the areas of NIR instrumentation, multivariate calibration, and high-performance polymeric materials provide a new incentive for research in NIR polymer analysis.

In this work, the ability of NIR spectroscopy to determine chemical, structural, and physical properties of several different polymeric materials is demonstrated. In most cases, multivariate techniques are used to determine the effect of various properties on the NIR spectrum. Quantitative studies are done to demonstrate the ability of NIR spectroscopy to quantitate several different polymer

properties. Qualitative studies are done to identify NIR spectral features that are used to determine various properties of interest.

1.2 Near-infrared Spectroscopy

1.2.1 Information Content of NIR Spectra

1.2.1.1 Standard Spectral Attributes

For the purpose of this discussion, the near-infrared spectral region is defined to be 780 nm (visible red) to 2500 nm (the boundary of the mid-infrared region). NIR spectroscopy provides information about vibrational overtones and vibrational combinations in a molecule (12-17). A vibrational overtone band occurs when a single photon excites a molecular vibration from the ground state (in which the vibrational quantum number, v, equals 0) to a second or higher excited state (in which v = 2 or greater). A first overtone band occurs from a v = 0 to 2 transition, a second overtone band occurs from a v = 0 to 3 transition, and so on. A combination band occurs when a single photon simultaneously excites two different molecular vibrations in the molecule. Overtones and combinations of vibrational transitions are affected by the same factors as the fundamental vibrational transitions (transitions from v = 0 to v = 1) , which are studied by mid-infrared and Raman

spectroscopy. As a result, much of the information provided by IR and Raman spectroscopy is also provided by NIR spectroscopy.

Overtone and combination transitions are forbidden for harmonic molecular vibrations. Therefore, the presence of anharmonicity in molecular vibrations is essential for the existence of overtone and combination bands (43-46). There are two types of anharmonicity that affect molecular vibrations: mechanical anharmonicity and electrical anharmonicity. Mechanical anharmonicity occurs if the potential energy of the vibration as a function of displacement of the vibration has terms of third or higher order. Electrical anharmonicity occurs if the dipole moment of the vibrating group is non-linearly related to the displacement of the vibration. In most real molecules, vibrations are not harmonic and dipole moments are not linear with displacement. As a result, overtone and combination bands are observed for most materials.

Estimated frequencies of overtone bands are integer multiples of the frequency of the fundamental band. Anharmonicity causes actual frequencies of overtone bands to be slightly less than estimated frequencies. The intensity of the first overtone band is at least one order of magnitude less than the intensity of the fundamental band. In general, as one moves from an n^{th} to a $(n+1)^{th}$ overtone band, the intensity of the band decreases by at least one order of magnitude and the bandwidth increases. The frequencies of combination bands are approximately the summation of the frequencies of the two or more vibrational transitions involved in the

combination. The intensities of combination bands are significantly less than the fundamental bands of the modes involved in the combination (46).

Figure 1.1 displays some of the overtone and combination bands for the CH group in chloroform (44). This figure shows that the overtone and combination bands in the NIR region are much weaker than the fundamental bands in the IR region. All of the NIR bands involve the CH stretching mode (3019 cm^{-1}). This result indicates that only the molecular vibrations with high frequency fundamental bands, such as CH, NH, OH, and C=O stretching modes, contribute to prominent overtone and combination bands in the NIR spectrum. Lower frequency vibrations, such as the CH bend in chloroform (1216 cm^{-1}), can combine with the higher frequency CH stretching vibration (3019 cm^{-1}) to make a combination band in the NIR spectrum (4217 cm^{-1}). In this case, the combination band depends on the character of both the CH bending and CH stretching vibrations in the molecule. Very low frequency vibrations, such as the C-Cl vibrations in chloroform, are not well-represented in the NIR spectrum. The sixth, seventh and higher overtone bands of these modes have frequencies in the NIR region, but they are expected to be very weak.

Although NIR spectra contain information from only a few different functional groups, they can be very complicated. The chloroform molecule, which has only one "NIR active" CH group, has many different overtone and combination bands in the NIR spectrum

Figure 1.1: Simplification of the absorbance spectrum of chloroform in the infrared and near-infrared regions. The absorptivities (a) are in units of $((g/l)\cdot cm)^{-1}$

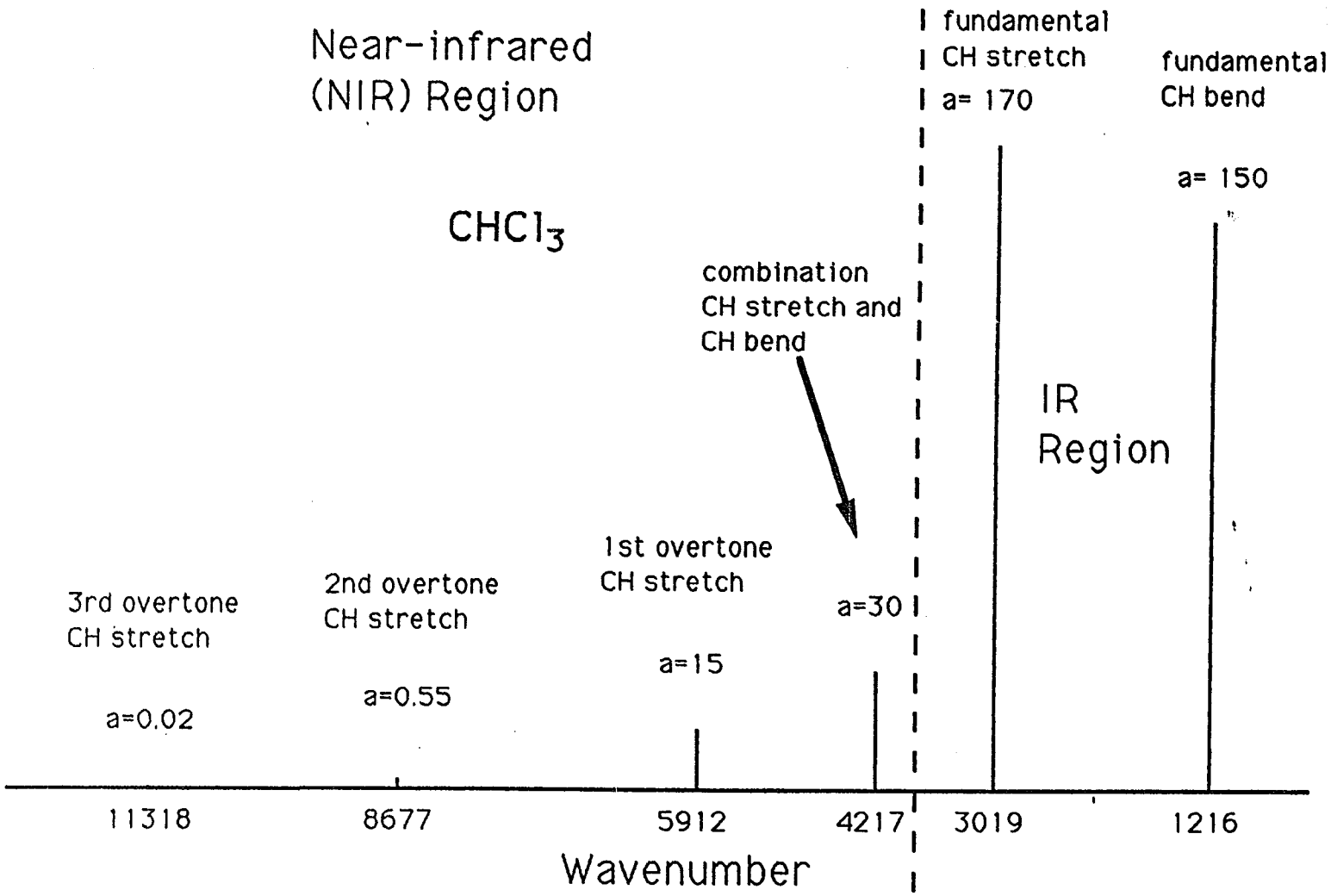
Near-infrared
(NIR) Region
$CHCl_3$
fundamental
CH stretch
a= 170
fundamental
CH bend
a= 150
combination
CH stretch and
CH bend
IR
Region
1st overtone
CH stretch
a=30
a=15
3rd overtone
CH stretch
a=0.02
2nd overtone
CH stretch
a=0.55
11318
8677
5912
4217
3019
1216
Wavenumber

(46). These bands arise from the multitude of possible combinations of fundamental and overtone vibrations in the molecule. For molecules with many different CH, NH, and OH groups, even more bands are expected. The complexity of NIR spectra, combined with the broadness of individual NIR bands, makes the interpretation of NIR spectra difficult.

1.2.1.2 Hydrogen-bonding

Hydrogen bonding is a significant factor in several of the properties studied in this work. Therefore, it is important that the effects of hydrogen bonding on overtone and combination bands be addressed. A hydrogen bond can form between a donor group, which is usually a OH or NH group, and an acceptor group, which has a lone pair of electrons. The vibrations of both the donor and acceptor groups are greatly affected by the formation of a hydrogen bond.

In most cases, hydrogen bonding causes a decrease in band frequency, an increase in band width, and a decrease in band intensity of the overtone and combination bands of the donor group (47,48). It should be noted that the band intensity trend is exactly the opposite for fundamental bands in the IR spectrum. In fact, several IR analyses of polymers indicate that the free NH and OH stretching bands are too weak (relative to bands from hydrogen-bonded groups) for useful interpretation (49,50). NIR spectroscopy

provides a better means to characterize hydrogen bond donor groups than IR spectroscopy, because bands from both free and hydrogen-bonded donor groups have significant intensities (51,52).

The effect of hydrogen bonding on the NIR bands of acceptor groups is not well-characterized, because the overtone and combination bands from acceptor groups are not as strong as the bands from donor groups. Several studies in this work (Chapters 6.2 and 7.2) (53,54) indicate that hydrogen bonding causes a decrease in the band frequency with no significant change in the band intensity of second overtone C=O bands.

1.2.2 NIR Band Assignment Techniques

In many applications of NIR spectroscopy, it is necesary to assign absorbances to support a conclusion or to validate a calibration. Unfortunately, NIR bands cannot be assigned on the basis of quantum-mechanical calculations, because the simulation of NIR bands requires a detailed knowledge of the anharmonicity of the vibrations in the molecule (which is seldom available). As a result, experimental methods of band assignment must be used for NIR analysis. Unfortunately, the high overlap and large number of NIR bands in a spectrum can cause experimental assignments to be tentative.

NIR bands can be assigned on the basis of previously assigned fundamental bands of the same material. Calculation of NIR band

frequencies from fundamental band frequencies is discussed in Chapter 1.2.1.1. There are several problems with this method of band assignment: 1) uncertainty in the calculated band frequency, arising from uncertainty in the anharmonicity of the vibration, 2) lack of band intensity information, and 3) the possible presence of many combinations or overtones at the same NIR frequency. As a result, NIR band assignments based on IR band positions are usually tentative.

More accurate band assignments can be made from NIR analysis of model compounds (53-56). In the case of NIR polymer analysis, several model compounds can be used, each of which contain unique functional groups that are present in the polymer. It is also possible to characterize hydrogen bonding effects by analysis of model compounds in the bulk and in solution (53,54). Model compound analyses provide good assignments of NIR bands because anharmonicity approximations are not necessary and band intensity information is available. However, suitable model compounds are not always available, and assignments can be difficult if there is a high overlap of NIR bands in the model compound spectra. In these cases, band frequencies calculated from the frequencies of fundamental bands can be used to assist the band assignments.

NIR bands can also be assigned on the basis of their behavior under certain changes in conditions. For example, a 1922 nm band that disappears upon drying of a polyurethane sample (Chapter 7.1.3.4) (54) is probably a water band. The isotope substitution

method has also been used to assign NIR bands (57), although it is not used in this work.

1.2.3 NIR Sampling Methods

One of the greatest advantages of NIR spectroscopy is sampling ease. Bulk materials can be analyzed with minimal preparation in many cases. Two different NIR sampling methods are used in this work: transmission and diffuse reflectance.

1.2.3.1 Transmission

NIR transmission spectroscopy can be used to analyze bulk non-scattering polymers and polymer solutions (Chapters 3 and 4) (58,59). A transmission measurement at a single wavelength involves the measurement of the intensity of an incident light beam (I_o) and the intensity of the light beam after it traverses the sample (I). The absorbance (A) can then be calculated:

$$A = -\log(I/I_o) \qquad (1.1)$$

If there is only one absorbing component in the sample, the absorbance is proportional to the concentration of that component, according to the Beer-Lambert law:

$$A = abc \qquad (1.2)$$

where a is the molar absorptivity of the component, b is the path length, and c is the molar concentration of the component in the sample.

Several analyses in this work involve transmission spectroscopy of polymers dissolved in a non-absorbing solvent. Carbon tetrachloride is the solvent used in all of these analyses. The path length (b in Equation 1.2), which corresponds to the width of the cuvette used for NIR sampling, can be held constant for all samples in the analysis. However, it is difficult to prepare solutions that each have the same dilution ratio (or total concentration of polymer in solution). As a result, it is often necessary to normalize each solution spectrum to the sample concentration prior to analysis of the spectra.

In transmission spectroscopy of bulk polymers, the sample thickness corresponds to the path length. Unfortunately, it is difficult to accurately measure the thickness of a bulk sample. This difficulty is especially severe if the bulk sample is relatively unprepared and does not have a well-defined thickness. As a result, it is usually not possible to normalize NIR spectra of bulk polymers to the sample thickness. However, several data correction methods can be used to approximately correct NIR spectra for thickness effects. Classical Least Squares (CLS) calibrations (Chapter 1.5.2.1) (19,24,25,59) can perform accurate predictions in the presence of

thickness effects. Other methods, such as Multiplicative Scatter Correction (MSC, Chapter 1.2.5) (21,60,61) and Path Length Correction with Chemical Modeling (PLC-MC, Appendix B) (62) can also be used to reduce thickness effects in the NIR spectra of bulk polymers.

The low absorptivities of NIR bands greatly simplify NIR transmission sampling. The analysis of polymer solutions in non-absorbing solvents can be made in thick path length (4 mm to 10 cm) cuvettes, which are easy to fill and clean. NIR transmission sampling of flowing streams (up to several centimeters in diameter) in a process environment is also possible. NIR transmission spectroscopy can also be used to analyze thick bulk polymers (1 mm to 10 mm thick), which are easy to prepare. As a result, NIR transmission sampling of polymers is much faster and easier than IR transmission sampling, which requires solution casting or pressing of the sample into thin films.

1.2.3.2 Diffuse Reflectance

NIR diffuse reflectance spectroscopy (63-67) can be used for the analysis of highly-scattering polymers, such as crystalline PET (Chapter 5) (56) and reaction injection molded (RIM) polyurethanes (Chapter 7) (54). In diffuse reflectance spectroscopy, the intensity of light reflected by the sample (R) is used to obtain a pseudo-absorbance value (A_r):

$$A_r = -\log(R/R_o) \qquad (1.3)$$

where R_o is a reference intensity value. R_o can be the reflected intensity of incident light from a highly-scattering, non-absorbing standard (such as a ceramic plate), or the intensity of the incident light. The intensity of light reflected from the sample (R) has contributions from specular and diffuse reflectance. Specular reflectance arises from incident light that is regularly reflected, but not absorbed, by the sample. Diffuse reflectance arises from incident light that has been absorbed and incoherently emitted by the sample. In NIR spectroscopy, absorbances are too weak to affect the specular reflectance of the material. As a result, only diffusely reflected light contains information about the chemistry of the sample.

Although the pseudo-absorbance value (A_r) is commonly used in quantitative NIR diffuse reflectance analysis (12), there is no theory that relates this value to concentration. Other quantities, such as the Kubelka-Munk function (63,65,67), have been used to linearize reflectance values with respect to concentration. The choice of the pseudo-absorbance value for use in this work is based solely on the success of earlier analyses that used this value (68).

In NIR diffuse reflectance spectroscopy, the scattering of incident light is caused by reflectance at refractive index interfaces in the sample. For a powdery material, such as powdered

poly(ethylene terephthalate), air/polymer interfaces and crystalline/amorphous polymer interfaces (Chapter 1.3.2.2) (56) cause much of the scattering. For a bulk polymer with trapped bubbles or voids, such as reaction injection molded (RIM) polyurethanes (Chapter 7) (54) and foams (Chapter 8) (69), scattering is caused by reflection at void/polymer interfaces. As a result, the magnitude of scattering by polymer samples depends on the particle size of powdery samples or on the void size and void density of porous samples.

The ability of a sample to scatter incident light strongly affects its specular and diffuse reflectance. Scattering differences cause differences in the overall intensity of specularly reflected light. This effect results in baseline offset differences in diffuse reflectance spectra. The effect of a scattering change on the diffuse reflectance is a change in the effective path length of the sample. This change, which is equivalent to a path length change in transmission spectroscopy, causes multiplicative differences in diffuse reflectance spectra. It is necessary to reduce baseline offset and multiplicative effects in diffuse reflectance spectra in order to perform accurate quantitative analyses. Derivative spectra (Chapter 1.2.5) can be used to reduce baseline offset effects. Multiplicative Scatter Correction (MSC, Chapter 1.2.5) (21,60,61) and Path Length Correction with Chemical Modeling (PLC-MC, Appendix B) (62) can be used to reduce multiplicative effects.

As stated before, the low absorptivities of NIR bands lead to several advantages for diffuse reflectance spectroscopy. The effective path length of a diffuse reflectance sample, which (for a given sample) is inversely related to the intensity of scattered light from the sample (63), can be very large for NIR spectroscopy. As a result, large particles (up to several mm in diameter) and bulk porous polymers with a low density of voids can be analyzed without preparation. Samples need not be ground into a fine powder or diluted in an inert scattering material, as in IR diffuse reflectance spectroscopy (70). In addition, the lack of intense absorptions eliminates the presence of *reststrahlen* bands, which complicate IR diffuse reflectance spectra (71).

1.2.4 NIR Instrumentation

1.2.4.1 Typical Instrumental Attributes

Recent developments in NIR instrumentation (13,17,72) have made NIR spectroscopy accessible to many potential users. Tungsten-halogen sources provide high intensities over the entire NIR spectral region (780 nm to 2500 nm). Concave holographic gratings blazed for the NIR region have few defects and high focusing power. Fixed filter NIR instruments have higher throughput and lower nominal resolution than grating monochomator instruments, and can be used for specific applications in hostile environments.

Tilting-interference filter instruments offer the ruggedness of fixed filter instruments and have rapid-scanning capabilities. An interferometer, which provides wavelength accuracy and throughput advantages, can also be used for NIR spectroscopy (73). Sensitive room temperature detectors, such as lead sulfide (with detection from 1000 nm to 3000 nm) and silicon (with detection from 780 nm to 1000 nm) are commonly used in commercial NIR spectrometers. Typical signal-to-noise ratios for NIR spectra obtained in this work are in the range of 100:1 to 1000:1, although ratios as great as 100,000:1 are possible (13).

Collection and detection optics in NIR spectroscopy depend on the sampling method. A single detector is used to collect transmitted light. An integrating sphere can be used to collect and focus diffusely reflected light onto several detectors. Diffusely-reflected light can also be detected by several detectors that are placed on the illuminated side of the sample. Figure 1.2 shows approximate sampling configurations for the NIR instruments used in this work.

There are several instrumental advantages of NIR spectroscopy over other spectroscopic methods. Because low-hydroxyl optical fibers efficiently transmit NIR light, remote NIR spectroscopy can be done over optical fibers (73,74). Inexpensive glass and quartz optics, which do not absorb NIR radiation, can be used in NIR instruments. Furthermore, the weakness of NIR water vapor absorptions eliminates the need for instrument purging for most instruments.

Figure 1.2: Simplified diagrams of the sampling geometries of the two near-infrared instruments used in this work.

PSCO 6250 NIR Spectrometer

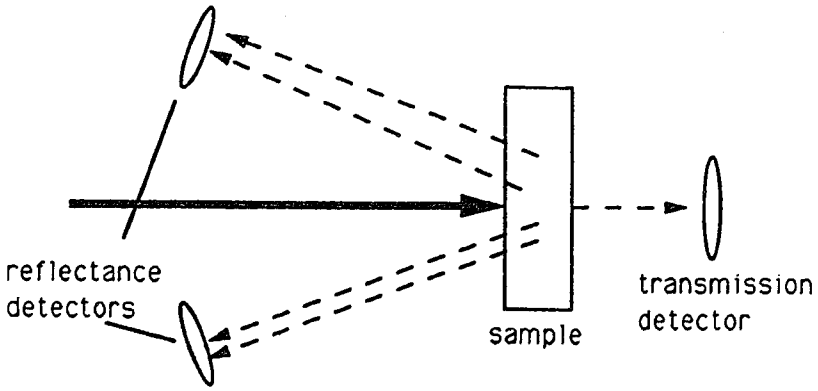

Technicon 500C NIR Spectrometer

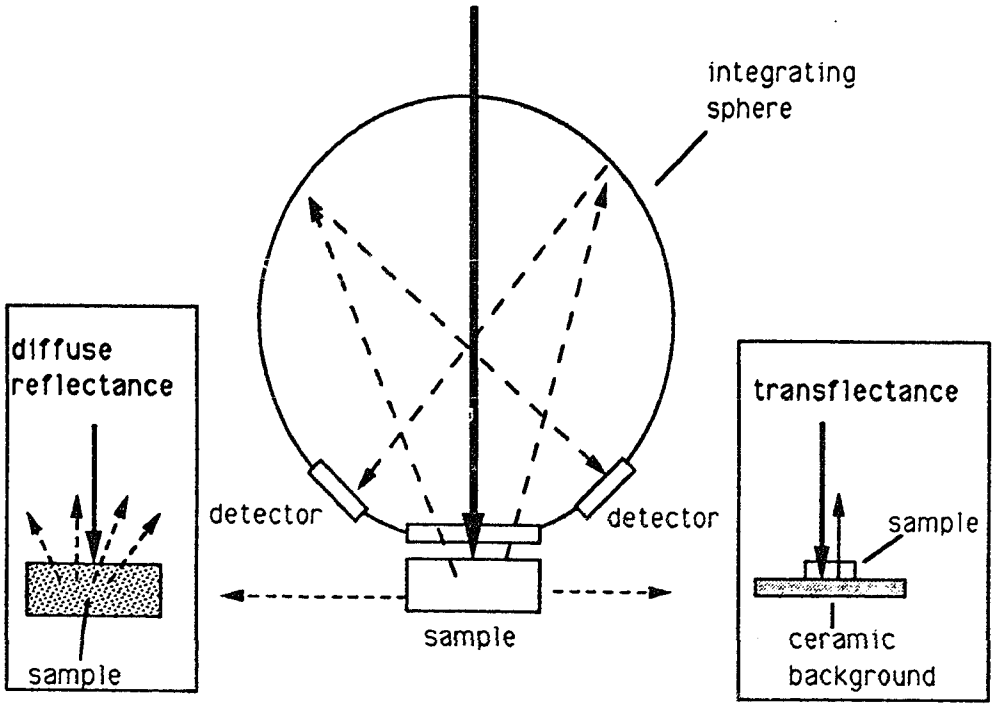

1.2.4.2 Instrumentation in This Work

A Pacific Scientific 6250 NIR instrument was used for the diffuse reflectance and transmission measurements in Chapters 3, 4 and 5. A lead sulfide detector was used to obtain transmission spectra (see Figure 1.2). The reference transmission intensity (I_o, in Equation 1.1) was obtained from the transmission spectrum of an empty cuvette. Other lead sulfide detectors, which are on the illuminated side of the samples and off the axis of the incident light path, are used for detection of diffusely reflected light. Reference reflectance intensity (R_o, in Equation 1.3) was obtained from the diffuse reflectance spectrum of a ceramic reflectance standard. Absorbance values (A in Equation 1.1) were used for analysis of transmission spectra, and pseudo-absorbance values (A_r, in Equation 1.3) were used for analysis of diffuse reflectance spectra.

A Technicon InfraAlyzer 500C NIR diffuse reflectance instrument was used for the studies in Chapters 2, 6, 7 and 8. This instrument uses an integrating sphere to efficiently collect diffusely reflected light (Figure 1.2). Although transmission measurements cannot be made on this instrument, "transflectance" measurements can be made for the analysis of bulk non-scattering polymers and polymer solutions. A transflectance measurement involves the placement of a sample on top of an inert scattering background at the sampling region of the spectrometer. For both diffuse reflectance

and transflectance measurements, the intensity of unattenuated source light was used as the reference intensity (R_o). Pseudo-absorbance values were used for the analysis of reflectance and transflectance spectra.

Both instruments have a tungsten-halogen source, a holographic grating, and lead sulfide detectors. The spectral range 1100 nm to 2500 nm was used for most experiments. Wavelength accuracy was +/- 1 nm, wavelength repeatability was 0.02 to 0.05 nm, and the nominal resolution was 10 nm for both instruments. NBS Standard Reference Material 1920 (75) was used for wavelength calibration of the Technicon InfraAlyzer instrument.

1.2.5 Spectral Pretreatment Methods

Non-reproducible sampling can cause baseline offset and multiplicative effects in NIR spectra (12). Variable sample placements in the spectrometer and differences in the intensity of scattered light from different diffuse reflectance samples (Chapter 1.2.3.2) cause baseline offset differences in the spectra. This effect can be reduced by taking the first derivative of each spectrum with respect to wavelength. If differences in baseline curvature of the spectra are significant, the second derivative of each spectrum can be used. The use of derivative spectra not only reduces baseline variabilities, but can also be used to resolve highly-overlapped

bands. Unfortunately, derivative spectra are noisier than the original spectra, and are very difficult to interpret qualititively.

Multiplicative effects in NIR spectra can arise from variations in the scattering properties of diffuse reflectance samples (Chapter 1.2.3.2) and from variations in the thickness of transmission samples (Chapter 1.2.3.1). Multiplicative Scatter Correction (MSC) has been used to reduce multiplicative and baseline offset effects in NIR spectra. The MSC model is given by the equation

$$\mathbf{x} = a\mathbf{1} + b\bar{\mathbf{x}} + \mathbf{e} \qquad (1.4)$$

where $\mathbf{x}$ is a NIR spectrum, $\bar{\mathbf{x}}$ is a reference NIR spectrum, $\mathbf{1}$ is a vector of ones, a is the MSC additive constant, and b is the MSC multiplicative constant. All of the vectors have *m* elements, where *m* is the number of wavelength responses in a single NIR spectrum. Given $\mathbf{x}$ and $\bar{\mathbf{x}}$, the estimates of a and b ($\hat{a}$ and $\hat{b}$) can be determined by the least-squares method. The MSC-corrected spectrum ($\mathbf{x}_c$) is then calculated from

$$\mathbf{x}_c = 1/\hat{b}\,(\mathbf{x} - \hat{a}\mathbf{1}). \qquad (1.5)$$

In most cases, the reference spectrum ($\bar{\mathbf{x}}$) is chosen as the average spectrum of a series of calibration spectra. The MSC method performs an accurate correction if additive and multiplicative spectral variations are much larger than the spectral variations from

chemical effects. However, when spectral variations from chemical effects are large, the MSC method performs inaccurate corrections. The Path Length Correction with Chemical Modeling (PLC-MC) method, described in Appendix B (62), can be used for accurate multiplicative correction when spectral variation from chemical effects is large.

1.3 Polymer Chemistry

A polymer is a material composed of molecules that have covalently-bonded chemical repeat units (11,76). Homopolymers, such as poly(ethylene terephthalate) (PET) (Chapter 5) and poly(octadecyl methacrylate) (POMA) (Chapter 2), contain only one chemical repeat unit; copolymers, such as styrene-butadiene copolymers (SBR) (Chapter 4), and polyurethanes (Chapter 6, 7 and 8), contain two different chemical repeat units; terpolymers, such as ethylene-propylene-diene terpolymers (Chapter 3), contain three different chemical repeat units. In this section, chemical, structural and physical properties of polymers are briefly reviewed. Only the properties studied in this thesis are discussed in detail.

1.3.1 Chemical Properties of Polymers

1.3.1.1 Composition

Composition refers to the mass percentages of the different chemical repeat units in a copolymer or terpolymer. FTIR spectroscopy (6,7), NMR spectroscopy (8), and elemental analysis (55) can be used to determine composition.

1.3.1.2 Moisture Content

Several polymer systems, such as poly(ethylene terephthalate) (Chapter 5.3.4) (56) and polyurethane block copolymers (Chapters 6.2.3 and 7.3.4) (53,54) are moderately hygroscopic. Moisture retention in these polymers is the result of hydrogen bonding of water molecules to hydrogen bond acceptor groups of the polymer, such as C=O, N-H, and C-O groups. Moisture content can be determined by thermogravimetry and Karl-Fischer titration.

1.3.2 Structural Properties of Polymers

1.3.2.1 Isomerism

There are several different types of isomerism in polymer molecules. Structural isomerism is a major source of variation in butadiene polymers (Chapter 4) (11,77). Three different structural isomers are possible in poly(butadiene) (PBD): *cis*-1,4, *trans*-1,4, and 1,2 butadiene (see Figure 1.3). These different structural isomers

Figure 1.3: Examples of structural and conformational isomers in polymers.

Structural Isomers:

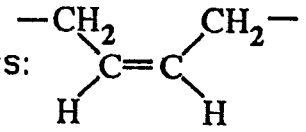

cis-1,4 butadiene

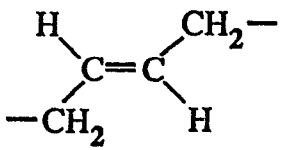

trans-1,4 butadiene

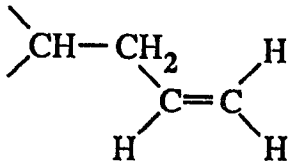

1,2 butadiene

Conformational Isomers:

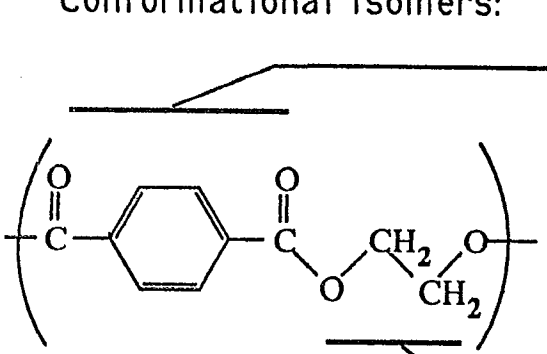

poly(ethylene terephthalate)

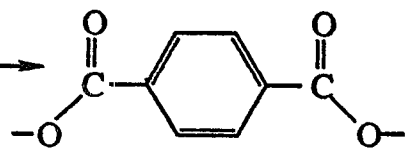

planar cis

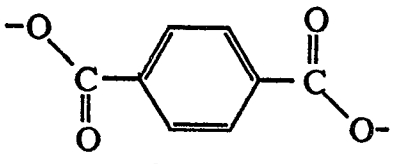

planar trans

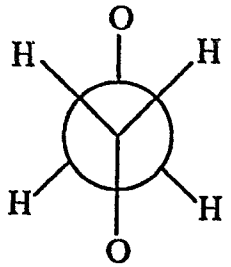

trans

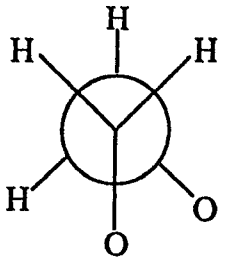

gauche

arise from three different addition reactions of monomers to growing polymer chain ends during polymerization (78). The relative amounts of the three structural isomers, also called the microstructure, can be controlled by the choice of polymerization catalyst and temperature. NMR (3,41,79,27) and FTIR (3,4,81) methods can be used to determine the microstructure of PBD and other materials that have structural isomers.

Conformational isomerism, which refers to the differences in conformational states of functional groups in a polymer chain, is an important factor in the analysis of poly(ethylene terephthalate) (PET) (Chapter 5) (82-84). There are two separate examples of conformational isomerism in PET: the terephthalic acid part of the molecule can assume a planar *cis* or planar *trans* conformation of the *p*-carboxylate groups about the phenyl ring, and 2) the ethylene glycol part of the molecule can assume a *trans* or *gauche* conformation (Figure 1.3). The relative amounts of *trans* and *gauche* ethylene glycol groups in PET is an indicator of the orientation of the polymer molecules. Conformational isomerism in polymer molecules can be determined by NMR (8) and FTIR spectroscopy (82-84).

1.3.2.2 Crystallinity

Crystallinity refers to the packing of polymer chains in an ordered configuration. In a typical semicrystalline polymer, regions of crystalline polymer are dispersed in a matrix of amorphous

polymer chains (Figure 1.4) (11,85). The polymer chain segments in crystalline regions are bound together by intermolecular forces, such as van der waals forces, hydrogen bonding and dipole-dipole forces. Like inorganic crystals, the crystalline regions of polymers give discrete X-ray diffractions. However, the sizes of crystalline regions in polymers are only on the order of 10 microns. In this situation, crystalline regions act as filler particles in the amorphous polymer, and provide strength to the material.

The thermodynamics of crystallinity are described by the equation

$$\Delta G_c = \Delta H_c - T\Delta S_c \qquad (1.6)$$

where ΔG_c is the free energy of crystallization, ΔH_c is the enthalpy of crystallization, ΔS_c is the entropy of crystallization and T is the absolute temperature. The temperature at which ΔG_c equals zero (T_m) is the melting temperature of a crystal. As a result, crystallization is thermodynamically favored at temperatures below T_m. For polymers, there is a strong dependence on the kinetics of crystallization, because the ordering process requires that the polymer chains rearrange themselves. Substantial rearrangements of polymer chains can occur at temperatures above the glass transition temperature (T_g) of the polymer. As a result, crystallization of polymers can occur at temperatures above T_g and below T_m.

Figure 1.4: The configuration of polymer chains in crystalline and amorphous regions of a semicrystalline polymer.

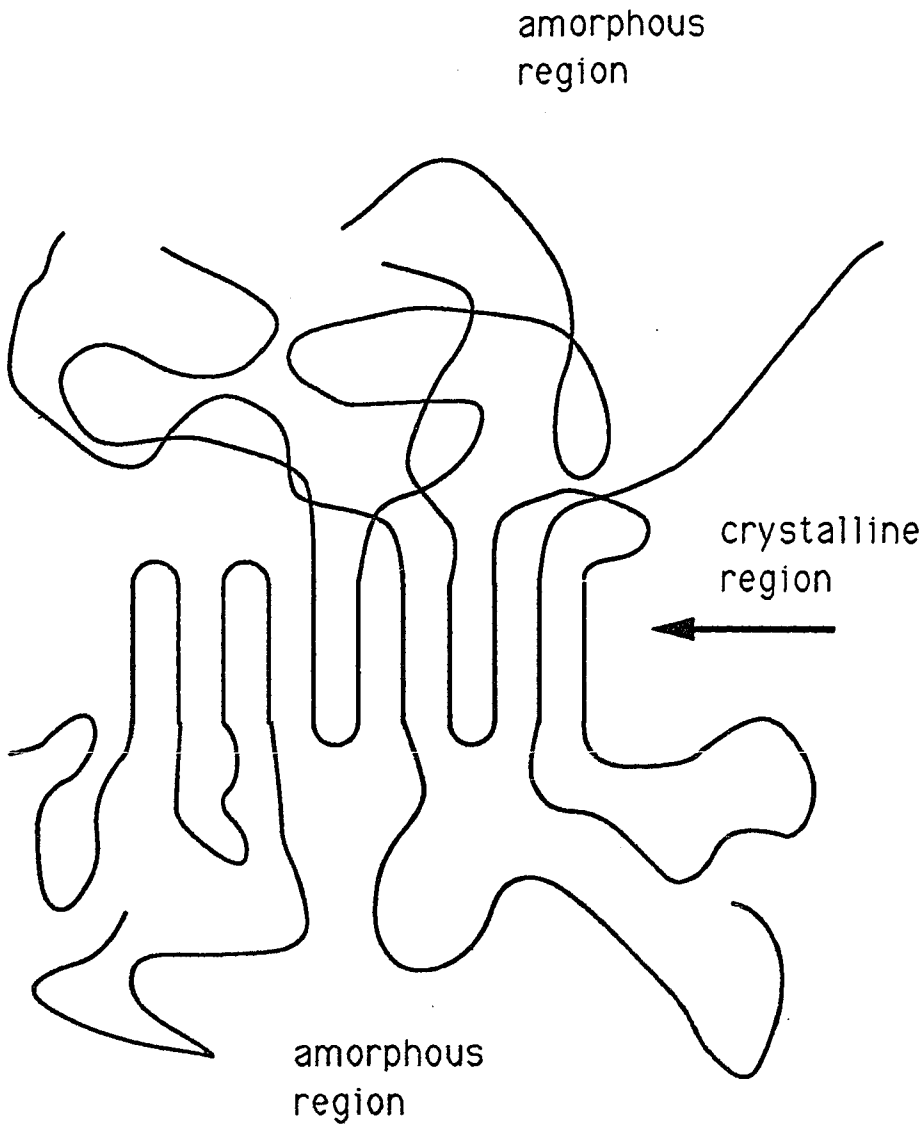
amorphous
region
crystalline
region
amorphous
region

Several methods can be used to determine crystallinity in polymers. Density measurements can be used (86), since the densities of crystalline and amorphous polymer differ. Differential Scanning Calorimetry (DSC) (9,86-89) and X-ray diffraction (86,90) methods can also be used to determine crystallinity. Neutron diffraction (91) yields detailed information about chain folding in polymer crystals.

1.3.2.3 Orientation

The orientation of amorphous polymer chains is a very important property for fibers and textiles (92). Orientation can develop in amorphous regions (Figure 1.4) of fibrous polymers as a result of spinning or drawing processes. In the case of PET fibers (Chapter 5), drawing causes the formation of crystalline polymer in addition to the orientation of amorphous polymer. The degree of amorphous orientation affects the shrinkage and strength of PET fibers. Amorphous orientation in polymer fibers is usually determined by birefringence measurements (92,93).

1.3.2.4 Sequencing

Sequencing refers to the ordering of repeat units in a polymer chain. There are three major types of sequencing in polymer molecules: 1) alternating, 2) block, and 3) random. These types of

sequencing are shown in Figure 1.5, where A and B refer to different chemical repeat units in a copolymer or different isomers of the same chemical repeat unit in a homopolymer. Alternating polymers can form crystalline domains, block polymers can phase separate (a phenomenon described in Chapter 1.3.2.5), and random polymers are generally incapable of crystallization or phase separation. As a result, the properties of a polymer depend greatly on the sequencing of monomer units in the polymer molecules (11).

The determination of sequencing in polymers requires a method that can distinguish between different sequences of several monomer units. NMR spectroscopy has been used to determine sequencing (8,80), because the technique has sufficient resolution to provide discrete peaks for sequences of up to 4 or 5 units. Vibrational spectroscopy methods, such as FTIR, Raman and NIR spectroscopy, do not have the necessary resolution to determine long sequences of repeat units. However, these methods can be used to distinguish between structures with large differences in sequencing.

1.3.2.5 Phase Separation

The different blocks in a block copolymer can behave like incompatible phases in a binary mixture. For example, polyurethane block copolymers (Chapters 6 and 7) contain hard blocks (with highly polar functionalities) and soft blocks (with non-polar functionalities). If the temperature is sufficiently high to cause mobility of the

Figure 1.5: Three different types of sequencing in polymer chains. A and B correspond to different repeat units in the polymer.

Sequencing in Polymers

Alternating: ABABABABAB

Block: AAAAABBBBB

Random: AABAABBBAB

polymer chains, these incompatible blocks can separate in the bulk copolymer. This process, known as phase separation, produces polar and non-polar domains in the copolymer (49,50,94-101). In the case of polyurethanes, the size of hard block (or polar) domains are on the order of tens to hundreds of angstroms. These hard block domains serve as crosslinks between different polymer chains, and therefore provide elastic properties to non-crosslinked polyurethane systems.

X-ray scattering (50,96,101,102) and differential scanning calorimetry (49,94,96,99) can be used to study phase separation. Several FTIR methods have been proposed for the analysis of phase separation (49,50,97-100,103).

1.3.2.6 Adsorption to Surfaces

The adsorption of polymers to surfaces is used for the production of several materials, such as storage media devices and ceramics (104). Polymers can adsorb to inorganic surfaces by hydrogen bonding or dipole-dipole interactions between functional groups on the surface and functional groups on the polymer. The bonding strength of polymers to surfaces depends on the adsorption mechanism. Spectroscopic methods, such as FTIR (105-107) and external reflectance-IR spectroscopy (108), can be used to characterize surface adsorption processes.

1.3.3 Physical Properties of Polymers

1.3.3.1 Density

The density of polymeric materials depends on chemical, structural and physical factors. Crystallinity and amorphous orientation affects the density of semicrystalline polymers (86). A density gradient tube, which contins a fluid with a known density gradient, can be used to determine the density of semicrystalline polymers. For porous bulk polymers, such as reaction injection molded (RIM) polyurethanes (Chapter 7) (54), and polyurethane foams (Chapter 8) (69), the density is affected by the size and concentration of voids in the polymer. The density of a foam sample can be obtained from volume and mass measurements of the sample.

1.3.3.2 Modulus

The modulus is the stress required to induce one unit of strain in an elastic material (11,76,109). Different types of moduli, such as tensile modulus, compression modulus, and flex modulus, refer to different geometries of stress and strain. At the elastic region of a stress/strain curve (Figure 1.6), the polymer behaves as a perfect elastic body. In many cases, excessive stress on the material causes failure of the material. The modulus can be calculated as the slope of the curve in the elastic region, as the strain approaches zero.

Figure 1.6: A typical stress-strain curve for an elastic material. s_f is the stress at failure and d_f is the deformation at failure.

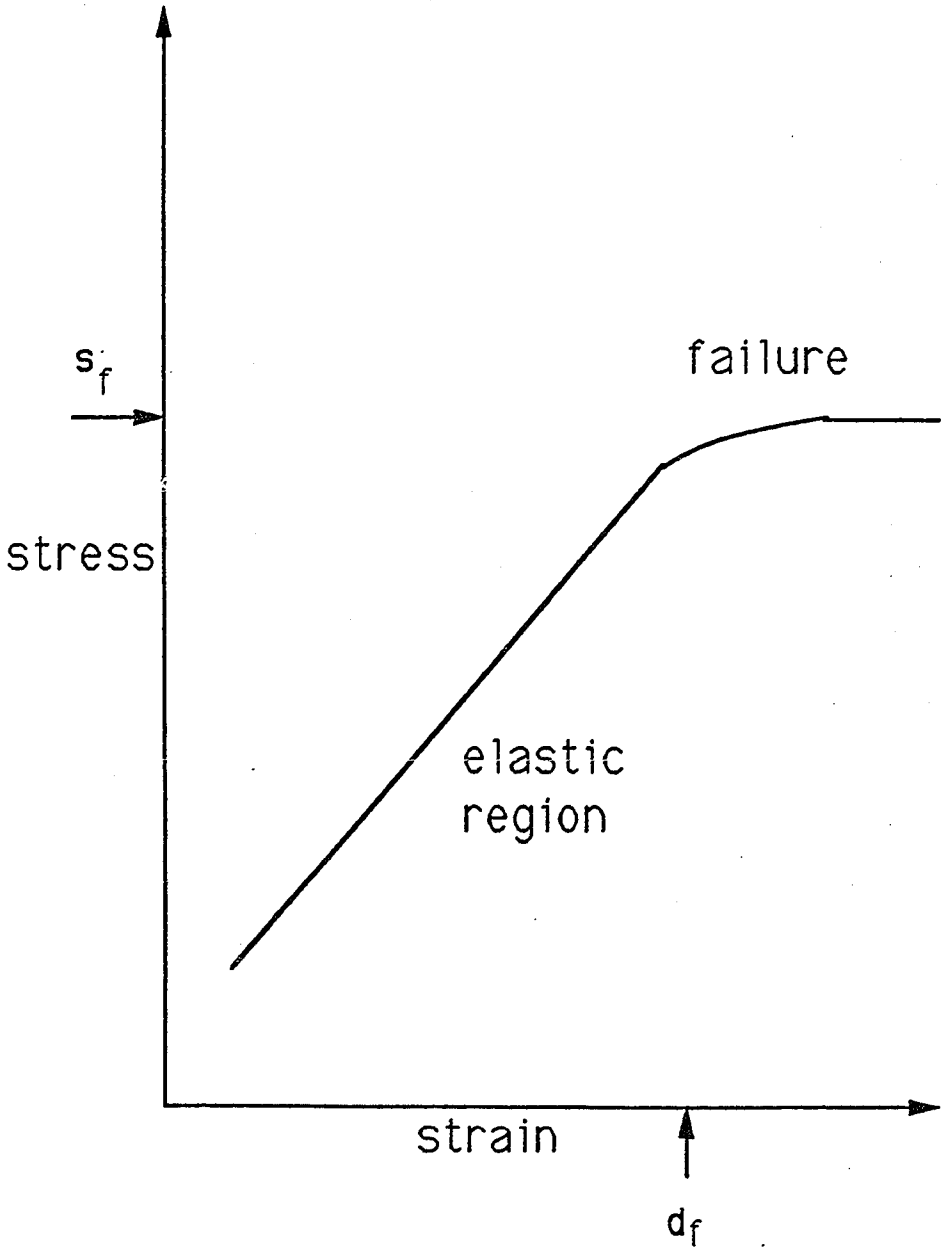
s_f
failure
stress
elastic
region
strain
d_f

Two different modulus measurements are used in this work: 1) flex modulus (Chapter 7.1.2) (110) and 2) compression modulus (Chapter 8.2) (111). The flex modulus measurement involves placement of a load in the center of a 1" by 3" by 1/4" sample, which is held at the two ends. A single flex modulus value is obtained from each measurement. The compression modulus measurement involves a biaxial compression of a 1" by 1" by 1" sample. A compression modulus test determines three properties of the material: 1) the compression modulus, 2) deformation at failure (d_f), and 3) compression strength (s_f). Details of flex modulus and compression modulus measurements are given in references 110 and 111.

1.3.3.3 Thermal Conductivity

Thermal conductivity is an important property of polymers that are used for insulation, such as rigid foams (69,112). This property is affected by the composition and structure of the polymer and the size and concentration of voids in the polymer. The determination of the thermal conductivity of a foam involves the placement of the sample between a hot and cold plate, and subsequent measurement of the heat flow through the sample. The thermal conductivity measurement used for this work, which is also called the K-factor test, is described in references 112 and 113.

1.3.3.4 Heat Sag

The heat sag of a material refers to the extent of deformation that the material experiences at elevated temperatures. This property is very important for RIM polyurethanes, which can deform during high temperature processing or paint application (1). A heat sag measurement involves the suspension of a 1" by 8" by 1/4" sample at one end, and observation of the deformation that occurs upon heating the sample at a fixed temperature for approximately one hour. The distance that the free end sags as a result of the heat treatment is equal to the heat sag (see Chapter 7.1.2, reference 114).

1.3.4 Correlation of Chemical and Structural Properties to Physical Properties

In many cases, the quality of a polymeric material is judged by its physical properties. However, the physical properties are directly affected by the chemical and structural properties of the polymer (11,76,115). Spectroscopic methods of analysis, such as NIR, FTIR, and Raman spectroscopy, provide information about chemical and structural properties. Therefore, data from these methods can be used to estimate physical properties.

Some of the analyses in this work involve the determination of chemical or structural properties by NIR spectroscopy (Chapters 2, 3, 4, 5 and 6). In these studies, it is important that the properties

directly influence absorbance bands in the NIR spectrum. Other analyses involve the correlation of physical properties to NIR spectra (Chapters 7 and 8). The success of these studies depends on the ability of NIR spectroscopy to determine chemical and structural properties that influence the physical property of interest. If little is known about the structure-property relations of a material, these studies can also be used to develop these relations.

1.4 Reaction Injection Molding

Reaction Injection Molding (RIM) (98,116-120) is a common method of preparation for polyurethane materials. In this method, reactants are rapidly mixed together and allowed to cure in a mold. Polyurethanes produced by RIM are used predominantly for automotive applications (1).

1.4.1 The Chemical Process

There are three main reactants in a RIM polymerization (Figure 1.7): 1) isocyanate (I), 2) polyol (II), and chain extender (III or IV) (121). The polymerization involves two competing reactions that occur during a RIM polymerization: 1) reaction of the polyol with the isocyanate (reaction 1) and 2) reaction of the isocyanate with the chain extender (reaction 2 or 3). If a diol chain extender (III) is

Figure 1.7: Reactions that occur during the preparation of a polyurethane by reaction injection molding.

Reaction 1:

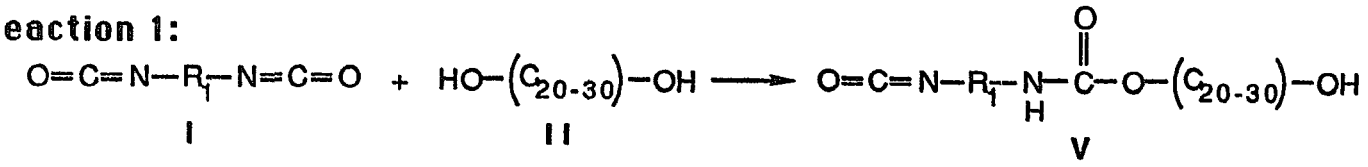

I II V

Reaction 2:

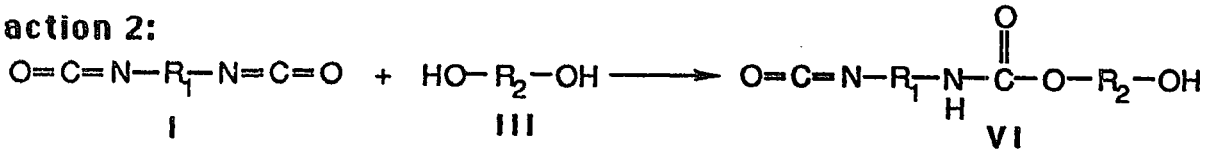

I III VI

Reaction 3:

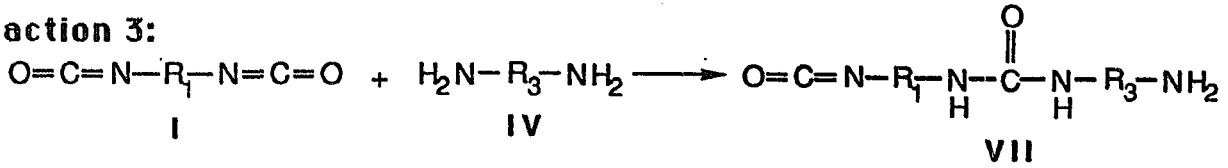

I IV VII

Reaction 4:

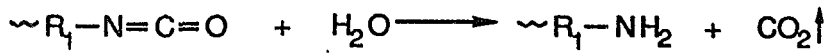

used, a polymer with urethane groups (as in products **V** and **VI**) will be formed. If a diamine chain extender (**IV**) is used, a polymer with urethane groups (as in product **V**) and urea groups (as in product **VII**) will be formed. It should be mentioned that side reactions of products (**V**, **VI**, and **VII**) with the isocyanate (**I**) also occur to a small extent. The finished polymer contains soft blocks (represented by **V**) and hard blocks (represented by **VI** or **VII**).

Reactions **1**, **2** and **3** in Figure 1.7 result in the formation of a linear polymer, because the functionalities (or number of reactive groups) of the isocyanate (**I**) and polyol (**II**) are each equal to two. Phase separated hard block domains (Chapter 1.3.2.5) provide crosslinks (and therefore elasticity) to linear polyurethane systems. If covalent crosslinks are desired, isocyanates or polyols with functionality greater than two can be used.

Phase separation of hard and soft blocks can occur during the polymerization (118-120). If too much phase separation occurs during the reaction, low molecular weight oligomers will be produced. In this case, the finished material will not exhibit elastic behavior. However, phase separation in the finished material is necessary to provide strength to the material. Reaction conditions can be manipulated to balance reaction and phase separation processes, and therefore optimize the physical properties of the product.

The process of nucleation, which involves the escape of dissolved nitrogen from the reactants, also occurs during the

polymerization (122). As the dissolved nitrogen attempts to escape the polymerizing mixture, many of the bubbles become trapped in the polymer and form voids in the finished material. The size and amount of voids in the finished material, which can be determined by density measurements, greatly affect the physical properties of the material. In many cases (as in Chapter 7), these voids are not equally distributed over the entire finished material. Nucleation can be controlled by several reaction parameters (see Chapter 1.4.2).

Polyurethane foams are also produced by the RIM process (121). Foaming can be accomplished in two ways: 1) addition of water to the polymerizing mixture, which reacts with isocyanate groups to produce CO_2 bubbles (Figure 1.7, reaction 4) during the reaction, or 2) addition of a blowing agent (usually a chlorofluorocarbon) to the reaction mixture, which volatilizes during the reaction process. These reactions produce large voids in the finished material. In most cases, these voids have a directional characteristic, which develops as the bubbles attempt to rise out of the polymerizing mixture. The compression properties of a foam greatly depend on the direction of elongation of the voids in the foam with respect to the compression direction (111).

1.4.2 The RIM Machine

A RIM machine takes in reactants and produces molded polyurethane plaques (116,120,123). A simplified diagram of a RIM

machine, adapted for polyurethane production, is shown in Figure 1.8. In most cases, the isocyanate resevoir contains only the di-isocyanate reactant (I). The polyol reservoir contains the polyol (II), the chain extender (III or IV), the catalyst, and the foaming agent (if foams are to be made). When an injection is made, the machine delivers reactants from the resevoirs to a mixing area, where impringement mixing occurs. The mixture is then injected into a mold and allowed to cure. After a specified reaction time, the mold can be opened and the polyurethane plaque removed.

There are several parameters (shown in Figure 1.8, labeled a through g) that can be manipulated to change the quality of a product. The polyol formulation (a) refers to the percentages of polyol (I) and chain extender (III or IV) in the polyol resevoir. Because the polyol exclusively forms soft blocks in the polymer (Figure 1.7, reaction 1) and the chain extender exclusively forms hard blocks in the polymer (Figure 1.7, reactions 2 and 3), this parameter affects the hard block percentage of the final polymer (98,117). The index (b) refers to the relative amounts of material in the isocyanate and polyol resevoirs that are mixed during the injection. An index of 100 corresponds to the mixing ratio for perfect reaction stoichiometry, which is fixed after the formulation (a) is determined. In practice, indices of 101 to 109 are used, which correspond to an excess of isocyanate groups in the reaction. The use of excess isocyanate in the reaction compensates for side reactions that consume isocyanate groups. The index affects the hard block

Figure 1.8: Simplified diagram of a reaction injection molding (RIM) machine. Important reaction parameters are shown in boldface.

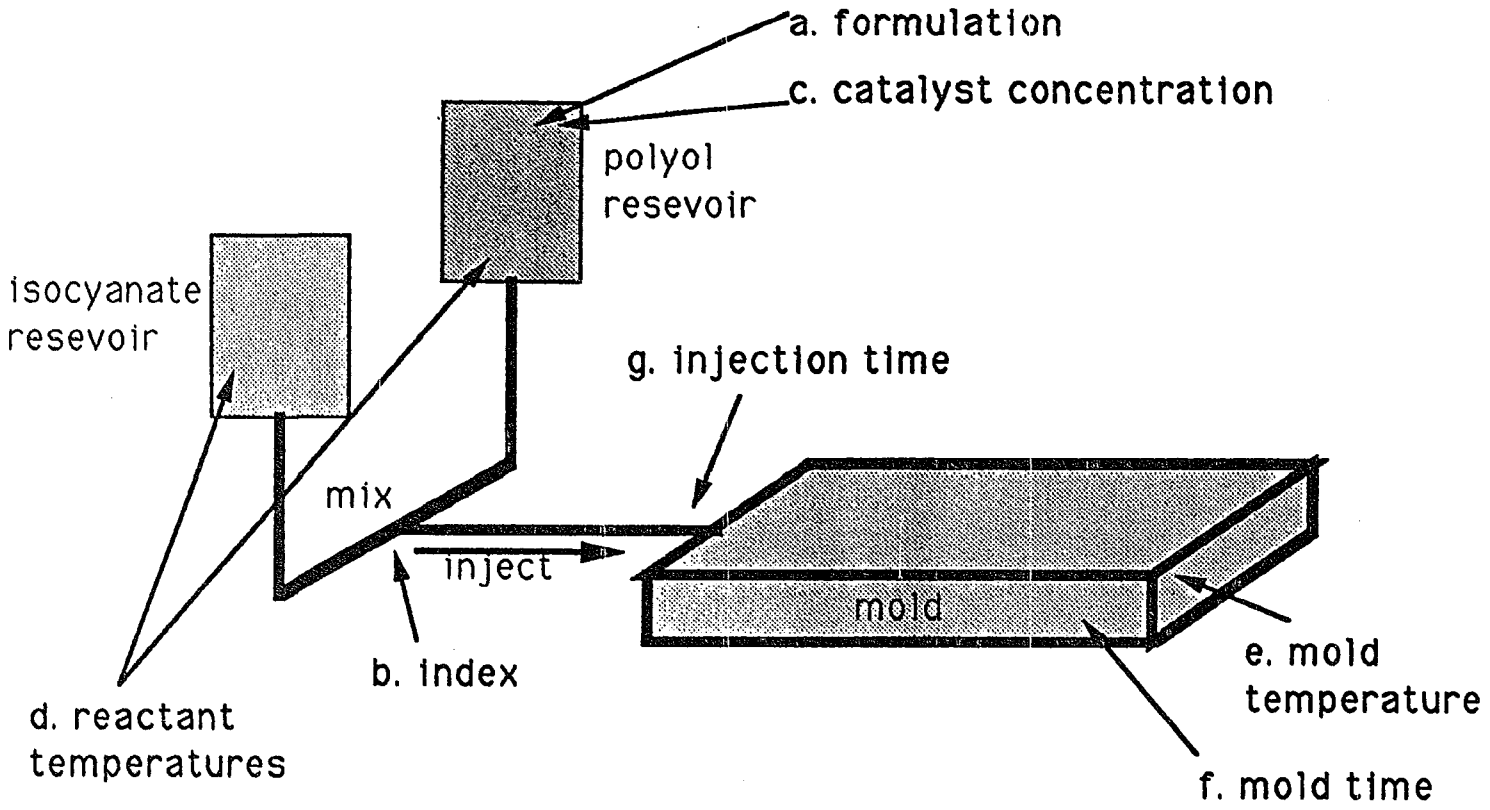
a. formulation
c. catalyst concentration
polyol
resevoir
isocyanate
resevoir
g. injection time
mix
inject
mold
b. index
d. reactant
temperatures
e. mold
temperature
f. mold time

percentage in the polymer and the concentrations of side products in the polymer.

Reaction kinetics can be controlled by the catalyst concentration (**c**), the reactant temperatures (**d**), and the mold temperature (**e**) (which is equivalent to reaction temperature). Earlier studies (118-120) indicate that an increase in catalyst concentration causes an increase in the molecular weight and a decrease in the phase separation of the final product. A recent study (120) has shown that an optimal reaction temperature exists for any polymer system. Below the optimal temperature, more phase separation occurs and lower molecular weight oligomers are obtained. If the reaction temperature is too high, the phase separation in the finished material is insufficient. The mold time (**f**), which is equivalent to the reaction time, must be sufficiently long to allow complete reaction of active groups in the polymerizing mixture. In some cases, a significant amount of unreacted isocyanate, hydroxyl, or amine groups are present in the finished polyurethane plaque. In these situations, post-curing of the polymer (which involves exposure to a temperature above the mold temperature for approximately one hour) can be used to cause further reaction of these groups. The post-curing process might also affect the phase separation of the material.

The injection time (**g**) affects the total amount of mixed reactants that is injected into the mold. This parameter can be adjusted to influence the density of voids in the finished material. If

the mold is underfilled, there is space in the mold available for the escape of gaseous nitrogen that is formed in the nucleation process. Various extents of underfilling result in various densities of voids in the finished polymer (122).

1.5 Multivariate Analysis- Full-Spectrum Methods

Each NIR spectrum contains a series of wavelength responses, or wavelength variables. These variables can be used to determine important properties of a sample. Because individual NIR bands are highly-overlapped (Chapter 1.2.1.1), it is usually necessary to use several NIR wavelength variables for the determination of a propertry. Two approaches can be used for multivariate analysis of NIR spectra: 1) several chosen wavelengths in the spectrum can be used (the wavelength-selection approach) (25,124,125), and 2) the entire NIR spectrum can be used (the full spectrum approach) (21). The studies in this work employ full spectrum methods, such as Partial Least Squares (PLS) (19-23), Classical Least Squares (CLS) (19,24,25), and Principal Components Analysis (PCA) (21,23,126).

There are several advantages of full-spectrum methods over wavelength-selection methods for NIR analysis. Full spectrum methods can perform better outlier sample detection than wavelength-selection methods, and can be used to identify unknown impurities in outlier samples. Use of all available wavelength

variables for analysis allows for a signal-averaging advantage over other methods that use only a few wavelength variables. Full spectrum methods also provide important qualitative information, such as the NIR absorbance peaks that correspond to the property of interest. The presence of large spectral regions with no absorbance bands can hinder the performance of full spectrum methods (127). However, NIR spectra seldom have regions of no absorption.

There are two types of full spectrum methods used in this work: exploratory data analysis methods, which determine patterns in the NIR spectra of different polymer samples, and calibration methods, which correlate NIR spectra to an important property of the polymers.

1.5.1 Exploratory Data Analysis

Although as many as 700 wavelength variables can be obtained for each NIR sample, many of these variables are correlated. Given a series of spectra of different samples, it is probable that only a few inherent trends in the spectra are displayed in the 700 variables. The major task of an exploratory data analysis method, such as Principal Components Analysis (PCA) (21,23,126), is to describe a set of spectra in terms of discrete factors which describe the few inherent variations in the spectra.

The matrix X is a m by n matrix containing the spectra of m samples at n wavelengths. If the NIR spectra in X have only f

inherent variations, **X** can be reduced to a product of two matrices, according to the PCA model:

$$\mathbf{X} = \mathbf{T}\mathbf{P}^t + \mathbf{E} \qquad (1.7)$$

where **T** is a m by f matrix of PCA scores, **P** is a n by f matrix of PCA loadings, and **E** contains the spectral variation not explained by the PCA model. Given the response matrix **X**, the PCA scores (**T**) and loadings (**P**) are determined by an iterative procedure.

The appropriate number of principal components for consideration in the data analysis (f), which equals the number of inherent variations in the spectra, can be determined by cross-validation (126). The cross-validation procedure involves the extraction of the spectra of some samples in the original data set (**X**) and the construction of PCA models with different numbers of principal components from the remaining samples. The ability of each of the models to describe the spectra of the extracted samples is then determined. The optimal number of factors (f) is the number of factors at which addition of another factor does not significantly improve the prediction ability of the PCA model.

Each principal component in the PCA model has a loading spectrum and corresponding score vector. The k^{th} principal component loading spectrum is obtained from the k^{th} column in the **P** matrix, and the k^{th} principal component scores are in the k^{th} column of the **T** matrix (Equation 1.7). The loading spectrum of a

principal component indicates the NIR absorbance bands that are used to describe that principal component of variation in the spectra. The score vector of a principal component indicates the relationship between different samples, with respect to that principal component. A two-dimensional PCA scores plot shows the scores of one principal component plotted against the scores of another principal component for each sample. Two-dimensional scores plots can be used to enable better discrimination between samples in the analysis.

A hypothetical example of PCA applied to NIR spectroscopy is shown in Figure 1.9. In this example, only two principal components of variation are found in the spectra of 8 samples. The first principal component loading spectrum has positive bands that correspond to water bands. The second principal component loading spectrum has positive methylene bands, which (for the sake of argument) are absorbances from fat in the samples. It should be noted that the two principal components have been rotated (see Equation 1.8) for clarity; in most situations, the principal components would not correspond exclusively to a single property (as they do in this case) These results indicate that the first principal component describes the variation in the water content of the samples, and the second principal component describes the variation in the fat content of the samples. The two-dimensional scores plot indicates that sample A, B and C have lower first principal component scores than samples D and E. Therefore, it can be concluded that samples D and E have more moisture than samples A, B and C. Similar reasoning reveals

Figure 1.9: An example of results obtained from Principal Components Analysis of NIR spectra. NOTE: the two principal components have been rotated for clarity; the loading spectra in this figure would not be obtained in a real Principal Components Analysis procedure.

Principal Component Loadings

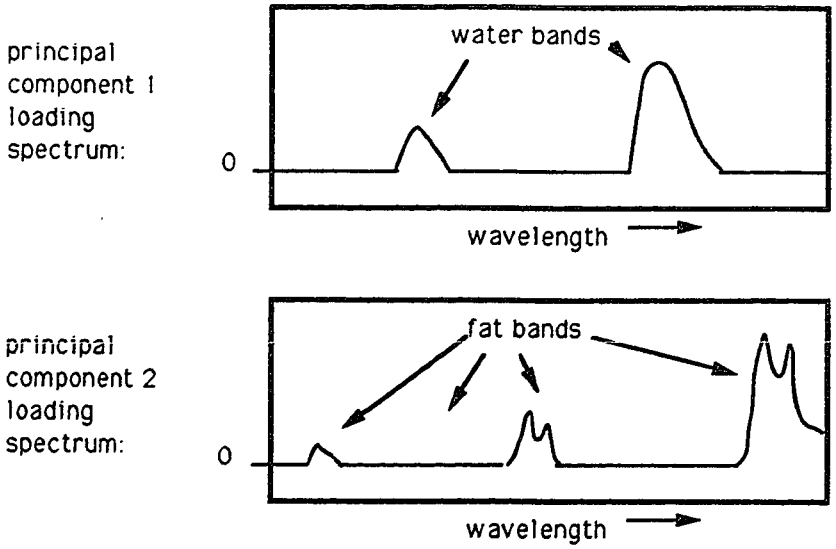

Principal Component Scores

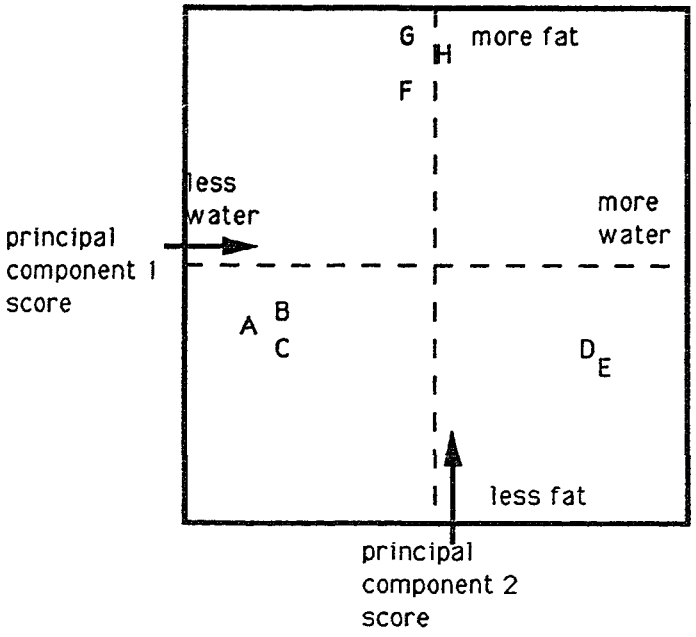

that samples F, G and H have greater fat content than the other samples. It is clear from this example that knowledge of the positions of characteristic NIR bands (for moisture and fat) is necessary to interpret PCA loading spectra. In addition, interpretation of two-dimensional scores plots can be aided by information that is known about the samples used in the analysis. For example, if the three sample groups in the scores plot (A, B and C; D and E; and F, G and H) correspond to three different sample classes, specific information about the moisture and fat contents of the three sample classes can be obtained.

In many cases, there are known variations in the samples used for PCA analysis. In the above example, each principal component corresponds to a single chemical phenomenon of the samples. In this case, this PCA results are easily interpreted. In other cases, the PCA procedure might produce principal components that are each influenced by several of the known variables of the samples. Fortunately, principal components rotation can be used to cause each principal component to correspond to a single known variable. Any two principal component loadings ($\mathbf{P}_2$) can be orthogonally rotated according to

$$\mathbf{P}_2^* = \mathbf{P}_2 \cdot \begin{bmatrix} \cos\alpha & -\sin\alpha \\ \sin\alpha & \cos\alpha \end{bmatrix} \qquad (1.8)$$

where $\mathbf{P}_2^*$ contains the rotated loadings, and α is the rotation angle. The PCA scores corresponding to the new rotated loadings ($\mathbf{T}_2^*$) are then given by

$$\mathbf{T}_2^* = \mathbf{X}\mathbf{P}_2^* \qquad (1.9)$$

Different values of α are used until the two-dimensional scores plot (obtained from $\mathbf{T}_2^*$) indicates that the optimal rotation angle has been reached. In the NIR analysis of RIM polyurethanes (Chapter 7) (54), it is found that principal component rotation improves the interpretability of PCA results.

1.5.2 Calibration Methods

1.5.2.1 Classical Least Squares

A Classical Least Squares (CLS) calibration (19,24,25) can be constructed if all of the possible analytes in the calibration samples are known, all spectra are corrected for multiplicative and baseline offset effects, and there are no spectral effects of interactions between analytes in the samples. The CLS model is given by

$$\mathbf{X} = \mathbf{C}\mathbf{K}^t + \mathbf{E} \qquad (1.10)$$

where **K** is a n by p matrix containing the spectra of each of the pure p analytes, **C** is a m by p matrix containing the concentrations of the p analytes in the n samples, and **X** and **E** are defined as before. CLS calibration is done by calculating the least-squares estimate of **K** ($\widehat{\mathbf{K}}$) according to

$$\widehat{\mathbf{K}} = \mathbf{X}^t\mathbf{C}(\mathbf{C}^t\mathbf{C})^{-1}. \qquad (1.11)$$

The estimated pure analyte spectra (in $\widehat{\mathbf{K}}$) are the spectra of each analyte as it exists in the calibration samples. These spectra can be used to determine the structure or interactions of analyte molecules in the samples.

The analyte concentrations of a future sample ($\hat{\mathbf{c}}_p$) are determined by curve-fitting the estimated pure analyte spectra ($\widehat{\mathbf{K}}$) to the spectrum of the future sample ($\mathbf{x}_p$) by means of

$$\hat{\mathbf{c}}_p = \mathbf{x}_p\widehat{\mathbf{K}}(\widehat{\mathbf{K}}^t\widehat{\mathbf{K}})^{-1}. \qquad (1.12)$$

A constant baseline spectrum can be fitted along with the pure analyte spectra during the prediction step (Equation 1.12), in order to correct for baseline offset effects in the prediction spectrum. If all absorbances in the spectrum are linear, the relative magnitudes of the predicted concentrations (in $\hat{\mathbf{c}}_p$) are independent of the multiplicative magnitude of the prediction spectrum (25). As a

result, accurate predictions can be obtained from spectra with unknown additive and multiplicative effects.

The advantages of the CLS method are the qualitative usefulness of estimated pure analyte spectra and the ability of calibrations to predict analyte concentrations from spectra with additive and multiplicative effects. The disadvantages of the CLS method are the difficult requirements for calibration, and the inability to account for interactions between analytes or the presence of unknown analytes in the samples.

1.5.2.2 Partial Least Squares

In contrast to the CLS method, the Partial Least Squares (PLS) method (19-23) involves separate models for the spectral responses and the property of calibration. The PLS calibration models are given by the equations

$$\mathbf{X} = \mathbf{T}\mathbf{P}^t + \mathbf{E}, \quad \text{(spectrum model)} \qquad (1.13)$$

$$\mathbf{y} = \mathbf{T}\mathbf{q} + \mathbf{f}, \quad \text{(property model)}, \qquad (1.14)$$

where $\mathbf{y}$ is a m by 1 vector containing the values of the property of interest for the m calibration samples, $\mathbf{q}$ is a f by 1 vector, $\mathbf{f}$ is the residual for the property model, and $\mathbf{X}$, $\mathbf{T}$, $\mathbf{P}$ and $\mathbf{E}$ are defined as before. Equation 1.13 is the calibration model for the spectral data,

and Equation 1.14 is the calibration model for the property data. The PLS calibration algorithm determines **T**, **P** and **q** such that the maximum variation in **y** is explained, and the maximum variation in **X** that is correlated to **y** is explained. The resulting calibration model relates the spectral absorbances (**X**) to the property data (**y**).

The PLS method can provide important qualitative information about the property of interest. The first PLS loading spectrum, obtained from the first column of the matrix **P** in Equation 1.13, indicates the NIR spectral features that are positively and negatively correlated to the property of interest. If the property of interest is a physical property, a correlation of the property to specific compositional and structural features can be obtained. The PLS regression coefficient spectrum, which can be multiplied by the spectrum of an unknown sample to obtain an estimate of the property, can also be used for qualitative analysis. However, this spectrum is strongly affected by the presence of spectral interferents, and must be interpreted with caution. As a result, the first PLS loading spectrum provides better qualitative information than the PLS regression coefficient spectrum.

The determination of the property of a prediction sample is done by calculation of the sample's scores (T) from the spectrum (using the spectral model, Equation 1.13), and subsequent calculation of the sample's property from the scores (using the property model, Equation 1.14). Details of PLS calibration and prediction procedures are given in references 20, 21 and 22.

The PLS method requires no assumption about the relationship between NIR absorbances and the property of interest. As a result, PLS can be used when unknown spectral interferences or analyte interaction effects are present. In addition, the PLS method can be used to calibrate NIR spectra directly to physical properties, which have unclear or complicated relationships to spectral absorbance. Although the PLS method cannot account for multiplicative effects in prediction spectra, these effects can be reduced by data pre-treatment methods (Chapter 1.2.5, Appendix B). However, in a situation where both CLS and PLS methods can be used, the qualitative information obtained from the CLS method (the estimated pure analyte spectra) is more interpretable than the qualitative information obtained from the PLS method (the first PLS loading spectrum or PLS regression coefficient spectrum).

1.5.2.3 Calibration Procedures

1.5.2.3.1 Cross Validation

The cross-validation procedure is used to determine the optimal number of factors (*f*) for a PLS calibration (22). The use of too few factors results in an insufficient calibration model. However, the use of too many factors results in overfitting of the calibration. Each cross-validation procedure involves the extraction of some samples from the set of samples used for calibration, and the

construction of PLS calibration models with different numbers of factors from the remaining samples. The properties of the extracted samples are then predicted from the different calibration models. A predicted residual error sum of squares (PRESS) value is obtained from each calibration model with use of the definition

$$PRESS_j = \sum_{i=1}^{NCV} (c_i - \hat{c}_{i,cv,j})^2 \qquad (1.15)$$

where c_i is the known property of sample i, $\hat{c}_{i,cv,j}$ is the property of sample i predicted by the model that excludes sample i, NCV is the number of extracted samples, and j indicates the number of factors in the PLS model. After predictions from all the different PLS models are made, the PRESS value can be plotted against the number of factors in the PLS calibration model (j). The optimal number of factors is the number at which the addition of another factor to the calibration model does not significantly lower the PRESS value. Results from several cross-validation analyses can be used to obtain a more confident estimate of the optimal number of factors. At this point, a PLS calibration with the appropriate number of factors can be constructed from the calibration samples.

1.5.2.3.2 Calibration/Prediction Analysis:

Most quantitative studies in this work involve the construction of a calibration model from a set of samples with known properties, and subsequent use of this model to predict the properties of a different set of samples with known properties. Results from this procedure are then used to determine calibration error and prediction error. The statistic used to describe calibration error is the Standard Error of Estimate (SEE), as defined by

$$SEE = \sqrt{\frac{\sum_{i=1}^{NC} (\hat{c}_{i,c} - c_i)^2}{(NC - 1)}} \qquad (1.16)$$

where $\hat{c}_{i,c}$ is the property of calibration sample i that is estimated from the calibration model that uses all calibration samples, and NC is the number of calibration samples. The Standard Error of Prediction (SEP) is a measure of prediction error:

$$SEP = \sqrt{\frac{\sum_{i=1}^{NP} (\hat{c}_{i,p} - c_{i,p})^2}{(NP)}} \qquad (1.17)$$

where $\hat{c}_{i,p}$ is the property of prediction sample i predicted from the calibration model, $c_{i,p}$ is the known property of prediction sample i,

and NP is the number of prediction samples. The SEP value is the best indicator of the ability of NIR spectra to predict the property of interest.

If there are not enough samples available to construct separate calibration and prediction sets, prediction error can be estimated from "leave-one-out" cross-validation. This prodecure involves N cross-validations, where N is the total number of samples in the analysis. Each cross-validation involves three steps: 1) extraction of one sample from the data set, 2) construction of a PLS model from the remaining samples, and 3) prediction of the property of the extracted sample by the model. A cross-validated SEP (SEP_{cv}) value can be calculated from

$$SEP_{cv} = \sqrt{\frac{\sum_{i=1}^{N} (c_i - \hat{c}_{i,cv})^2}{N-1}} . \qquad (1.18)$$

Here, $\hat{c}_{i,cv}$ is the property of sample i predicted by a PLS model that excludes sample i, c_i is the known property of sample i and N is the total number of samples in the analysis.

1.5.2.3.3 Spectral Residual of Prediction

The spectral residual of prediction is the variation in the spectrum of a prediction sample that is not explained by the

calibration model (21). For the CLS method, the residual spectrum of a prediction sample (e_p) is obtained from

$$e_p = x_p - \hat{K}\hat{c}_p \qquad (1.19)$$

where $\hat{K}$ is determined from Equation 1.11, and $\hat{c}_p$ is determined from Equation 1.12. The residual spectrum for the PLS method is obtained in a similar manner (from the PLS spectrum model, Equation 1.12). If the intensities in the residual spectrum are much larger than the spectral noise level, the sample might be an outlier. In addition, the residual spectrum might contain significant spectral features that identify impurities, spectral anomalies, or other unexpected spectral effects that cause the sample to be an outlier.

1.6 NIR Polymer Analysis, a Review

Several earlier analyses demonstrated the ability of NIR spectroscopy to determine several important properties of polymers. Composition determinations for ethylene-propylene copolymers (26) and polymer blends in food packaging (27) were made by NIR spectroscopy. Several NIR studies of molecular order in proteins and synthetic polymers were also done (29-32). NIR spectroscopy was also used to study the swelling of gelatin by water (28), and to monitor polymerization reactions (35,36). Hydrogen bonding in

polyamides (128), crystallinity in cellulose fibers (33), thermal history of nylon (34), geometrical isomerism in poly(butadiene) (38), hydroxyl groups in fatty acids (37), and terminal epoxide groups (39) were also determined by NIR spectroscopy. NIR molecular weight determinations were done for poly(butadiene) (41) and poly(ethylene glycols) (42).

There are several main departures of the work in this thesis from previous NIR polymer analysis work: 1) direct analysis of bulk polymers (past work has focused on the analysis of polymer solutions), 2) use of current NIR instrumentation, which yields higher-quality spectra than the instrumentation used in most previous work, 3) use of multivariate calibration methods, which enables the determination of properties that previously could not be determined by NIR spectroscopy, and 4) analysis of polymers that are currently relevant.

1.7 Notes to Chapter 1

(1) *Modern Plastics*, **1987**, *64(10A)*.

(2) Reisch, M.S., *Chem. and Eng. News*, **1989**, *67(36)*, 21.

(3) Koenig, J.L., *Chemical Microstructures of Polymer Chains*, Wiley: N.Y., 1980.

(4) Zbinden, R., *Infrared Spectroscopy of High Polymers*, Academic: N.Y., 1964.

(5) Zerbi, G., *Appl. Spectrosc. Rev.*, **1968**, *2*, 193.

(6) Ward, I.M., in *Advances in Polymer Science*, Springer-Verlag: Berlin, 1985.

(7) Drushel, H.V., *CRC Crit. Rev. in Anal. Chem.*, **1970**, *1*, 161.

(8) Bovey, F.A., *High Resolution NMR of Macromolecules*, Academic Press: N.Y., 1972.

(9) Wendlandt, W.W., *Thermal Analysis*, Wiley: N.Y., 1986.

(10) Yau, W.W., *Gel Permeation Chromatography*, Wiley-Interscience: N.Y., 1979.

(11) Hiemenz, P.C., *Polymer Chemistry*, Marcel Dekker: N.Y., 1984.

(12) Williams, P.C., Norris, K., *Near-infrared Technology in the Agricultural and Food Industries*, Williams, P, Norris, K., Eds., American Association of Cereal Chemists: St. Paul MN, 1987.

(13) Stark, E., Luchter, K., Margoshes, M., *Appl. Spectrosc. Rev.*, **1986**, *22(4)*, 335.

(14) Weyer, L.G., *Appl. Spectrosc. Rev.*, **1985**, *21*,1.

(15) Kaye, W., *Spectrochimica Acta*, **1954**, *6*, 257.

(16) Wetzel, D.L., *Anal. Chem.*, **1983**, *55(12)*, 1165A.

(17) Honigs, D.E., doctoral dissertation, Indiana University, Bloomington, IN, 1984.

(18) Mark, H., *Anal. Chem.*, **1986**, *58*, 2814.

(19) Beebe, K., Kowalski, B.R., *Anal. Chem.*, **1987**, *59*, 1007A.

(20) Geladi, P., Kowalski, B.R., *Anal. Chim. Acta*, **1986**, *185*, 1.

(21) Martens, H., Naes, T., in *Near-infrared Technology in the Agricultural and Food Industries*, American Association of Cereal Chemists: St. Paul MN, 1987, Chapter 4.

(22) Haaland, D.M., Thomas, E.V., *Anal. Chem.*, **1988**, *60*, 1202.

(23) Sharaf, M.A., Illman, D.L., Kowalski, B.R., *Chemometrics*, John Wiley and Sons: N.Y., 1986.

(24) Haaland, D.M., Easterling, R.G., Vopicka, D.A., *Appl. Spectrosc.*, **1985**, *39*, 73.

(25) Brown, C.W., Obremski, R.J., *Appl. Spectrosc. Rev.*, **1984**, *20*, 373.

(26) Bly, R.M., Kiener, P.E., Fries, B.A., *Anal. Chem.*, **1966**, *38*, 217.

(27) Davies, A.M.C., Grant, A., Gavrel, G.M., Steeper, R.V., *Analyst*, **1985**, *110*, 643.

(28) Ellis, J.W., Bath, J., *J. Chem. Phys.*, **1938**, *6*, 723.

(29) Glatt, L., Ellis, J.W., *J. Chem. Phys.*, **1951**, *19*, 459.

(30) Glatt, L., Webber, D.S., Seaman, C., Ellis, J.W., *J. Chem. Phys.*, **1950**, *18*, 413.

(31) Ambrose, E.J., Elliot, A., *Proc. Roy. Soc. (London)*, **1951**, *208A*, 75.

(32) Elliot, E., *Proc. Roy. Soc. (London)*, **1951**, *211A*, 490.

(33) Basch, A., Wasserman, J., Lewin, M., *J. Poly. Sci*, **1974**, *12*, 1143.

(34) Ghosh, S., Rodgers, J.E., *Text. Res. J.*, **1985**, *55*, 556.

(35) Crandall, E.W., *J. Appl. Poly. Sci.*, **1975**, *19*, 897.

(36) Buback, M., Vogele, H., Winkels, H., *Makromol. Chem., Macromol. Symp.*, **1986**, *5*, 69.

(37) Holman, R.J., Edmondson, P.R., *Anal. Chem.*, **1956**, *28*, 1533.

(38) Goddu, R.F., *Anal. Chem.*, **1957**, *29*, 1790.

(39) Goddu, R.F., Delker, D.A., *Anal. Chem.*, **1958**, *30*, 2009.

(40) Evans, A., Hibbard, R.R., Powell, A.S., *Anal. Chem.*, **1951**, *23*, 1604.

(41) Durbetaki, A.J., Miles, C.M., *Anal. Chem.*, **1965**, *37*, 1231.

(42) LeFevre, R.J.W., Parkins, G.M., Roper, R., *Aust. J. Chem.*, **1959**, *13*, 169.

(43) Wilson, E.B., Decius, J.C., Cross, P.C., *Molecular Vibrations*, McGraw-Hill: N.Y., 1955.

(44) Colthup, N.B., Daly, L.H., Wiberly, S.E., *Introduction to Infrared and Raman Spectroscopy, 2nd edition*, Academic: N.Y., 1975.

(45) Sverdlov, L.M., Kovner, M.A., Krainov, E.P., *Vibrational Spectra of Polyatomic Molecules*, John Wiley and Sons: N.Y., 1974.

(46) Murray, I., Williams, P.C., in *Near-infrared Technology in the Agricultural and Food Industries*, Williams, P, Norris, K., Eds.,

American Association of Cereal Chemists: St. Paul MN, 1987, Chapter 2.

(47) Pimental, G., McClellan, A.L., *The Hydrogen Bond*, W.H. Freeman: San Fransisco, 1960.

(48) Schuster, P., Zundel, G., Sandorfy, C., *The Hydrogen Bond, II. Structure and Spectroscopy*, North-Holland: Amsterdam, 1976.

(49) Lee, H.S., Hsu, S.L., *Macromolecules*, **1989**, *22*, 1100.

(50) Pollack, S.K., Shen, D.Y., Hsu, S.L., Wang, Q., Stidham, H.D., *Macromolecules*, **1989**, *22*, 551.

(51) Davies, A.M.C., Miller, C.E., *Appl. Spectrosc.*, **1988**, *42*, 703.

(52) Miller, C.E., Honigs, D.E., *Spectroscopy*, **1989**, *4*, 44.

(53) Miller, C.E., Edelman, P.G., Ratner, B.D., Eichinger, B.E., "Near-infrared Spectroscopic Analysis of Polyether(urethaneurea) Block Copolymers, II. Phase Separation", *Appl. Spectrosc.*, **1990**, in press.

(54) Miller, C.E., "Analysis of Reaction-Injection-Molded Polyurethanes by NIR Diffuse Reflectance Spectroscopy", unpublished work, 1989.

(55) Miller, C.E., Edelman, P.G., Ratner, B.D., "Near-infrared Spectroscopic Analysis of Polyether(urethaneurea) Block Copolymers, I. Bulk Composition", *Appl. Spectrosc.*, **1990**, in press.

(56) Miller, C.E., Eichinger, B.E., "Determination of Crystallinity and Morphology of Fibrous and Bulk Poly(ethylene terephthalate) by NIR Diffuse Reflectance Spectroscopy", *Appl. Spectrosc.*, **1990**, in press.

(57) Davies, A.M.C, Rutland, S.G., *Spectrochim. Acta*, **1988**, *45A*, 1143.

(58) Miller, C.E., *Appl. Spectrosc.*, **1989**, *43(8)*, 1435.

(59) Miller, C.E., Eichinger, B.E., Gurley, T.W., Hermiller, J.G., "Determination of Microstructure and Composition of Butadiene and Styrene-butadiene polymers by NIR Spectroscopy", *Anal. Chem.*, submitted 1989.

(60) Geladi, P., MacDougall, D., Martens, H., *Appl. Spectrosc.*, **1985**, *39*, 491.

(61) Ilari, J.L., Martens, H., Isaksson, T., *Appl. Spectrosc.*, **1988**, *42*, 722.

(62) Miller, C.E., Naes, T., "A Path Length Correction Method for Near-infrared Spectroscopy", *Appl. Spectrosc.*, submitted 1989.

(63) Birth, G.S., Hecht, H.G., in *Near-infrared Technology in the Agricultural and Food Industries*, Williams, P, Norris, K., Eds., American Association of Cereal Chemists: St. Paul MN, 1987, Chapter 1.

(64) Hecht, H.G., in *Modern Aspects of Reflectance Spectroscopy, Symposium Proceedings*, Plenum Press: N.Y., 1968, pp. 1-26.

(65) Kortum, G., *Reflectance Spectroscopy*, Springer-Verlag: N.Y., 1969.

(66) Kortum, G., Braun, W., Herzog, G., *Angew. Chem.*, **1963**, *2(7)*, 333.

(67) Kubelka, P., Munk, F., *Z. Tech. Phys.*, **1931**, *12*, 593.

(68) Honigs, D.E., *Anal. Instr.*, **1985**, *16*, 1.

(69) Miller, C.E., Eichinger, B.E., "Determination of Compression and Thermal Properties of Rigid Polyurethane Foams by NIR Diffuse Reflectance Spectroscopy", *Appl. Spectrosc.*, submitted 1989.

(70) Tenge, B.J., doctoral dissertation, University of Washington, Seattle, WA, 1989.

(71) Brimmer, P.J., doctoral dissertation, University of California, Riverside, 1987.

(72) McClure, W.F., in *Near-infrared Technology in the Agricultural and Food Industries*, Williams, P, Norris, K., Eds., American Association of Cereal Chemists: St. Paul MN, 1987, Chapter 5.

(73) Archibald, D.D., Miller, C.E., Lin, L.T., Honigs, D.E., *Appl Spectrosc.*, **1988**, *42(8)*, 1549.

(74) Buchanan, B.R., doctoral dissertation, University of Washington, Seattle WA, 1987.

(75) Weidner, V.R., Barnes, P.Y., Eckerle, K.L., *NBS Journal of Research*, **1986**, in press

(76) Flory, P.J., *Principles of Polymer Chemistry*, Cornell Univ. Press: Ithaca NY, 1953.

(77) Morton, M., *Rubber Technology*, Robert E. Kreiger Co.: Malabar FL, 1981.

(78) Odian, G., *Principles of Polymerization, 2nd edition*, Wiley and Sons: N.Y., 1970.

(79) Alaki, Y., Yoshimoto, T., Dnanari, M., Takenchi, M., *Rubber Chem. and Technol.*, **1973**, *46*, 350.

(80) Claque, A.D.H., vanBroekhoven, J.A.M., Blaavin, R.P., *Macromolecules*, **1974**, *7*, 348.

(81) Binder, J.L., *Anal. Chem.*, **1954**, *26*, 1877.

(82) Lin, S-B, Koenig, J.L., *J. Poly Sci, Poly. Phys. Ed.*, **1982**, *20*, 2277.

(83) Lin, S-B, Koenig, J.L., *J. Poly Sci, Poly. Phys. Ed.*, **1983**, *21*, 2365.

(84) Schmidt, P.G., *J. Poly. Sci., A*, **1963**, *1*, 1271.

(85) Mandelkern, L., *Crystallization of Polymers*, McGraw-Hill: N.Y., 1964.

(86) Farrow, G., Ward, I.M., *Polymer*, **1960**, *1*, 330.

(87) Gupta, V.B., Kumar, S., *J. Appl. Poly. Sci.*, **1981**, *26*, 1865.

(88) Groeninckx, G., Reynaers, H., Berghmans, H., Smets, G., *J. Poly. Sci., Poly Phys. Ed.*, **1980**, *18*, 1311.

(89) Ito, E., Yamamoto, K., Kobayashi, Y., Hatakeyama, T., *Polymer*, **1978**, *19*, 39.

(90) Ladd, M.F.C., Palmer, R.A., *Structure Determination by X-ray Diffraction*, Plenum Press: N.Y., 1977.

(91) Fischer, E.W., *Polymer J.*, **1985**, *17*, 397.

(92) Samuels, R.T., in *Structured Polymer Properties*, Wiley-Interscience: N.Y., 1974.

(93) Zachmann, H.G., *Poly. Eng. and Sci.*, **1979**, *19*, 966.

(94) Liu, L.B., Sumita, M., Miysaka, K., *Macromolecules*, **1988**, *21*, 3424.

(95) Yoon, S.C., Ratner, B.D., *Macromolecules*, **1986**, *19*, 1068.

(96) Sung, C.S.P., Hu, C.B., Wu, C.S., *Macromolecules*, **1980**, *13*, 111.

(97) Sung, C.S.P., Smith, T.W., Sung, N.H., *Macromolecules*, **1980**, *13*, 117.

(98) Chen, Z.S., Yang, W.P., Mackosko, C.W., *Rubber Chem. and Tech.*, **1988**, *61*, 86.

(99) Yoon, S.C., Ratner, B.D., *Macromolecules*, **1988**, *21*, 2392.

(100) Yoon, S.C., Ratner, B.D., *Macromolecules*, **1988**, *21*, 2401.

(101) Blackwell, J., Lee, C.P., *J. Poly. Sci., Poly. Phys. Ed.*, **1984**, *22*, 759.

(102) Blackwell, J., Nagarajan, M.R., *Polymer*, **1981**, *22*, 202.

(103) Lee, H.S., Wang, Y.K., MacKnight, W.J., Hsu, S.L., *Macromolecules*, **1988**, *21*, 270.

(104) Yin, T-K, Eichinger, B.E., Aksay, I.A., "Lubricating Polymers for Powder Compaction" in *Proceedings of First International Conference on Ceramic Powder Processing Science*, Orlando FL, 1987.

(105) Fontana, B.J., Thomas, J.R., *J. Phys. Chem.*, **1961**, *65*, 480.

(106) Calvert, P.D., Tormey, E.S., Pober, R.L., *Am. Ceram. Soc. Bull.*, **1986**, *65*, 669.

(107) Korn, M., Killmann, E., Eisenlauer, J., *J. Colloid and Interface Sci.*, **1980**, *76*, 7.

(108) Porter, M.D., *Anal. Chem.*, **1988**, *60*, 1143A.

(109) Mark, J.E., Erman, B., *Rubberlke Elasticity, A Molecular Primer*, John Wiley and Sons: N.Y., 1988.

(110) ASTM Method D790-86, *1989 Annual Book of ASTM Standards*, ASTM: Philadelphia PA, **1989**, volume *08.01*, p.280.

(111) ASTM Method D1621-73, *1989 Annual Book of ASTM Standards*, ASTM: Philadelphia PA, **1989**, volume *08.02*, p.11.

(112) Smith, S.A., Galbraith, C.J., Cartmell, M.J., Moore, M.L., Brown, R.K., *Polyurethanes World Congress*, **1987**, *Sept. 29 to Oct. 2*, 1987, 74.

(113) ASTM Method C518-85,*1988 Annual Book of ASTM Standards*, ASTM: Philadelphia PA, **1988**, volume *04.06*, p.151.

(114) ASTM Method D3769-85, *1989 Annual Book of ASTM Standards*, ASTM: Philadelphia PA, **1989**, volume *09.02*, p.370.

(115) Seymour, R.B., Carraher, C.E., *Structure-Property Relationships in Polymers*, Plenum Press: N.Y., 1984.

(116) Macosko, C.W., *RIM, Fundamentals of Reaction Injection Molding*, Hanser: Munich, 1989.

(117) Blackwell, J., Quay, J.R., Turner, R.B., *Poly. Eng. and Sci.*, **1983**, *23*, 816.

(118) Camargo, R.E., Macosko, C.W., Tirrell, M.V., Wellinghoff, S.T., *Polymer*, **1985**, *26*, 1145.

(119) Camargo, R.E., Macosko, C.W., Tirrell, M.V., Wellinghoff, S.T., *Poly. Eng. and Sci.*, **1982**, *22*, 719

(120) Yang, W.P., Macosko, C.W., *Makromol. Chem., Macromol. Symp.*, **1989**, *25*, 23.

(121) Saunders, J.H., Frisch, K.C., *Polyurethanes, Chemistry and Technology, Part I: Chemistry*, Wiley-Interscience: N.Y., 1962.

(122) Camargo, R.E., private communication, 1989.

(123) Macosko, C.W., *Plast. Eng.*, **1983**, *39(4)*, 21.

(124) Martens, H., Naes, T., *Trends Anal. Chem.*, **1984**, *3(8)*, 204.

(125) Hruschka, W.R., in *Near-infrared Technology in the Agricultural and Food Industries*, Williams, P, Norris, K., Eds., American Association of Cereal Chemists: St. Paul MN, 1987, Chapter 3.

(126) Jolliffe, I.T., *Principal Components Analysis*, Springer-Verlag: New York, 1986.

(127) Seasholtz, M.B., Archibald, D.D., Lorber, A., Kowalski, B.R., *Appl. Spectrosc.*, **1989**, *43*, 1067.

(128) Cannon, C.G., *Mikrochim. Acta*, **1955**, *2-3*, 555.

Chapter 2

Near-infrared Diffuse Reflectance Analysis of Poly(octadecyl methacrylate) Adsorbed on Alumina

2.1 Introduction to Chapter 2

The coating of refractory powders by methacrylate polymers has beneficial effects on the processing of ceramic precursors (1). The mass of adsorbed polymer, the amount of surface covered with polymer, the thickness of the polymer coating, and the configuration of the polymer at the surface are important properties that can potentially affect the quality of a ceramic product.

Methacrylate polymers adsorb to refractory surfaces through hydrogen-bonding between carbonyl groups of the polymer and hydroxyl groups of the surface (2). It has been shown (2-4) that mid-infrared spectroscopy can successfully characterize hydrogen-bonding processes. Frequency and intensity changes in polymer carbonyl stretching bands in IR spectra resulting from polymer adsorption have been used to investigate the effects of adsorption on the polymer. Likewise, changes in surface hydroxyl stretching bands in IR spectra resulting from polymer adsorption have been used to investigate the effects of adsorption on the surface.

Near-infrared (NIR) diffuse reflectance spectroscopy (5,6) can also be used for the analysis of polymer-coated refractories. Coated particle specimens usually require substantial preparation for IR

spectroscopy, but require little or no preparation for NIR spectroscopy. However, because near-infrared spectra are dominated by absorbance bands from O-H, C-H, and N-H bonds in the specimen, NIR spectroscopy is generally applicable only to the analysis of surface hydroxyl groups and C-H, N-H, and O-H bonds in the polymer.

NIR spectroscopy usually provides better information about hydrogen-bonding states of hydroxyl groups than IR spectroscopy. Absorptivities of free hydroxyl bands in near-infrared spectra are generally higher than the absorptivities for hydrogen-bonded hydroxyl bands (7,8). As a result, a better discrimination between free and hydrogen-bonded hydroxyl groups can be made using NIR spectra. Earlier, near-infrared analyses of cellulose (9), sucrose (10), and nylon (11) demonstrated the ability of NIR spectroscopy to determine relative amounts of different hydrogen-bonded states of O-H and N-H groups. In this work, the ability of NIR spectroscopy to study the adsorption of poly[octadecyl methacrylate] (POMA) on alumina is considered.

2.2 Experimental

Alumina particles (AKP-30, 0.4 μm, Sumitomo) were placed in a 1.04 mg/ml solution of POMA (Polysciences, Inc.) in heptane. After stirring for 24 hours, the excess solution was decanted, and the

particles were rinsed twice with the solvent. The coated particles were then air-dried for 48 hours.

Near-infrared reflectance spectra of uncoated alumina, coated alumina, and pure POMA were obtained with a Technicon InfraAlyzer 500C near-infrared reflectance instrument with a tungsten filament lamp and a lead sulfide detector. See Chapter 1.2.4.2 for details of instrumentation. A reflectance sampling cell (12) was used to introduce the powder specimens to the reflectance spectrometer. The pure POMA was analyzed as a thin film on a ceramic disk. Each scan covered a spectral range of 1100 to 2500 nm, and each scan required about 2 minutes.

2.3 Results

The hydroxyl groups on the alumina surface can assume three possible states (see Figure 2.1): free (I), self-associated (II), and associated with polymer (III). For the uncoated alumina, only states I and II are present. As the polymer adsorbs to the alumina, hydroxyl groups in state I convert to state III. It is also possible that some hydroxyls in state II convert to state III during adsorption.

Near-infrared reflectance spectra of pure POMA, uncoated alumina, and POMA-coated alumina are shown in Figure 2.2, A, B, and C. The polymer spectrum has absorption bands at 1212, 1395, 1728, 1761, 2309, and 2349 nm which result from methyl and

Figure 2.1: Simplified diagram of three possible states for surface hydroxyl groups: free (**I**), self-associated (**II**), and associated with polymer (**III**).

I

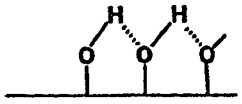

II

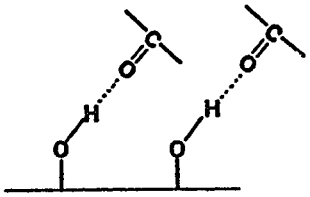

III

Figure 2.2: Near-infrared reflectance spectra of pure POMA (A), uncoated alumina (B), POMA-coated alumina (C), and "ideal" POMA-coated alumina spectrum (D). All four spectra are offset for clarity. Wavelengths (in nanometers) referred to in text are labeled.

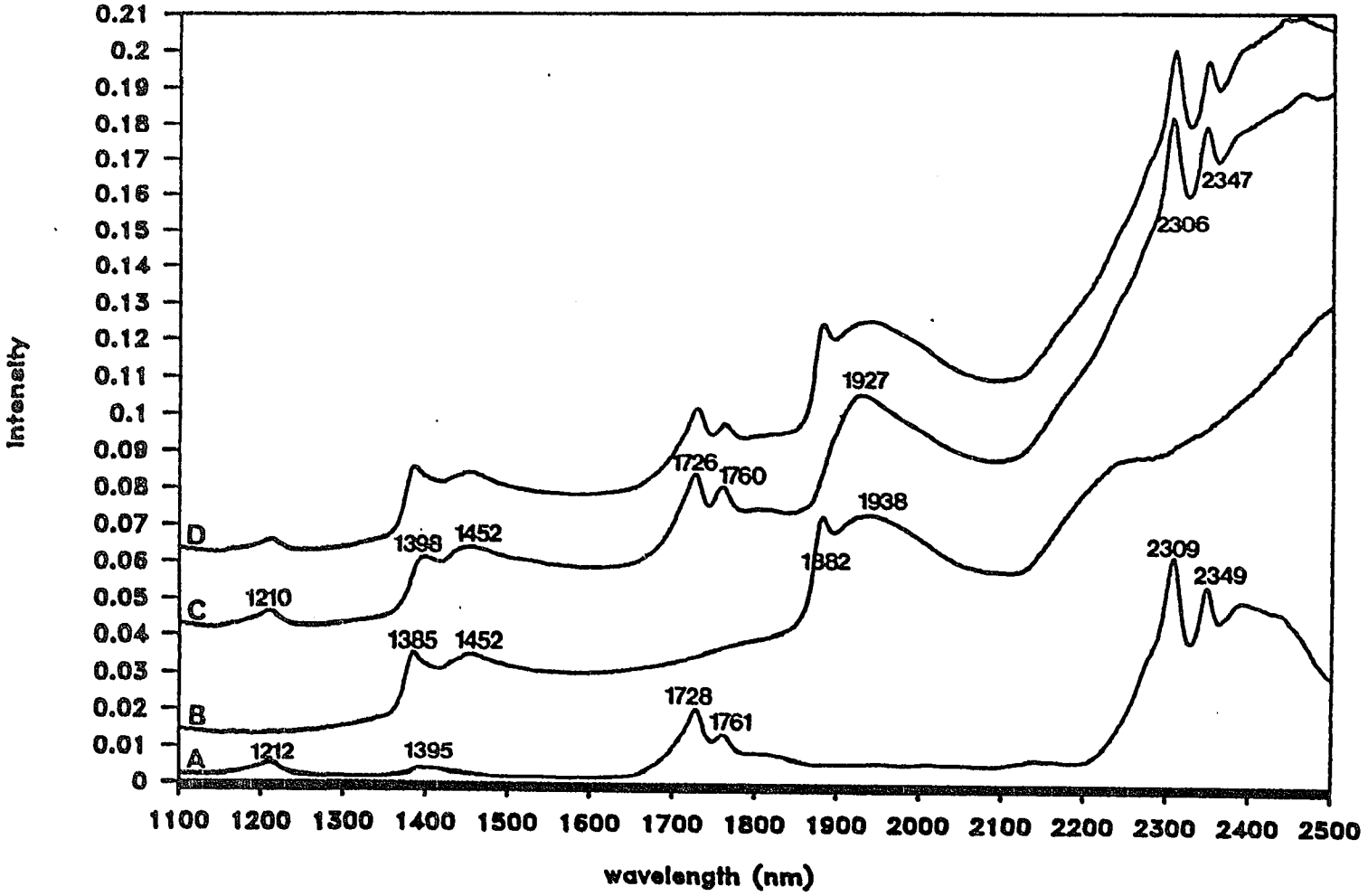
0.21
0.2
0.19
0.18
0.17
0.16
0.15
0.14
0.13
0.12
0.11
0.1
0.09
0.08
0.07
0.06
0.05
0.04
0.03
0.02
0.01
0
Intensity
D
C
B
A
1726
1760
1927
2347
2306
1398
1452
1938
1882
2309
2349
1210
1385
1452
1728
1761
1212
1395
1100 1200 1300 1400 1500 1600 1700 1800 1900 2000 2100 2200 2300 2400 2500
wavelength (nm)

methylene groups in the polymer. The spectrum of the uncoated alumina shows sharp bands at 1385 nm and 1882 nm from free surface hydroxyl groups (Figure 2.1(**I**)), and broader bands centered at 1452 nm and 1938 nm from self-associated sufrace hydroxyl groups (Figure 2.1(**II**)). The free hydroxyl bands are well-resolved from the broader self-associated hydroxyl bands.

In the POMA-coated alumina spectrum (Figure 2.2(**C**)), the bands from methylene groups on the pendant octadecyl chains in the polymer, observed at 1210, 1726, 1760, 2306, and 2347 nm, are each shifted to slightly shorter wavelength than the bands in the pure polymer spectrum. In addition, the free O-H bands at 1385 nm and 1882 nm are absent as a result of conversion of surface hydroxyl groups from state **I** to state **III**.

To further investigate the near-infrared spectral shifts associated with adsorption, an "ideal" POMA-coated alumina spectrum was constructed from the pure alumina and pure POMA spectra (Figure 2.2(**D**)). The weights of the two pure spectra used to construct the "ideal" spectrum were determined by least-squares curve-fitting the pure component spectra to the coated alumina spectrum (excluding the spectral regions with surface hydroxyl bands). The difference of the "ideal" POMA-coated alumina spectrum and the real POMA-coated alumina spectrum is shown in Figure 2.3. Sharp negative peaks at 1382 nm and 1879 nm indicate depletion of free surface hydroxyl groups, and a weak positive peak at 1927 nm indicates production of polymer-bound hydroxyl groups (Figure

Figure 2.3: Subtraction of the "ideal" POMA-coated alumina spectrum (Figure 2.2, D) from the real POMA-coated alumina spectrum (Figure 2.2, C). Wavelengths referred to in the text are labeled.

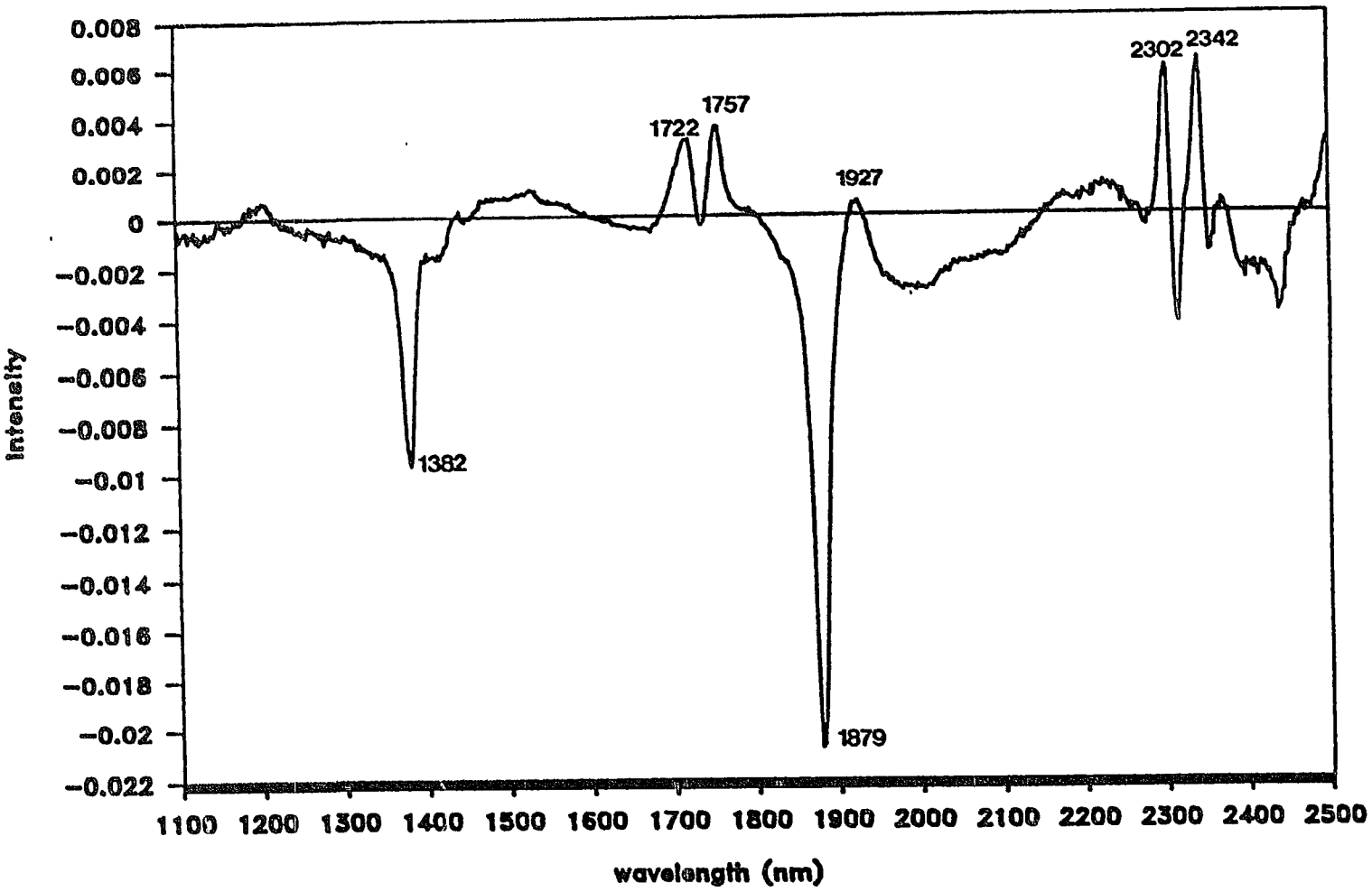
0.008
0.006
0.004
0.002
0
−0.002
−0.004
−0.006
−0.008
−0.01
−0.012
−0.014
−0.016
−0.018
−0.02
−0.022
Intensity
1382
1722
1757
1927
1879
2302
2342
1100 1200 1300 1400 1500 1600 1700 1800 1900 2000 2100 2200 2300 2400 2500
wavelength (nm)

2.1(III)) upon adsorption. In addition, peaks at 1722, 1757, 2302, and 2342 nm indicate that the bands from groups on the pendant octadecyl chains in the polymer shifted upon adsorption. These results suggest that polymer adsorption can be monitored by observation of small shifts of methyl and methylene polymer bands or disappearence of free surface hydroxyl bands in the near-infrared spectrum.

It is possible that self-associated hydroxyl groups (Figure 2.1(II)) were converted to polymer-bound hydroxyl groups (Figure 2.1(III)) during polymer adsorption. However, because the hydrogen bond acceptor strengths of hydroxyl and carbonyl groups are nearly equal (13), no major spectroscopic differences between the hydroxyl bands of states **II** and **III** are expected. IR spectral information about carbonyl band shifts is needed to determine the extent of conversion from state **II** to state **III**.

The shift of methylene bands to shorter wavelengths upon adsorption suggests that the structure of the pendant octadecyl chains in the bulk polymer and in the adsorbed polymer are different. An NIR study of ethylene-propylene-diene terpolymers (Chapter 3) (14) showed similar spectral shifts that probably resulted from decreased crystallinity of ethylene blocks in the terpolymer. Infrared and NMR investigations might provide specific information regarding the change in polymer chain conformation upon adsorption.

This analysis has demonstrated the ability of NIR spectroscopy to analyze polymer-coated refractories. Determination of relative amounts of the surface states **I, II,** and **III** is currently being investigated. NIR spectroscopy can be combined with IR spectroscopy to perform extensive and detailied investigations of similar adsorption processes.

2.4 Notes to Chapter 2

(1) Yin, T.K., Eichinger, B.E., Aksay, I.A., "Lubricating Polymers for Powder Compaction", in *Proceedings of First International Conference on Ceramic Powder Processing Science* (Orlando, FL, 1987).

(2) Fontana, B.J., Thomas, J.R., *J. Phys. Chem.*, **1961**, *65*, 480.

(3) Calvert, P.D., Tormey E.S., Pober, R.L., *Am. Ceram. Soc. Bull.*, **1986**, *65*, 669.

(4) Korn, M., Killmann E., Eisenlauer, J., *J. Colloid and Interface Sci.*, **1980**, *76*, 7.

(5) Stark, E., Luchter, K., Margoshes, M., *Appl. Spectrosc. Rev.*, **1986**, *22*, 335.

(6) Weyer, L.G., *Appl. Spectrosc. Rev.*, **1985**, *21*, 1.

(7) Pimental, G., McClellan, A.L., *The Hydrogen Bond*, W.H. Freeman and Co.: San Fransisco, 1960.

(8) Schuster, P., Zundel, G., Sandorfy, C.,*The Hydrogen Bond, II. Structure and Spectroscopy*, North-Holland Publishing Co.: Amsterdam, 1976.

(9) Basch, A., Wasserman T., Lewin, M., *J. Poly. Sci.*, **1974**, *12*, 1143.

(10) Davies, A.M.C., Miller, C.E., *Appl. Spectrosc.*, **1988**, *42*, 703.

(11) Ghosh, S., Rodgers, J.E., *Text. Res. J.*, **1985**, *55*, 556.

(12) Yeo, P., Honigs, D.E., *Appl. Spectrosc.*, **1988**, *42*, 1128.

(13) Kamlet, M.J., Abboud, J.M., Abraham, M.H., Taft, R.W., *J. Org. Chem.*, **1983**, *48*, 2877.

(14) Miller, C.E., *Appl. Spectrosc.*, **1989**, *43(8)*, 1435.

Chapter 3

Analysis of Ethylene-Propylene-Diene Terpolymers by NIR Spectroscopy

3.1 Introduction to Chapter 3

Ethylene-propylene-diene monomer rubbers (EPDMs) are used for many different applications, including automotive belts, hoses, and tires, non-automotive hoses, and electrical insulation. These terpolymers are mostly composed of ethylene and propylene units, but also contain diene functionalities in the polymer backbone that are used to make crosslinks. Earlier studies have shown that important physical properties such as modulus, relaxation, and thermal transitions are greatly influenced by the composition of these polymers (1,2).

Near-infrared (NIR) spectroscopy (3,4), which has been used to determine important properties of bulk agricultural materials, can also be used to analyze bulk EPDM terpolymers. Earlier NIR analyses of ethylene-propylene co-polymer films (5-7) demonstrated the ability of NIR spectroscopy to determine chemical composition. However, these calibrations used only one or two absorbance bands at user-chosen wavelengths. Furthermore, only the combination region was used for these analyses. Improvements in NIR instrumentation and multivariate data analysis made after the earlier analyses have provided abilities both to improve calibrations

and to use spectral regions other than the combination region for quantitative analysis.

In this work, near-infrared spectroscopy in the combination, first overtone, and second overtone region is combined with the multivariate methods of Classical Least Squares (CLS) (8,9) (Chapter 1.5.2.1) and Partial Least Squares (PLS) (8,10,11) (Chapter 1.5.2.2) to provide calibrations for chemical components in ethylene-propylene-diene monomer (EPDM) terpolymers. EPDM samples with 1,4-hexadiene (HD) and ethylidene norbornene (ENB) diene monomers were used for this study. Results indicate that the combination, first overtone, and second overtone regions of the spectrum can be used to determine ethylene and propylene concentrations in the terpolymers, and the combination region can be used to determine diene concentrations.

3.2 Experimental

Commercially available EPDMs were used in this analysis (labeled sample 1 to 14): samples 1 to 5 are Nitriflex EPDMs, samples 6 to 8 are Royalene EPDMs, and samples 9 to 14 are Nordel EPDMs. The diene unit used in the Nitriflex amd Royalene samples is 5-ethylidene bicyclo[2.2.1] hept-2-ene (or ethylidene norbornene, ENB), and the diene unit used in the Nordel samples was 1,4-hexadiene (HD). All samples were obtained as un-crosslinked polymers. Reference chemical composition values of the EPDM polymers were

obtained by FT-NMR spectroscopy of the samples dissolved in $CDCl_3$. The compositions of the samples ranged from 52 to 73.6% ethylene, 21.8 to 44% propylene, 0 to 8.1% ENB and 0 to 4.6% HD. Estimated errors in the NMR composition values are 2 % (mass) for ethylene and propylene, and 0.5 % (mass) for ENB and HD.

NIR spectra of the polymers were obtained using a Pacific Scientific 6250 Near-infrared grating spectrophotometer (Chapter 1.2.4.2). Each scan lasted about 30 seconds. Spectral data was saved on an IBM-AT microcomputer for later data processing. The polymers were sampled by NIR as solutions in CCl_4 and as bulk samples. For the bulk sampling, a thin piece of material (approximately 1 mm thick) was cut and placed in a reflectance sample cup with a ceramic background and a quartz window. Reflectance spectra were obtained by illuminating the sample with NIR light and collecting back-scattered light. Each sample was analyzed in duplicate, using two different pieces of the bulk sample.

EPDM solutions of approximately 5 % (w/v) were prepared by placing approximately 0.2 grams of polymer and 40 ml of CCl_4 (Aldrich) in an 80 ml vial. After 24 hours, several samples had significant gel fractions. As a result, each solution was homogenized (Helvitica homogenizer) for approximately 30 seconds to disperse the non-soluble portion of the polymer. The concentration of polymer in each solution was determined by pipetting 10 ml of the homogenized solution into a pre-weighed aluminum pan and weighing the pan again after solvent evaporation. The samples were then placed in a 4

mm thick quartz cuvette and analyzed by NIR transmission spectroscopy. The spectrum of pure CCl_4 solvent was then subtracted from each solution spectrum.

NIR reflectance spectra of high-density polyethylene (HD-PE) (Aldrich) and isotactic polypropylene (*ISO*-PP)(Aldrich) were obtained by placing the samples in a reflectance sampling cup with a quartz window. The HD-PE sample was obtained in pellet form, and had to be ground before NIR reflectance analysis.

Spectral data pre-treatment (Chapter 1.2.5) consisted of one or two data corrections. The bulk sample spectra were corrected with Multiplicative Scatter Correction (MSC) (12). Each solution spectrum was corrected by subtracting the absorbance value at 1100 nm from all other absorbance values, and dividing the resulting absorbance values by the concentration of polymer in the sample (in g/10 mL). For both rubber and solution spectra, second derivative correction (Pacific Scientific Co.) was sometimes used prior to subsequent correction methods.

The NIR spectra were split into three spectral regions: region 1 (1100 nm to 1350 nm), region 2 (1570 nm to 1850 nm) and region 3 (1950 nm to 2500 nm). Each region was used separately for multivariate analysis. A program developed by the Center for Process Analytical Chemistry (10) was used for PLS analyses, and a LOTUS-123 spreadsheet was used for CLS analyses. Mean-centered spectral data were used for all PLS analyses. The prediction ability

of CLS and PLS calibrations was estimated by a "leave-one-out" cross-validation procedure (Chapter 1.5.2.3.2, Equation 1.18).

3.3 Results and Discussion

3.3.1 NIR Spectra

NIR reflectance spectra of a high-ethylene and low-ethylene EPDM terpolymer in the bulk are shown in Figure 3.1. Regions of significant absorption are designated as region 1 (1100 nm to 1350 nm), region 2 (1570 nm to 1850 nm), and region 3 (1950 nm to 2500 nm). Although significant absorptions are found in the region 1350 nm to 1570 nm, instrumental anomalies in this region prevent its use for quantitative analysis. Regions 1,2, and 3 are used separately for multivariate analysis because they have different NIR sampling characteristics. Region 1 is dominated by 2nd overtone C-H stretching bands. The low absorptivity of these bands permits the use of this region for the sampling of thick films (up to several cm thick) and large pellets. Region 2 is dominated by 1st overtone C-H stretching bands, which have about an order of magnitude higher absorptivity than the bands in region 1. As a result, region 2 can be used for thinner films (about 0.5 to 2 mm thick) and dilute solutions. Region 3 contains C-H combination bands with much higher absorptivities than bands in regions 1 and 2. This region is appropriate for very thin films (less than 0.1 mm thick) and dilute

Figure 3.1: Near-infrared reflectance spectra of bulk EPDM sample 14 (A) and sample 2 (B). Region 1 is 1100 nm to 1350 nm, region 2 is 1570 nm to 1850 nm, and region 3 is 1950 nm to 2500 nm.

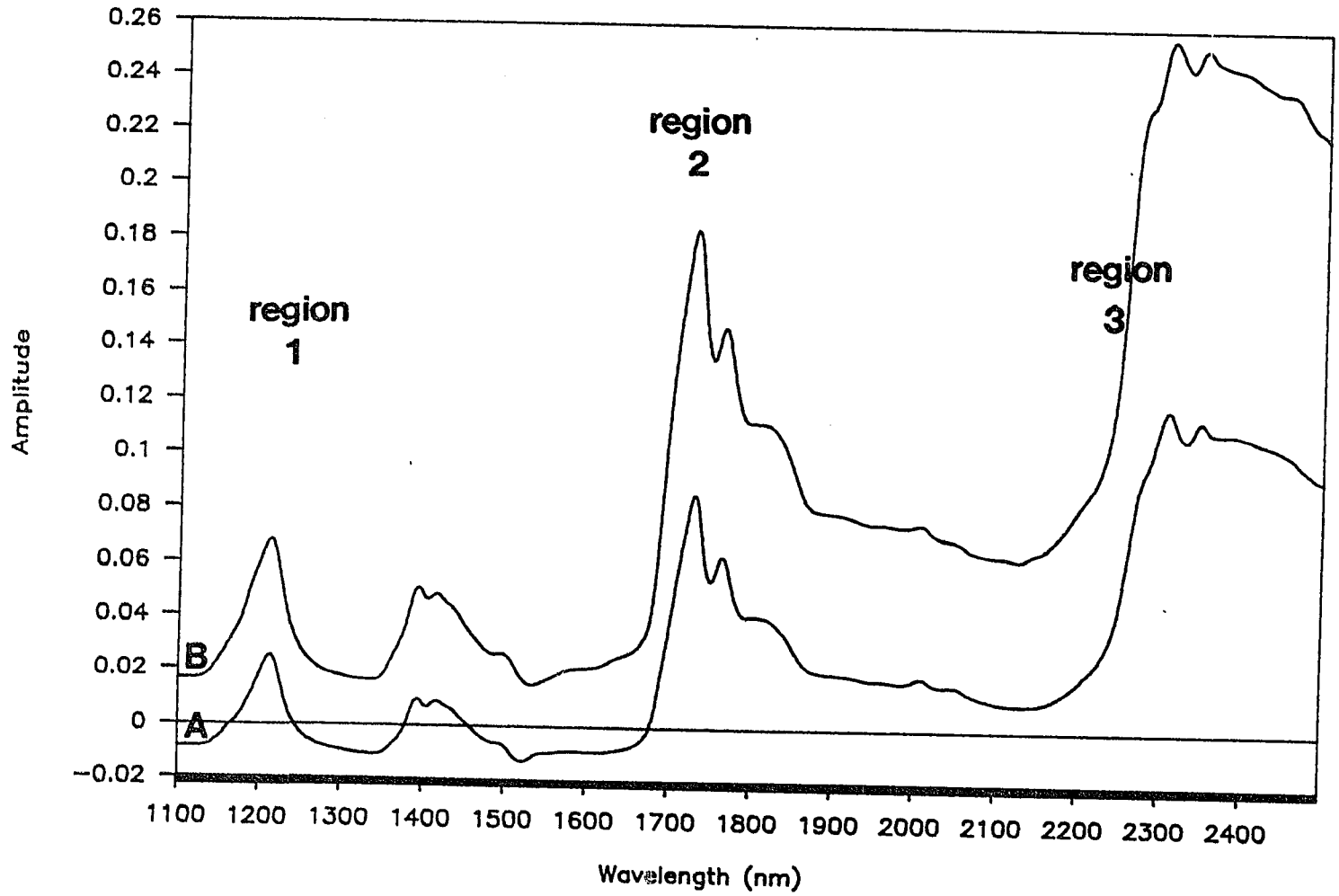
0.26
0.24
0.22
0.2
0.18
0.16
0.14
0.12
0.1
0.08
0.06
0.04
0.02
0
−0.02
Amplitude
region 1
region 2
region 3
B
A
1100 1200 1300 1400 1500 1600 1700 1800 1900 2000 2100 2200 2300 2400
Wavelength (nm)

solutions. Because the bulk samples were approximately 1 mm thick, region 3 was not useful for bulk EPDM analysis. However, this region was used for the analysis of dilute EPDM solutions.

Although sampling difficulty increases as one goes from region 1 to region 3, spectral information and spectral resolution increases also (Chapter 1.2.1.1). Unlike the overtone bands in regions 1 and 2, the combination bands in region 3 are affected by fundamental vibrations in the low-energy (approximately 600 cm^{-1} to 2000 cm^{-1}) IR spectrum, and therefore contain much more information than the former regions.

3.3.2 CLS Results

Table 3.1 lists the "leave-one-out" SEP values of CLS calibrations for EPDM rubber and solution samples. Second derivative spectral correction improved the results of many calibrations, but worsened the results for some calibrations. In most cases, the SEP values were significantly reduced as the spectral region changed from region 1 to region 2 (to region 3, for the solution samples). This result is expected, because the spectral information content and spectral resolution increases as one moves from region 1 to region 3.

The SEP values for ethylene and propylene were, for the most part, slightly greater than the estimated error of the reference NMR method for determination of ethylene and propylene concentration

Table 3.1: Prediction errors for NIR-determined compositions of EPDM terpolymers, using the CLS method.

TABLE 3.1

Spectral region	Data Correction[a]	Analyte SEP (in mass %) ethylene	propylene	ENB	HD
EPDM Solutions:					
1	normal	3.6	5.3	9.1	5.2
1	2nd deriv.	3.9	4.0	6.1	5.2
2	normal	2.9	3.2	4.0	4.1
2	2nd deriv.	2.3	2.1	4.2	2.4
3	normal	2.5	3.8	5.0	2.0
3	2nd deriv.	2.2	4.5	2.8	2.2
Bulk EPDM:					
1	MSC	5.9	11	8.9	5.6
1	MSC-2D	6.5	5.9	12	2.3
2	MSC	2.9	4.5	5.1	2.3
2	MSC-2D	3.4	2.9	5.6	3.8

[a] *normal*: subtraction of baseline at 1100 nm and normalization to solution concentrations only

2nd deriv.: second derivative correction, then normalization to solution concentration

MSC: Multiplicative Scatter Correction (see reference 12)

MSC-2D: second derivative correction, then Multiplicative Scatter Correction

(2 %). SEP values for ethylene were generally below 4 % (mass) and SEP values for propylene were below 6 %. The prediction errors for ethylene and propylene in bulk EPDM elastomers were much higher than the prediction errors for these analytes in their solutions. This difference could have been caused by inadequate removal of sampling effects from the bulk polymer spectra, or by the presence of unknown effects in the bulk polymer spectra that were not present in the polymer solution spectra.

Predictions of ENB and HD in EPDM are expected to be more difficult than for ethylene and propylene, because the concentrations of these monomer units are much lower than the concentrations of ethylene and propylene units. In addition, there are few functional groups in these monomer units that can give unique spectral signals, especially at low spectral resolution. Region 3, which has the best spectral resolution and most information of all three regions, provides the best possibility for quantitative analysis of ENB and HD. The errors for ENB and HD calibrations in region 3 were within 35 to 65 % of the range of concentration values of these analytes in the samples.

3.3.3 PLS Results

The first step in all PLS calibrations was the determination of the optimal number of spectral factors. If all chemical components are known, and there are no interactions between them, the optimal

number of factors for PLS calibrations using mean-centered EPDM spectra is three, because there are 4 different chemical components in the polymers (ethylene, propylene, ENB, and HD units). However, additional factors might be necessary to explain unknown spectral components. In an attempt to determine a more confident number of factors for PLS calibrations, cross-validations were performed with each PLS calibration using 2 user-selected prediction sets. The cross-validation results indicate that the optimal number of factors is three for all calibrations that use solution spectra and four for all calibrations that use bulk polymer spectra. As a result, three factors were used in all PLS calibrations that use solution spectra, and four factors were used in all calibrations that use bulk polymer spectra.

The SEP results of the PLS calibrations are shown in Table 3.2. For the most part, SEP values for PLS calibrations were significantly lower than the SEP values for CLS calibrations (Table 3.1). The use of second derivative-corrected spectra caused a decrease in prediction error in most cases.

The lower prediction errors obtained from the PLS method relative to the CLS method suggests that there are spectral variations in the EPDM solution and bulk spectra that cannot be modeled by the CLS method. It is possible that the NIR spectra of EPDMs are affected by varying amounts of block and random segments, or sequencing effects (Chapter 1.3.2.4), in the different polymers. It is expected that the PLS method is better able to model sequencing effects than the CLS method.

Table 3.2: Prediction errors for NIR-determined compositions of EPDM terpolymers, using the PLS method.

TABLE 3.2

spectral region	data correction[a]	analyte SEP (in mass %) ethylene	propylene	ENB	HD
EPDM Solutions:					
1	normal	3.7	5.0	3.7	2.4
1	2nd deriv.	2.7	3.8	2.7	2.0
2	normal	1.9	1.6	3.0	2.2
2	2nd deriv.	1.7	1.7	3.0	2.0
3	normal	1.4	2.4	2.4	1.6
3	2nd deriv.	1.6	2.5	1.4	1.3
Bulk EPDM:					
1	MSC	1.9	1.9	2.6	1.7
1	MSC-2D	1.8	1.7	1.8	1.4
2	MSC	1.6	1.7	1.8	1.3
2	MSC-2D	1.7	1.7	1.0	1.0

[a] same abbreviations as in Table 3.1

The difference in performance of the PLS and CLS methods is especially large for analyses that use bulk polymer spectra. This difference is probably caused by morphology, or interchain interaction effects in the bulk polymers. EPDM terpolymers with high ethylene contents can have significant crystallinity (13,14). It is probable that crystallinity also affects the NIR spectra of these substances. This effect can be used to explain the cross-validation results for PLS analyses of bulk polymer spectra, which indicate that the number of independent spectral variations (four) is one greater than the number of variations expected for a system without interaction effects. The extra spectral factor in the PLS calibration enabled better modeling of the bulk polymer spectra and resulted in better prediction results relative to the CLS analyses.

For the EPDM solution calibrations, many ethylene and propylene prediction errors were below the estimated error of the NMR reference method. Because the SEP values cannot be less than the actual error in the reference method, it is suspected that the estimated error in the NMR reference method is too high. The PLS calibrations for ENB and HD in region 3 were greatly improved relative to the CLS calibrations. The results for the PLS calibrations with the bulk samples are also very encouraging. The relatively low SEP values for the calibrations in region 1 are particularly noteworthy, because this region is tolerant of wide sample variations.

3.3.4 Spectral Residuals

In CLS and PLS calibrations, all variations in the calibration spectra must be explained to obtain an optimal calibration. The variations in the calibration spectra that are not explained by the multivariate model are called the spectral residuals (Chapter 1.5.2.3.3, Equation 1.19). A spectral residual of zero indicates that all spectral variations (including noise) are modeled by the multivariate calibration. A large spectral residual can be caused by low signal-to-noise ratio in the spectral region used for the calibration, or by the presence of spectral effects not modeled by the calibration method.

Table 3.3 lists the residual SS for all of the PLS and CLS calibrations and the percent residual SS for the PLS calibrations. The percent residual SS is the residual SS divided by the sum-of-squares of the mean-centered calibration spectra. Note that only one residual value is reported for each CLS calibration, because all 4 analytes are calibrated in the same procedure. For the PLS calibrations in this work, one calibration model was constructed for each analyte.

The residuals for CLS calibrations are consistently higher than the residuals for corresponding PLS calibrations. This result is a further indication that significant spectral effects explained by the PLS calibration are not explained in the CLS calibrations. Of particular note is the large difference in spectral residuals for PLS and CLS calibrations that used bulk polymer spectra. This difference corresponds to a large difference in prediction errors (see Tables 3.1 and 3.2). Earlier, it was mentioned that crystallinity could have

Table 3.3: Spectral residuals of prediction from CLS and PLS analyses of NIR spectra of EPDM terpolymers.

TABLE 3.3

Sum of Squares of Spectral Residuals - times 1000
(Percent Sum of Squares of Spectral Residuals)

spectral region	data correction[a]	PLS Calibrations ethylene	propylene	ENB	HD	CLS Calibration
EPDM Solutions:						
1	normal	0.22 (1.9)	0.23 (1.9)	0.36 (3.0)	0.46 (3.8)	0.44
1	2nd deriv.	0.18 (5.0)	0.19 (5.4)	0.18 (4.9)	0.17 (4.8)	0.20
2	normal	1.8 (4.8)	1.9 (4.8)	2.0 (5.1)	2.0 (5.2)	2.3
2	2nd deriv.	1.5 (2.9)	2.1 (4.1)	2.3 (4.4)	1.8 (3.6)	1.7
3	normal	18 (1.7)	21 (2.0)	22 (2.1)	26 (2.5)	28
3	2nd deriv.	8.2 (0.90)	7.7 (0.84)	7.8 (0.85)	7.8 (0.85)	14.7
Bulk EPDM:						
1	MSC	0.0090 (0.25)	0.010 (0.30)	0.012 (0.32)	0.039 (1.1)	0.34
1	MSC-2D	0.014 (2.7)	0.0084 (1.6)	0.014 (2.7)	0.014 (2.7)	0.93
2	MSC	0.32 (0.89)	0.24 (0.67)	0.35 (0.97)	0.34 (0.93)	0.75
2	MSC-2D	0.095 (1.9)	0.096 (1.9)	0.091 (1.8)	0.09 (1.8)	0.35

[a] same abbreviations as in Table 3.1

affected the spectra of the bulk samples. It is probable that this effect, if it exists, is not accounted for by the CLS calibrations.

Comparison of PLS calibrations that use spectra in different regions and with different data corrections can be made from observation of percent residual SS values (the values in parenthesis in Table 3.3). For the PLS solution calibrations, second derivative correction caused a decrease in percent residual SS values for regions 2 and 3, but caused an increase in percent residual SS values for region 1 calibrations. Despite this discrepancy, the prediction errors for all regions were slightly improved or unchanged by the use of second derivative correction (Table 3.2). For regions 2 and 3, the deconvolution and baseline correction abilities of second derivative correction dominated, and caused improved calibration fit and decreased spectral residuals. In region 1, where the signal-to-noise ratio was much less than in regions 2 and 3, the noise increasing effect of second derivative correction became significant, which caused the spectral residuals to increase despite slight improvements in prediction results.

3.3.5 Qualitative Information

Although the monomer units in EPDM polymers (ethylene, propylene, ENB, and HD) were covalently bonded in the polymer chains, they were considered as separate chemical components in the

polymers. Interactions between these components can be of two types: intrachain and interchain.

Intrachain interactions involve adjacent monomer units in a polymer chain. For example, differences in the infrared spectra of block and random ethylene-propylene co-polymers were observed (7) because the vibrational spectroscopy of the ethylene and propylene groups is sensitive to the identities of adjacent groups in the polymer chain. Interchain interactions occur between monomer units that are not adjacent in the same polymer chain. Polymer crystallinity and morphology are a result of interchain interactions.

Because both intrachain and interchain interactions have been found to affect infrared spectra of polymers (5,7), they are also expected to affect the near-IR spectra of polymers. The nature and extent of these interactions for the EPDM samples used in this work can be studied by observation of CLS-estimated pure analyte spectra and PLS regression coefficient spectra. For this discussion, spectra corrected with the second derivative operation will not be used, because they are more difficult to interpret qualitatively.

Figure 3.2 shows the region 1 CLS estimated pure analyte spectra of ethylene in EPDM solution (C) and in bulk (D), the PLS coefficient spectrum for ethylene in EPDM solution (A), and a NIR reflectance spectrum of high-density polyethylene (HD-PE) (B). Note that the CLS estimated pure analyte spectra (C and D) closely resemble the spectrum of HD-PE (B). The difference between the CLS estimated pure analyte spectra of ethylene in EPDM solution (C) and

Figure 3.2: *upper plot*- **A**: PLS coefficient spectrum of ethylene in EPDM solution, **B**: NIR reflectance spectrum of high-density polyethylene, **C**: CLS reconstructed spectrum of ethylene in EPDM solution, **D**: CLS reconstructed spectrum of ethylene in bulk EPDM; *lower plot*- **E**: PLS coefficient spectrum of propylene in EPDM solution, **F**: NIR reflectance spectrum of isotactic polypropylene, **G**: CLS reconstructed spectrum of propylene in EPDM solution, **H**: CLS reconstructed spectrum of propylene in bulk EPDM. All spectra are in region 1. Spectra **B, C, D, F, G** and **H** were vertically offset and scaled for clarity; spectra **A** and **E** were only scaled for clarity.

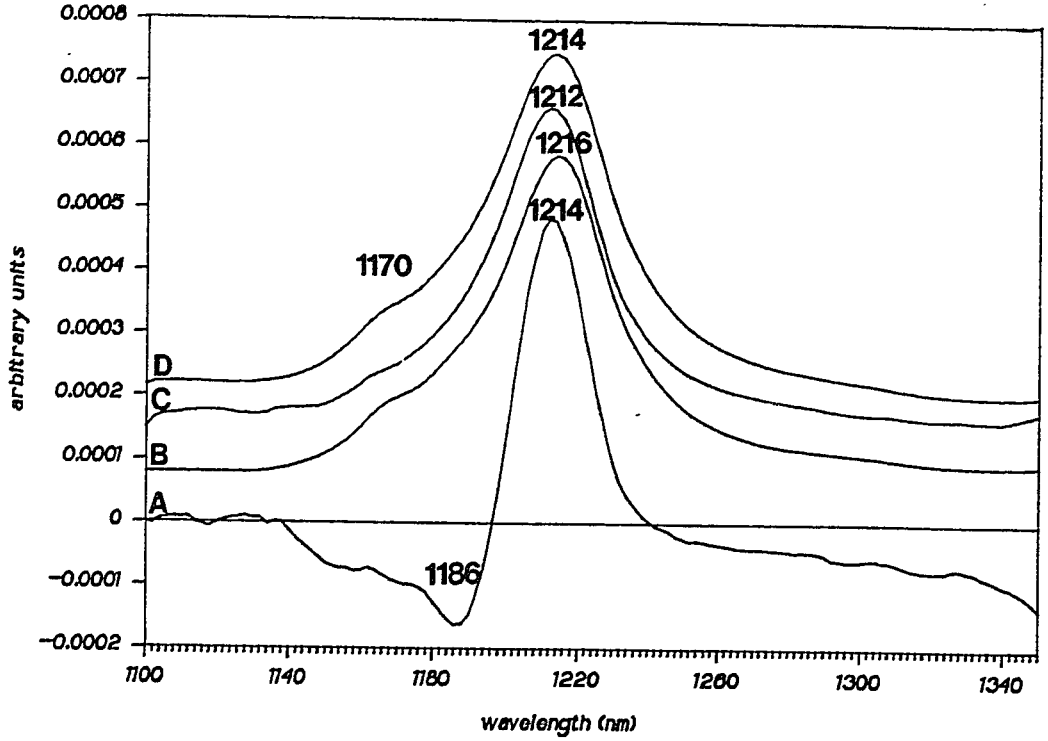
0.0008
0.0007
0.0006
0.0005
0.0004
0.0003
0.0002
0.0001
0
-0.0001
-0.0002
arbitrary units
1214
1212
1216
1214
1170
D
C
B
A
1186
1100
1140
1180
1220
1260
1300
1340
wavelength (nm)

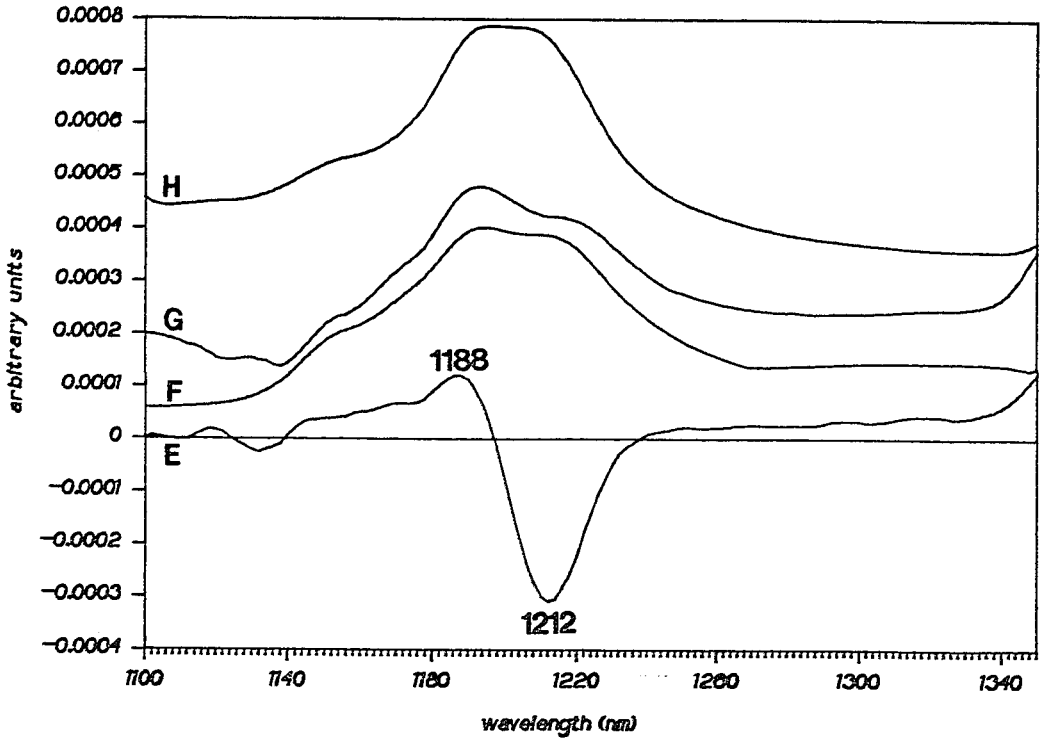
0.0008
0.0007
0.0006
0.0005
0.0004
0.0003
0.0002
0.0001
0
-0.0001
-0.0002
-0.0003
-0.0004
arbitrary units
H
G
F
E
1188
1212
1100
1140
1180
1220
1260
1300
1340
wavelength (nm)

in bulk (**D**) is small, but significant. The estimated pure analyte spectrum in solution has a peak maximum at 1212 nm, and the estimated pure analyte spectrum in the bulk has a peak maximum at 1214 nm, which is closer to the peak maximum for HD-PE (1216 nm). Because the estimated wavelength repeatability of the NIR instrument is 0.02 to 0.05 nm, these peak shifts are significant. In addition, a very small shoulder at 1170 nm was observed only in the estimated pure analyte spectrum in the bulk (**D**) and in the HD-PE spectrum (**B**). These observations suggest that the ethylene units in bulk EPDM were arranged more like the ethylene units in HD-PE than the ethylene units in EPDM solutions. If one assumes that HD-PE is highly crystalline, and the EPDM polymers do not exhibit crystallinity in solution, these results suggest that the ethylene units in the bulk EPDM samples have significant crystallinity.

The PLS coefficient spectrum for ethylene in EPDM solution (Figure 3.2, **A**) also resembles the spectrum of HD-PE (**B**), except for the negative peak at 1186 nm. This negative peak is most likely caused by the presence of propylene absorbance bands overlapping with the ethylene band. Its presence indicates that interfering propylene absorbances are accounted for in the ethylene calibration.

Figure 3.2 also shows the CLS estimated pure analyte spectra for propylene in EPDM solution (**G**) and in bulk (**H**), the PLS coefficient spectrum for propylene in EPDM solution (**E**), and the NIR reflectance spectrum of isotactic polypropylene (*ISO*-PP) (**F**). As is the case for ethylene, the two CLS estimated pure analyte spectra

closely resemble the spectrum of the homopolymer (*ISO*-PP) (**F**). However, slight differences between the estimated pure analyte spectra and the *ISO*-PP spectrum are observed. These differences might be caused by differences in intra-chain interactions of the propylene units in the two polymer systems. In *ISO*-PP, the propylene units are connected in an ordered "head-to-tail" configuration. In EPDM polymers, the propylene units might be isolated between ethylene units in the chain, or arranged randomly in "head-to-head" and "head-to-tail" configurations in propylene blocks. This difference should cause a difference in the NIR spectrum of the propylene group in the two substances. The crystallinity effect, discussed earlier, might contribute to the observed deviations of the estimated pure analyte spectrum of propylene in bulk EPDM (**H**) from the estimated pure analyte spectrum of propylene in EPDM solution (**G**). Although the propylene units in EPDM elastomers do not exhibit crystallinity themselves, they can be incorporated into crystalline domains of ethylene units (13), thus causing their spectral properties to differ from those of propylene units in solution.

The PLS coefficient spectrum for propylene in EPDM solutions (Figure 3.2, **E**) is almost exactly opposite to the PLS coefficient spectrum for ethylene (Figure 3.2, **A**). A positive peak at 1188 nm indicates propylene absorption, and the negative peak at 1212 nm compensates for overlapping absorption from ethylene units.

Figure 3.3 is the region 2 analog of Figure 3.2. Note the shift in peak maxima between the CLS estimated pure analyte spectrum for ethylene in EPDM solution (Figure 3.3, **C**) and the spectrum of HD-PE (Figure 3.3, **B**). The magnitude and direction of this shift are identical to that for region 1 mentioned earlier. This further indicates the large difference in morphology of ethylene units in EPDM solutions and in HD-PE. The estimated pure analyte spectrum for ethylene in EPDM rubber (**D**) has peak maxima at approximately the same position as for HD-PE (1730 nm and 1762 nm). However, the peak at 1730 nm is much less intense than expected. This effect is probably caused by the non-linear behavior of the strong ethylene band at 1730 nm, which resulted from the use of bulk samples that were too thick, or too absorbing.

The CLS estimated pure analyte spectrum of propylene in EPDM solution (Figure 3.3, **G**) and the *ISO*-PP spectrum (**F**) are very similar, but they do show small differences. For example, the peak at 1770 nm in the estimated pure analyte spectrum in EPDM solution (**G**) is not present in the *ISO*-PP spectrum. As mentioned earlier, these differences could be caused by differences in intrachain and interchain interactions between propylene units in *ISO*-PP and in EPDM solution. The estimated pure analyte spectrum of propylene in EPDM elastomer (**H**) differs greatly from the *ISO*-PP spectrum, much of which is likely caused by the non-linear absorbance at 1730 nm.

The non-linear absorbance at 1730 nm is considered to be caused by an unknown spectral effect, which should increase the

Figure 3.3: *upper plot-* **A**: PLS coefficient spectrum of ethylene in EPDM solution, **B**: NIR reflectance spectrum of high-density polyethylene, **C**: CLS reconstructed spectrum of ethylene in EPDM solution, **D**: CLS reconstructed spectrum of ethylene in bulk EPDM in region 2; *lower plot-* **E**: PLS coefficient spectrum of propylene in EPDM solution, **F**: NIR reflectance spectrum of isotactic polypropylene, **G**: CLS reconstructed spectrum of propylene in EPDM solution, **H**: CLS reconstructed spectrum of propylene in bulk EPDM. All spectra are in region 2. Offset and scaling were similar to that of Figure 3.2.

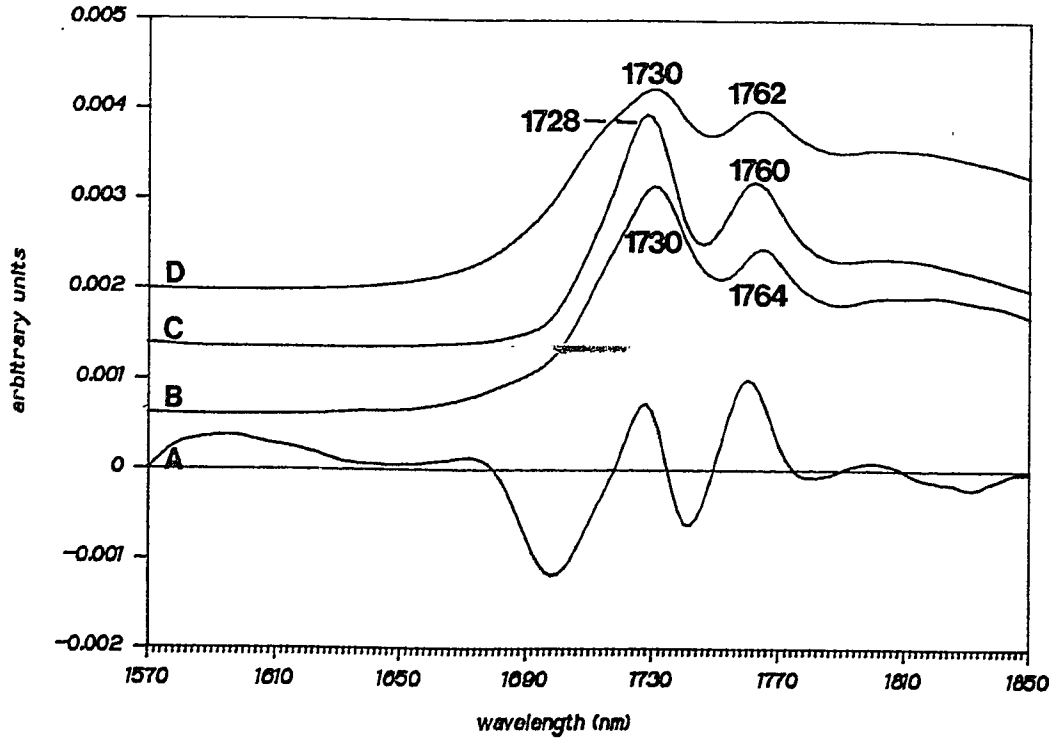
0.005
0.004
0.003
0.002
0.001
0
-0.001
-0.002
arbitrary units
1730
1762
1728
1760
1730
1764
D
C
B
A
1570
1610
1650
1690
1730
1770
1810
1850
wavelength (nm)

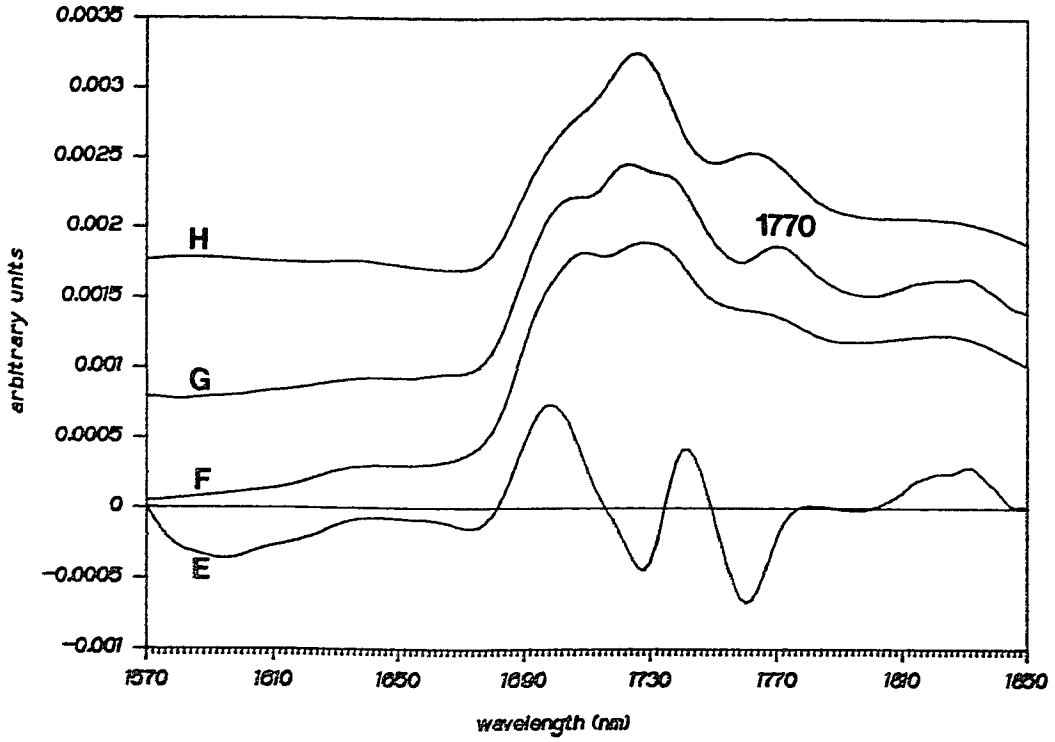
0.0035
0.003
0.0025
0.002
0.0015
0.001
0.0005
0
-0.0005
-0.001
arbitrary units
1770
H
G
F
E
1570
1610
1650
1690
1730
1770
1810
1850
wavelength (nm)

number of independent spectral variations by one. PLS can explain the extra spectral effect more easily than CLS. This assertion is reflected in the CLS and PLS calibration results for EPDM elastomers (Tables 3.1 and 3.2), and in the spectral residuals of the CLS and PLS calibrations for the bulk elastomers in region 2 (Table 3.3). As a result, the PLS method performs better quantitation than the CLS method for bulk polymers in region 2.

Figure 3.4 is the region 3 analog of Figure 3.2. The CLS estimated pure analyte spectrum for ethylene in EPDM solution (Figure 3.4, C) is very similar to the HD-PE spectrum (**B**). As in regions 1 and 2, the major ethylene peaks (at 2310 nm and 2350 nm) are shifted to lower wavelength for the estimated pure analyte spectrum of ethylene in EPDM solution. This result further indicates the large difference in morphology and intrachain interactions of ethylene units in EPDM solutions and in HD-PE. The PLS coefficients for ethylene in EPDM solution showed positive features where ethylene peaks exist and negative peaks where interfering absorptions exist. Small, but significant differences between the CLS estimated pure analyte spectrum of propylene in EPDM solution (Figure 3.4, **F**) and the *ISO*-PP spectrum (**E**) are also observed. As mentioned earlier, this difference is the result of differences in interactions for propylene units in *ISO*-PP and in EPDM solution.

The PLS coefficient spectrum for propylene (Figure 3.4, **D**) is almost an exact opposite of the PLS coefficient spectrum for ethylene, with the exception of a major positive feature at 2198 nm. This

Figure 3.4: *upper plot*- **A**: PLS coefficient spectrum of ethylene in EPDM solution, **B**: NIR reflectance spectrum of high-density polyethylene, **C**: CLS reconstructed spectrum of ethylene in EPDM solution; *lower plot*- **D**: PLS coefficient spectrum of propylene in EPDM solution, **E**: NIR reflectance spectrum of isotactic polypropylene, **F**: CLS reconstructed spectrum of propylene in EPDM solution. All spectra are in region 3. Offset and scaling were similar to that of Figure 3.2.

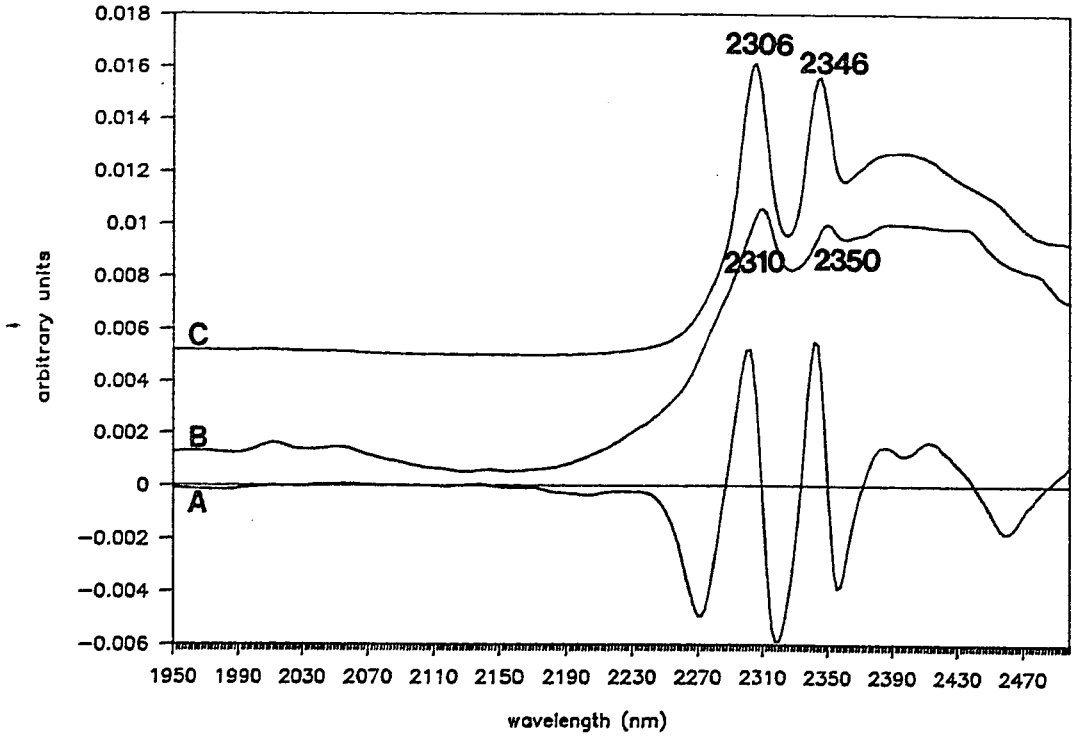
0.018
0.016
0.014
0.012
0.01
0.008
0.006
0.004
0.002
0
−0.002
−0.004
−0.006
arbitrary units
2306
2346
2310
2350
C
B
A
1950 1990 2030 2070 2110 2150 2190 2230 2270 2310 2350 2390 2430 2470
wavelength (nm)

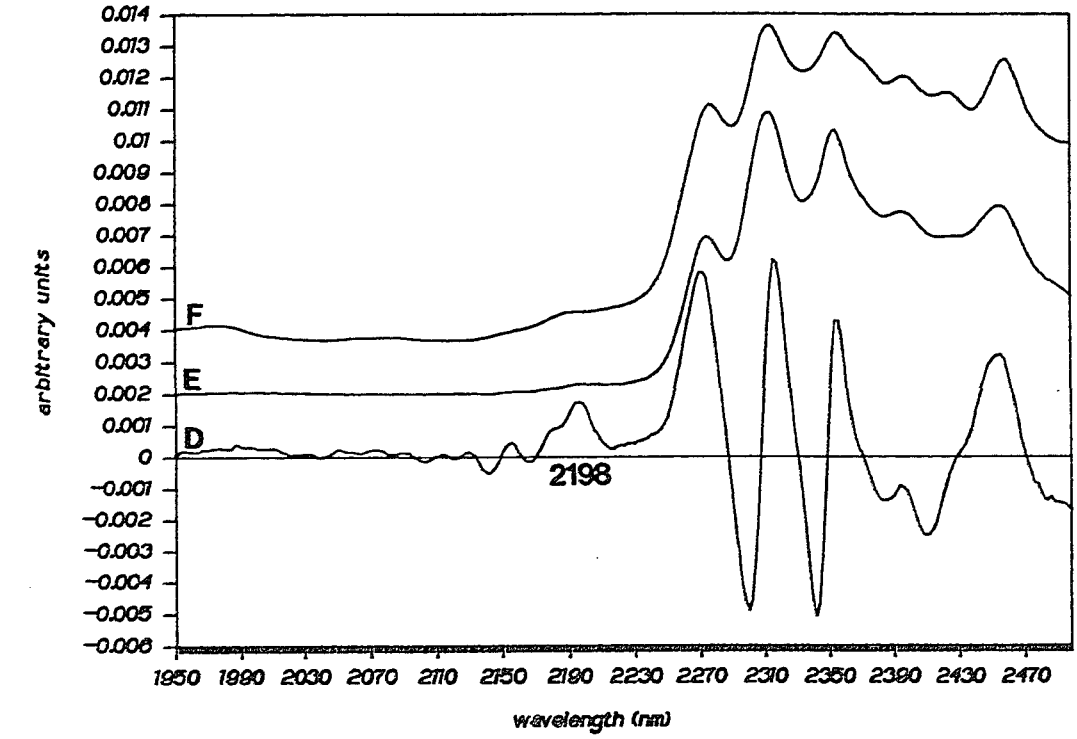
0.014
0.013
0.012
0.011
0.01
0.009
0.008
0.007
0.006
0.005
0.004
0.003
0.002
0.001
0
−0.001
−0.002
−0.003
−0.004
−0.005
−0.006
arbitrary units
F
E
D
2198
1950 1990 2030 2070 2110 2150 2190 2230 2270 2310 2350 2390 2430 2470
wavelength (nm)

feature is slightly visible in the CLS estimated pure analyte spectrum of propylene in EPDM solution (Figure 3.4, **F**) and the ISO-PP spectrum (**E**). However, it is probably free of interferent peaks, and was therefore weighted highly in the PLS calibration. In this case, the PLS regression method demonstrates that the best absorbances used for calibration of an analyte are not necessarily the strongest analyte peaks, but the peaks with fewest interferences from other components.

In region 3, spectral resolution was much better than in regions 1 and 2. As a result, calibrations were greatly improved for all four analytes. The CLS estimated pure analyte spectra for all 4 analytes in EPDM solution are shown in Figure 3.5. A peak at 2274 nm, present in the estimated pure analyte spectra of propylene, ENB, and HD, has been previously assigned as a methyl combination band (7). The relative number of methyl groups per monomer unit in the 3 monomers decreases as one goes from propylene to HD to ENB; this trend is reflected in the intensity above baseline of the 2274 nm band in the 3 estimated pure analyte spectra **A**, **B**, and **D**. Weak, but significant bands are observed in the region 2130 nm to 2200 nm only for the ENB and HD estimated pure analyte spectra. These bands are characteristic of unsaturation (15), which is only present in the HD and ENB units. Absorptions from methylene and methyne groups in the polymer are observed in the region 2290-2450 nm. The most prominent of these are the 2306 and 2346 nm bands in the

Figure 3.5: CLS reconstructed spectra of ENB (**A**), propylene (**B**), ethylene (**C**), and HD (**D**). Spectra are offset for clarity.

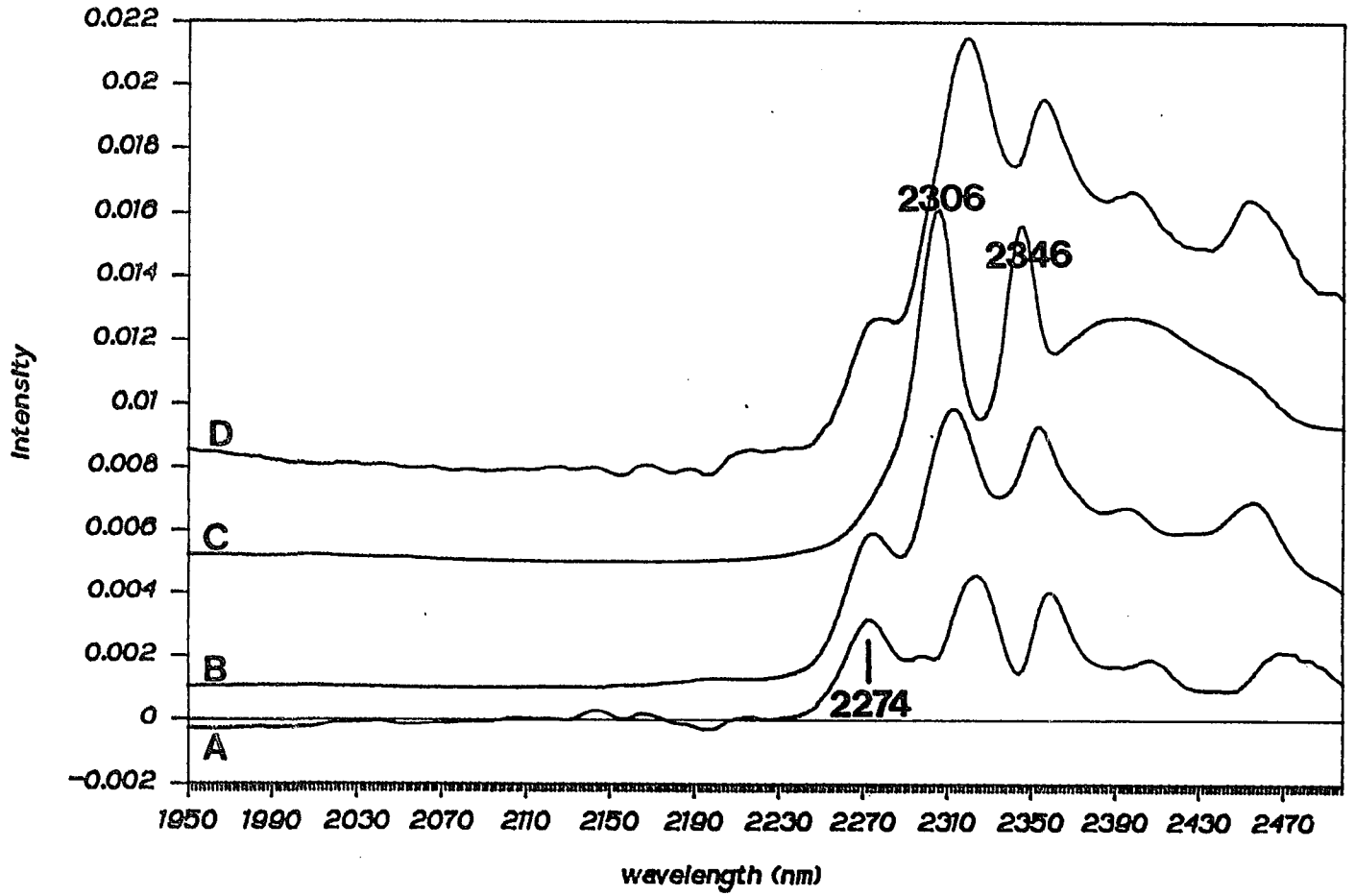
0.022
0.02
0.018
0.016
0.014
0.012
0.01
0.008
0.006
0.004
0.002
0
−0.002
Intensity
D
C
B
A
2306
2346
2274
1950 1990 2030 2070 2110 2150 2190 2230 2270 2310 2350 2390 2430 2470
wavelength (nm)

estimated pure analyte spectrum of ethylene, which were previously assigned to ethylene group vibrations (7).

3.4 Conclusion

NIR spectroscopy can be used to rapidly sample EPDM elastomers and solutions. This work has shown that the full potential of NIR for quantitative analysis cannot be realized unless multivariate calibration methods are used. Unlike univariate, or 2-wavelength calibrations used earlier, PLS and CLS methods can account for overlap between analyte signals. In addition, PLS can account for unknown interferents and spectral effects. Not only do PLS and CLS provide better quantitative results, but they also provide important qualitative information, which is observed in PLS coefficient spectra and CLS estimated pure analyte spectra. This additional information can be used to verify the presence of spectral interactions, interferents and non-linearities, and to improve the confidence of calibrations.

3.5 Notes to Chapter 3

(1) Baranwal, K.C., Lindsay, G.A., *Rubber Chem. Tech.*, **1972**, *45*, 1334.

(2) Kirkham, M.C., *J. Appl. Poly. Sci.*, **1973**, *17*, 1101.

(3) Stark, E., Luchter, K., Margoshes, M., *Appl. Spectrosc. Rev.*, **1986**, *22*, 335.

(4) Weyer, L.G., *Appl. Spectrosc. Rev.*, **1985**, *21*, 1.

(5) Bly, R.M., Kiener, P.E., Fries, B.A., *Anal. Chem.*, **1966**, *38*, 217.

(6) Takeuchi, T., Tsuge, S., Sugimura, Y., *Anal. Chem.*, **1969**, *41*, 184.

(7) Drushel, H.V., Iddings, F.A., *Anal. Chem.*, **1963**, *35*, 28.

(8) Beebe, K., Kowalski, B.R., *Anal. Chem.*, **1987**, *59*, 1007A.

(9) Haaland, D.M., Easterling, R.G., Vopicka, D.A., *Appl. Spectrosc.*, **1985**, *39*, 73.

(10) Veltkamp, D., Kowalski, B.R., Center for Process Analytical Chemistry, BG-10, Seattle WA 98195, *PLS-2 Block Modeling, Version 1.9 (IBM)*, 1986.

(11) Geladi, P., Kowalski, B.R., *Anal. Chim. Acta.*, **1986**, *185*, 1.

(12) Geladi, P., MacDougall, D., Martens, H., *Appl. Spectrosc.*, **1985**, *39*, 491.

(13) Gilbert, M., Briggs, J.E., Omana, W., *Br. Poly. J.*, **1979**, *11*, 81.

(14) Shih, C.K., Cluff, E.F., *J. Appl. Polym. Sci.*, **1977**, *21*, 2885.

(15) Goddu, R.F., *Anal. Chem.*, **1957**, *29*, 1790.

Chapter 4

Determination of Microstructure and Composition of Poly(butadiene) and Styrene-butadiene polymers by Near-infrared Spectroscopy

4.1 Introduction to Chapter 4

Poly(butadiene) (PBD) and styrene-butadiene copolymer (SBR) are used extensively in the tire and rubber industries (1). These polymers contain sites of unsaturation that can react with crosslinking agents to form elastomers. Three different types of unsaturation can be present in PBD polymer chains (1,2) (refer to Figure 1.3): 1,2 butadiene, cis-1,4 butadiene, and trans-1,4 butadiene, which result from different stereospecific additions of monomers to growing polymer chain ends during polymerization. The relative amount of these three structures (called the microstructure) greatly affects the physical properties of PBD elastomers formed from the polymers (2). For SBR copolymers, the butadiene microstructure and the amount of styrene incorporated into the polymer affect physical properties. As a result, microstructure and composition information about PBD and SBR polymers can be used to predict physical properties of their elastomers.

NMR (3-6) and infrared (7,8) spectroscopy can accurately determine the microstructure and composition of PBD and SBR. However, these methods usually require extensive sample

preparation, typically dissolving the polymer in a solvent or pressing the polymer into a thin film. Both of these preparations are time-consuming, and might alter the spectroscopy of the samples. In contrast, near-infrared (NIR) spectroscopy can rapidly analyze bulk polymers with minimal or no sample preparation.

In this work, transmission spectroscopy in the NIR region (1100 nm to 2500 nm) (9-11) is combined with the multivariate method of Classical Least Squares (CLS) (12-14) (Chapter 1.5.2.1) to determine microstructure and composition in poly(butadiene) polymers (PBD) and styrene-butadiene co-polymers (SBR). Earlier NIR analyses of PBD polymers (6) and unsaturated hydrocarbons (15) demonstrated that NIR spectroscopy can be used to determine microstructure. However, these analyses used calibrations with only one or two specific NIR absorbances, which had difficulty discriminating between highly-overlapped cis-1,4 butadiene and trans-1,4 butadiene absorptions. In contrast, the multivariate CLS method is able to make accurate microstructure predictions despite the high overlap of individual analyte bands in the spectra.

4.2 Experimental

23 PBD polymer samples and 17 SBR copolymer samples were obtained from the Goodyear Tire and Rubber Co. All polymers were obtained in a bulk state. Reference microstuctures and styrene contents of the polymers were obtained by carbon-13 NMR

spectroscopy (at 300 MHz) of the polymers dissolved in $CDCl_3$. The estimated error of the NMR reference method is 1% mass for all analytes.

The PBD samples ranged from 0.4 to 86.2 mass % 1,2 butadiene, 3.3 to 98.3 mass % 1,4-cis butadiene, and 1.2 to 84.3 mass % 1,4-trans butadiene. The covariances of the 1,2 butadiene, 1,4-cis butadiene and 1,4-trans butadiene concentrations were very low for the samples used in this work. The SBR samples ranged from 10.3 to 33.2 mass % styrene, 7.1 to 55.3 mass % 1,2 butadiene, 10.8 to 32.9 mass % cis-1,4 butadiene and 18.4 to 47.8 mass % trans-1,4 butadiene. The covariance of the 1,4-cis and 1,4-trans butadiene concentrations was very high for the SBR samples used in this work. As a result, there are only there are only three components that vary in the SBR samples: styrene, 1,2 butadiene, and total 1,4-butadiene (cis-1,4 butadiene plus trans-1,4 butadiene).

All polymers were analyzed by NIR spectroscopy in the bulk and in CCl_4 solution. Polymer solutions of approximately 1% (w/v) were prepared by dissolving a weighed amount of polymer (approximately 0.25 g) into 25 ml of CCl_4. A polystyrene solution was prepared by placing approximately 0.25 g of polystyrene (M_n = 5.56 x 10^5, Goodyear Tire and Rubber Co.) into 25 ml of CCl_4.

NIR spectra were taken with a Pacific Scientific 6250 grating monochromator instrument with a lead sulfide detector. The nominal resolution was 10 nm, the wavelength accuracy was +/- 1

nm, and the spectral region was 1100 to 2500 nm. All spectra were obtained in transmission mode. Each scan lasted about 30 seconds.

Spectra of solutions were obtained by placing approximately 10 ml of the solution in a 4 mm thick quartz cuvette with a teflon cover. The cuvette was then placed in the spectrometer for NIR sampling. A cuvette filled with CCl_4 was used as a reference. Each solution spectrum was corrected by subtraction of the CCl_4 reference spectrum, subtraction of the absorbance value at 1100 nm from all absorbance values, and subsequent division of each absorbance in the spectrum by the total concentration of polymer in the solution (in grams/25 mL).

Bulk polymers were analyzed by placing a piece of polymer, approximately 0.5 to 1.0 mm thick and 10 mm wide, on one quartz plate of a 2-plate quartz cell. The cover plate was then placed on the sample to form a "polymer sandwich" between quartz plates. For some samples, the thickness of the sample was reduced by compression of the sample between the two plates. The 2-plate cell containing the sample was then placed in the spectrometer for NIR analysis. Reference spectra were obtained by scanning the empty 2-plate cell. Each bulk polymer spectrum was corrected by subtraction of a reference spectrum before multivariate analysis.

A thickness experiment was done using the NIR spectra of five samples of a PBD polymer that have thicknesses between 0.17 and 21.8 mm. The thicknesses of the samples used in this study were determined with a caliper (Randall and Stuckney).

All CLS analyses were performed on a IBM-AT microcomputer. The NIR spectra of the polymers were split into three spectral regions for quantitative analyses: region I (1100 nm to 1350 nm), region II (1570 nm to 1850 nm) and region III (1950 nm to 2500 nm). Regions I and II contain second and first overtone bands from C-H vibrations, and are useful for analysis of polymer solutions and bulk polymers. Region III contains combination bands from C-H vibrations, which are stronger than the overtone bands in regions I and II. Region III can be used for analysis of polymer solutions, because the solvent used in this work (CCl_4) is transparent in the near-infrared region. In general, spectral resolution and absorptivites of bands increase as one moves from region I to region III.

PBD and SBR analyses were performed separately. In each case, a polymer solution and bulk polymer analysis were performed using each of the three spectral regions. In polymer solution analyses, solution spectra were used for calibration, and solution spectra were used for prediction. In bulk polymer analyses, CLS calibrations constructed from solution spectra were used to correct bulk polymer spectra for baseline and multiplicative effects; the corrected bulk polymer spectra were then used to construct CLS calibrations for bulk polymers, which were used to determine microstructure and composition from other bulk polymer spectra. For some analyses, second derivative spectra (Pacific-Scientific Co.) were used for calibration and prediction.

For each analysis, the ability of the NIR/CLS method to determine microstructure and composition was determined by using approximately half of the available samples to construct a calibration, and using the calibration to predict microstructures and compositions of the remaining samples. The statistic used to evaluate the prediction ability of the NIR/CLS method is the Standard Error of Prediction (SEP) (Chapter 1.5.2.3.2) (Equation 1.17).

The ability of CLS calibrations to describe the spectra of prediction samples is investigated using two different analyses: 1) comparison of spectral residuals of prediction with spectral noise levels and 2) estimation of the number of independent spectral variations by Principal Components Analysis (PCA). The percent spectral residual of prediction (abbreviated %SR) is calculated according to Equation 4.1:

$$\%\,SR = \left(\frac{\sqrt{\sum_{j=1}^{NP}\sum_{k=1}^{NW}\left(a_{j,k}-\hat{a}_{j,k}\right)^2}}{\sqrt{\sum_{j=1}^{NP}\sum_{k=1}^{NW}\left(a_{j,k}\right)^2}} \right) 100 \qquad (4.1)$$

where $a_{j,k}$ is the absorbance value of prediction sample j at wavelength k, $\hat{a}_{j,k}$ is the value of the modeled spectrum (the part of the spectrum explained by the CLS calibration model) of prediction sample j at wavelength k, NP is the number of prediction samples,

and NW is the number of wavelength responses in the spectrum. For the purposes of residual analysis, baseline shifts in bulk polymer spectra were not considered to be meaningful spectral variations. As a result, only CLS analyses that use second derivative spectra were considered for residual analysis.

The spectrum of a SBR solution (about 1% w/v in CCl_4) and a bulk SBR sample (about 1 mm thick) were used to estimate the noise levels for NIR spectra in all three regions. For both samples, the percent root mean square of spectral noise (abbreviated $\%RMS_e$) was determined:

$$\%RMS_e = \left(\frac{\sqrt{\sum_{k=1}^{NW} \left(a_{e,k} - \overline{a_{e,k}}\right)^2}}{\sqrt{\sum_{k=1}^{NW} a_{N,k}^{\ 2}}} \right) 100 \qquad (4.2)$$

where $a_{e,k}$ is the absorbance of a "noise spectrum" (obtained by subtracting two spectra of the same sample taken in rapid succession) at wavelength k, $\overline{a_{e,k}}$ is the average absorbance value of the noise spectrum, and $a_{N,k}$ is the absorbance of the sample spectrum at wavelength k. Only second derivative spectra were used for determination of $\%RMS_e$ values.

Principal Components Analysis (PCA) (12,16) is used to determine the number of independent spectral variations for several sets of near-infrared spectra. These determinations were done for second derivative spectra of PBD and SBR in the bulk and in solution in each of the spectral regions. In each determination, a PCA model with six principal components is constructed, and the percentage of spectral variance described by each principal component is obtained. The number of independent spectral variations in the data set is estimated as the number of principal components at which an additional principal component does not describe a significant additional amount of the spectral variation.

4.3 Results and Discussion

4.3.1 PBD Analyses

The prediction results for PBD solution analyses are shown in Table 4.1. In most cases, the SEP value for 1,2 butadiene content is the lowest of all three analytes. This result is caused by the unique near-infrared spectral features of the 1,2 butadiene group, which will be shown later. Predictions that use second derivative spectra in region II have very low SEP values for all three analytes. The errors of solution predictions that use region III are comparable to or greater than the errors from predictions that use region II, even though spectral resolution is better in region III than in region II.

Table 4.1: Prediction errors for NIR-determined microstructures of poly(butadiene) samples, using the CLS method.

TABLE 4.1

spectral region used	spectral correction[1]	Standard Error of Prediction for Different Analytes (in % mass) 1,2 butadiene	cis-1,4 butadiene	trans-1,4 butadiene
Solution analyses:				
I	none	11.2	33.8	25.9
I	second der.	3.31	7.46	5.01
II	none	4.27	0.978	2.29
II	second der.	0.947	1.03	1.15
III	none	2.37	2.44	2.59
III	second der.	0.952	2.46	3.29
Bulk analyses:				
I	none	17.1	7.45	22.3
I	second der.	1.90	5.31	6.17
II	none	1.78	2.93	3.89
II	second der.	1.51	1.80	2.57

[1] second der.= second derivative spectral correction

Second derivative spectral correction greatly improves prediction results in all spectral regions. The improvement of predictions with the use of second derivative spectra is caused by two factors: 1) decrease of spectral overlap, and 2) removal of baseline offset and linear baseline variations in calibration and prediction spectra (11).

The CLS-estimated spectra in region II for cis-1,4 butadiene, trans-1,4 butadiene and 1,2 butadiene in PBD solution are shown in Figure 4.1, A. Note the sharp 1,2 butadiene band at 1636 nm, which is not present in the spectra of trans-1,4 butadiene and cis-1,4 butadiene. This unique spectral feature of 1,2 butadiene enables accurate determination of 1,2 butadiene in PBD. Note also the high degree of overlap of the cis-1,4 butadiene and trans-1,4 butadiene spectra. This high degree of overlap causes higher prediction errors for cis-1,4 butadiene and trans-1,4 butadiene by CLS analysis, and essentially prevents prediction of these analytes by univariate analysis (6). Similar situations are encountered for pure analyte spectra in the other spectral regions. The pure analyte spectra in region III (Figure 4.1, B) indicate the presence of unique 1,2 butadiene peaks (at 2118 nm and 2230 nm). Spectral features of cis-1,4 butadiene and trans-1,4 butadiene are more separable in region III (Figure 4.1, B) than in region II (Figure 4.1, A) as a result of increased spectral resolution. However, the shape of the trans-1,4 butadiene peak at 2316 nm suggests the presence of non-linear absorption at that wavelength for the solution samples. This effect probably causes the errors of cis-1,4 butadiene and trans-1,4

Figure 4.1 : CLS-estimated spectra of 1,2 butadiene, cis-1,4 butadiene, and trans-1,4 butadiene in PBD solution in region II (A) and in region III (B).

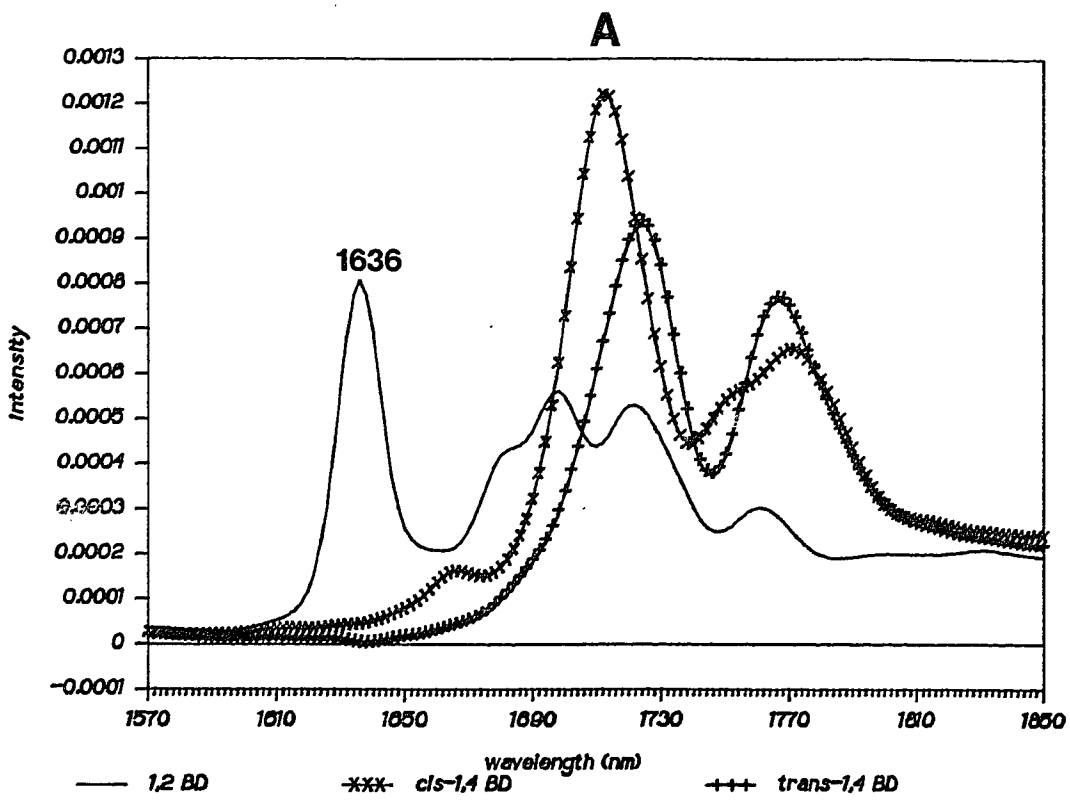
A
1636
Intensity
0.0013
0.0012
0.0011
0.001
0.0009
0.0008
0.0007
0.0006
0.0005
0.0004
0.0003
0.0002
0.0001
0
-0.0001
1570
1610
1650
1690
1730
1770
1810
1850
wavelength (nm)
1,2 BD
cis-1,4 BD
trans-1,4 BD

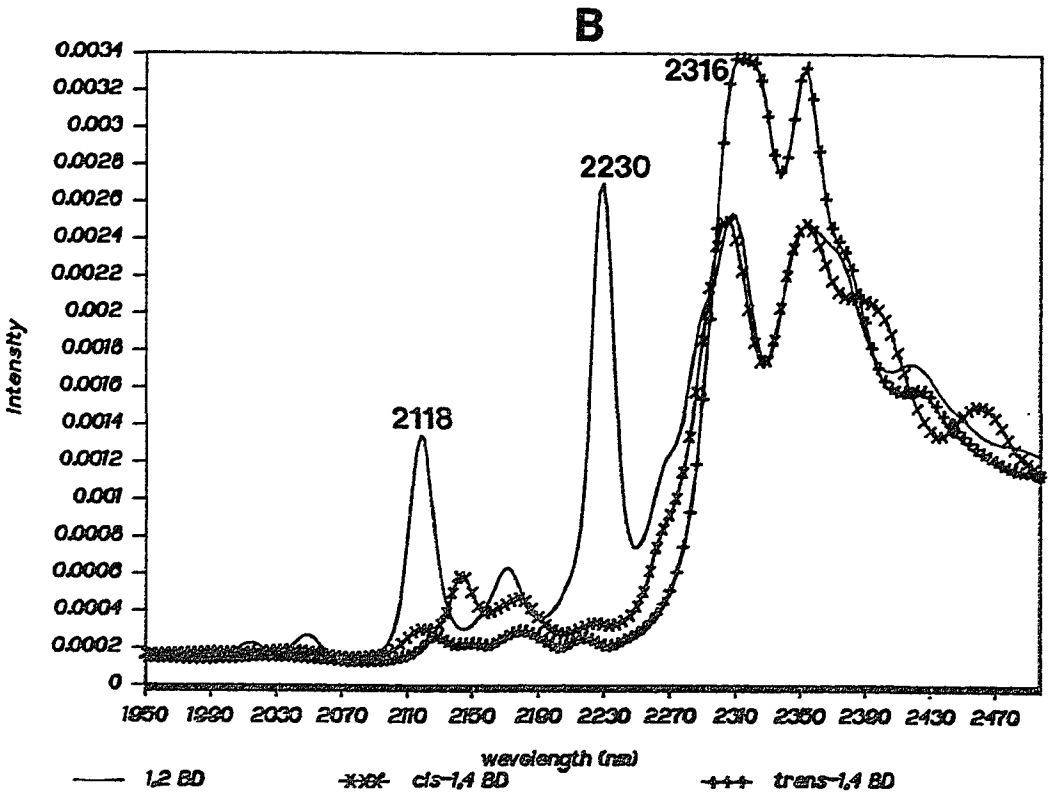
B
2316
2230
2118
Intensity
0.0034
0.0032
0.003
0.0028
0.0026
0.0024
0.0022
0.002
0.0018
0.0016
0.0014
0.0012
0.001
0.0008
0.0006
0.0004
0.0002
0
1950
1990
2030
2070
2110
2150
2190
2230
2270
2310
2350
2390
2430
2470
wavelength (nm)
1,2 BD
cis-1,4 BD
trans-1,4 BD

butadiene predictions that use region III to be greater than the errors of predictions that use region II.

The PBD bulk polymer prediction results are also shown in Table 4.1. Prediction errors for bulk and solution analyses that use region I are comparable. However, prediction errors for bulk analyses that use region II are significantly greater than prediction errors for solution analyses that use region II. This result could be caused by the error associated with multiplicative and baseline correction of bulk polymer calibration spectra or by the inability of the CLS method to describe all variations in bulk polymer spectra. Nevertheless, the results of bulk PBD analyses are encouraging. They indicate that the microstructure of bulk PBD polymers of unknown thicknesses can be determined within 1.51% (mass) for 1,2 butadiene, 1.80 % for cis-1,4 butadiene, and 2.57 % for trans-1,4 butadiene. Of course, the thickness of the polymer samples used for predictions must not be too large, or non-linearity of NIR peaks will cause increased prediction errors. The maximum allowable thickness for bulk PBD sampling by NIR using regions I and II will be determined in a later section.

Differences in the spectra of PBD polymer in bulk and in solution are indicated by comparison of estimated pure analyte spectra in the two states. Comparison of CLS-estimated spectra of trans-1,4 butadiene and 1,2 butadiene in PBD bulk and solution revealed no significant differences. However, there are significant differences between the CLS-estimated spectra in region II of cis-1,4

butadiene in PBD solution and in bulk PBD (Figure 4.2). The most notable difference is the relative height of the peaks at 1712 and 1772 nm for the two spectra. It is possible that non-linear absorbances of the bulk samples in region II cause this difference. The cis-1,4 butadiene band at 1712 nm is the strongest of all bands for all analytes in region II (see Figure 4.1, A). It is quite possible that the thicknesses of the bulk PBD samples are large enough to cause non-linearity of this band for samples with high-cis-1,4 butadiene contents.

4.3.2 SBR Analyses

As mentioned earlier (Chapter 4.2), the correlation between cis-1,4 butadiene and trans-1,4 butadiene contents in the SBR copolymers is very high. As a result, discussion of results of SBR analyses will focus on the 1,2 butadiene and styrene components.

The prediction results for SBR solution analyses are shown in Table 4.2. In most cases, 1,2 butadiene content is more accurately predicted than styrene content. In fact, the SEP value for the 1,2 butadiene prediction that uses second derivative spectra in region III is below the estimated error of the NMR reference method (+/- 1% mass). SEP values for styrene predictions are below 2% mass for analyses that use second derivative spectra in regions II and III. The SEP value for styrene obtained using second derivative spectra

Figure 4.2 : CLS-estimated spectra in region II of cis-1,4 butadiene in PBD solution and in bulk PBD polymer.

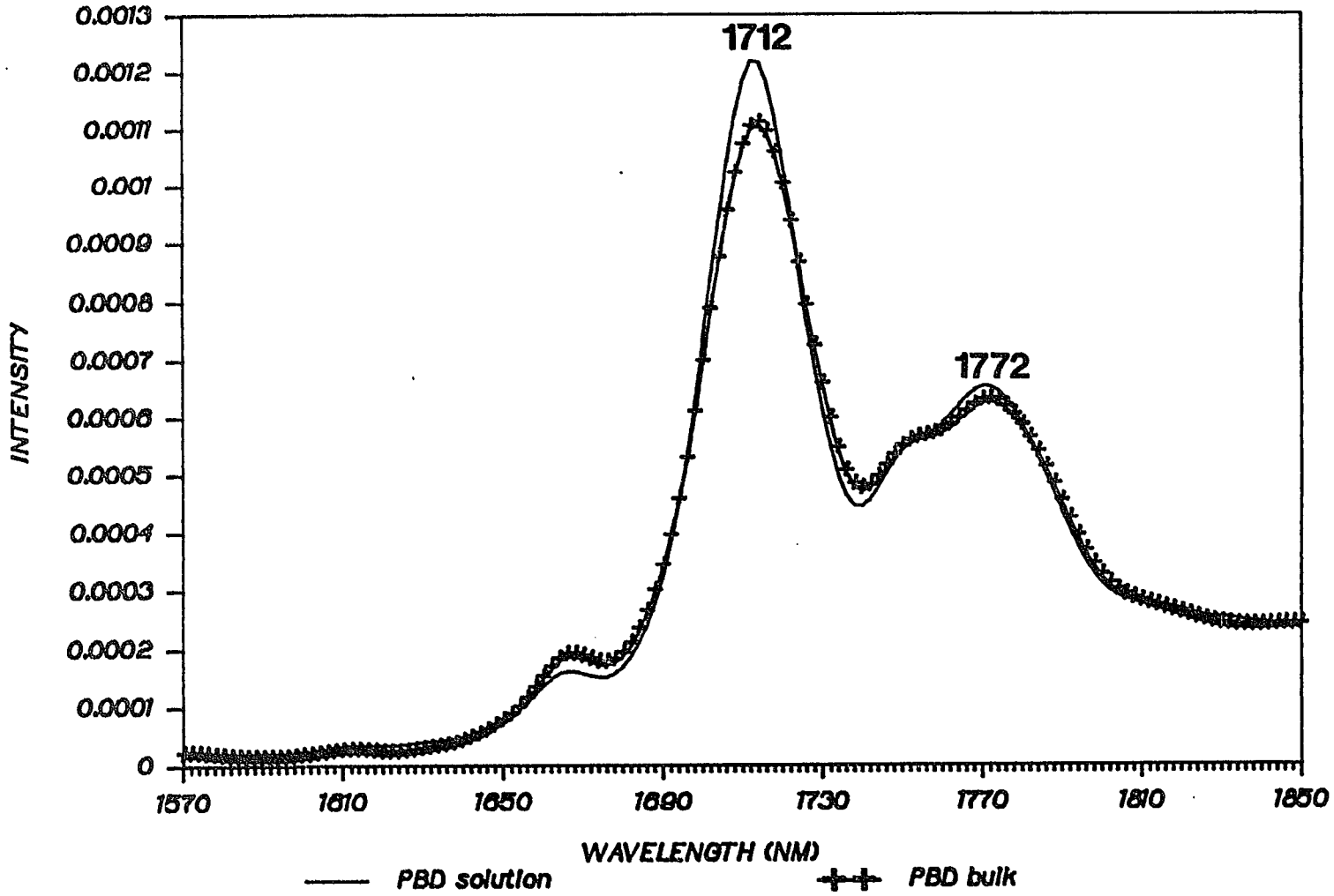
0.0013
0.0012
0.0011
0.001
0.0009
0.0008
0.0007
0.0006
0.0005
0.0004
0.0003
0.0002
0.0001
0
INTENSITY
1712
1772
1570
1610
1650
1690
1730
1770
1810
1850
WAVELENGTH (NM)
PBD solution
PBD bulk

Table 4.2: Prediction errors of NIR-determined styrene and 1,2 butadiene contents of styrene-butadiene copolymers, using the CLS method.

TABLE 4.2

spectral region used	spectral correction	Standard Error of Prediction for Different Analytes (in % mass) styrene	1,2 butadiene
Solution Analyses:			
I	none	7.78	21.6
I	second der.	3.67	7.40
II	none	2.75	2.65
II	second der.	1.40	1.12
III	none	1.38	1.23
III	second der.	1.92	0.852
Bulk Analyses:			
I	none	3.10	4.39
I	second der.	2.37	3.30
II	none	1.83	0.861
II	second der.	2.56	1.47

in region I is also encouraging, because region I can be used to analyze solution samples with path lengths up to several centimeters.

The accurate predictions of both styrene and 1,2 butadiene in the SBR copolymers is caused by the unique NIR spectral features of these two groups. The distinguishing peak for 1,2 butadiene at 1636 nm (Figure 4.1) enables accurate determination of 1,2 butadiene content in the samples. It will be shown later (Chapter 4.3.4, Figure 4.3) that the major styrene absorbance peak is located at approximately 1680 nm. This band is also experiences very little overlap with the bands of the other analytes in the samples.

Results of SBR bulk polymer analyses are also shown in Table 4.2. SBR bulk and solution analyses that use region II have comparable prediction errors. However, bulk analyses that use region I have significantly lower prediction errors than solution analyses that use region I. The lowest prediction errors for bulk analyses, 1.83 % mass for styrene and 0.861 % mass for 1,2 butadiene, which are obtained using uncorrected spectra in region II, are very encouraging.

4.3.3 Assessment of CLS Modeling Errors

Although the CLS method has multiplicative and baseline correction abilities, it can be a less than optimal multivariate technique when unknown spectral variations are present (17). In the CLS method, it is assumed that the maximum number of

independent variations in the spectra of different samples is equal to the number of known analytes in the polymer. If unknown spectral variations, such as non-linear absorbances or interaction effects, are present, a CLS calibration might not adequately model the variations in the polymer spectra. In order to determine the presence and extent of CLS modeling errors in this work, two analyses are performed: 1) analysis of spectral residuals of prediction and 2) Principal Components Analysis of the calibration spectra.

In Table 4.3, spectral residual of prediction values (determined by Equation 4.1) are compared to estimated spectral noise levels (determined by Equation 4.2) for bulk and solution spectra in all three spectral regions. In each case, the spectral residual exceeds the estimated noise level. This result indicates the presence of CLS modeling errors, which reflect the inability of the CLS method to describe the polymer spectra. For the solution spectra, in which the spectral residuals are not much greater than the corresponding noise levels, CLS modeling errors are very small. However, the amount that the spectral residual exceeds the noise level is much greater for the bulk polymer spectra. This result suggests that significant CLS modeling errors are encountered for bulk polymer spectra. These modeling errors indicate the presence of significant spectral effects of interaction between analytes in the bulk polymer. Results of PCA analyses indicate that three independant spectral variations are present in all of the data sets represented in Table 4.3. It should be noted that three independant spectral variations are expected in

Table 4.3: Comparison of spectral residuals for CLS predictions and estimated spectral noise levels.

Table 4.3

sample type	spectral region[1]	%SR values PBD	SBR	%RMS$_e$
solution	I	17.7	22.0	15.5
	II	2.28	2.51	0.760
	III	4.59	2.46	1.47
bulk	I	6.62	6.28	1.50
	II	4.60	2.69	0.194

[1] : only second derivative spectra are used for residual analyses

both the PBD data sets, from the 1,4-cis, 1,4-trans and 1,2 butadiene components, and in the SBR data sets, from the styrene, 1,2 butadiene, and combined 1,4 butadiene components (1,4-cis and 1,4-trans butadiene contents are covariant in this analysis). Therefore, even though significant CLS modeling errors are indicated by the spectral residual results, the PCA results indicate that the three-component CLS models for PBD analyses and four-component CLS models for SBR analyses sufficiently account for the number of independant variations in the spectra.

4.3.4 Interaction Effects in SBR Copolymers:

The estimated spectra in region II of styrene in SBR bulk and solution (Figure 4.3) show significant differences. The major peak in these spectra, at about 1680 nm, is most probably an aromatic C-H stretching first overtone peak, previously observed in the NIR spectrum of a polystyrene wavelength standard (11). The difference in the wavelength at the peak maximum in the two spectra is 2 nm, which is significant. In addition, significant differences between the two spectra are observed in the region 1720 nm to 1770 nm, where aromatic, methylene, and methyne C-H overtone bands are found. These observations indicate significant differences in the structure of styrene units in SBR solutions and in bulk SBR.

Earlier fluorescence analyses of SBR (18) indicated the presence of significant interactions between phenyl rings in SBR copolymers

Figure 4.3 : CLS-estimated spectra in region II of styrene in bulk SBR polymer (A), and in SBR solution (B). Spectra are offset for clarity.

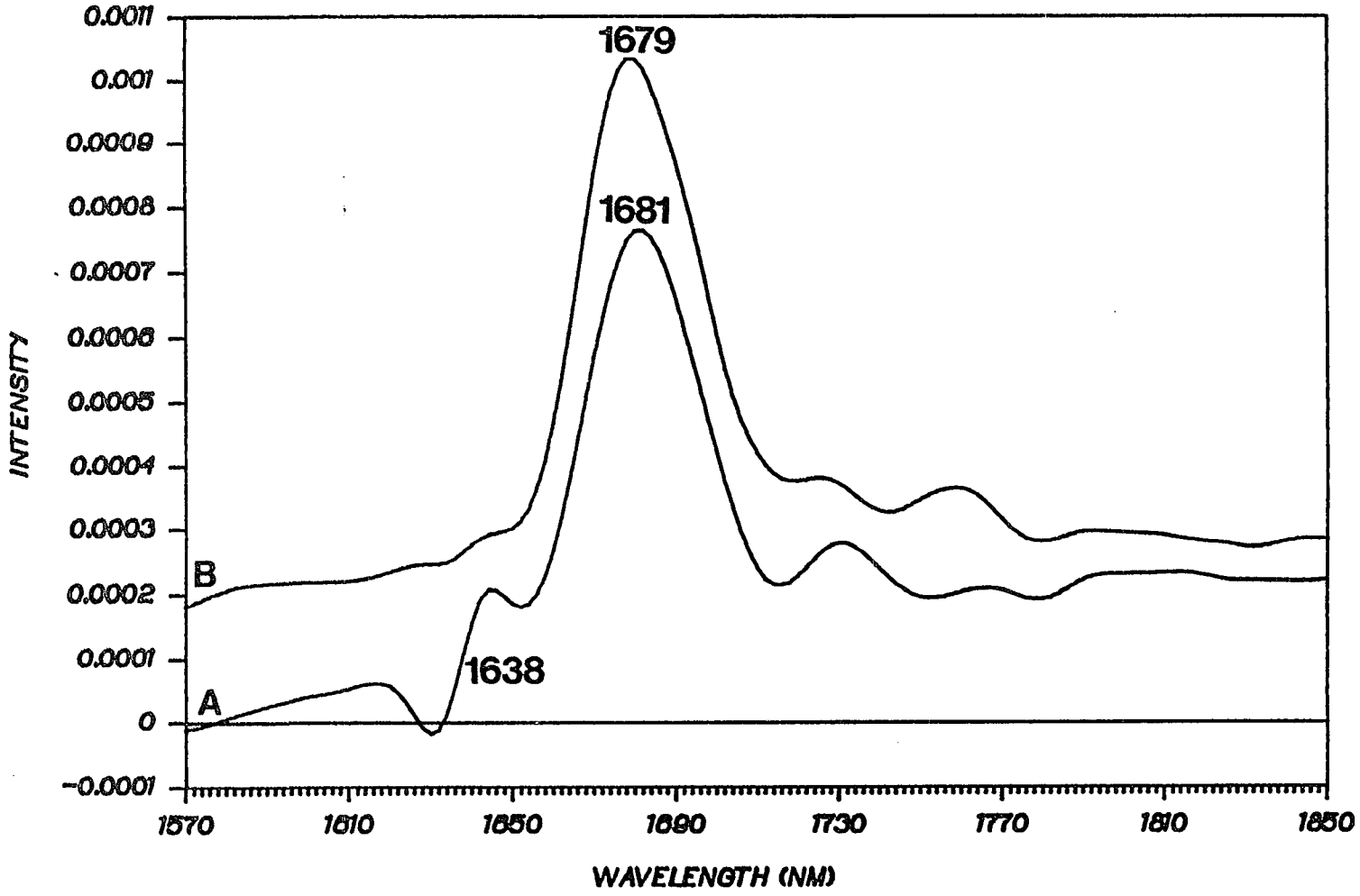
0.0011
0.001
0.0009
0.0008
0.0007
0.0006
0.0005
0.0004
0.0003
0.0002
0.0001
0
-0.0001
INTENSITY
1679
1681
1638
B
A
1570
1610
1650
1690
1730
1770
1810
1850
WAVELENGTH (NM)

for concentrated solutions and bulk polymers. This phenyl-phenyl interaction was observed to decrease with increasing dilution. The observed differences in the estimated NIR spectra of styrene in bulk SBR and in SBR solution also indicate the presence of this interaction. However, the nature of this interaction cannot be determined without detailed assignments of observed near-infrared peaks.

Of particular note in the spectrum of styrene in bulk SBR (Figure 4.3) is the first derivative-like feature at 1638 nm, which is precisely in the same position as a strong 1,2 butadiene band (see Figure 4.1, A). This feature indicates that the 1,2 butadiene peak is shifted to higher wavelength as a function of styrene content for bulk SBR, which suggests the presence of an interaction between 1,2 butadiene groups and styrene groups in bulk SBR. This interaction probably involves the phenyl group of styrene and the vinyl group of 1,2 butadiene, which are the only pendant groups in SBR polymer chains. The low intensity of the derivative-like feature relative to the intensity of the 1636 nm band in the estimated spectrum of 1,2 butadiene (in Figure 4.1, A) indicates that a very small fraction of 1,2 butadiene groups participate in this interaction.

Unfortunately, very little evidence of vinyl-phenyl interactions has been found in the literature. In ultraviolet spectroscopic analyses of (2-vinyloxy ethoxy)styrenes and (2-ethoxy ethoxy)styrenes (19), evidence of interactions between vinyl and phenyl groups was presented. However, the authors noted that the

spectral effects were too small to confirm the presence of such interactions.

The presence of vinyl-phenyl interactions in bulk SBR can be inferred from thermodynamic data of mixtures of aromatics with n-alkanes and 1-alkenes. Theromodynamic data for mixtures of benzene with n-hexane (20), 1-hexene (21), n-octane (22), and 1-octene (23) indicate that the excess enthalpy of mixing for benzene and n-alkanes is about 0.3 kJ/mol greater than the excess enthalpy of mixing for benzene and 1-alkenes. Equations of state for n-hexane and 1-hexene, indicated by thermal expansion (24) and compressibility (25) coefficients, are identical within experimental error. According to one theory of polymer solutions (26), differences in excess enthalpies of mixing of a polymer with two different solvents can be attributed to differences in the interaction enthalpies for the two solvents with the polymer if the equations of state of the solvents are identical. With this in mind, the thermodynamic data support the suggestion that exothermic vinyl-phenyl interactions are present in SBR copolymers.

4.3.5 Neighboring Group Effects

In order to demonstrate the sensitivity of NIR spectroscopy to neighboring group effects in polymer chains, the estimated spectrum of styrene in SBR solution is compared to a spectrum of polystyrene homopolymer in CCl_4 solution in region III (Figure 4.4). In this

Figure 4.4: CLS-estimated spectrum of styrene in SBR solution (**A**), and a spectrum of 1% (w/v) polystyrene in CCl_4 (**B**). Spectrum **A** is offset, and spectrum **B** is scaled and offset for clarity.

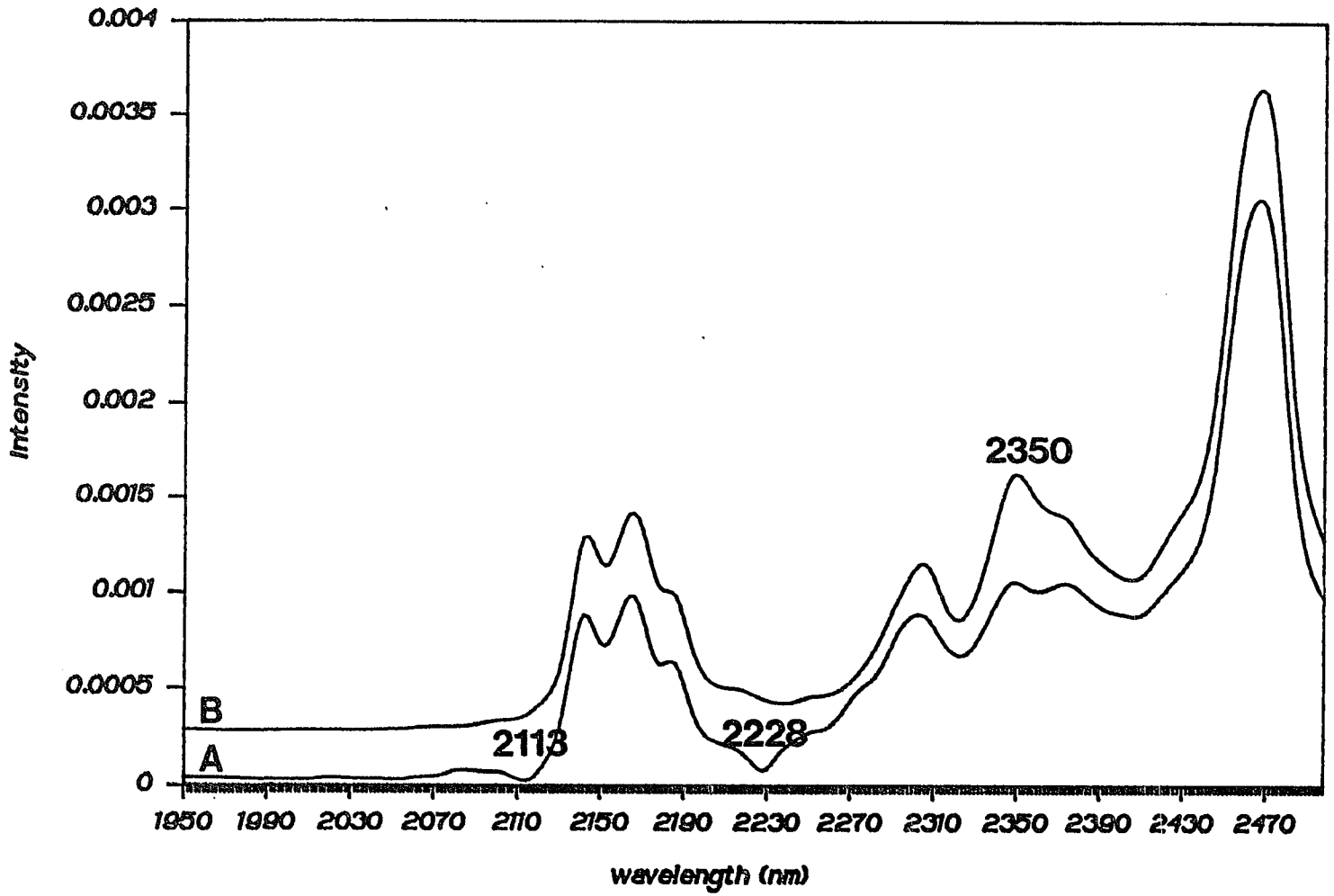
0.004
0.0035
0.003
0.0025
0.002
0.0015
0.001
0.0005
0
Intensity
B
A
2113
2228
2350
1950 1990 2030 2070 2110 2150 2190 2230 2270 2310 2350 2390 2430 2470
wavelength (nm)

region, absorbances from aromatic C-H groups (in the regions 2110 to 2210 nm and 2430 to 2500 nm) and absorbances from aliphatic C-H groups (in the region 2270 to 2400 nm) are well-separated. Weak negative peaks at 2113 and 2228 nm in the spectrum of styrene in SBR solution, which are at the same wavelengths as sharp 1,2 butadiene absorbances (Figure 4.1, **B**), are probably a result of weak non-linearities of strong 1,2 butadiene absorptions in the SBR solutions. The aromatic C-H combination bands from 2110 nm to 2210 nm are very similar in the two spectra. However, a major difference is observed in the region of 2350 nm, where bands from C-H vibrations of methylene and methyne groups in the polymer backbone are found. This result is expected, because the vibrations of backbone groups are greatly affected by the identities of neighboring groups on the polymer chains.

4.3.6 Maximum Allowable Thickness for Bulk Polymer NIR Analysis

In Chapter 1.5.2.1, it was mentioned that the relative amplitudes of the CLS-predicted concentrations (in $\hat{c}_p$, Equation 1.12) are independent of the path length of the prediction sample. However, the sum of the CLS-predicted concentrations is linearly related to the path length of the prediction sample. For bulk polymer analyses, this linear relationship will hold if the sample thickness is not large enough to cause isolated non-linear absorbances from stray light effects.

The maximum allowable thicknesses for NIR sampling of bulk PBD and SBR polymers in regions I and II are estimated by performing CLS predictions of a PBD polymer using the spectra obtained from samples with five different thicknesses. Uncorrected spectra of the bulk samples are used for prediction. Two values are used to estimate the maximum allowable thickness of the polymer sample: the sum of the CLS-predicted concentrations and the sum of squared prediction errors for all three analytes (hereby abbreviated SSPE).

Figure 4.5, A shows the relationship between the sum of the CLS predicted concentrations and the thickness of the bulk polymer sample for analyses using regions I and II. The plot for region I shows a linear relationship for all thicknesses considered, which indicates that region I has linear absorptions for samples up to 22 mm thick. The plot for region II, however, shows a linear relationship for low thicknesses and a change in slope at a point corresponding to a thickness of approximately 2 to 3 mm. This trend is observed because at sample thicknesses greater than 2 to 3 mm the absorbances in region II become non-linear from stray light effects in the spectrometer. As a result, it can be tentatively concluded that region II is useful for sampling of bulk polymers up to approximately 2 to 3 mm thick. Although this maximum allowable thickness for bulk sampling depends on sample placement,

Figure 4.5 : Sum of CLS-predicted concentrations versus bulk sample thickness (**A**), and sum of squared prediction errors versus bulk sample thickness (**B**), for CLS predictions of the microstructure of a poly(butadiene) sample that used normal spectra in regions I and II.

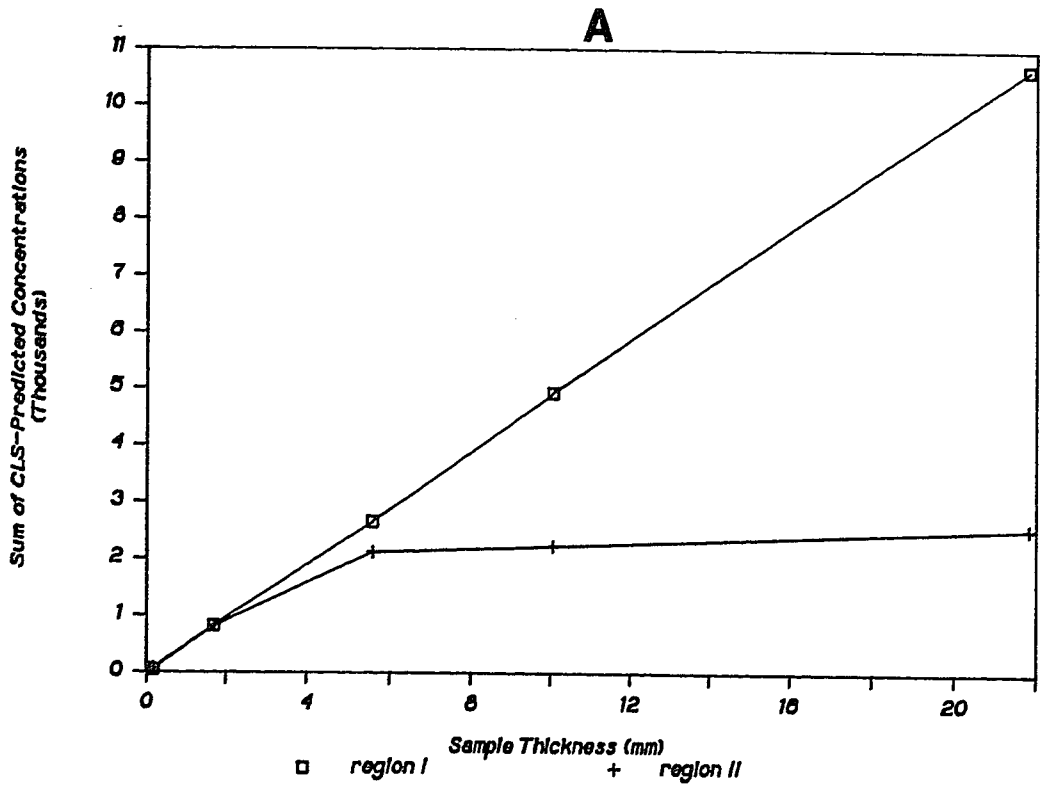
A
Sum of CLS-Predicted Concentrations (Thousands)
11
10
9
8
7
6
5
4
3
2
1
0
0
4
8
12
16
20
Sample Thickness (mm)
region I
region II

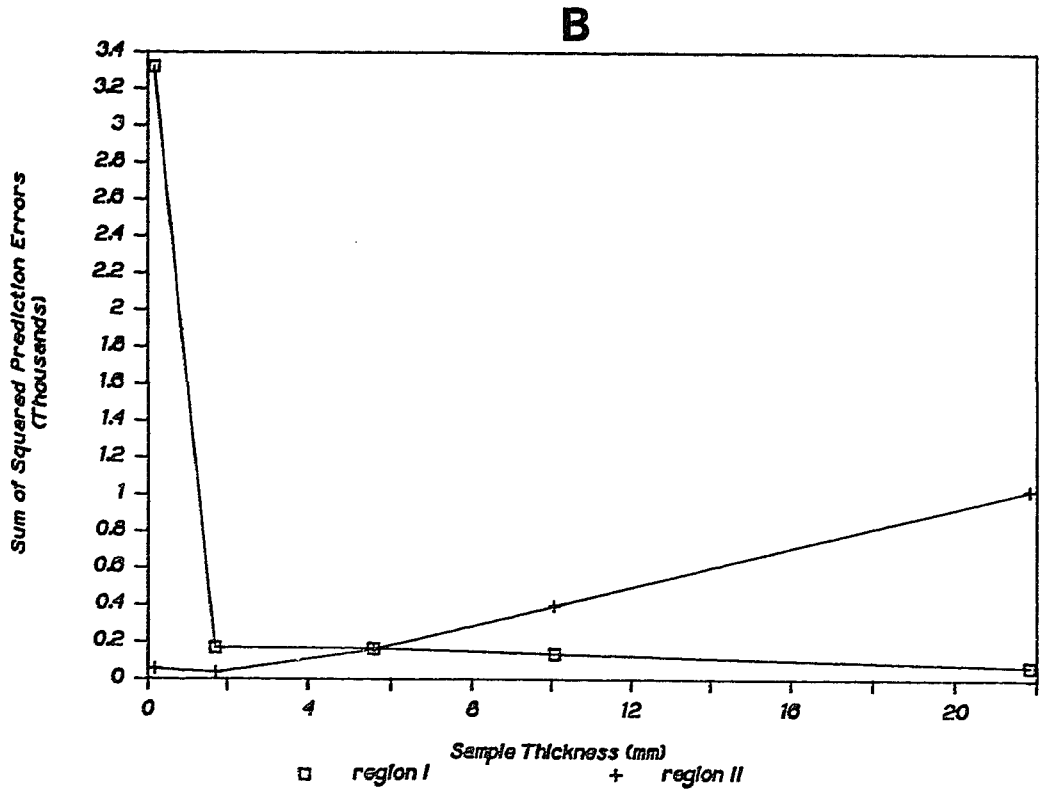
B
Sum of Squared Prediction Errors (Thousands)
3.4
3.2
3
2.8
2.6
2.4
2.2
2
1.8
1.6
1.4
1.2
1
0.8
0.6
0.4
0.2
0
0
4
8
12
16
20
Sample Thickness (mm)
region I
region II

sample shape, instrumental conditions, and sample composition, it should be a good approximation.

The effect of sample thickness on prediction errors are indicated by plots of SSPE vs. thickness for regions I and II (in Figure 4.5, B). For region I, the SSPE decreases sharply with increasing thickness for thin samples, and then gradually decreases as the sample thickness increases. The results described in the previous paragraph indicate that linear absorption in region I was observed for all thicknesses studied. Therefore, the gradual decrease in SSPE with thickness for region I indicates that increased thickness of bulk samples increases spectral signal versus a slightly changing spectral noise level, which should cause prediction errors to decrease. For region II, this trend is also observed, but only for thin samples. After the prediction error reaches a minimum value at approximately 2 to 3 mm thickness, it continually increases with sample thickness. The thickness at the minimum of this plot roughly corresponds to the thickness at the discontinuity in the region II curve in the previous plot (Figure 4.5, A). This coincidence indicates that as the non-linear absorptions become more severe, the CLS prediction errors increase.

4.4 Conclusion

This study has demonstrated the usefulness of near-infrared spectroscopy and the Classical Least Squares method for the

determination of microstructure and composition in PBD polymers and SBR copolymers. Although pure analyte spectra are highly overlapped in the near-infrared region, the CLS method enables discrimination between analyte signals and results in accurate predictions. Comparison of CLS-estimated spectra of pure analytes in bulk polymer and in polymer solution indicate specific differences in the states of the polymers in bulk and in solution. The results of this work show that NIR spectroscopy is a valuable analytical technique for analysis of bulk polymers and polymer solutions.

4.5 Notes to Chapter 4

(1) Morton, M., *Rubber Technology*; Robert E. Kreiger Co: Malabar FL, 1981.

(2) Odian, G., *Principles of Polymerization, 2nd edition*;John Wiley and Sons: N.Y., 1970.

(3) Koenig, J.L., *Chemical Microstructures of Polymer Chains*; John Wiley and Sons: N.Y., 1980.

(4) Alaki, Y., Yoshimoto, T., Dnanari, M, Takenchi, M., *Rubber Chem. and Tech.*, **1973**, *46*, 350.

(5) Claque, A.D.H., vanBroekhoven, J.A.M., Blaavin, R.P., *Macromolecules*, **1974**, *7*, 348.

(6) Durbetaki, A.J., Miles, C.M., *Anal. Chem.*, **1965**, *37*, 1231.

(7) Zbinden, R., *Infrared Spectroscopy of High Polymers*; Academic: N.Y., 1964.

(8) Binder, J.L., *Anal. Chem.*, **1954**, *26*, 1877.

(9) Stark, E., Luchter, K., Margoshes, M., *Appl. Spec. Rev.*, **1986**, *22*, 335.

(10) Weyer, L.G., *Appl. Spec. Rev.*, **1985**, *21*, 1.

(11) Williams, P., Norris, K., *Near-infrared Technology in the Agricultural and Food Industries*; American Association of Cereal Chemists: St. Paul MN, (1987).

(12) Beebe, K., Kowalski, B.R., *Anal. Chem.*, **1987**, *59*, 1007A.

(13) Haaland, D.M., Easterling, R.G., Vopicka, D.A., *Appl. Spec.*, **1985**, *39*, 73.

(14) Brown, C.W., Obremski, R.J., *Appl. Spec. Rev.*, **1984**, *20*, 373.

(15) Goddu, R.F., *Anal. Chem.*, **1957**, *29*, 1790.

(16) Jolliffe, I.T., *Principal Component Analysis*; Springer-Verlag: New York, 1986.

(17) Miller, C.E., *Appl. Spectrosc.*, **1989**, 43(8), 1435.

(18) Renyuan, Q., Xigao, J., *Scientia Sinica*, **1982**, *25*, 137.

(19) Thompson, R.E., Butler, G.B., *J. Poly. Sci. Poly. Chem Ed.*, **1978**, *16*, 1367.

(20) *International Data Series, Selected Data for Mixtures, Ser. A*, **1973**, 100.

(21) *International Data Series, Selected Data for Mixtures, Ser. A*, **1975**, 186.

(22) *International Data Series, Selected Data for Mixtures, Ser. A*, **1976**, 55.

(23) *International Data Series, Selected Data for Mixtures, Ser. A*, **1975**, 188.

(24) ASTM Committee D-2 and API Research Project 44, *Physical Constants of Hydrocarbons C1 to C10*; ASTM: Philadelphia PA, 1971; pp. 2, 14.

(25) Buchat, R. K., Richard, A. J., *J. Chem. Thermodyn.*, **1975**, 7, 271.

(26) Eichinger, B.E., Flory, P.J., *Trans. Faraday Soc.*, **1968**, *64*, 2035.

Chapter 5

Determination of Crystallinity and Morphology of Fibrous and Bulk Poly(ethylene terephthalate) by Near-infrared Diffuse Reflectance Spectroscopy

5.1 Introduction to Chapter 5

Poly(ethylene terephthalate) (PET) is currently being used for a wide range of applications. Blow-molded PET is used for food and beverage containers, and drawn PET fibers are used for tire reinforcement (1). The physical properties of PET depend on several structural factors, such as percent crystallinity (Chapter 1.3.2.2), crystallite dimension, and orientation (Chapter 1.3.2.3) (2). These structural factors can be influenced by various treatments, such as annealing or drawing, to provide a product with properties appropriate for a specific application. As a result, it is important to determine the effects of these treatments on the structure in order to determine the physical properties of the polymer.

Many different analytical methods have been used to determine structural factors in PET. Infrared and Raman spectroscopy have been used to determine orientation, percent crystallinity, and chain folding at crystalline-amorphous boundaries (3-12). NMR spectroscopy has been used to characterize the structure of amorphous PET (13). Wide angle X-ray scattering (WAXS) can be used to determine percent crystallinity and structure of crystalline domains (4,14,15), and small angle X-ray scattering

(SAXS) is useful for the determination of crystallite dimensions and orientation of amorphous polymer chains (14,16,17). The orientation of polymer chains in PET fibers can be determined from birefringence measurements (2,12,13,18), and differential scanning calorimetry (DSC) yields the percent crystallinity and the presence of different phases in the polymer (14,18-22).

These methods can provide important structural information about PET. However, they often require extensive sample preparation and long analysis times. As a result, they might not be useful for rapid process analysis. For situations where a rapid analysis is desired, near-infrared (NIR) spectroscopy is very effective (23-25). The linearity of NIR absorptions and sensitivity of commercial NIR spectrometers allow rapid and accurate analyses of relatively unprepared samples, such as wheat (23,26) and bulk polymers (24,27).

In this work, the ability of NIR spectroscopy to determine crystallinity and other structural factors in PET is demonstrated. The multivariate method of Partial Least Squares (PLS) (28-30) is used to correlate NIR spectra to percent crystallinity in fibrous PET. In addition, Principal Components Analysis (PCA) (31) of bulk PET crystallized at different temperatures is used to demonstrate the sensitivity of NIR spectroscopy to both crystal growth and crystal perfection mechanisms. Finally, the ability of NIR spectroscopy to distinguish between orientation and crystallinity in PET is demonstrated by Principal Components Analysis of bulk and fibrous PET spectra.

5.2 Experimental

Bulk PET (M_n = 18000) was obtained from the Goodyear Tire and Rubber Company. Although the exact crystallinity of the bulk PET was unknown, it was assumed that it was mostly amorphous. The pellets were then ground to produce particles in the 500 to 1000 micron range. Eight 5 gram portions of the bulk PET were taken; seven of these were heat-treated at seven different temperatures (ranging from 110 °C to 230 °C) for 5 minutes in an oil bath with a dry air purge. After heat-treatment, each sample was placed in a vial and allowed to cool to room temperature.

Five different PET tire yarns were also obtained from the Goodyear Tire and Rubber Company. A spun yarn, a fully-drawn yarn, and 3 underdrawn yarns (10%, 20% and 30% underdrawn) were obtained, using the procedure outlined in Reference 32. X-ray diffraction analyses of the yarns were performed using a Rigaku D-max X-ray Spectrometer. The scattering curve for the spun yarn (used as an amorphous reference) was fitted to the diffraction patterns of the other yarns to determine the amorphous fraction of polymer in each, and the remainder of the diffraction pattern for each sample indicated the amount of crystalline polymer. The percent crystallinity values for the PET tire yarns are shown in Table 5.1. The estimated error of the X-ray-determined crystallinity values is 2 to 3% crystallinity.

Table 5.1: Names and percent crystallinity values (determinated by X-ray diffraction) of PET tire yarn samples used in this analysis.

Table 5.1

sample type	sample code	percent crystallinity[1]
spun	Y0	0
30% underdrawn	Y1	37
20% underdrawn	Y2	42
10% underdrawn	Y3	44
fully drawn	Y4	42

[1] estimated error of 2 to 3 % crystallinity

NIR diffuse reflectance spectra of PET powders and yarns were obtained using a Pacific Scientific 6250 NIR grating spectrometer. The spectral range was 1100 nm to 2400 nm, the wavelength accuracy was +/- 1 nm, and the nominal resolution was 10 nm. Bulk samples were packed into a reflectance sample cup with a quartz window, which was then placed in the spectrometer for NIR analysis. Yarn samples were rolled into a ball and placed into a reflectance sample cup for NIR analysis. Each scan lasted about 30 seconds. Four scans for each bulk and yarn sample were taken with the sample packed twice in the cell and scanned in two different orientations in the spectrometer.

A near-infrared transmission spectrum of ethylene glycol (EG) (Aldrich) in a 1 mm path length cell and a diffuse reflectance spectrum of terephthalic acid (TPA) (Goodyear Tire and Rubber Co.) in a reflectance sampling cup were used to assist band assignments of PET spectra.

Before multivariate analysis, each spectrum was corrected for multiplicative and baseline scattering effects by the method of Multiplicative Scatter Correction (MSC) (Chapter 1.2.5) (33). In some cases, the second derivative of the spectra were taken before MSC correction. The spectra were then split into four different spectral regions for multivariate analysis: I (1100 nm to 1350 nm), II (1570 nm to 1850 nm), III (1850 nm to 2000 nm), and IV (2000 nm to 2400 nm).

Principal Components Analysis (PCA) was performed for each spectral region using two different data sets: A) bulk PET spectra only, and B) bulk and fibrous PET spectra. Mean centered spectra were used for all analyses. For each PCA analysis, the number of factors present in the NIR spectra was determined by cross-validation (31).

PLS calibrations of the yarn spectra to percent crystallinity were constructed using a program provided by the Center for Process Analytical Chemistry (34). The method of cross-validation (Chapter 1.5.2.3.1) was used to determine the optimal number of PLS factors for each calibration. Accuracy of PLS calibrations was expressed using the Standard Error of Estimate (SEE) value (Chapter 1.5.2.3.2, Equation 1.16). Prediction ability of PLS calibrations were expressed using cross-validated Standard Error of Prediction (CVSEP) values (Chapter 1.5.2.3.2, Equation 1.18). Only three samples (Y1, Y2 and Y4), which had intermediate crystallinity values (see Table 5.1), were used as prediction samples to determine CVSEP values.

5.3 Results and Discussion

5.3.1 Discussion of PET Spectrum

The NIR diffuse reflectance spectra of bulk PET before and after crystallization at 230 ^{o}C for 5 minutes are shown in Figure 5.1.

Figure 5.1: NIR diffuse reflectance spectra of bulk PET uncrystallized (**A**), and crystallized at 230 °C for 5 minutes (**B**). Specific NIR spectral regions used for analysis are labeled.

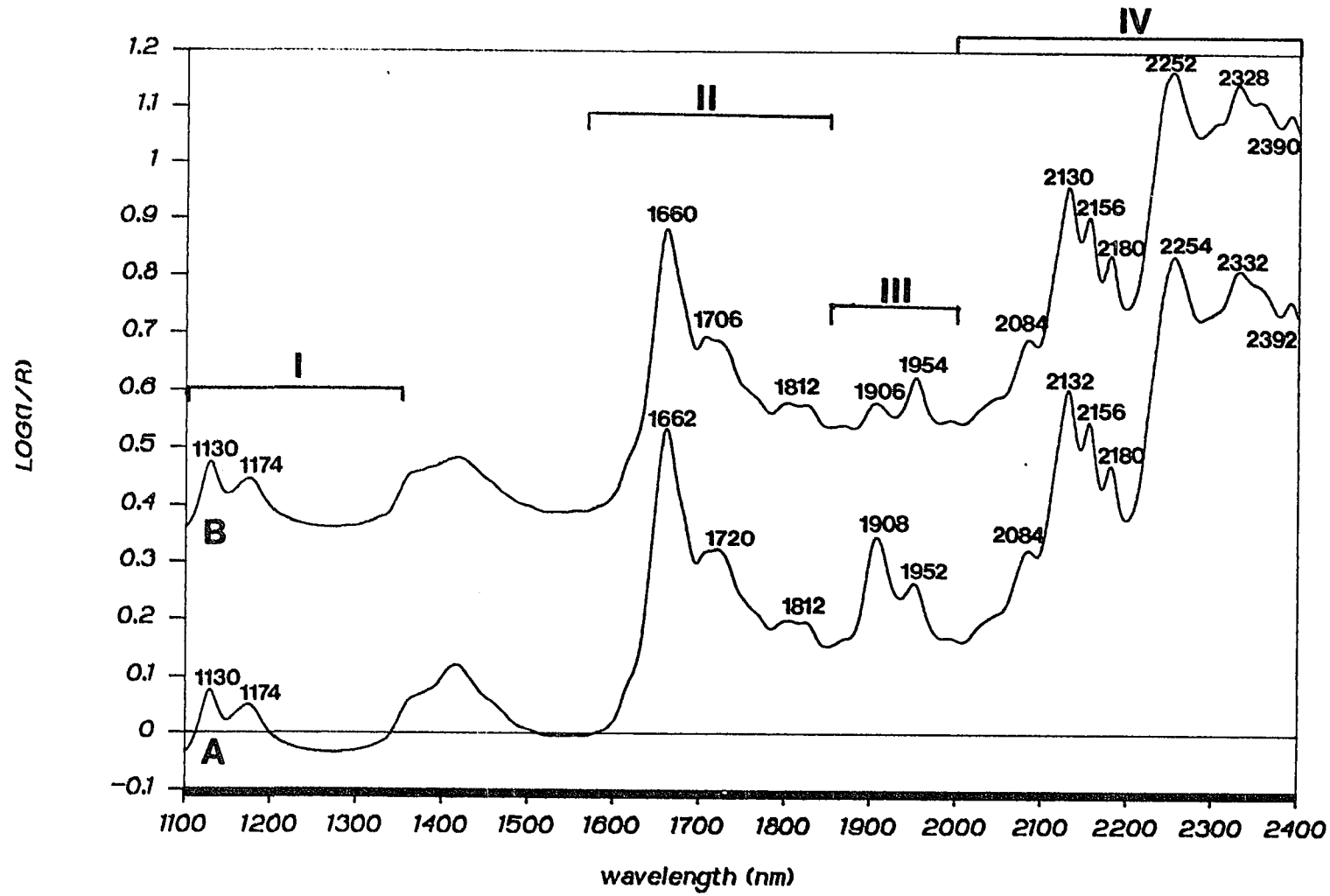
IV
II
III
I
2252
2328
2390
2130
2156
2180
1660
2254
2332
1706
2084
2392
1954
1812
1906
2132
2156
1662
1130
1174
2180
1720
1908
2084
1952
1812
1130
1174
B
A
1.2
1.1
1
0.9
0.8
0.7
0.6
0.5
0.4
0.3
0.2
0.1
0
-0.1
LOG(1/R)
1100
1200
1300
1400
1500
1600
1700
1800
1900
2000
2100
2200
2300
2400
wavelength (nm)

The different spectral regions used for analysis are labeled. As one moves from region I to region IV, the absorptivities of the bands increase and the spectral resolution improves. The strong absorbances in region IV have the best spectral resolution, but are highly susceptible to non-linear behavior. As a result, this region might not provide accurate quantitative results for highly absorbing (or low scattering) samples.

The chemical structure of PET is shown in Figure 1.3 (in Chapter 1.3.2.1). All of the NIR absorbances are overtone and combination bands of the stretching modes of aromatic C-H groups, methylene groups, and carbonyl groups in the polymer. Regions I, II, and IV contain second overtone, first overtone, and combination bands from aromatic C-H groups in the terephthalic acid (TPA) part and methylene groups in the ethylene glycol (EG) part of PET. Region III contains the second overtone carbonyl stretching band and absorbances from moisture in the polymer.

Specific assignments of NIR bands are difficult to determine, because the absorptions from each vibrational overtone and combination are highly overlapped. However, approximate assignments can be made from previously assigned bands in the IR and Raman spectra of PET (3,6-8,11) and from NIR spectra of ethylene glycol and terephthalic acid (refer to Chapter 1.2.2). The assignments of NIR bands in the PET spectra are listed in Table 5.2. It should be mentioned that the 2254 nm methylene combination band for PET is at a significantly higher frequency than the

Table 5.2: Positions and assignments for peak maxima in NIR spectra of PET and model compounds.

Table 5.2

spectral region	Band Maxima (nm) PET NC[1]	PET C(230C)[2]	Models TPA[3]	Models EG[4]	Band Assignment
I	1130	1130	1126	----	2nd overtone aromatic C-H stretch
I	1174	1174	----	1206	2nd overtone methylene stretch
II	1662	1660	1656	----	1st overtone aromatic C-H stretch overlapped with 1st overtone methylene stretch
II	1720	1706	----	1713	1st overtone methylene stretch
II	1812	1812	----	----	(3rd overtone methylene bend)
III	1908	1906	----	----	O-H stretch and bend combination, water (ref. 23)
III	1952	1954	----	----	2nd overtone C=O stretch (ref. 23)
IV	2084	2084	2090	----	3rd overtone C-O stretch (ref. 23)
IV	2132	2130	2131	----	combination aromatic C-H stretch and ring vibration
IV	2156	2156	2155	----	combination aromatic C-H stretch and ring vibration
IV	2180	2180	2180	----	combination aromatic C-H stretch and ring vibration
IV	2254	2252	----	2285	combination methylene stretch and bend
IV	2332	2328	2332	----	overlap of absorbances
IV	2392	2390	----	----	involving methylene and aromatic C-H groups and COO^- groups

[1] NC= uncrystallized bulk PET; [2] C(230C)= bulk PET crystallized at 230°C for 5 min; [3] terephthalic acid; [4] ethylene glycol

methylene combination band for ethylene glycol (2285 nm). The cause of this difference is probably the larger electron withdrawing effect of neighboring carboxyl groups in PET relative to neighboring hydroxyl groups in ethylene glycol.

Although the spectroscopic differences between uncrystallized and crystallized PET in the NIR region (Figure 5.1) are not as dramatic as in the IR region (3,6-8,11), significant differences are observed. In region IV, the ethylene combination bands at 2254 nm and 2332 nm (Figure 5.1, A) each shift to higher frequency (lower wavelength) with crystallization. Because the methylene bending and wagging vibrations are each higher for the trans conformer than for the gauche conformer of the EG segment (refer to Chapter 1.3.2.1, Figure 1.3) and the methylene stretching frequency is relatively unaffected by crystallization (3), the positive energy shifts of these combination bands are a result of an increase in the trans/gauche conformer ratio with crystallization. It should also be noted that the spectrum of the crystallized sample (Figure 5.1,B) has more fine structure than the spectrum of the uncrystallized sample (Figure 5.1,A) in the region 2300 nm to 2400 nm. This discrepancy is probably caused by crystal field splitting of bands in this region.

The bands in region II, which are primarily first overtone C-H aromatic and methylene stretching bands, also change upon crystallization. These differences might be a result of differences in inter or intramolecular order for the two samples. Intermolecular order is characterized by the ordered chain packing present in

crystalline material, and intramolecular order depends on the conformational structure of individual chains. The weaker and broader second overtone C-H stretching bands in region I do not appear to change with crystallization. However, more detailed multivariate analyses can detect small spectral shifts in this region and in other regions.

In region III, a large decrease in the 1908 nm water band with crystallization is observed (Figure 5.1). This result indicates that moisture originally present in the polymer was removed during annealing at 230 °C. A more detailed discussion of this effect will be presented later.

5.3.2 PLS Analysis- Percent Crystallinity in Yarns

The results of PLS calibrations for crystallinity in PET fibers are shown in Table 5.3. A successful crystallinity determination for PET yarns requires the ability to distinguish between crystalline polymer, oriented amorphous polymer, and random amorphous polymer. Crystalline domains are characterized by specific intermolecular and intramolecular order, whereas oriented amorphous PET is characterized by intramolecular order. In spectroscopic terms, the vibrations of methylene, aromatic C-H and carbonyl groups in the polymer (and therefore the spectrum of the polymer) must be sensitive not only to intramolecular order, but also to intermolecular interactions.

Table 5.3: Calibration and prediction results for PLS calibrations of NIR spectra to percent crystallinity in PET tire yarns.

Table 5.3

Calibration Statistics
(in % crystallinity)

spectral region	spectral correction	calibration SEE	prediction SEP	Number of Factors [2]
I	none	4.44	5.84	2
I	second deriv.[1]	2.54	3.68	2
II	none	1.88	3.51	2
II	second deriv.	1.05	2.76	2
III	none	3.89	5.43	1
III	second deriv.	2.89	3.98	1
IV	none	1.87	2.72	2
IV	second deriv.	1.37	2.11	2

[1] second derivative
[2] determined by cross-validation

The PLS cross-validation results, which indicate the number of independent spectral factors present in the NIR spectra of the PET yarns, are shown in the last column of Table 5.3. For spectral regions I, II, and IV, the PLS calibration required the use of two factors. Therefore, one can assume the presence of two independent spectral variations in the PET yarn spectra in these regions. It is quite possible that these two independent variations correspond to changes in intermolecular and intramolecular states in the polymer. It is therefore possible that the NIR spectra in these regions contain enough information to determine percent crystallinity in the yarns.

For the most part, the use of second derivative spectra improves PLS prediction results. This improvement is caused by removal of baseline variations and enhancement of spectral resolution. NIR spectral regions II and IV provide the best results for crystallinity determinations. Because the combination bands in region IV are better resolved than the overtone bands in region II, the prediction results for region IV are the most favorable. However, the weaker absorbances in region II are less likely to be non-linear as a result of stray light effects. Therefore, region II might provide the best results for highly absorbing (low scattering) samples. The prediction results for region I are less favorable, because the absorptions are weak and highly overlapped. However, this region might be optimal for analysis of thick (1 to 2 cm) PET films, which would produce stronger absorbances in this region and non-linear absorbances in the other regions.

It should be mentioned that the calibration and prediction errors for the calibrations that use regions II and IV are close to the estimated error of the X-ray crystallinity values (2 to 3% crystallinity). This result suggests that the error in the X-ray crystallinity values is the limiting error for these calibrations. As a result, better calibrations might be possible if a more accurate reference crystallinity measurement is used.

The calibration curve for the PLS calibration that uses second derivative spectra in region II is shown in Figure 5.2. Although five different yarn samples are used to construct the calibration, there are essentially three different crystallinities represented in the calibration, because differences in the crystallinities of the fully-drawn, 10% underdrawn, and 20% underdrawn samples are within the error of the X-ray crystallinity measurement. Furthermore, these crystallinity values are not well-distributed over the range of crystallinities. Therefore, it could be argued that a poor design of the calibration samples, which is not intentional but dependent on the yarn samples that are available, results in overfitting of the calibrations. However, the cross-validation results, which indicate the maximum number of PLS factors that can be used to avoid overfitting, are very reliable. As a result, it is probable that overfitting did not occur in the PLS calibrations, despite the relatively poor design of the calibration samples.

The regression coefficient spectrum for the PLS calibration that uses normal spectra in region IV is shown in Figure 5.3, A. The first

Figure 5.2: PLS calibration curve for percent crystallinity in PET yarns. Second derivative spectra in region II are used for the calibration. Sample labels are listed in Table 5.1.

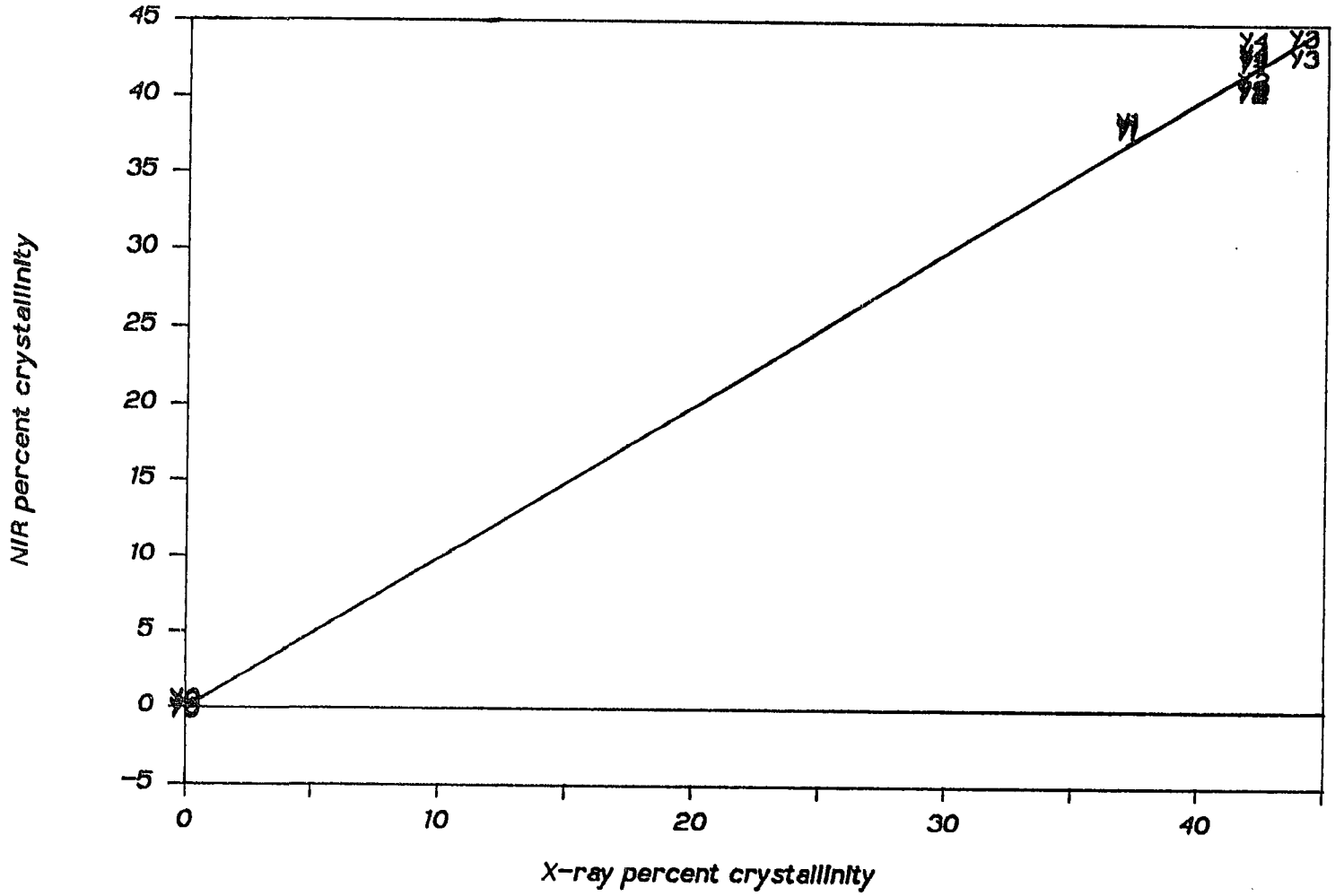
45
40
35
30
25
20
15
10
5
0
-5
0
10
20
30
40
NIR percent crystallinity
X-ray percent crystallinity

Figure 5.3: PLS regression coefficient spectra for the percent crystallinity calibrations that use normal spectra in region IV (A) and region III (B).

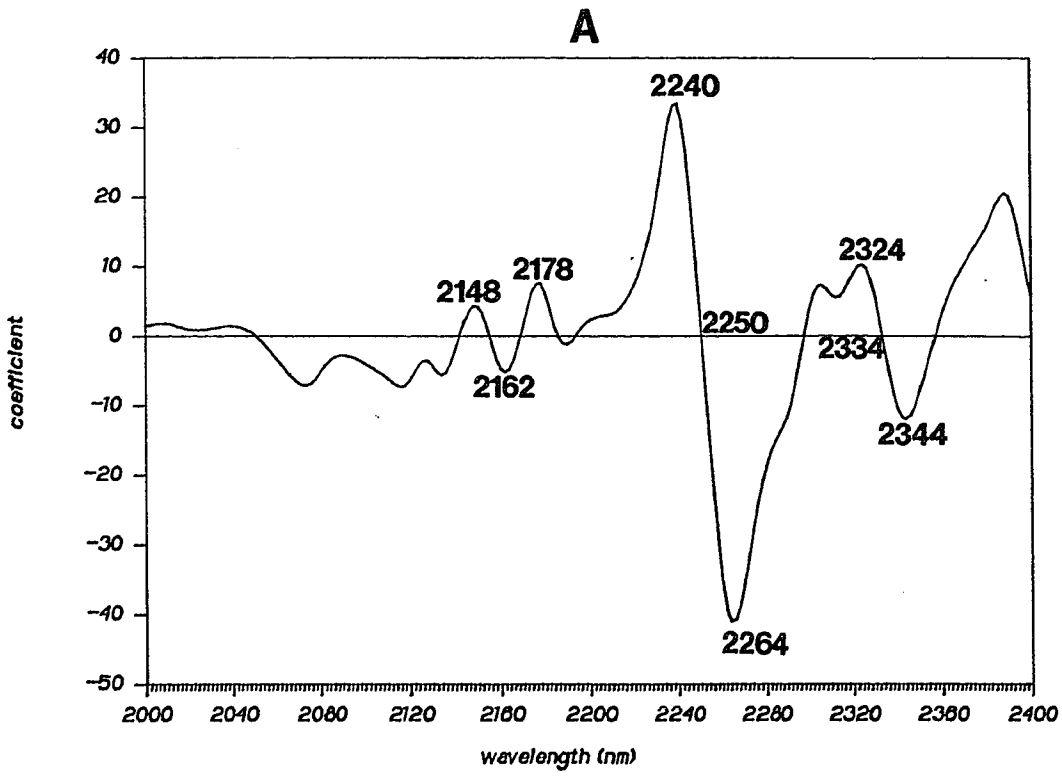
A
40
30
20
10
0
-10
-20
-30
-40
-50
coefficient
2240
2148
2178
2324
2250
2334
2162
2344
2264
2000
2040
2080
2120
2160
2200
2240
2280
2320
2360
2400
wavelength (nm)

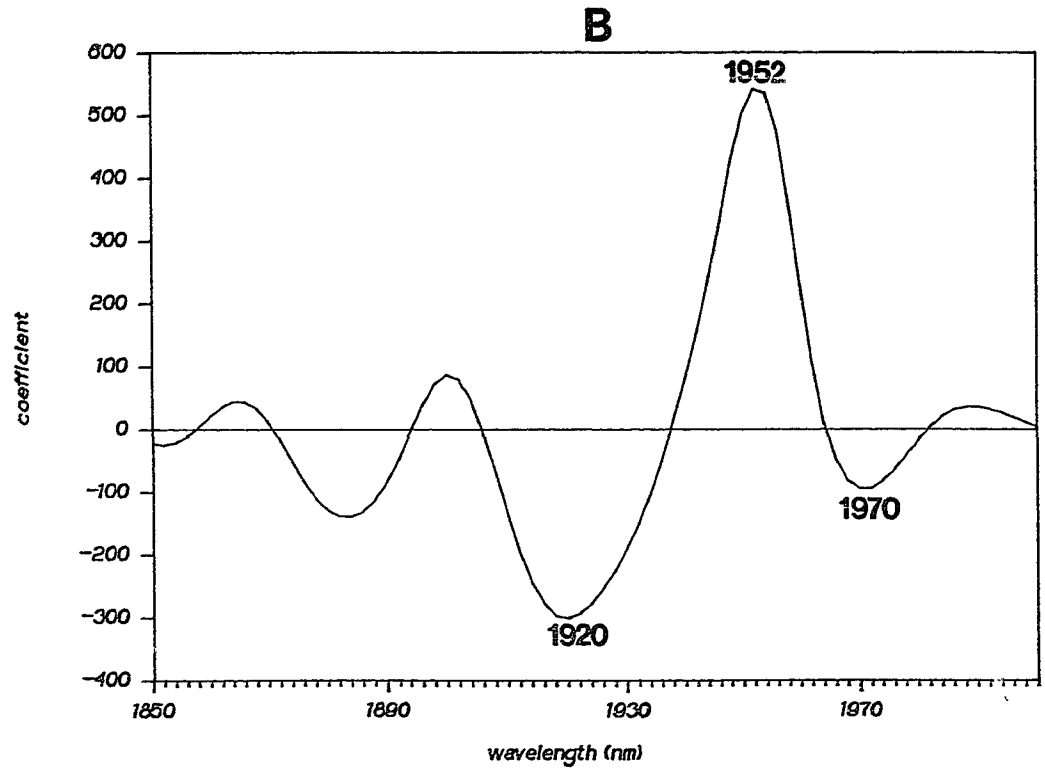
B
600
500
400
300
200
100
0
-100
-200
-300
-400
coefficient
1952
1970
1920
1850
1890
1930
1970
wavelength (nm)

derivative features at 2250 nm and 2334 nm indicate negative wavelength shifts (positive frequency shifts) of the methylene combination bands with increasing crystallinity. As mentioned earlier, these shifts indicate an increase in the trans/gauche conformer ratio with increasing crystallinity. This result is expected, because only the trans conformer of the ethylene glycol unit is present in crystalline PET (15). The weaker features at 2148 nm, 2162 nm, and 2178 nm indicate changes in aromatic C-H combination bands with crystallinity. These features are probably a result of the increased intermolecular order associated with increasing crystallinity.

Only one PLS factor was necessary for each calibration that used spectral region III (Table 5.3). Therefore, it is doubtful that this region provides enough information to accurately determine crystallinity in PET yarns. Prediction errors are significantly greater for this spectral region than for regions II and IV, which have comparable absorbance intensities and spectral resolution. However, region III contains enough information to provide an approximate crystallinity determination.

The PLS regression coefficient spectrum for the calibration that uses region III is shown in Figure 5.3, **B**. A positive peak at 1952 nm is flanked by two negative side lobes at 1920 nm and 1970 nm. This feature suggests that an increase in crystallinity is accompanied by a slight narrowing of the carbonyl band at 1952 nm. This result is in agreement with results from earlier Raman analyses of PET (6),

which indicated that the half-width of the fundamental carbonyl stretching band decreases with increasing crystallinity.

5.3.3 PCA of PET Powder Spectra

The PCA cross-validation results for the NIR spectra of bulk PET crystallized at different temperatures (data set A) are shown in Table 5.4. These results indicate that there are two independent spectral trends with crystallization temperature for regions I, II, and IV. The presence of 2 independent spectral variations in the NIR spectra indicates that 2 independent structural variations of PET polymer chains occur as a function of annealing temperature.

Detailed theoretical (35) and experimental (36,37) work on polymer crystallization have provided information about structural changes that occur with crystallization. In general, structural changes result from crystal growth and crystal perfection mechanisms. Crystal growth involves the aggregation of previously amorphous polymer chains into crystalline domains. This process is characterized by an increase in intramolecular and intermolecular order. Crystal perfection involves rearrangements of polymer chains that eliminate defects in the crystalline domains. These rearrangements might involve the formation of polymer chain folds at the surface of crystalline domains, diffusion of internal defects from the crystalline domains, or elimination of the tie chains that span different crystalline domains. Earlier results of thermal

Table 5.4: Number of factors used in PCA analyses of NIR spectra of PET, as determined by cross-validation.

Table 5.4

Spectral Region	Spectral Correction	Number of PCA Factors used[1]
Data Set A: = Spectra of bulk PET crystallized at different temperatures:		
I	none	3
I	second derivative	2
II	none	2
II	second derivative	2
III	none	1
III	second derivative	1
IV	none	2
IV	second derivative	2
Data Set B: Spectra of bulk PET crystallized at different temperatures and spectra of PET yarns spun and drawn to different extensions:		
I	none	2
I	second derivative	2
II	none	2
II	second derivative	2
III	none	1
III	second derivative	1
IV	none	2
IV	second derivative	2

[1] determined by cross-validation

analyses of PET (19,20) suggested that crystal growth occurs at 100 to 245 °C, but substantial rearrangements and crystal thickening can occur only at crystallization temperatures above 200 °C.

Both crystal growth and perfection involve major structural changes that should be detectable by vibrational spectroscopy. Indeed, IR analyses (10) of crystallized PET indicated the presence of two distinct spectral trends with crystallization temperature. It was suggested that a crystal growth process can occur at annealing temperatures below 160 °C, and a rearrangement process occurs at crystallization temperatures above 160 °C. As expected, the crystal growth mechanism involved an increase in the trans/gauche conformer ratio. In contrast, the rearrangement mechanism involved a decrease in the trans/gauche ratio for the amorphous polymer phase.

The PCA scores and loading spectra for the analysis of data set A that uses spectral region IV are shown in Figures 5.4, A and B, respectively. Despite the scatter between replicate samples in the PCA scores plot (Figure 5.4, A), a distinct non-linear spectral trend with crystallization temperature is indicated. For low crystallization temperatures (samples B0 to B4) a fairly linear decrease in the first principal component with crystallization temperature is observed. A curve in the trend occurs at samples B4 and B5, which are crystallized at 170 and 190 °C. The samples crystallized at higher temperatures (B6 and B7) follow a different trend, which is a decrease in the second principal component with crystallization

Figure 5.4:Plot of first and second principal component scores (**A**) and first and second principal component loading spectra (**B**), obtained from the principal components analysis of spectra (in region IV) of bulk PET samples crystallized for 5 minutes at different temperatures. For the scores plot (**A**), crystallization temperatures corresponding to different labels are as follows: B0: uncrystallized sample, B1: 110 ^{o}C, B2: 130 ^{o}C, B3: 150 ^{o}C, B4: 170 ^{o}C, B5: 190 ^{o}C, B6: 210 ^{o}C, B7: 230 ^{o}C. Primes on sample labels denote repacked samples. For the loading plots (**B**), the solid line is the first principal component loading and the dotted line is the second principal component loading.

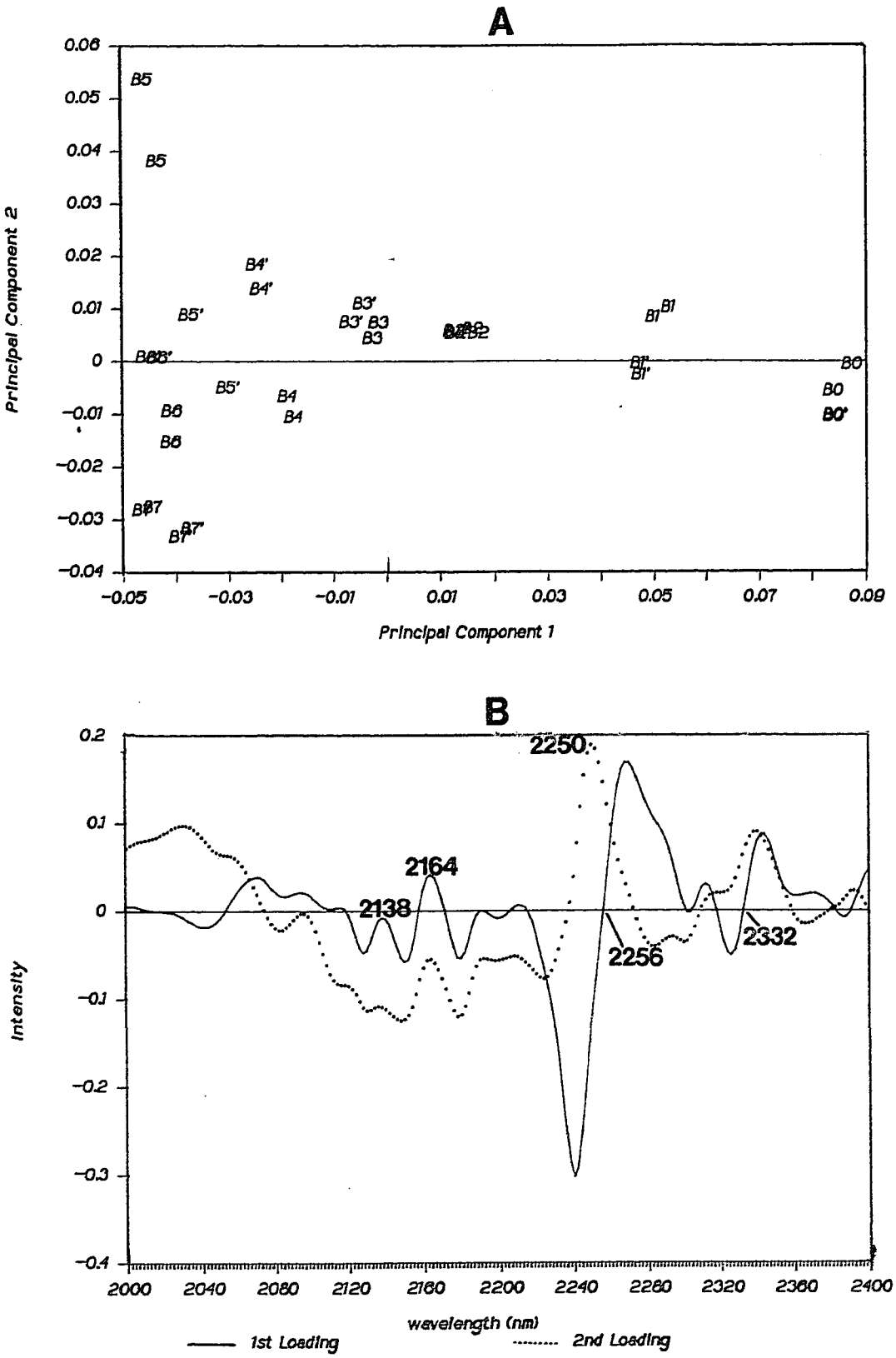
A
Principal Component 2
Principal Component 1
0.06
0.05
0.04
0.03
0.02
0.01
0
-0.01
-0.02
-0.03
-0.04
-0.05
-0.03
-0.01
0.01
0.03
0.05
0.07
0.09
B5
B5
B4'
B4'
B5'
B3'
B3' B3
B3
B1 B1
B1"
B1"
B0
B0
B0'
B5'
B4
B4
B6
B6
B7
B7
B7"
B7
B
Intensity
wavelength (nm)
0.2
0.1
0
-0.1
-0.2
-0.3
-0.4
2000
2040
2080
2120
2160
2200
2240
2280
2320
2360
2400
2250
2164
2138
2256
2332
1st Loading
2nd Loading

temperature. As a result, the scores plot indicates that two different spectral trends with crystallization temperature occur: one that dominates for crystallization temperatures below 170 to 190 °C, and one that dominates for higher crystallization temperatures. This result is in agreement with IR and thermal analyses of PET (10,19,20). To a first approximation, the first principal component (X-axis) is inversely related to the low crystallization temperature trend (affecting samples B0 to B5), and the second principal component (Y-axis) is inversely related to the high crystallization temperature trend (which affects samples B6 and B7).

The loading spectra for the first two principal components are shown in Figure 5.4, **B**. The most prominent features in the first principal component loading spectrum are first derivative features at 2256 nm and 2332 nm, where the strong ethylene combination bands (Table 5.2) are situated. These derivative features indicate negative energy band shifts with increasing principal component score 1, which correspond to positive energy shifts of these bands with crystallization temperature for low crystallization temperatures. This result indicates that the low crystallization temperature trend corresponds to an increase in the trans/gauche conformer ratio with crystallization temperature. As a result, the NIR spectral data support a crystal growth mechanism for the low crystallization temperature trend.

The first principal component loading spectrum shows features at 2138 nm and 2164 nm, where aromatic C-H combination bands

are found. These features suggest that aromatic C-H stretching and bending vibrations in the terephthalic acid part of the polymer are affected by crystal growth. Both the planar cis and planar trans configurations of the carbonyl groups about the aromatic ring in the TPA part of PET (refer to Figure 1.3) are possible in amorphous material (38), but only the planar trans configuration is observed in crystalline material (15). Because the aromatic vibrations in a given TPA segment are affected by the configuration of the neighboring carbonyl groups, a change in aromatic C-H combination absorbances with percent crystallininty is expected. In addition, the increase in intermolecular order associated with crystalline material probably perturbs the aromatic vibrations.

The structural origin of the high crystallization temperature trend is indicated by the second principal component loading spectrum (in Figure 5.4, B). The most distinguishing feature of the second principal component loading spectrum is the positive band at 2250 nm. Because this band is located at the high frequency side of the ethylene combination band in PET (Table 5.2), it indicates an increase in the trans conformer in the ethylene glycol unit with increasing principal component score 2. This result translates to a decrease in the trans/gauche ratio with crystallization temperature. This result is in agreement with results of earlier IR analyses of crystallized PET, in which the trans conformer content in the amorphous phase was found to decrease at crystallization temperatures above 170 ^{o}C (8).

There are several aspects of crystal perfection that could explain the observed high crystallization temperature trend. Earlier, it was proposed that depletion of tie chains (which are polymer chains that connect crystalline domains) occurs at high crystallization temperatures (8). It was also concluded that because these tie chains contain a disproportionately large fraction of trans conformers in the amorphous phase, loss of them would result in a decrease in the total number of trans conformers. The decrease in tenacity of PET fibers annealed at high temperatures supports this explanation, because tenacity of PET fibers is directly related to the number of tie chains (2).

If loss of tie chains occurs at high crystallization temperatures, a gain in other structural features (which contain more gauche conformers) must also occur. Sharpening of the phase interfaces between crystalline and amorphous material might cause an increase in the gauche conformer content. The sharpening of a phase interface corresponds to the narrowing of the interfacial region between amorphous and crystalline polymer, and requires an increase in the number of polymer chains that escape and re-enter the same crystallite (39). In order for a chain to escape and reenter the same crystallite, a turn or fold of the chain must be present. Because a chain fold must contain more gauche conformers than trans conformers, it is expected that an increase in chain folding (corresponding to a shapening of phase boundaries) would cause an overall increase in the number of gauche conformers.

5.3.4 Moisture Effect

The principal component scores for the analysis that uses normal spectra in region III are shown in Figure 5.5, A. The uncrystallized samples and the samples crystallized at 110 °C (samples B0 and B1) fall into tightly bound clusters. However, the scores for the samples crystallized at 130 °C and at higher temperatures indicate a significant and reproducible repacking effect. For sample B5, which is crystallized at 170 °C, the effect is not large. In all other cases, the effect is characterized by a decrease in the first principal component score as a result of repacking the sample. The trend with crystallization temperature, which is obscured by the repack effect, is an increase in the first principal component score.

The first principal component loading spectrum for region III is shown in Figure 5.5, B. The minimum at 1910 nm indicates that the first principal component corresponds to a decrease in the absorbance of the water band. Because the repack effect involves a decrease in the first principal component score, it correlates to an increase in the moisture content. Apparently, moisture originally present in the uncrystallized bulk PET is removed during crystallization at temperatures above 110 °C. Subsequent exposure of the samples to the atmosphere before original sampling and

Figure 5.5: Plot of the first principal component score versus sample number (**A**) and the first principal component loading spectrum (**B**), from the principal component analysis of spectra (in region III) of bulk PET samples crystallized for 5 minutes at different temperatures. Sample labels are identical to those used in Figure 5.4, **A**.

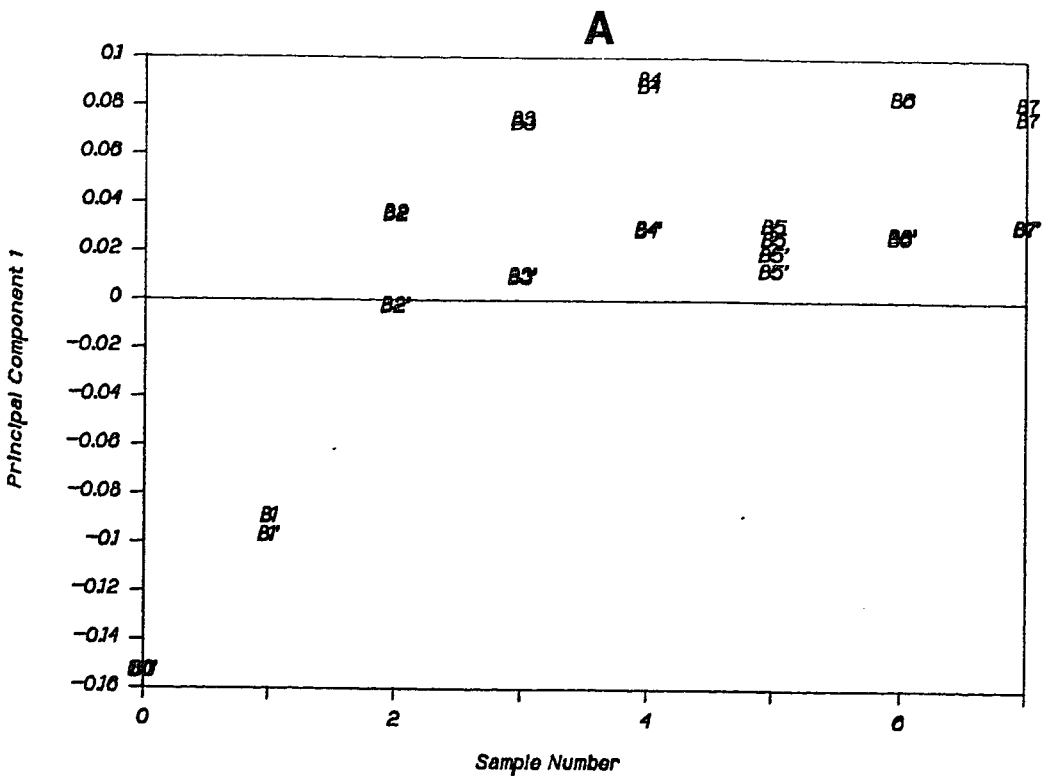
A
Principal Component 1
Sample Number
0.1
0.08
0.06
0.04
0.02
0
-0.02
-0.04
-0.06
-0.08
-0.1
-0.12
-0.14
-0.16
0
2
4
6
B1
B1'
B2
B2'
B3
B3'
B4
B4'
B5
B5'
B6
B6'
B7
B7'

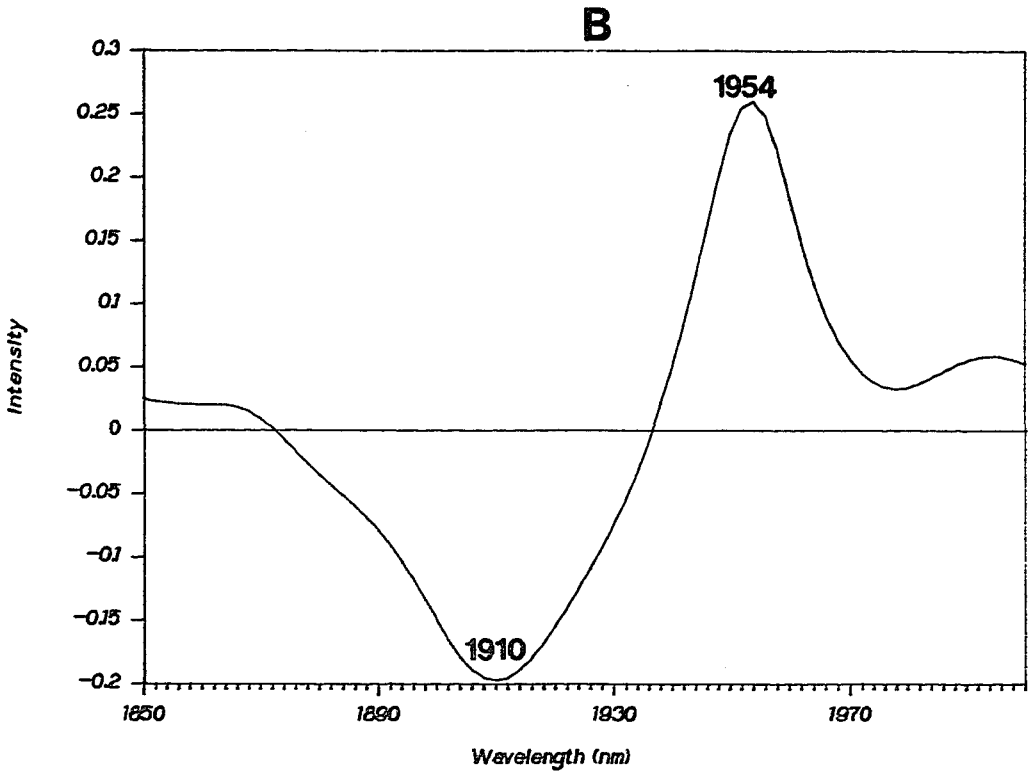
B
Intensity
Wavelength (nm)
0.3
0.25
0.2
0.15
0.1
0.05
0
-0.05
-0.1
-0.15
-0.2
1850
1890
1930
1970
1954
1910

during the repack procedure allowed the samples to absorb moisture from the air.

The sample vials used to contain the samples after crystallization and before NIR analysis and the reflectance sampling cup protected the samples from atmospheric moisture. However, the samples were exposed to the atmosphere during the transfer from sampling vial to sampling cup and during the repack procedure. The PCA results indicate that the samples absorb moisture from the atmosphere during the repack procedure. The anomalous behavior of sample B5 (Figure 5.5, A) might be caused by a leaky sample vial, which allowed the sample to absorb a significant amount of atmospheric moisture before NIR analysis.

There are two important implications of the observed moisture effect. The presence of water in the amorphous polymer might cause hydrolysis of the polymer during crystallization (1). However, the absorptivity of the 1908 nm water band is approximately 25 times higher than the absorptivity of the 1952 nm carbonyl band (40), and the intensities of these two bands in the spectrum of the amorphous PET (Figure 5.1, A) are comparable. Therefore, the amount of water in the amorphous polymer is rather small, and it is expected that only a small amount of hydrolysis occurred in the crystallized samples. In addition, regions I, II and IV are dominated by CH bands, and are therefore insensitive to the small amount of hydrolysis that might occur upon crystallization.

The second implication of the moisture effect is the ability of NIR spectroscopy to determine moisture in PET. The moisture content of the amorphous polymer before processing is a very important control variable in many applications. As mentioned before, water in the pre-processed polymer might cause hydrolysis of the polymer during high-temperature processing, which decreases the average molecular weight and therefore degrades the quality of the processed material (1).

5.3.5 PCA of Powder and Fiber Spectra

The ability of NIR spectroscopy to discriminate between orientation and crystallinity in PET is demonstrated by Principal Components Analysis of a data set comprising of both fibrous and bulk PET spectra. For analyses that use regions I,II, and IV, the optimal number of PCA factors is two (Table 5.4). Because the PCA analyses of bulk PET spectra alone also indicated the presence of two factors, it can be concluded that the same spectral trends in these regions used to describe variations in the bulk PET spectra can also be used to distinguish between fibrous and bulk PET spectra.

The scores and loading spectra for PCA analysis of normal spectra in region II are shown in Figures 5.6 A and B, respectively. The first principal component score is inversely related to the draw ratio (or percent extension) of the yarns, and discriminates between bulk and fibrous PET samples. As a result, the first principal

Figure 5.6: Plot of the second principal component score versus the first principal component score (A) and the first and second principal component loading spectra (B), from the principal components analysis of spectra (in region II) of both fibrous PET drawn to different extensions and bulk PET crystallized for 5 minutes at different temperatures. For the scores plot (A), sample labels are identical to those used in Figure 5.4, A and Table 5.1, and average principal component scores values for replicate samples are used for clarity. For the loading plot (B), the solid line is the first principal component loading and the dotted line is the second principal component loading.

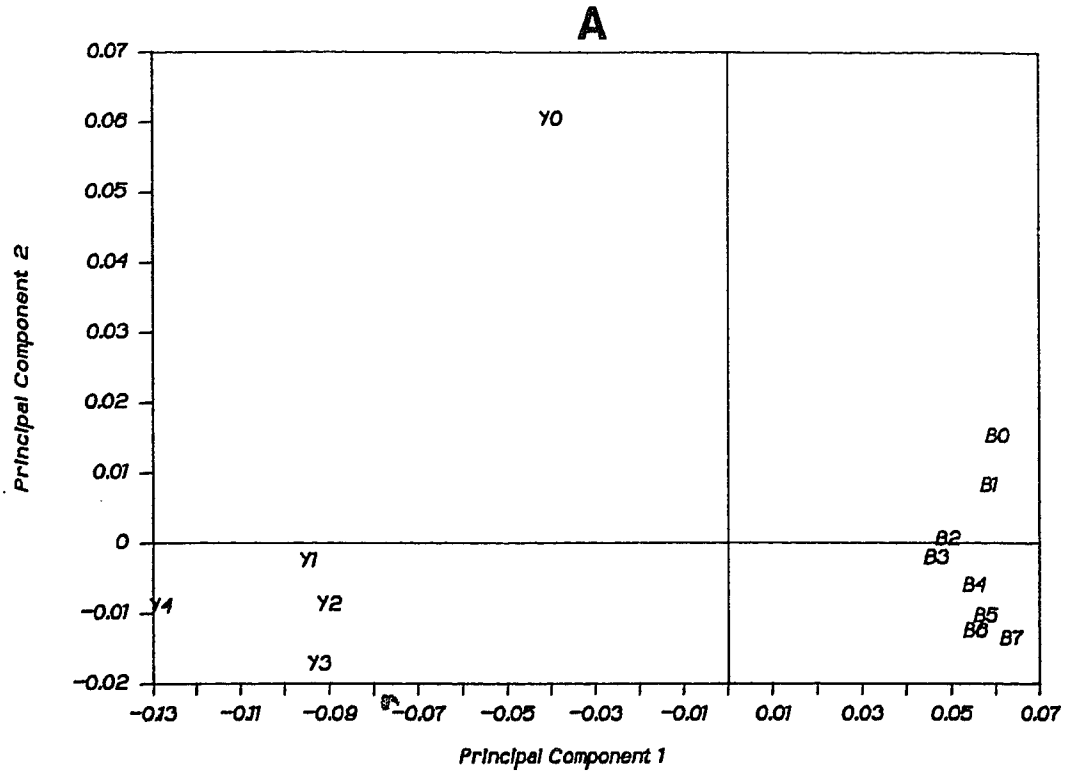
A
0.07
0.06
0.05
0.04
0.03
0.02
0.01
0
-0.01
-0.02
Y0
Y1
Y2
Y3
Y4
B0
B1
B2
B3
B4
B5
B6
B7
-0.13
-0.11
-0.09
-0.07
-0.05
-0.03
-0.01
0.01
0.03
0.05
0.07
Principal Component 2
Principal Component 1

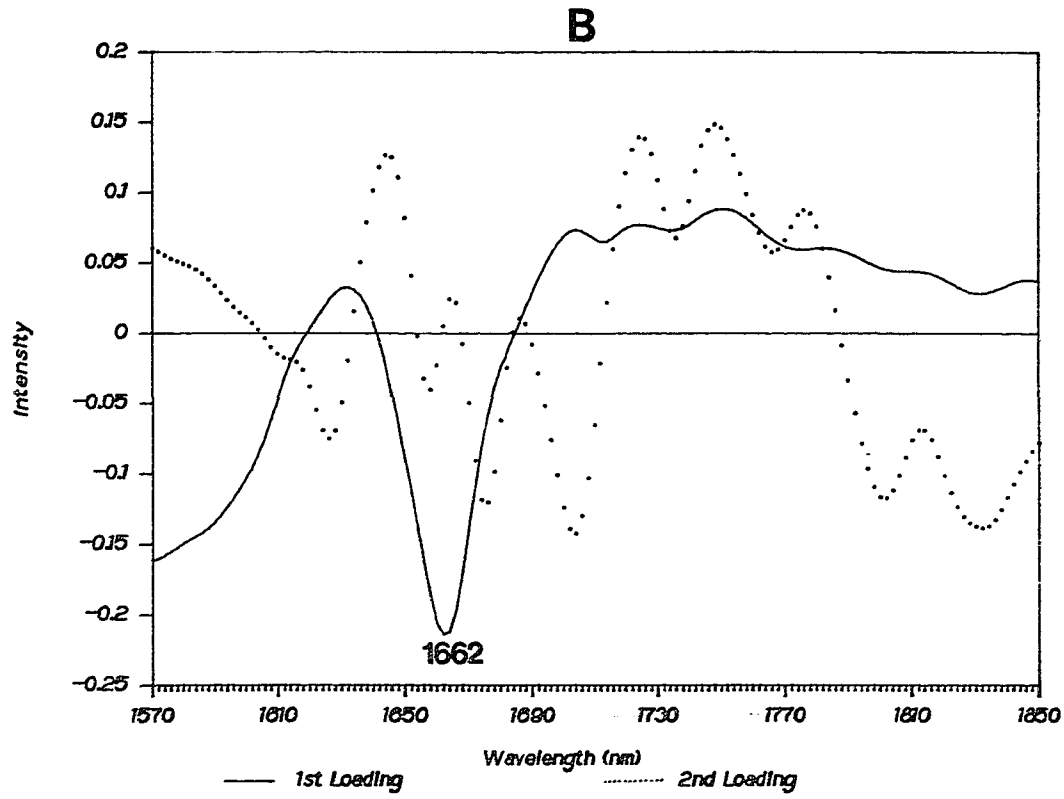
B
0.2
0.15
0.1
0.05
0
-0.05
-0.1
-0.15
-0.2
-0.25
1662
1570
1610
1650
1690
1730
1770
1810
1850
Intensity
Wavelength (nm)
1st Loading
2nd Loading

component is inversely related to chain orientation in the polymer. The second principal component score is inversely related to crystallinity of the PET yarns and inversely related to the low crystallization temperature trend for bulk PET samples. These results indicate that the second principal component is inversely related to crystallinity.

Note that the high crystallization temperature trend for the bulk PET samples, which involves samples B6 and B7 (Figure 5.6, A), corresponds to an increase in the first principal component score with increasing crystallization temperature. This result suggests that a structural trend involving decreased orientation can be used to describe the high crystallization temperature trend for crystallized bulk PET. This structural trend is most likely a decrease in the trans/gauche conformer ratio, which is consistent with results discussed earlier and with results of past IR analyses of PET (8).

The principal component loading spectra are shown in Figure 5.6, B. Because the spectral resolution in region II is significantly lower than in region IV, detailed structural information is difficult to obtain from the loading spectra. However, the two loading spectra show striking differences. The first loading, which describes spectral variation inversely related to orientation, is very featureless. The negative peak at 1662 nm is at the same position as the peak assigned to the first overtone aromatic C-H stretch (Table 5.2), and might indicate a sharpening of this band with increased orientation. However, it is probable that a large overlap of methylene and

aromatic C-H absorbances is present in this region. Therefore, it is quite possible that a change in the trans/gauche conformer ratio is also indicated in this loading spectrum. The second principal component loading spectrum, which indicates spectral changes inversely related to crystallinity, is very different from the first principal component loading spectrum. This loading spectrum indicates the sharpening or shifting of many absorbances in this region, which is indicative of an increase in intramolecular and intermolecular order caused by crystallization.

5.4 Conclusion

This study has shown that NIR spectroscopy can be used to perform rapid and accurate analyses of fibrous and bulk PET for various processing applications. Results of PLS calibrations for percent crystallinity in PET fibers and PCA analyses of spectra of fibrous and bulk PET indicate that NIR spectroscopy can characterize both intramolecular and intermolecular effects, and thus distinguish between crystallinity and orientation. Although other analytical methods are better-suited for detailed structural investigations, this work has shown that NIR spectroscopy is sensitive to the structural features in PET that influence the physical properties and quality of PET products.

5.5 Notes to Chapter 5

(1) *Modern Plastics*, **1987**, *64(10A)*, pp. 44-47.

(2) Samuels, R.T, in *Structured Polymer Properties*, Wiley-Interscience: N.Y., p211, 1974.

(3) Ward, I.M., *Chem. Ind. (London)*, **1957**, *1957*, 905.

(4) Farrow, G., Ward, I.M., *Polymer*, **1960**, *1*, 330.

(5) Schmidt, P.G., *J. Poly. Sci., A*, **1963**, *1*, 1271.

(6) Melveger, A,J., *J. Poly. Sci., A-2*, **1972**, *10*, 317.

(7) D'Esposito, L., Koenig, J.L., *J. Poly. Sci., Phys. Ed.*, **1976**, *14*, 1731.

(8) Lin, S-B., Koenig, J.L., *J. Poly. Sci., Phys. Ed.*, **1982**, *20*, 2277.

(9) Stokr, J., Schneider, B., Doskocilova, D., Lovy, J., Sedlacek, P., *Polymer*, **1982**, *23*, 714.

(10) Lin, S-B., Koenig, J.L., *J. Poly. Sci., Phys. Ed.*, **1983**, *21*, 2365.

(11) Fina, L.J., Koenig, J.L., *Macromolecules*, **1984**, *17*, 2572.

(12) Heuvel, H.M., Huisman, R., *J. Appl. Poly. Sci.*, **1985**, *30*, 3069.

(13) Zachmann, H.G., *Poly. Eng. and Sci.*, **1979**, *19*, 966.

(14) Fakirov, S., Fischer E.W., Hoffmann, R., Schmidt, G.F., *Polymer*, **1977**, *18*, 1121.

(15) Daubeny, R.P., Bunn, C.W., Brown, C.J., *Proc. Roy, Soc. A*, **1954**, *226*, 531.

(16) Palys, L.H., Phillips, P.J., *J. Poly. Sci., Phys. Ed.*, **1980**, *18*, 829.

(17) Burnshlegl, E., Bonart, R., *Colloid and Poly. Sci.*, **1980**, *258*, 319.

(18) Gupta, V.B., Kumar, S., *J. Appl. Poly. Sci.*, **1981**, *26*, 1865.

(19) Groeninckx, G., Reynaers, H., Berghmans, H., Smets, G., *J. Poly. Sci., Phys. Ed.*, **1980**, *18*, 1311.

(20) Groeninckx, G., Reynaers, H., *J. Poly. Sci., Phys. Ed.*, **1980**, *18*, 1325.

(21) Ito, E., Yamamoto, K., Kobayashi, Y., Hatakeyama, T., *Polymer*, **1978**, *19*, 39.

(22) Roberts, R.C., *Polymer*, **1969**, *10*, 117.

(23) Williams, P., Norris, K., *Near-infrared Technology in the Agricultural and Food Industries*; American Association of Cereal Chemists: St. Paul, MN, 1987.

(24) Weyer, L.G., *Appl. Spectrosc. Rev.*, **1985**, *21*, 1.

(25) Stark, E., Luchter, K., Margoshes, M., *Appl. Spectrosc. Rev.*, **1986**, *22*, 335.

(26) Norris, K., Williams, P.C., *Cereal Foods World*, **1979**, *24*, 459.

(27) Miller, C.E., *Appl. Spectrosc.*, **1989**, *43(8)*, 1435.

(28) Beebe, K., Kowalski, B.R., *Anal. Chem.*, **1987**, *59*, 1007A.

(29) Geladi, P., Kowalski, B.R., *Anal. Chim. Acta.*, **1986**, *185*, 1.

(30) Haaland, D.M., Thomas, E.V., *Anal. Chem.*, **1988**, *60*, 1202.

(31) Jolliffe, I.T., *Principal Component Analysis*, Springer-Verlag: New York, 1986.

(32) Brown, D.L., Weissert, J.T., Bhakuni, R.S., Rogowski, G.S., *U.S. Patent 4,654,253*, March 31, 1987.

(33) Geladi, P., MacDougall, D., Martens, H., *Appl. Spectrosc.*, **1985**, *39*, 491.

(34) Veltkamp, D., Kowalski, B.R., Center for Process Analytical Chemistry, BG-10, Seattle WA, 98195, *PLS-2 Block Modeling, Version 1.9*, (IBM), 1986.

(35) Sadler, D.M., Gilmer, G.H., *Polymer*, **1984**, *25*, 1446.

(36) Yoon, D-Y., Flory, P.J., *Faraday Discuss. Chem. Soc.*, **1979**, *68*, 288.

(37) Fischer, E.W., *Polymer J.*, **1985**, *17*, 397.

(38) Williams, A.D., Flory, P.J., *J. Poly. Sci., A-2*, **1967**, *5*, 417.

(39) Mandelkern, L., *Crystallization of Polymers*, McGraw-Hill: N.Y., 1964.

(40) Goddu, R.F., Delker, D.A., *Anal. Chem.*, **1960**, *32*, 140.

Chapter 6

Near-infrared Analysis of Polyether(urethaneurea) Block Copolymers

6.1 Bulk Composition

6.1.1 Introduction to Chapter 6.1

Segmented poly(ether urethane urea) (PEUU) copolymers, which are composed of alternating hard and soft blocks, are commercially useful materials with interesting properties worthy of fundamental investigation (1-6). The polyether soft block provides flexibility and elasticity to the polymer. The hard block, generally comprised of the reaction products of a diisocyanate and a low molecular weight diamine (Chapter 1.4.1), can non-covalently self-associate (or phase separate, see Chapter 1.3.2.5) to form domains that act as effective crosslinks and reinforce the polymers. The physical properties of these polymers greatly depend on the composition and the degree of phase separation.

Some physical properties of segmented PEUU copolymers can be measured directly by mechanical analyses (3,5,6). Other methods, such as thermal analysis (2,5,6), X-ray scattering (2), X-ray photoelectron spectroscopy (4) and FT-IR spectroscopy (3) also provide valuable information that can be used to probe composition and morphology. These techniques are useful for polymer analysis,

but require specific and careful sample preparation leading to long analysis times. For those situations where a rapid determination of chemical composition of polymers is required, near-infrared (NIR) spectroscopy can be valuable (7,8). Earlier NIR determinations of octane numbers in gasolines (9), functional groups in hydrocarbons (10), and ethylene and propylene contents in EPDM terpolymers (11) illustrate the ability of NIR spectroscopy to determine important compositional and structural properties.

In this chapter, the ability of near-infrared (NIR) diffuse reflectance spectroscopy to perform rapid bulk composition analyses of poly(ether urethane urea) (PEUU) block copolymers is demonstrated. The multivariate method of Classical Least Squares (CLS) (11,12) (Chapter 1.5.2.1) was used to relate NIR spectra to composition of the polymers.

6.1.2 Experimental

Materials: PEUU polymers were synthesized from 4,4'-methylenebis(phenylene isocyanate) (MDI), (The Upjohn Company), hydroxy-terminated poly(tetramethylene oxide) of approximately 2000 g/mol (PTMO-2000) (Quaker Oats Co.) and 1,3-propylenediamine (PD) (Aldrich). MDI and dimethylacetamide (DMA) (Burdick and Jackson Lab. Inc.) were vacuum-distilled. MDI was refrigerated until needed. PD was distilled under an argon blanket. PTMO-2000 was dried in a vacuum oven for 24 hours at

60°C. Dibutyltin dilaurate (ICN Pharmaceuticals, Inc.) was used as received.

Synthesis: A two step solution synthesis was used for the PEUU samples from MDI, PD and PTMO-2000 reactants. Synthesis of the 2:1:1 polymer will be described in detail as being representative of the procedure for the series. The 2:1:1 refers to the mole ratio of MDI to PD to PTMO-2000, respectively. A 3-necked 250 ml round bottom flask was set up with a mechanical stirrer, pressure-equalizing dropping funnel and argon inlet. To remove moisture, the glassware was flamed-out under argon. To MDI (4.14 g, 16.5 mmol) dissolved in DMA at room temperature, a solution of PTMO-2000 (16.55 g, 8.28 mmol) and 2 drops catalyst were added. The solution concentration was 10-15% w/v. The temperature was slowly raised to 60°C and maintained for 1 hour. After cooling back to room temperature, the dropping funnel was charged with a 5% solution of the diamine (0.614 g, 8.28 mmol) which was then added dropwise with rapid stirring. In all cases, the solution thickened considerably after about 80% of the diamine had been added, so more DMA had to be added to facilitate uniform mixing. After complete addition, the temperature was again raised to 60°C for about 4 additional hours. The product was then separated by precipitation into 600 ml methanol, filtered, rinsed five times in methanol and vacuum dried at 80°C for 12 hours. Additionally, to insure more complete removal of low molecular weight products, the polymers were redissolved in DMA and reprecipitated in methanol.

The basic structure of the polymers after an ideal reaction is shown in Figure 6.1.

A hard block model compound was prepared by reaction of a 1:1 molar mixture of MDI and PD. Pure PTMO-2000 was used as a soft block model. Six PEUU polymers were prepared using reaction stoichiometries of 1:0:1, 2:1:1, 3:2:1, 4:3:1, 5:4:1, and 6:5:1 (MDI:PD:PTMO-2000); these polymers were used as calibration samples. The percent (mass) of nitrogen in the six polymers, determined from elemental analysis (Huffman Laboratories, Golden CO), are shown in Table 6.1. The mass percent hard block value for each sample was obtained from the percent nitrogen value as follows: a calibration curve of mass percent hard block versus mass percent nitrogen for an ideal reaction was constructed, and this curve was used to determine experimental mass percent hard block values from experimental mass percent nitrogen values. The percent soft block value was determined as 100 minus the mass percent hard block value. It should be noted that this method of determining hard and soft block contents does not take into account the formation of side products in the polymers.

NIR Bulk Polymer Analysis: The PEUU samples were analyzed in the form that they existed immediately after synthesis and purification. The different polymer samples had different physical appearances and consistencies (e.g., fibrous, powdery). Each sample was packed in a sampling cup with a quartz window, and subsequently analyzed by the spectrometer.

Figure 6.1: Chemical structure of PEUU copolymers.

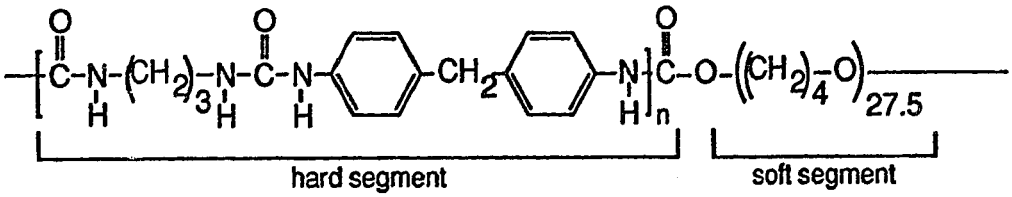
hard segment
soft segment

Table 6.1: Bulk compositions of PEUU samples.

TABLE 6.1

Sample Name	Experimental Mass Percent Nitrogen	Mass Percent Hard Segment[1]
1:0:1	1.27	11.3
2:1:1	2.25	16.8
3:2:1	4.16	27.4
4:3:1	5.36	34.0
5:4:1	6.25	38.9
6:5:1	6.89	42.5

[1] calculated from experimental mass percent nitrogen values

The near-infrared reflectance spectra of the six calibration samples, the hard block model, and the soft block model, were obtained using a Technicon InfraAlyzer 500C near-infrared reflectance spectrometer. The spectral range was 1100 nm to 2200 nm; the region 1350 nm to 1450 nm deleted because of instrumental anomalies. The wavelength accuracy was +/- 1 nm, and the nominal resolution was 10 nm. Four spectra of each sample were obtained, one spectrum each with the specimen in four different orientations in the spectrometer. Each individual scan lasted 1.5 minutes. In some cases, second derivative spectra were used (Technicon IDAS software, Tarrytown NY).

Data Analysis- Bulk Polymers: CLS calibrations were constructed from both log(1/reflectance) and second derivative log(1/reflectance) NIR spectra of the bulk polymers. In each case, the method of multiplicative scatter correction (MSC) was used to correct the spectra for multiplicative and baseline effects before CLS calibration (13,14). Replicate samples were treated separately in the calibration procedure. All calibrations were evaluated using the Standard Error of Estimate (SEE) value (Chapter 1.5.2.3.2, Equation 1.16).

6.1.3 Results and Discussion

6.1.3.1 Calibration Results

The SEE for the CLS calibration for percent hard block in the PEUU copolymers is 2.6 % mass if normal NIR spectra are used and 2.5 % mass if second derivative NIR spectra are used. This result indicates that the NIR spectroscopic method can determine bulk composition within 2.5% mass over a range of 31% mass. Second derivative NIR spectra provide better results than uncorrected spectra, because the second derivative operation reduces sampling effects and improves spectral resolution. Because percent hard and soft block values are inversely proportional, calibration errors for both quantities are equal for a given calibration. These calibration results are encouraging, because they indicate that rapid, accurate analyses of bulk polymers can be performed.

In order to further assess the ability of NIR spectroscopy to perform bulk polymer analyses, the sources of errors in the calibrations were investigated. Calibration errors can be caused by errors in the spectral data or by errors in the elemental analysis data for the polymers. Errors in the spectral data might arise from non-linear absorbances, instrumental anomalies, or inadequate removal of sampling effects by MSC. Errors in the reference hard and soft block concentration data might result from random errors in elemental analysis results. However, systematic errors in the reference hard and soft block concentrations might result from the presence of side products in the polymers, which is not accounted for in the determination of hard and soft block concentrations from percent nitrogen data.

The calibration curve for percent hard block that used second derivative spectra is shown in Figure 6.2. Note that the points that correspond to replicate samples fall into tightly-bound clusters with deviations of approximately 1 to 3 % mass, which are similar or lower than the overall calibration error of 2.5% (see Table 6.1). This result indicates that sampling errors, caused by a combination of baseline shifts, multiplicative spectral effects, and sample non-homogeneity, contribute only a fraction to the calibration error. It should also be noted that the calibration error is not distributed equally over all of the samples. The clusters for the 4:3:1 and 5:4:1 samples are located far from the calibration line, but the other clusters are close to the line. This result indicates the presence of two possible error sources in the calibration: 1) non-representative sampling of the 4:3:1 and 5:4:1 samples, or 2) the presence of unexpected side products in these samples. It is unlikely that differences in phase separation of these samples is responsible for the error, because the effect of phase separation on the NIR spectra of these polymers is small (15).

The sources of error in the CLS calibrations can be investigated by comparison of CLS-estimated spectra of the hard and soft blocks in the polymer with spectra of hard and soft block model compounds. If non-representative sampling is the source of the calibration error, systematic errors in the CLS-estimated spectra will be present. These errors are indicated by the presence of bands from groups in the hard block in the CLS-estimated soft block spectrum, and vice

Figure 6.2: Calibration curve for CLS calibration for percent hard block that uses second derivative NIR spectra.

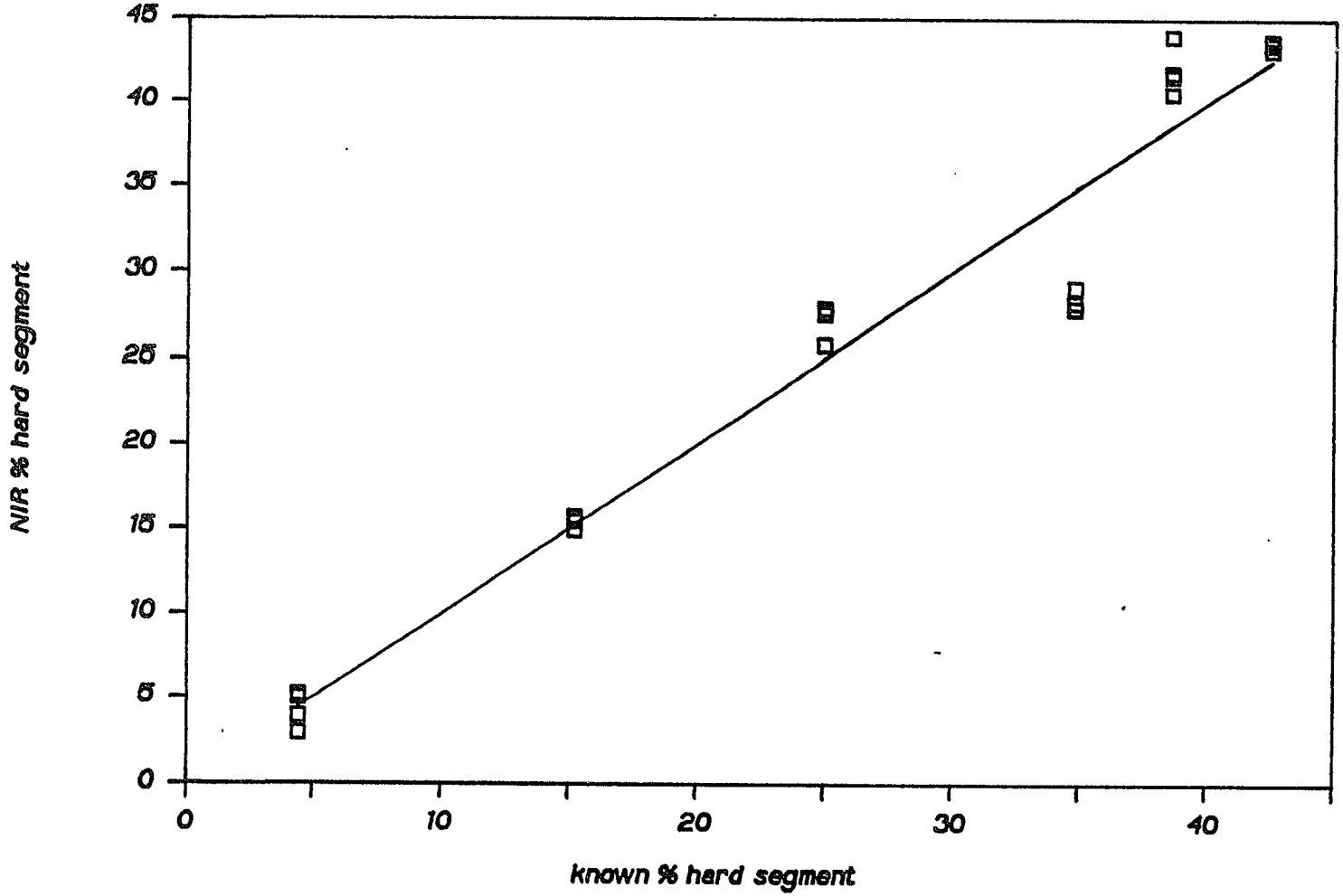
45
40
35
30
25
20
15
10
5
0
0
10
20
30
40
NIR % hard segment
known % hard segment

versa. If the presence of side products is the source of the calibration error, spectral features from the side products, not present in the spectra of the model compounds, will be present in the CLS-estimated spectra. Furthermore, if it is assumed that side product formation primarily affects urea and urethane groups in the polymers, only the regions of carbonyl and N-H absorption (1450 nm to 1600 nm and 1900 nm to 2100 nm) (7,16,17) will be affected by side product formation.

Figure 6.3 shows the CLS-estimated spectrum and model compound spectrum for the hard block and soft block. Comparison of the estimated spectrum of the hard block in the polymer (Figure 6.3, **B**) and the hard block model spectrum (Figure 6.3, **A**) reveals significant differences in the C-H stretching overtone region (1650 nm to 1800 nm) and the N-H and carbonyl absorption region (1900 nm to 2100 nm). The band at 1748 nm in the estimated hard block spectrum, which is at the same position as a band in the soft block model spectrum (Figure 6.3, **C**), indicates the occurrence of non-representative sampling. In the carbonyl and N-H region (1900 nm to 2100 nm), a shoulder at 1920 nm in the hard block model spectrum (Figure 6.3, **A**) is not present in the estimated hard block spectrum (Figure 6.3, **B**). Although this difference might be caused by a difference in the morphology of the hard block model and the hard block in the polymers, it might also indicate the presence of side products in the polymers.

Figure 6.3: *upper plot-* NIR diffuse reflectance spectrum of the hard block model polymer (**A**), and the CLS-estimated spectrum of the hard block in PEUU copolymer (**B**); *lower plot-* NIR diffuse reflectance spectrum of the soft block model polymer (**C**), and the CLS-estimated spectrum of the soft block in PEUU copolymer (**D**).

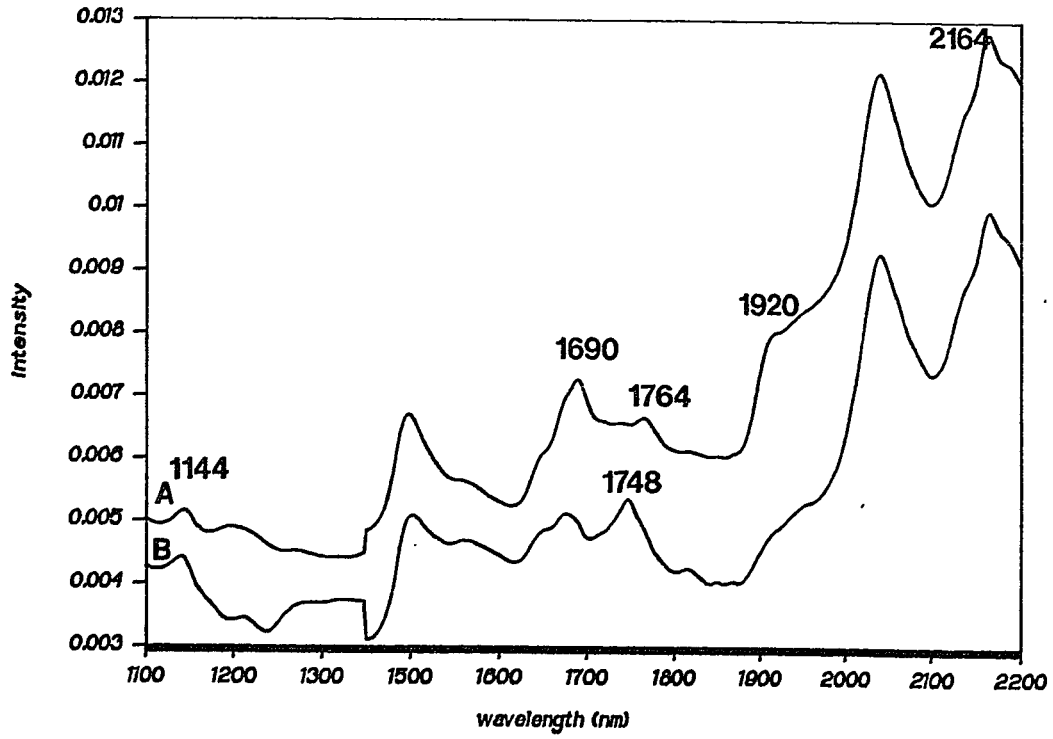
0.013
0.012
0.011
0.01
0.009
0.008
0.007
0.006
0.005
0.004
0.003
Intensity
2164
1920
1690
1764
1144
1748
A
B
1100
1200
1300
1500
1600
1700
1800
1900
2000
2100
2200
wavelength (nm)

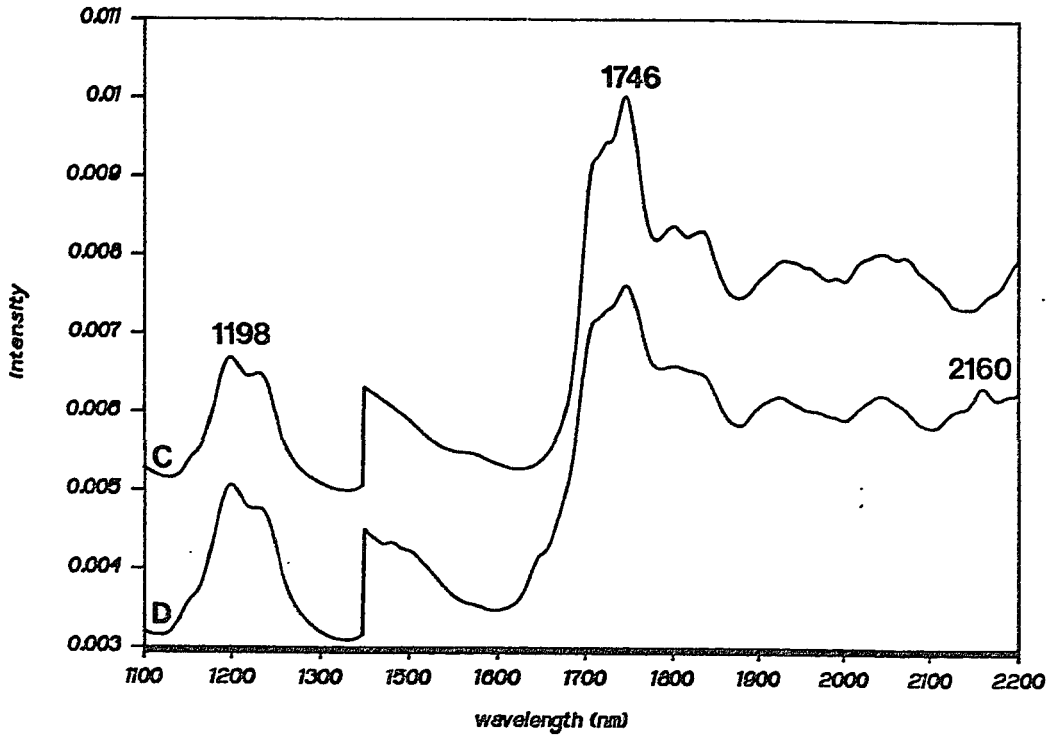
0.011
0.01
0.009
0.008
0.007
0.006
0.005
0.004
0.003
Intensity
1746
1198
2160
C
D
1100
1200
1300
1500
1600
1700
1800
1900
2000
2100
2200
wavelength (nm)

The estimated soft block spectrum (Figure 6.3, **D**) and soft block model spectrum (Figure 6.3, **C**) are very similar. However, the band at 2160 nm in the estimated soft block spectrum, which is in approximately the same position as the 2164 nm band in the hard block model spectrum (Figure 6.3, **A**), is a clear indication of non-representative sampling. Other differences between the soft block spectra in Figure 6.3, **C** and **D** might be weaker indicators of non-representative sampling, or results of morphological differences between the soft block model and the soft block in the polymers. In summary, comparison of CLS-estimated spectra and model compound spectra indicate the occurrence of non-represenataive sampling, and possibly the presence of side products in the polymers. Additional results from a reference method that measures functional group concentrations (e.g., NMR or IR spectroscopy, might allow identification and determination of side products.

6.1.3.2 Band assignments

Although NIR bands are highly-overlapped, assignments of NIR absorptions to specific functional groups can be made. NIR bands at 1144 nm, 1690 nm and 2164 nm in the hard block model spectrum (Figure 6.3, **A**) correspond to the second overtone, first overtone, and combination bands of the aromatic C-H stretch in the MDI unit. These bands are in close proximity to aromatic C-H bands present in the NIR spectra of polystyrene (7). The absorbance at 1764 nm,

which is in the region of previously observed bands in the NIR spectra of aliphatic hydrocarbons (7,10) and ethylene-propylene-diene terpolymers (11) (Chapter 3), are from the methylene group in the MDI unit and from methylene groups in the chain extender (1,3 propylenediamine). Absorbances in the region 1450 nm to 1600 nm arise from overlapped N-H stretching first overtone bands and second overtone carbonyl stretching bands. The region 1900 nm to 2100 nm also contains contributions from combination N-H stretching and amide bands and from second overtone carbonyl stretching bands. Absorptions in these regions are observed in NIR spectra of proteins (7,16) and amino acids (17). More detailed assignments of absorbances in the region 1900 nm to 2100 nm are made in Chapter 6.2.

The NIR spectrum of the soft block model (Figure 6.3, C) is dominated by methylene stretching overtone bands. The absorbances in the region of 1198 nm are second overtone methylene stretching bands, and the absorbances at 1746 nm are first overtone methylene stretching bands. Similar absorbances are observed in spectra of ethylene-propylene-diene terpolymers (11) and of aliphatic hydrocarbons (7,10). Note that these absorbances are not highly-overlapped with absorbances from aromatic C-H groups in the hard block (Figure 6.3, A and B). As a result, accurate determinations of hard and soft block concentrations are possible.

6.1.4 Conclusion for Chapter 6.1

This analysis has shown that rapid composition determinations of bulk PEUU polymers can be made using NIR diffuse reflectance spectroscopy. The method of CLS provided accurate calibrations of NIR spectra to hard block and soft block fractions in the polymers. The observed calibration errors were caused by non-representative NIR sampling of the polymers. It is also possible that the presence of side products in the polymers contributed to the calibration errors.

6.2 Phase Separation

6.2.1 Introduction to Chapter 6.2

Phase separation in PEUU block copolymers can be probed by several different analytical methods. Mechanical studies (5,6), X-ray methods (2,4,18-20), thermal analysis methods (2,5,18,21), FT-IR spectroscopy (3,6,18-22) and NMR spectroscopy (5) have been used to determine the nature and extent of phase separation in PEUU copolymers and similar systems. Although these methods provide specific information about phase separation, they usually require extensive sample preparation and long analysis times. In contrast, near-infrared (NIR) spectroscopy can rapidly analyze bulk materials (7,8,11,23).

In earlier IR studies of phase separation in diol-extended polyurethanes (18,19,21,22), the primary band of interest is the fundamental stretching band of the urethane carbonyl group. Changes in the relative magnitude of absorbances from the free carbonyl group and from carbonyl groups hydrogen-bonded to N-H groups are used to monitor phase separation. The carbonyl group is a good indicator of phase separation in these polymers because self-association of hard blocks involves intermolecular hydrogen bonding of urethane carbonyl groups to urethane N-H groups. In contrast, the phase-mixed state has a large number of urethane N-H groups hydrogen-bonded to ether oxygens in the soft block and a significant number of free carbonyl groups. Although other IR bands have been used to monitor phase separation (21), the carbonyl band is the most affected by phase separation.

Spectral analysis of phase separation of PEUU block copolymers is slightly more complex than for diol-extended block polyurethanes. These copolymers (Figure 6.1) contain urea carbonyl groups, which are at the interior of hard blocks, and urethane carbonyl groups, which are located at the boundaries of hard and soft blocks. The urea carbonyl groups are, therefore, sensitive to hard block aggregation and changes in hard block domain structure. In contrast, the urethane carbonyl groups are more sensitive to effects at the phase boundaries. As a result, spectral analysis of urea and urethane carbonyl groups can distinguish between processes involving phase boundaries and those involving the interior of hard block domains.

Phase separation analysis by NIR spectroscopy relates the spectral shifts of overtone stretching bands with changes in hydrogen bonding states of urethane and urea carbonyl groups. Although the effects of hydrogen bonding on the fundamental transitions of carbonyl vibrations (observed in IR spectra) have been well-characterized (24), effects on overtone transitions (observed in NIR spectra) are less characterized. In addition, because of the broadness of NIR bands relative to IR bands, assignment of NIR absorbances to specific functional groups is difficult. With these considerations in mind, the positions of NIR urea and urethane carbonyl bands are best determined by analysis of model compounds.

In this work, the ability of NIR spectroscopy to monitor phase separation in PEUU copolymers is investigated. Spectra of model compounds are used to assign second overtone bands for free urethane and urea carbonyls, and these bands are used to monitor phase separation.

6.2.2 Experimental

Sample Preparation: The synthesis of PEUU samples is discussed in Chapter 6.1.2. The chemical structure of the PEUU block copolymers used in this work is shown in Figure 6.1. PEUU samples 2:1:1, 4:3:1, and 6:5:1 were dissolved to approximately 4% (w/v) in N,N'-dimethylacetamide (DMA). For each analysis, approximately 3

mL of solution was placed in a Teflon casting dish and vacuum-dried for 8 to 9 days at room temperature to remove the solvent. The polymer film was then placed in a sealed sample cell with a ceramic background and a quartz window (see Figure 6.4). The sample was sealed from the environment by placing a rubber O-ring between the quartz and ceramic and applying pressure on 2 stainless steel cover rings with screws. The sample remained in the cell until the completion of annealing and NIR scanning. When necessary, the sealed sample was conveniently placed in the reflectance spectrometer for NIR analysis.

The film was annealed in an oven at 100 ^{o}C. NIR scans were taken before annealing and after 11 different total annealing times (up to 70 hours). After each annealing interval, the sample was removed from the oven and allowed to cool at room temperature for 30 minutes before NIR scanning.

Model Compunds: Model compounds were used to study the effects of hydrogen bonding on urethane and urea carbonyl groups. The urethane model was the reaction product of methylene diphenyl isocyanate (MDI) with ethanol (Figure 6.5, I), and the urea model was 1,3-diethylurea (II) (Aldrich). Diffuse reflectance NIR spectra of the model compound powders were obtained using a diffuse reflectance sampling cup that was specially designed for small samples (25). NIR spectra of THF (Baker) solutions of the model compounds (approximately 1% w/v) were obtained using a sealed glass cuvette. The spectra of the model compounds in THF

Figure 6.4: Diagram of the sample cell used to contain polymer films for annealing and NIR scanning.

Top View

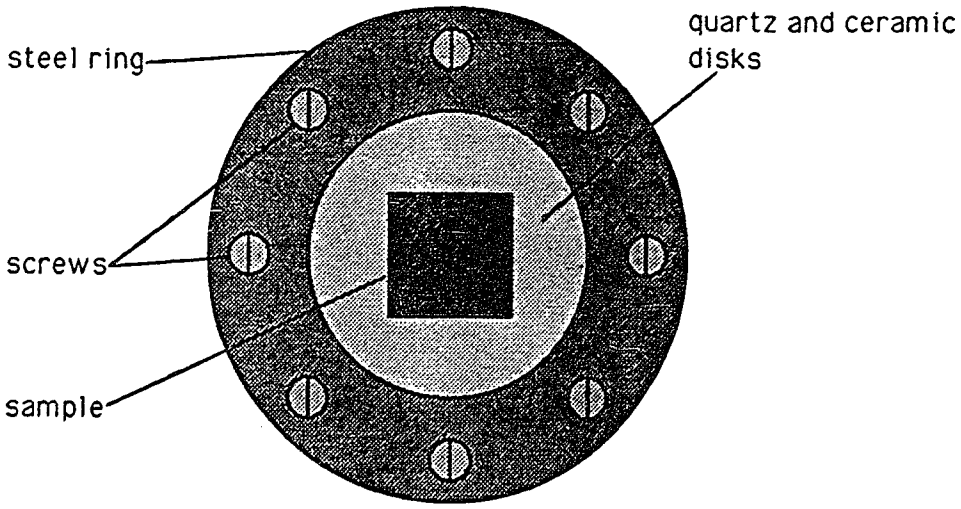

Side View

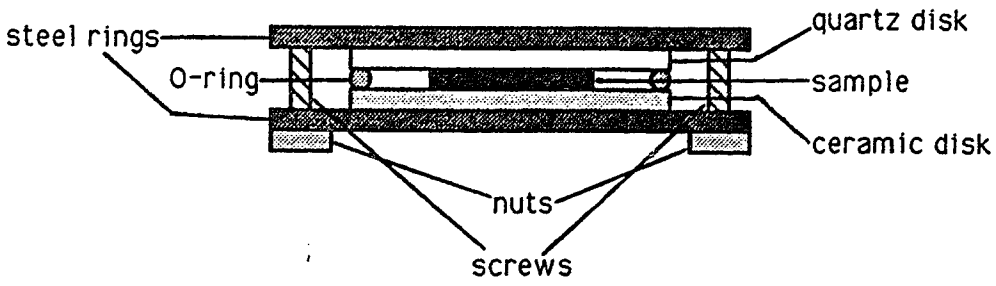

Figure 6.5: Chemical structures the urethane model compound (I), and the urea model compound (II).

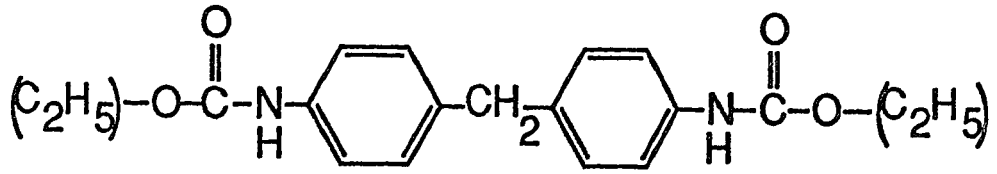

I

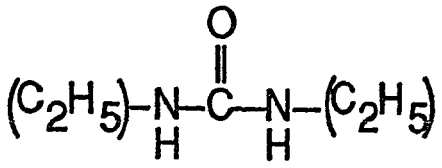

II

solution were obtained by subtraction of the solvent spectrum from the solution spectrum until prominent solvent peaks disappeared.

Spectroscopy: All NIR spectra were obtained using a Technicon InfraAlyzer 500C NIR reflectance spectrometer (Chapter 1.2.4.2). Although the total spectral range used was 1100 nm to 2500 nm, only the region 1800 nm to 2100 nm was used for phase separation analysis. The wavelength accuracy of the instrument was +/- 1 nm, and the nominal resolution was 10 nm. Each scan lasted about 1.5 minutes. Each solution spectrum was obtained by averaging 9 replicate scans of the solution.

6.2.3 Results and Discussion

NIR spectra of the urethane model compound (in the spectral region 1800 nm to 2100 nm) in bulk and in THF solution are shown in Figure 6.6, **A** and **B**. This region of the NIR spectrum is dominated by second overtone carbonyl stretching bands and N-H combination bands (8,23). In the spectrum of the bulk material (Figure 6.6, A), the only strong absorbances are at wavelengths above 1960 nm. The band at 1980 nm might be a second overtone band for a hydrogen-bonded carbonyl in the bulk material. Upon dissolution in THF, a strong band at 1918 nm appears, and the 1980 nm band disappears. In the dilute solution, it is assumed that all N-H groups in the material are bound to solvent molecules, and the carbonyl groups should be free from hydrogen bonding. Therefore, the 1918 nm

Figure 6.6: *upper plot-* NIR diffuse reflectance spectrum of the solid urethane model compound (**A**), and the NIR spectrum of the urethane model compound diluted 1% (w/v) in THF (**B**); *lower plot-* NIR diffuse reflectance spectrum of the solid urea model compound (**C**), and the NIR spectrum of the urea model compound diluted 1% (w/v) in THF (**D**).

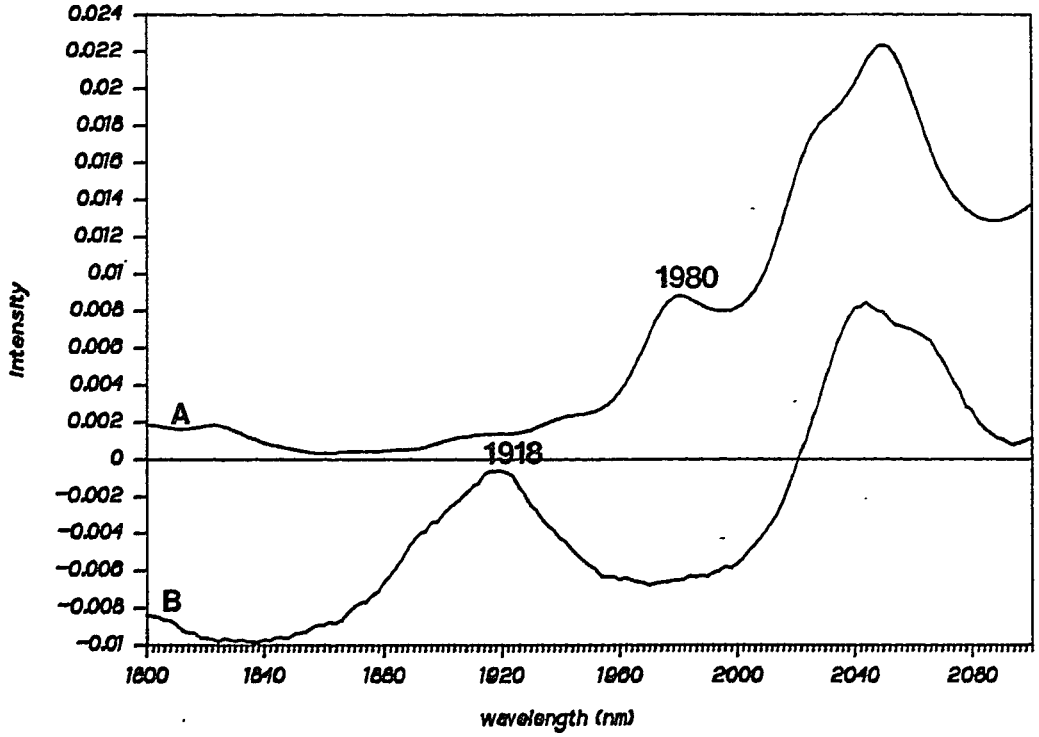
0.024
0.022
0.02
0.018
0.016
0.014
0.012
0.01
0.008
0.006
0.004
0.002
0
-0.002
-0.004
-0.006
-0.008
-0.01
Intensity
1980
A
1918
B
1800
1840
1880
1920
1960
2000
2040
2080
wavelength (nm)

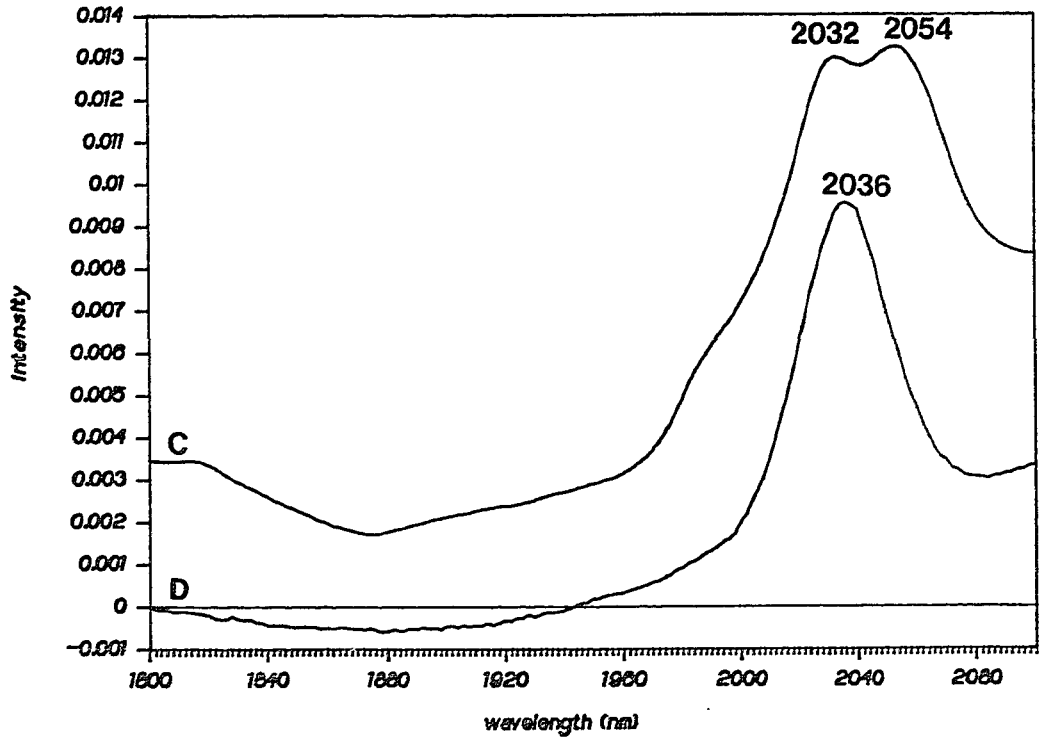
0.014
0.013
0.012
0.011
0.01
0.009
0.008
0.007
0.006
0.005
0.004
0.003
0.002
0.001
0
-0.001
Intensity
2032
2054
2036
C
D
1800
1840
1880
1920
1960
2000
2040
2080
wavelength (nm)

band can be assigned to the second overtone band of the free urethane carbonyl. Although the 1980 nm band in the bulk urethane spectrum is probably a second overtone band from a bound urethane carbonyl, it corresponds to a specific type of hydrogen bond present in the specific structure of the bulk urethane model. Because the hydrogen bond geometry of urethane carbonyls in the PEUU copolymers might be substantially different than in the bulk urethane model compound, use of this band for phase separation analysis is avoided.

Similar spectra for the urea model compound are shown in Figure 6.6, **C** and **D**. Overlapped bands at 2032 nm and 2054 nm are observed in the spectrum of the bulk urea model (**C**). However, only a single absorbance at 2036 nm is observed in the spectrum of the urea model dissolved in THF (**D**). As a result, the 2036 nm absorbance is assigned to the second overtone of the free urea carbonyl. The 2054 nm band in the spectrum of the bulk urea model compound probably corresponds to a specific hydrogen-bonded state of the urea carbonyl group.

Assignments of the NIR bands from urea and urethane carbonyls are confirmed by estimating overtone vibrational frequencies from previously assigned fundamental vibrational frequencies (3). To a first order approximation, second overtone bands occur at frequencies three times that of the fundamental band. Table 6.2 shows the estimated positions of second overtone carbonyl bands (in nanometers). A close agreement with results obtained

Table 6.2: Estimated and observed positions of second overtone carbonyl bands for PEUU copolymers.

Table 6.2

group	observed wavelength (nm)	estimated wavelength[2] (nm)
free urea carbonyl	2036	2020
hydrogen-bonded urea C=O	2054[1]	2034
free urethane carbonyl	1918	1922
hydrogen-bonded urethane C=O	1980[1]	1960

[1] denotes bands corresponding to specific hydrogen bonds in bulk model compounds

[2] calculated as 3 times the frequency of an assigned IR band (reference 5)

from model compound analysis is observed. The discrepancies between observed and estimated band positions is attributed to positive anharmonicity of the carbonyl vibrations, which commonly causes estimated NIR band positions to be blue-shifted from actual band positions (7).

NIR spectra of the 6:5:1 film before annealing and after several annealing times are shown in Figure 6.7. Although the spectral trends with annealing are not obvious from this plot, the spectral regions that change with annealing are identified. Changes in absorbances in the region of the assigned free urethane carbonyl band (1918 nm) are quite large. Weaker changes in the free urea carbonyl absorbance at 2036 nm are also observed. In contrast, absorbances in the C-H stretching first overtone region (1600 nm to 1800 nm) are relatively unaffected by annealing. Differences in spectral baselines are caused by non-reproducible sample placement in the spectrometer or by changes in the refractive indices of the film with phase separation. As a result, the absorbance at 1800 nm is used as a baseline reference for subsequent analyses.

Figure 6.8, A shows the free urea carbonyl absorbance at 2036 nm plotted as a function of annealing time for the three PEUU films. The absorbance for each film at time zero is arbitrarily set to zero. In each case, the free urea carbonyl absorbance decays continuously with annealing. The parameters obtained from the fit of an exponential function to these annealing profiles are shown in Table 6.3. The A parameter, which is the magnitude of the decay, indicates

Figure 6.7: NIR spectra of the 6:5:1 polymer film before annealing, and after annealing times of 20 min., 1 hr., 4 hr., 24 hr., and 70 hr.

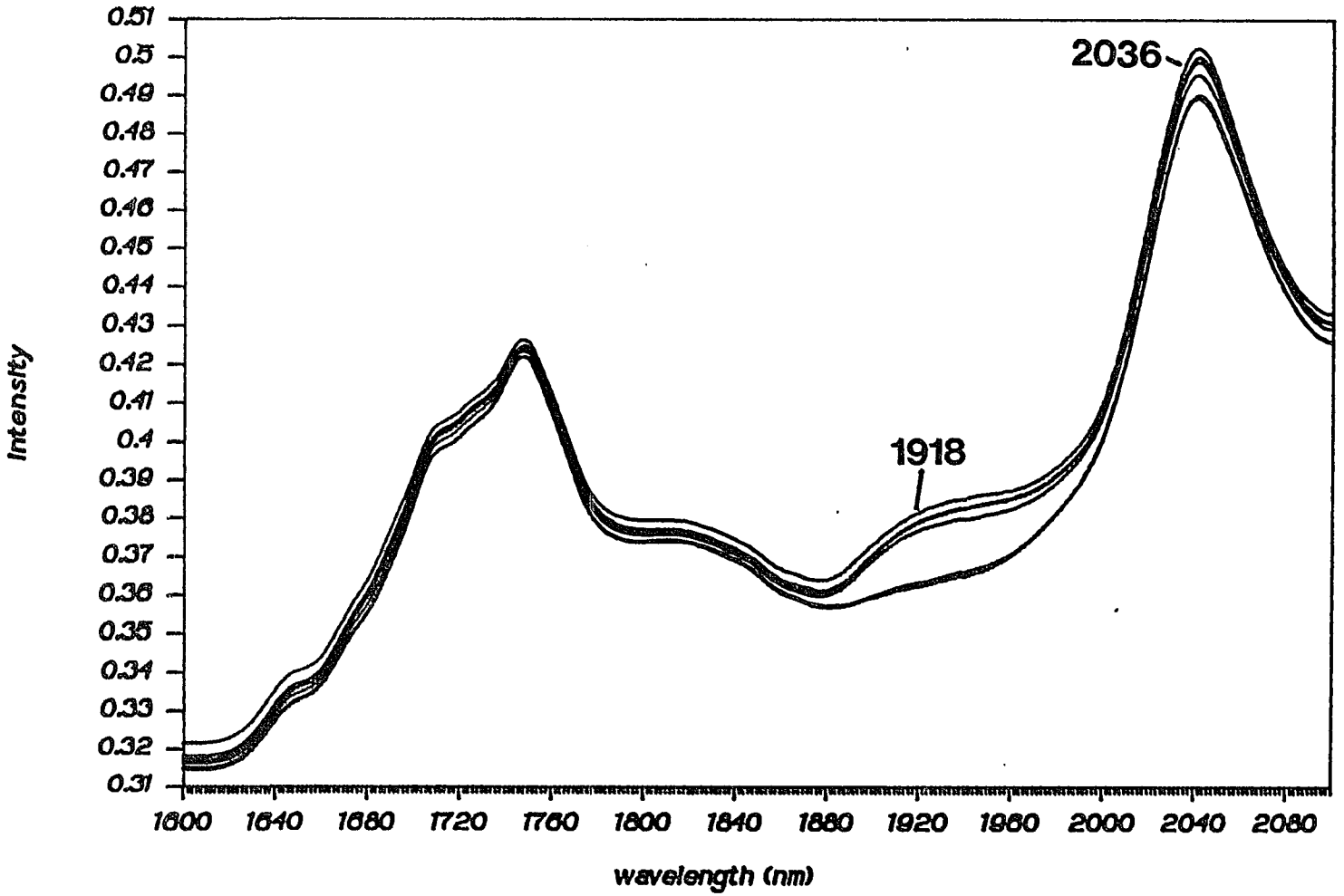
0.51
0.5
0.49
0.48
0.47
0.46
0.45
0.44
0.43
0.42
0.41
0.4
0.39
0.38
0.37
0.36
0.35
0.34
0.33
0.32
0.31
Intensity
2036
1918
1600
1640
1680
1720
1760
1800
1840
1880
1920
1960
2000
2040
2080
wavelength (nm)

Figure 6.8: Absorbance at 2036 nm (**A**) and at 1918 nm (**B**) versus annealing time at 100 ^{o}C for all three PEUU copolymer films. For plot **A**, the absorbance at 2036 nm at time zero is arbitrarily set to zero for each sample.

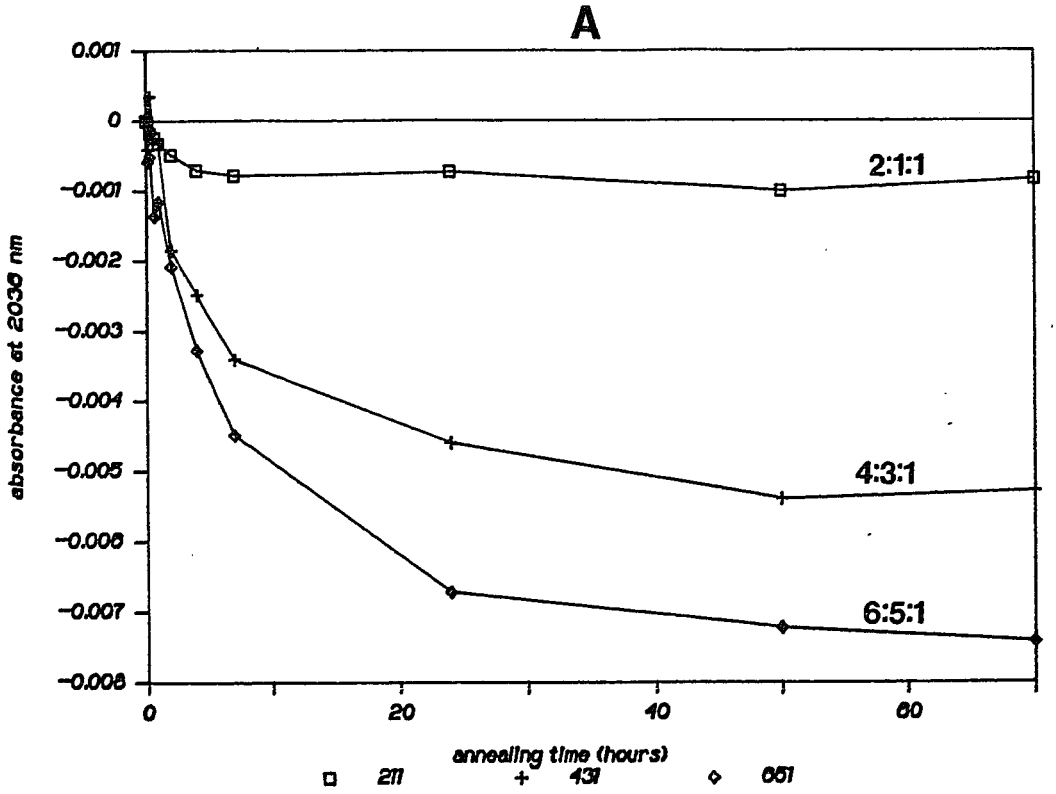
A
absorbance at 2030 nm
0.001
0
-0.001
-0.002
-0.003
-0.004
-0.005
-0.006
-0.007
-0.008
0
20
40
60
annealing time (hours)
2:1:1
4:3:1
6:5:1
211
431
651

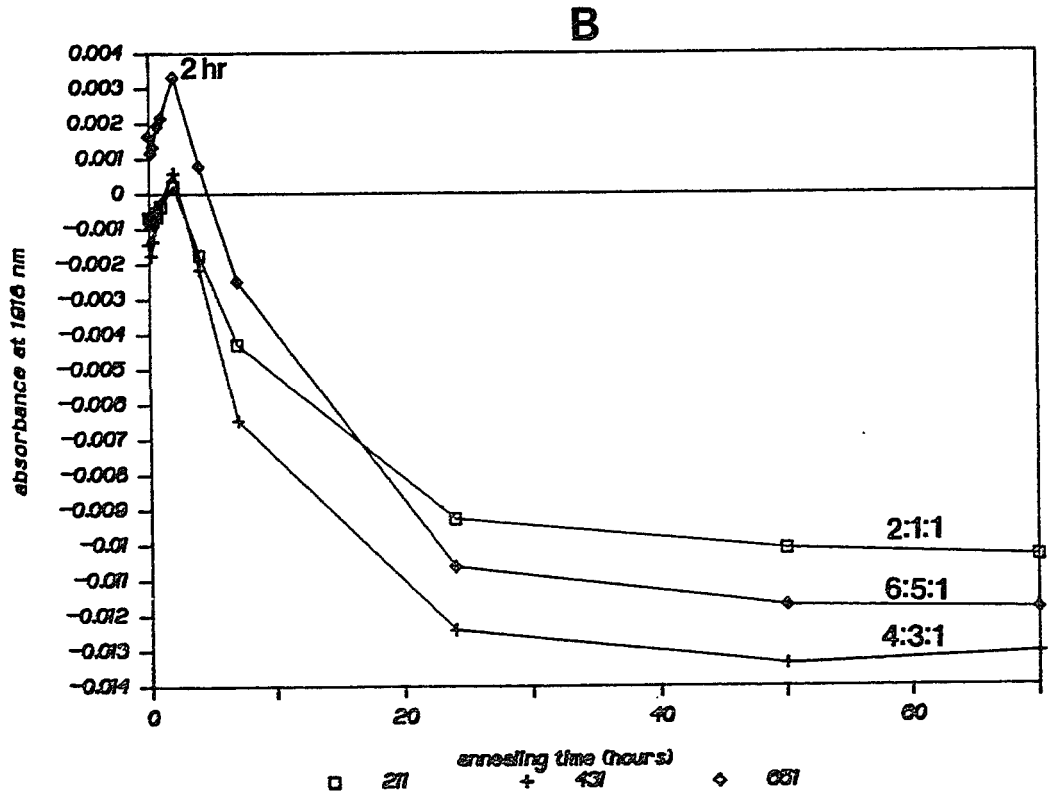
B
absorbance at 1616 nm
0.004
0.003
0.002
0.001
0
-0.001
-0.002
-0.003
-0.004
-0.005
-0.006
-0.007
-0.008
-0.009
-0.01
-0.011
-0.012
-0.013
-0.014
2 hr
0
20
40
60
annealing time (hours)
2:1:1
6:5:1
4:3:1
211
431
651

Table 6.3: Results of exponential fits to 100 °C annealing profiles.

Table 6.3

2036 nm absorbance : fit function = $A*\exp(-k_1 t)$
1918 nm absorbance : fit function = $B*(1-\exp(-k_2 t)) + C*\exp(-k_3 t)$;

	PEUU Sample		
Parameter	2:1:1	4:3:1	6:5:1
A	0.00084	0.0053	0.0069
$k_1(hr^{-1})$	0.44	0.17	0.14
B	0.0072	0.020	0.011
$k_2(hr^{-1})$	0.53	0.48	0.48
C	0.016	0.031	0.024
$k_3(hr^{-1})$	0.14	0.20	0.13

the magnitude of change in the free urea carbonyl absorbance with annealing. This parameter increases with increasing hard block content of the film (from sample 2:1:1 to sample 6:5:1). This result is expected, because the number of urea groups in the polymer increases with the hard block content. The decay rate constants (k_1) indicate the rate of change of the free urea carbonyl absorbance with annealing. The decay rate constants obtained from the annealing profiles of the 4:3:1 and 6:5:1 films closely agree. The decay rate constant for the annealing profile of the 2:1:1 film is highly suspect, because the magnitude of the decay is very small.

Figure 6.8, **B** shows the free urethane carbonyl absorbance at 1918 nm as a function of annealing time. For all films, an increase in free carbonyl absorption is observed until a total annealing time of 2 hours. After two hours of annealing, the free urethane carbonyl absorption decays in a manner similar to that of the free urea carbonyl absorption (Figure 6.8, **A**). This result suggests two different mechanisms occuring for urethane groups in PEUU copolymers during annealing. The parameters obtained from the fit of two exponentials to these annealing profiles are shown in Table 6.3. These parameters indicate that the faster process has a rate constant of approximately 0.5 hr^{-1}, and shows no pronounced trend with composition. The slower process (with a rate constant of 0.13 to 0.2 hr^{-1}) is of larger magnitude than the faster process, and shows no obvious trend with composition.

It should be noted that the A, B and C parameters are subject to significant errors because of the uncertainty of film thicknesses and unknown degrees of phase mixing of the polymers before annealing. Smaller errors in the rate constants (k_1, k_2 and k_3) might arise from high overlap of individual absorbances that change with annealing. In this work, it is assumed that the absorbances at 1918 nm and 2036 nm are affected only by changes in the free urethane carbonyl and free urea carbonyl content, respectively.

The exponential fit data in Table 6.3 suggest that three different structural processes occur as a result of annealing at 100 ^{o}C. Solution-cast PEUU copolymers are assumed to be mostly phase-separated, because of the high affinity of hydrogen bond donors (N-H groups) in the hard blocks towards hydrogen bond acceptors (carbonyl groups) in the hard blocks. However, a substantial amount of phase-mixing, characterized by hydrogen bonding interactions between N-H groups in the hard block and ether oxygens in the soft block, might be present. At the higher temperature used for annealing, the polymer chains can undergo substantial rearrangements that enhance phase separation by eliminating impurities in each of the phases and by maximizing hydrogen bonding interactions in the hard block phases.

The annealing trend of the 2036 nm absorbance, described by A and k_1, indicates a continuous decrease in the free urea carbonyl content with annealing. This trend is consistent with a phase separation mechanism in which free urea carbonyl groups in the soft

block phase become hydrogen-bonded to N-H groups in various hard block portions of the polymer. It is most likely that urea groups hydrogen-bond to each other to form hard block domains.

The faster trend of the 1918 nm absorbance, described by B and k_2, indicates an increase in the number of free urethane carbonyl groups with annealing. This trend is also observed in the infrared spectra of these polymers (26). Although this result might seem anomalous, it should be noted that the urethane groups are only situated at the boundaries of hard and soft blocks in the polymers. Therefore, it is possible that as urea-urea hydrogen bonding between hard blocks increases, several urethane groups at the phase boundary are forced into the soft block phase. This process would cause an increase in the free urethane carbonyl, because no hydrogen bond donors exist in the soft block phase. Diffusion of soft block impurities from hard block domains could also explain this trend, becuase this process would cause expulsion of urethane groups from the interiors of hard block domains. Studies by Blackwell, et. al. (27,28) indicate that rigid hard block domains are present in similar polyurethane systems. If such a rigid hard block system is present in these polymers, it is expected that hydrogen bonding between groups at the interior of hard block domains are maximized, but groups at the phase boundary might be isolated in the soft block phase.

The slower trend of the 1918 nm absorbance, described by C and k_3, is a decrease in the free urethane carbonyl content with

annealing. This trend suggests that the hard block domains, once they are formed, can slowly move toward each other. This process would allow free urethane carbonyls at the edges of hard block domains to become hydrogen bonded to N-H groups of other hard block domains.

Another possible source of the slower trend in the 1918 nm absorbance is the desorption of water from the samples. It is unfortunate that water has a very strong absorbance band at 1920 nm (7), which overlaps the free urethane carbonyl absorbance at 1918 nm. Although great care was taken to avoid water contamination of the polymer samples, a very small amount of water might have been present in the samples before annealing. If this was the case, desorption of water from the sample into the surrounding space in the sample cell (most of which is not sampled by the NIR spectrometer) would cause a decrease in absorbance at 1918 nm during annealing. However, the amount of water corresponding to the observed absorbance decrease at 1918 nm would be very small. As a result, if water desorption is responsible for the slower trend at 1918 nm, other annealing trends in the spectra can still be attributed to phase separation of the polymer. In this case, the NIR results would agree with IR annealing studies of these polymers (26), which indicate only an increase in the free urethane carbonyl absorbance with annealing.

It should be mentioned that the molecular interpretation presented here is one possible model that explains the trends in the

NIR spectra. Further information from annealing studies at different temperatures, FTIR spectroscopy and X-ray diffraction are necessary to obtain more detailed information about the annealing process.

6.2.4 Conclusion for Chapter 6.2

NIR spectroscopy can be used to perform rapid analyses of bulk polymers. This analysis suggests that NIR spectroscopy can characterize the degree of phase separation in PEUU copolymers and therefore provide an accurate assessment of physical properties of these polymers. The NIR spectra indicate the presence of several structural changes that occur with annealing, but further information is required to fully characterize these trends.

6.3 Notes to Chapter 6

(1) Lelah, M.D., Cooper, S.L., *Polyurethanes in Medicine*, (CRC press, Boca Raton FL, 1986).

(2) Sung, C.S., Hu, C.B., Wu, C.S., *Macromolecules*, **1980**, *13*, 111.

(3) Sung, C.S., Smith, T.W., Sung, N.H., *Macromolecules*, **1980**, *13*, 117.

(4) Yoon, S.C., Ratner, B.D., *Macromolecules*, **1986**, *19*, 1068.

(5) Liu, L.B., Sumita, M., Miyasaka, K., *Macromolecules*, **1988**, *21*, 3424.

(6) Chen, Z.S., Yang, W.P., Macosko, C.W., *Rubber Chem. and Technol.*, **1988**, *61*, 86.

(7) Williams, P., Norris, K., *Near-infrared Technology in the Agricultural and Food Industries*, American Association of Cereal Chemists: St. Paul MN, 1987.

(8) Stark, E., Luchter, K., Margoshes, M., *Appl. Spectrosc. Rev.*, **1986**, *22*, 335.

(9) Kelly, J.J., Barlow, C.H., Jinguji, T.M., Callis, J.B., *Anal. Chem.*, **1989**, *61*, 313.

(10) Honigs, D.E., Hirschfeld, T.B., Hieftje, G.M., *Anal. Chem*, **1985**, *57*, 443.

(11) Miller, C.E., *Appl. Spectrosc.*, **1989**, *43(8)*, 1435.

(12) Haaland, D.M., Easterling, R.G., Vopicka, D.A., *Appl. Spectrosc.*, **1985**, *39*, 73.

(13) Geladi, P., MacDougall, D., Martens, H., *Appl. Spectrosc.*, **1985**, *39*, 491.

(14) Ilari, J.L, Martens, H., Isaksson, T., *Appl. Spectrosc.*, **1988**, *42*, 722.

(15) Miller, C.E., Edelman, P.G., Ratner, B.D., Eichinger, B.E., "NIR Spectroscopic Analyses of Polyether(urethaneurea) Block Copolymers, II. Phase Separation", *Appl. Spectrosc.*, **1990**, in press.

(16) Hecht, K.T., Wood, D.L., *Proc. Roy. Soc. London*, **1956**, *235*, 174.

(17) Miller, C.E., Honigs, D.E., *Spectroscopy*, **1989**, *4*, 44.

(18) Yoon, S.C., Ratner, B.D., *Macromolecules*, **1988**, *21*, 2392.

(19) Pollack, S.K., Shen, D.Y., Hsu, S.L., Wang, Q., Stidham, H.D., *Macromolecules*, **1989**, *22*, 551.

(20) Yoon, S.C., Ratner, B.D., *Macromolecules*, **1988**, *21*, 2401.

(21) Lee, H.S., Hsu, S.L., *Macromolecules*, **1989**, *22*, 1100.

(22) Lee, H.S., Wang, Y.K, Macknight, W.J., Hsu, S.L., *Macromolecules*, **1988**, *21*, 270.

(23) Miller, C.E., Edelman, P.G., Ratner, B.D., "NIR Spectroscopic Analyses of Polyether(urethaneurea) Block Copolymers, I. Bulk Composition", *Appl. Spectrosc.*, **1990**, in press.

(24) Pimental, G.C., McClellan, A.L., *The Hydrogen Bond*, (W.H. Freeman and Co., San Fransisco CA, 1960).

(25) Yeo, P., Honigs, D.E., *Appl. Spectrosc.*, **1988**, *42*, 1128.

(26) Edelman, P.G., Ratner, B.D., unpublished results, 1988.

(27) Blackwell, J., Lee, C-D., *J. Poly. Sci., Poly. Phys.*, **1984**, *22*, 759.

(28) Blackwell, J., Nagarajan, M.R., *Polymer*, **1981**, *22*, 202.

Chapter 7

Analysis of Reaction Injection Molded Polyurethanes by Near-infrared Diffuse Reflectance Spectroscopy

7.1 Introduction to Chapter 7

Reaction Injection Molding (RIM) (Chapter 1.4) is a common method of preparation for polyurethane products (1). Polyurethane block copolymers produced by RIM are used predominantly for automotive applications (2). RIM process parameters (Chapter 1.4.2), such as polymeric formulation, catalyst concentration, and mold temperature can be altered to change the composition (3,4), density, and the degree of phase separation (5-7) of the polymer, which affect the physical properties of the finished material.

Thermal conductivity (8) and Dynamic Mechanical Analysis (9,10) tests can be used to directly determine physical properties. Other analytical methods, such as FTIR (6,7,9,11-15), Differential Scanning Calorimetry (3,5,9,16), and X-ray scattering (4-6,16) determine compositional and structural properties, which affect physical properties. However, all of these methods require substantial sample preparation, and some of them are destructive. As a result, these methods cannot be used for rapid quality evaluation in a process environment. In contrast, near-infrared (NIR) spectroscopy has been used to rapidly determine compositional and structural properties of polymeric materials (17-22).

In this work, near-infrared (NIR) spectroscopy is used to determine compositional and physical properties of block polyurethane copolymers produced by Reaction Injection Molding (RIM). Principal Components Analysis (PCA) (23-25) is used to identify variations in the spectra of samples with differences in composition, density and phase separation. In addition, Partial Least Squares (PLS) (23,26-28) regression is used to correlate NIR spectra to various physical properties.

7.2 Experimental

Two different sets of RIM samples were used in this study; these sets will be identified as sample set **a** and sample set **b**. Refer to Chapter 1.4 for specific information regarding the general chemistry and processing aspects of reaction injection molding.

7.2.1 Sample Set a

Sample set **a** samples were prepared by the ICI Polyurethanes Group (Sterling, Hgts. Michigan). The polyol formulations consisted of various mixtures of an ethylene-oxide-capped poly(propylene oxide) triol (with a molecular weight of approximately 6000) and diethyl toluene diamine (DETDA) chain extender. A small amount (approximately 0.24 mass %) of a typical polyurethane catalyst was added to each polyol formulation. The isocyanate formulation

consisted of a glycol-modified 4,4'-diphenylmethane diisocyanate (MDI) with a functionality of approximately two. The ratio of polyol and chain extender concentrations was varied to produce RIM polymers with four different hard block percentages (approximately 55, 51, 46 and 42.5 mass %). The chemical structure of the finished polyurethanes in sample set a is shown in Figure 7.1, A. After the samples were prepared, they were post-cured at 120 °C for one hour.

A production-scale RIM machine (ICI Polyurethanes) was used to prepare the samples. This machine produced polyurethane plaques 3 ft. by 4 ft. and 1/8" thick. A heat sag sample (1" by 8") and a flex modulus sample (1" by 3") were cut from three different regions of each plaque: 1) the gate, corresponding to the part of the plaque closest to the injection point, 2) the middle, corresponding to the middle of the plaque, and 3) the end, corresponding to the part of the plaque farthest from the injection point. A total of 54 samples, which came from 18 different plaques, were used for both heat sag and flex modulus measurements. The naming scheme for the samples used in this set is shown in Table 7.1.

Duplicate NIR diffuse reflectance spectra of each heat sag sample were obtained and four spectra of each flex modulus sample were obtained. All NIR sampling was done near the center of each sample. A ceramic background was used for NIR sampling of the flex modulus samples. All samples were cleaned with hexane before analysis. NIR pseudo-absorbance values (Chapter 1.2.3.2) were obtained at every 8 nm from 1100 nm to 2236 nm for the flex

Figure 7.1: Chemical structures of RIM polyurethanes in sample set **a** (**A**) and sample set **b** (**B**), and the chemical structure of the hard block model compound for the sample set **b** samples (**C**).

A:

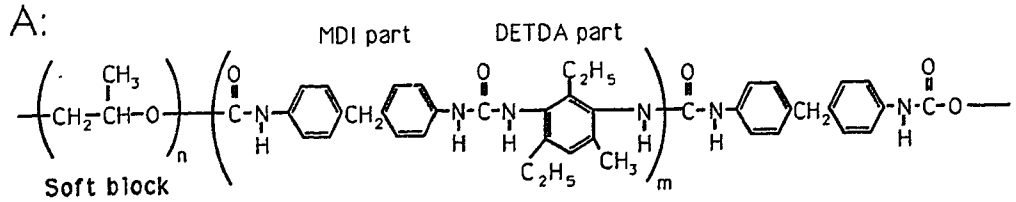
MDI part
DETDA part
Soft block
(molecular weight
approx. 6000)
Hard Block

B:

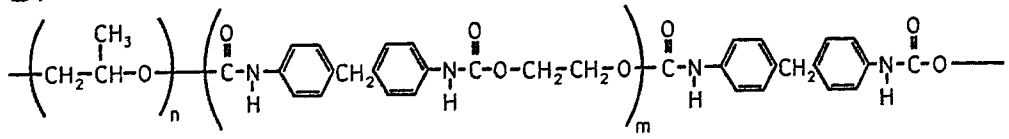

C:

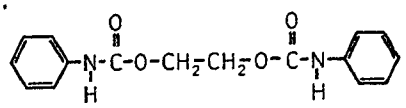

Table 7.1: Sample naming scheme for polyurethane samples in sample set **a** and sample set **b**.

Table 7.1

Sample Set a:

-First Character: composition group

A : approximately 55 mass% hard block
B : approximately 51 mass% hard block
C : approximately 46 mass% hard block
D : approximately 42.5 mass% hard block

-Second Character: sample number within composition group

1 to 3 for group A
1 to 5 for groups B,C and D

-Third Character: location of sample in RIM plaque:

G : gate; from one-third of panel closest to injection point
M : middle; from middle one-third of plaque
E : end; from one-third of panel farthest from injection point

Sample Set b:

	% of ethylene glycol in polyol resevoir (approximate hard block percentage[1])			
	9.1	12.4	16.4	20.0
index[1]	(40)	(47.5)	(55)	(60)
101	D1N	C1N	B1N	A1N
	D1Y	C1Y	B1Y	A1Y
104	D2N	C2N	B2N	A2N
	D2Y	C2Y	B2Y	A2Y
106	D3N	C3N	B3N	A3N
	D3Y	C3Y	B3Y	A3Y
109	D4N	C4N	B4N	A4N
	D4Y	C4Y	B4Y	A4Y

[1] : hard block percentage is also affected by index, see Chapter 1.4.2 for details

modulus samples, and at every 4 nm from 1101 nm to 2249 nm for the heat sag samples. For each sample, an average spectrum was calculated from the 2 or 4 original spectra of the sample. Multiplicative Scatter Correction (MSC) (29,30) (Chapter 1.2.5) was then used to reduce baseline offset and multiplicative scatter effects in the spectra.

7.2.2 Sample Set b

The polyurethanes used in sample set **b** were prepared from the same polyol and diisocyanate that were used for preparation of the samples in set **a**. However, an ethylene glycol chain extender was used. The chemical structure of the polymers in sample set **b** is shown in Figure 7.1,**B**. In addition, a hard block model compound (Figure 7.1,**C**) was prepared from reaction of ethylene glycol (Aldrich) and phenyl isocyanate (Aldrich) in a dry nitrogen atmosphere. The model compound was rinsed five times with methanol and vacuum-dried for 24 hours before use.

A production-scale RIM machine was used to prepare 1 ft. by 1 ft. and 1/8" thick polyurethane plaques. The mold temperature was 93 °C, the mold time was 3 minutes, and the reactant temperatures were 38 °C for the preparation of all plaques. The formulation was varied between four different levels (9.1, 12.4, 16.4 and 20 mass % ethylene glycol in the polyol, which resulted in hard block percentages of approximately 40, 47.5, 55 and 60 mass %,

respectively). The index (Chapter 1.4.2) was also varied between four different levels (101, 104, 106 and 109). Two samples were prepared from each possible combination of formulation and index. In each case, one of the samples was post-cured at 120 °C for 1 hour and the other was left alone. The experimental design and naming scheme for the 32 plaques are shown in Table 7.1. Three 1" by 3" samples for flex modulus testing and three 1" by 8" samples for heat sag testing were cut from each of the 32 original plaques. Some of the plaques, which had visible non-homogeneities (presumably from incomplete mixing), yielded fewer physical test samples. A total of 90 1" by 3" flex modulus samples and 83 1" by 8" heat sag samples were prepared.

NIR diffuse reflectance spectra of the physical test samples were obtained in the same way as in the spectra of the sample set a samples. Duplicate spectra of each physical testing sample were obtained, and a ceramic diffuse reflectance background was used in all NIR measurements. The spectral range was 1100 nm to 2200 nm, in 4 nm increments. Duplicate spectra were averaged and every two adjacent wavelengths in each spectrum were averaged. MSC correction (29,30) (Chapter 1.2.5) was used to reduce sampling effects in the spectra. The resulting spectra, which spanned the spectral region 1102 nm to 2200 nm in 8 nm increments, were used for multivariate analysis. Spectra of the 1" by 3" flex modulus samples were used for both the PCA study and for the PLS

calibration to flex modulus, and the spectra of the 1" by 8" heat sag samples were used for the PLS calibration to heat sag.

NIR spectra of the pure polyol, pure diisocyanate and a 1% (w/v) solution of the hard block model compound in THF (Baker) were obtained with the samples in a 1 mm path length glass cuvette. In each case, the spectrum was collected in transflectance mode (Chapter 1.2.4.2). The spectrum of the model compound in THF was obtained from a weighted subtraction of the spectrum of pure THF from the solution spectrum. The diffuse reflectance spectrum of the bulk hard block model compound was obtained with a sampling cell that was developed for small samples (31).

7.2.3 NIR Spectroscopy and Physical Testing:

NIR diffuse reflectance spectra were obtained with a Technicon InfraAlyzer 500C grating instrument. The nominal resolution of the instrument was 10 nm, and the wavelength accuracy was +/- 1 nm. After the samples were analyzed by NIR spectroscopy, they were tested for flex modulus and heat sag. These tests were performed with a Universal Testing Machine (Instron). The flex modulus was determined by ASTM Method D-790-86 (32). Single flex modulus measurements at 23 °C, 38 °C, and 70 °C were done for each 1" by 3" sample in sample set **a**, and a single flex modulus measurement at 23 °C was done for each 1" by 3" sample in sample set **b**. The heat sag measurement of each 1" by 8" sample involved the exposure of the

sample to 120 °C for 1 hour (ASTM Method D-3769-85) (33). A single heat sag measurement was made for each 1" by 8" sample.

For the moisture study, sample A2E (in sample set a) was dried by heating in a dry nitrogen-purged oven at 120 °C for 1.5 hours. The sample was then exposed to the atmosphere at room temperature for 20 additional hours. The mass of the sample (obtained from a Mettler balance) and its NIR spectrum were obtained before drying, after drying, and after exposure to the atmosphere. After the drying step, the sample was allowed to cool at room temperature for 20 minutes before weighing and NIR sampling.

7.2.4 Data Analysis

Principal Components Analysis of the NIR spectra of the flex modulus samples was done with software provided by the Center For Process Analytical Chemistry (34). Two analyses were done, one each for the two sample sets. Mean-centered spectra were used, and cross-validation was used to determine the optimal number of principal components. For the analysis of the spectra of the sample set a samples, it was found that a rotation of the first two principal components would yield more interpretable results. Details of principal component rotation are described in Chapter 1.5.1 (Equation 1.8). It was found that a rotation of -38° provided the most interpretable results.

PLS correlations of NIR spectra to physical properties were done with software provided by the Center for Process Analytical Chemistry (Seattle, WA) (35). For each analysis, the samples were split into calibration and prediction sets. Samples in the calibration set were used to construct PLS models, and samples in the prediction set were used to test the validity of the PLS models. The method of cross-validation was used to determine the optimal number of spectral factors for all calibrations. Four different properties were calibrated to NIR spectra of the sample set **a** samples (flex moduli at 23 °C, 38 °C and 70 °C, and heat sag) and two properties were calibrated to NIR spectra of the sample set **b** samples (flex modulus at 23 °C and heat sag). For each analysis, all spectra were mean-centered before PLS modeling.

Two error statistics were obtained for each PLS calibration: the Standard Error of Estimate (SEE) and the Standard Error of Prediction (SEP). These quantities are defined in earlier references (Chapter 1.5.2.3.2) (18,19,21). The SEE value is an indication of calibration error and the SEP value is an indication of prediction error. Relative error was calculated as the standard error divided by the range of values used in the analysis. The first PLS loading spectrum for each calibration was used to determine the spectral absorbances that are correlated to the property of interest.

7.3 Results and Discussion

7.3.1 Band Assignments

7.3.1.1 Functional Groups in the Polymers

Figure 7.2 shows the NIR spectrum of polyurethane sample B4Y in sample set **b** (**A**) and the spectrum of the diisocyanate (**B**) and polyol (**C**) that were used to prepare the polymers in both sample sets. The bands in the polymer spectrum (**A**) at 1184 nm, 1220 nm, 1416 nm, 1688 nm, and 1732 nm, which are also observed in the spectrum of the polyol (**C**), correspond to aliphatic CH groups in the soft block of the polymers. Bands at 1146 nm, 1648 nm and 2162 nm in the polymer spectrum, which are the approximate positions of bands in the diisocyanate spectrum (**B**), correspond to aromatic CH groups in the MDI part of the hard block of the polymer. The band at 1764 nm in the polymer spectrum probably corresponds to the bridging methylene group of MDI (**B**). The band at 1874 nm in the spectrum of the diisocyanate (**B**) is from the isocyanate group. Several bands in the polymer spectrum that are not observed in the polyol or isocyanate spectrum (1496 nm, 1920 nm, and 2048 nm) correspond to urethane groups in the polymer. The 1496 nm and 2048 nm bands are from NH vibrations in the urethane group. The absorbance at 1920 nm is probably the result of overlapping bands from the urethane carbonyl group and from water in the polymer (Chapters 6.2 and 7.1.3.4) (22). The NIR spectra of the samples in sample set **a** are very similar to the spectra of the samples in sample

Figure 7.2: *upper plot* - Near-infrared diffuse reflectance spectrum of polyurethane sample B4Y (in sample set **b**) (**A**), and near-infrared transflectance spectra of the modified 4,4'-diphenylmethane diisocyanate (**B**) and polyol (**C**), which were used to prepare the polymers; *lower plot* - the NIR diffuse reflectance spectrum of the bulk hard block model compound for the sample set **b** samples (**D**), and the transflectance spectrum of the hard block model compound in THF solution (**E**). The calculation of spectrum **E** is described in the text.

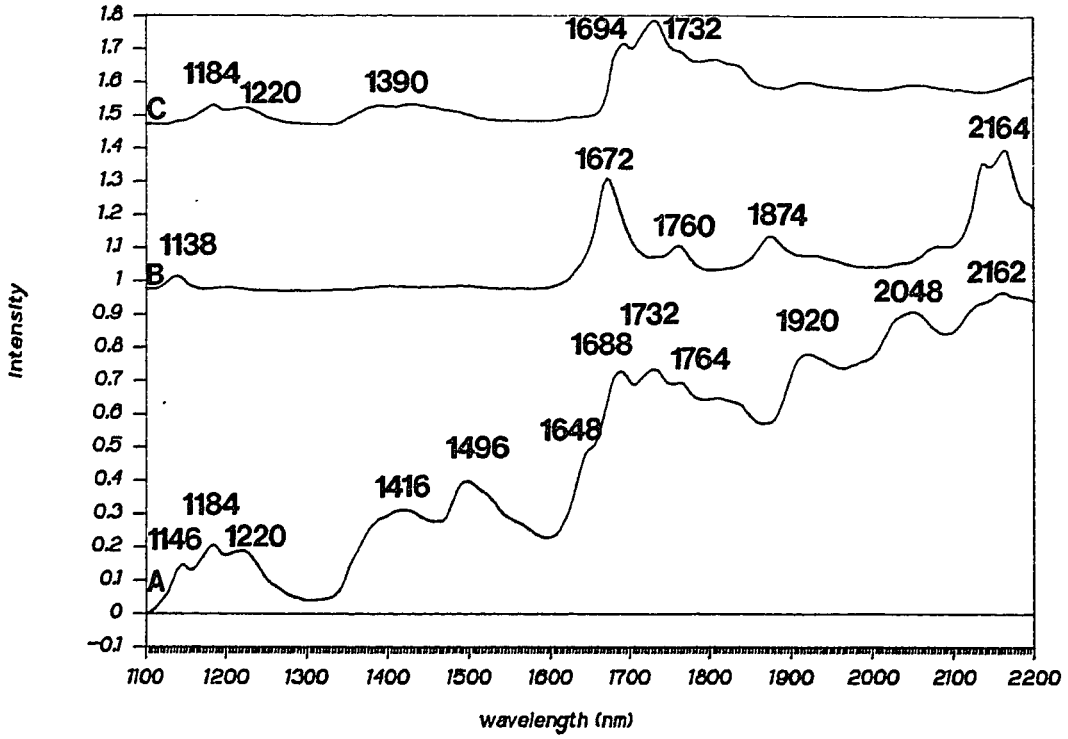
Intensity
wavelength (nm)
A
B
C
1694
1732
1184
1220
1390
1672
1760
1874
2164
1138
2162
2048
1920
1732
1688
1764
1648
1496
1416
1184
1146
1220

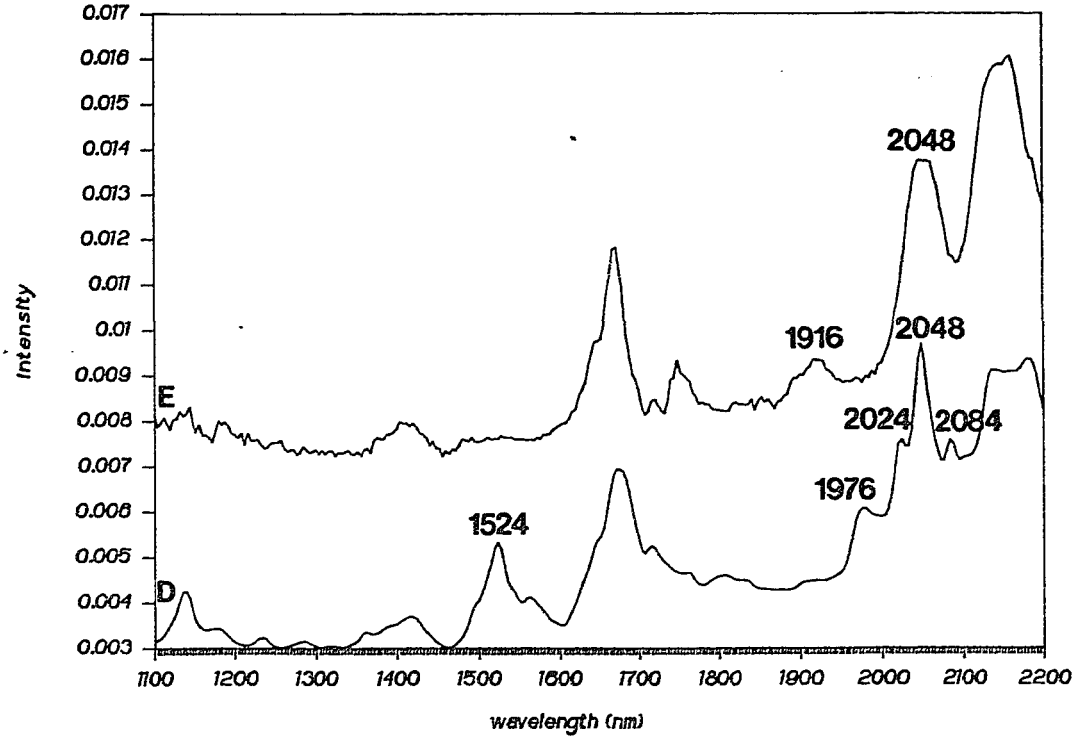
Intensity
wavelength (nm)
E
D
2048
1916
2048
2024
2084
1976
1524

set **b**. As a result, these band assignments for functional groups are reasonably accurate for samples in both sample sets.

7.3.1.2 Phase Separation

Phase separation in polyurethane block copolymers involves hydrogen bonding between hard blocks in the polymer (Chapter 1.3.2.5) (14,15). Therefore, the effect of phase separation in the polyurethanes in sample set **b** is approximated by comparison of the spectrum of the bulk hard block model compound (Figure 7.2, **D**) and the model compound in dilute THF solution (Figure 7.2, **E**). In the bulk compound, discrete hydrogen bonds between urethane NH and carbonyl groups are present. In solution, most urethane NH groups are hydrogen-bonded to solvent molecules, and the urethane carbonyl groups are free from hydrogen-bonding. Major differences in these spectra are observed in the regions of carbonyl and NH absorptions (1900 nm to 2100 nm and 1500 nm to 1600 nm). The 1976 nm band in the bulk model compound spectrum (**D**) corresponds to a carbonyl group that is hydrogen-bonded to NH groups in the bulk model compound. The 1916 nm band in the solution spectrum (**E**) corresponds to the free urethane carbonyl group. Three seperate combination bands in the NH region (2024 nm, 2048 nm, and 2084 nm) are observed in the spectrum of the bulk model compound (**D**). It is unlikely that these three bands correspond to three hydrogen-bonded states of the NH group in the

bulk model compound, because earlier studies (36) indicate that only one type of hydrogen bond is formed in the crystal structure of a similar model compound. Therefore, these three bands might arise from the combinations of the NH stretching mode with three different vibrational modes in the crystal structure. The spectrum of the model compound in solution has only a single broad NH combination band at 2048 nm. This band results from a multitude of similar hydrogen bonded states of the urethane NH groups in solution.

A strong band at 1524 nm in the spectrum of the bulk model compound, which is not present in the spectrum of the model compound in solution, is a first overtone band of the NH group in the crystalline bulk model compound. The reason for the absence of the 1524 nm band in the solution spectrum is uncertain. However, these results indicate that this band corresponds to an aggregated state of hard segments in the sample set **b** polymers.

Unfortunately, the NIR spectral effects of phase separation of the samples in sample set **a** are different than the effects of phase separation observed in this study, because the hard blocks of the polymer are different for the two sample sets (see Figure 7.1, **A** and **B**). The phase separation studies in Chapter 6.2 (22), which used polyurethanes with urea hard blocks (like the samples in sample set **a**), indicate that phase separation in these polymer is accompanied by increased hydrogen bonding of urea carbonyl groups (which involves a decrease in absorbance at 2034 nm) and decreased

hydrogen bonding of urethane carbonyl groups (which involves an increase in absorbance at 1918 nm).

7.3.2 Principal Components Analysis Results

7.3.2.1 Sample Set a

PCA cross-validation results indicate that three spectral factors are necessary to explain the variations in the NIR spectra of the RIM polyurethanes in sample set a. There are two properties of these samples that are known to vary: the composition and the position of the sample on the original RIM plaque. The original PCA results indicated that the first two principal components correspond to these two properties of the samples. However, because the original first two principal components each corresponded to a mixture of these two properties, results were difficult to interpret. Therefore, a rotation of the first two principal components was done (Chapter 1.5.1, Equations 1.8 and 1.9), in order to have each principal component correspond entirely to a single property.

The first, second and third principal components in the rotated PCA model explain 49.45%, 44.38% and 3.34% of the spectral variation, respectively. The principal component 1 and 2 scores are plotted in Figure 7.3, A. This plot indicates that principal component 1 describes the variation between samples at the gate, middle, and

Figure 7.3: Plot of the second versus the first principal component scores (**A**) and the loadings for principal component 1 (**B**, bottom) and principal component 2 (**B**, top), from principal components analysis of NIR spectra of RIM polyurethanes in sample set **a**.

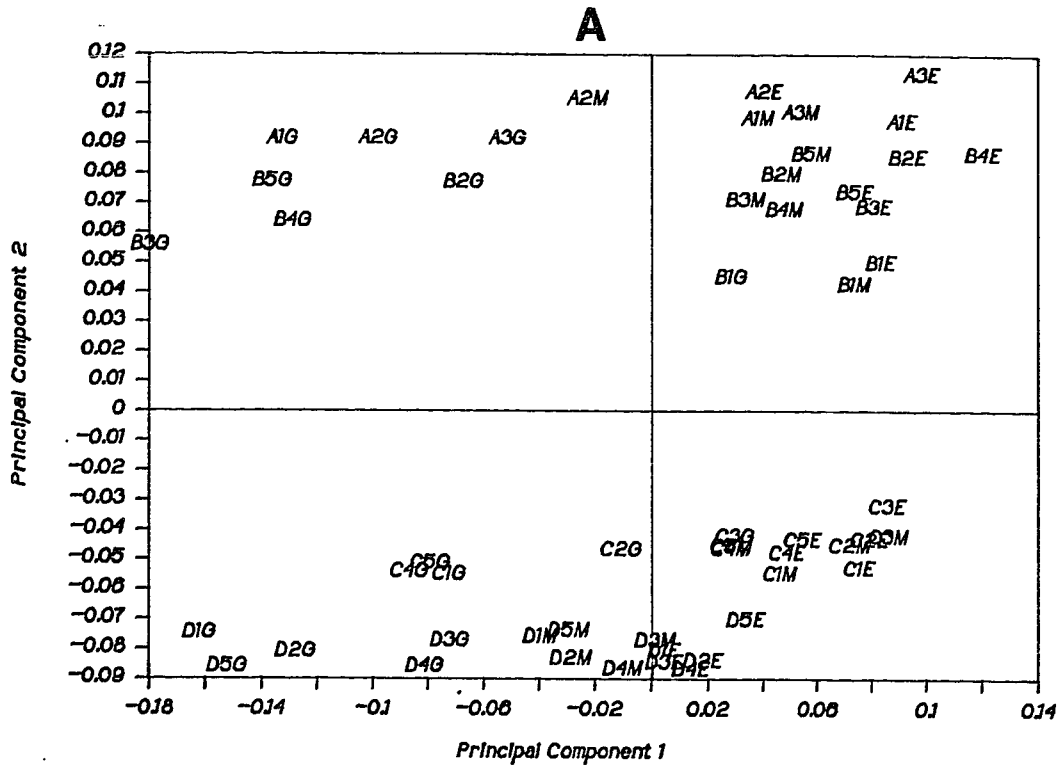
A
Principal Component 2
Principal Component 1
0.12
0.11
0.1
0.09
0.08
0.07
0.06
0.05
0.04
0.03
0.02
0.01
0
-0.01
-0.02
-0.03
-0.04
-0.05
-0.06
-0.07
-0.08
-0.09
-0.18
-0.14
-0.1
-0.06
-0.02
0.02
0.06
0.1
0.14
A1G
A2G
A3G
A2M
A2E
A1M
A3M
A3E
A1E
B5G
B2G
B5M
B2E
B4E
B2M
B4G
B3G
B3M
B4M
B5E
B3E
B1G
B1E
B1M
C3E
C2G
C5E
C4E
C1M
C1E
C4G
C1G
D1G
D2G
D5G
D3G
D4G
D1M
D5M
D2M
D4M
D5E
D2E
B4E

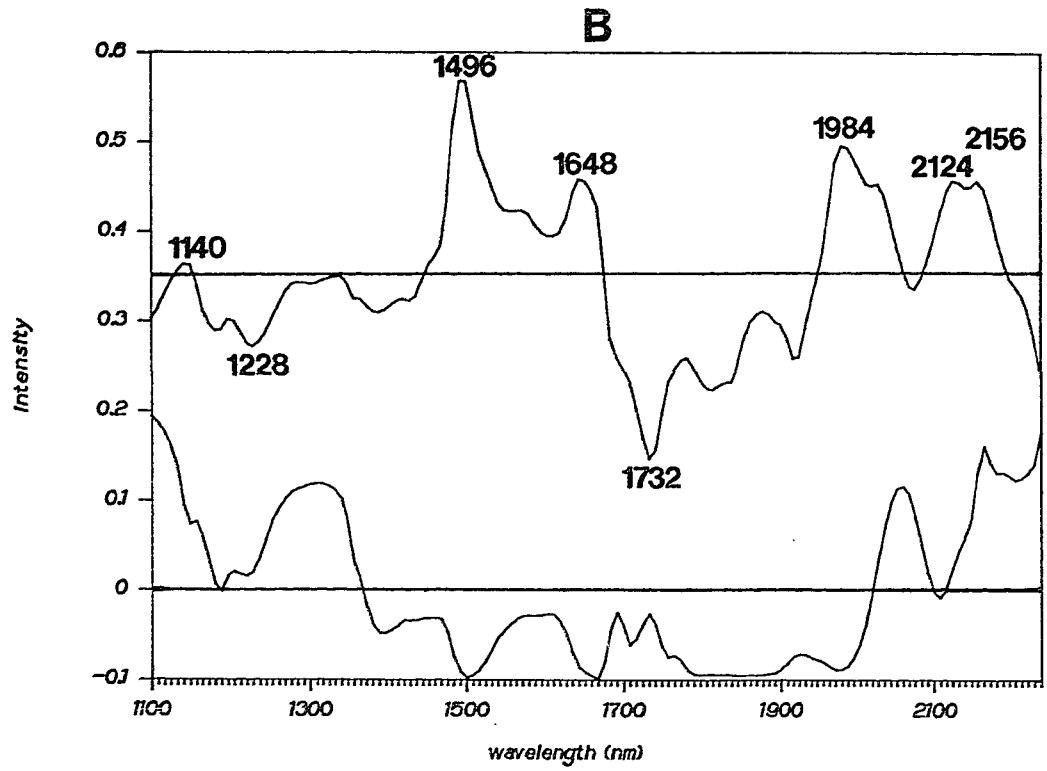
B
Intensity
wavelength (nm)
0.6
0.5
0.4
0.3
0.2
0.1
0
-0.1
1100
1300
1500
1700
1900
2100
1496
1648
1984
2156
2124
1140
1228
1732

end of the RIM piece, and principal component 2 describes the variation between samples in different composition groups (A, B, C and D).

The first 2 principal component loading spectra are shown in Figure 7.3, **B**. The first principal component loading spectrum (Figure 7.3, **B**, bottom), which explains the spectral variation that corresponds to differences in the gate, middle, and end portions of the same RIM piece, is very interesting. Comparison of this loading spectrum with the spectrum of a typical polyurethane used in this analysis (Figure 7.2, **A**) indicates that the loading spectrum has negative bands of the polymer spectrum at short wavelengths (1100 nm to 1600 nm) and positive bands of the polymer spectrum at longer wavelengths (1600 nm to 2250 nm). In summary, the first principal component loading indicates an enhancement of longer wavelength intensities relative to shorter wavelength intensities.

The only known property that varies between samples at the gate, middle and end of a given RIM piece is the concentration of voids. The process of nucleation (Chapter 1.4.1), which occurs during the RIM process (Chapter 1.4), involves the liberation of nitrogen that was formerly dissolved in the reactants. As the polymer cures, the liberated nitrogen gas becomes trapped in the polymer. The voids produced by this process enhance the diffuse reflectance and decrease the density of the product. The density of a RIM sample is a very important property, because it strongly affects the physical properties of the sample. In this study, it is observed that the

concentration of voids in a polyurethane plaque increases (and thus the density decreases) as one moves from the injection end of the plaque to the end of the plaque.

Although it is probable that the first principal component explains the variation in the density of the RIM materials, it is difficult to explain this correlation from the first principal component loading spectrum (Figure 7.3, **B**, bottom). The intensities in the diffuse reflectance spectra in this work are expressed in pseudo-absorbance units (Equation 1.3, Chapter 1.2.3.2) which are calculated as $\log(R_0/R)$, where R_0 is usually the incident light intensity, and R is the intensity of collected diffusely reflected light (if no specular reflection is present). An increase in pseudo-absorbance occurs both from absorption of light, and from loss of diffusely-reflected light. In several illustrations, Birth and Hecht (37) indicate that increasing scattering ability of a sample causes more diffuse reflectance at wider angles from the incident light. In this work, diffusely-reflected light is collected within a confined range of angles. Therefore, an increase in scattering ability of the sample would be expected to cause an increase in undetected diffusely reflected light, and thus an increase in measured pseudo-absorbance for a sample.

It is possible that the scattering ability (and thus the loss of diffusely reflected light) is not constant for all wavelengths. The scattering ability of a RIM sample depends on the regular reflection of light at each void/polymer interface in the material, which is described by one of the Fresnel Equations (37,38):

$$R_{\text{void/polymer}} = \frac{(n_2-n_1)^2 + n_2^2k^2}{(n_2+n_1)^2+ n_2^2k^2} \qquad (7.1)$$

where $R_{\text{void/polymer}}$ is the reflectance at a void/polymer interface, n_1 is the refractive index of the void, n_2 is the refractive index of the polymer, and k is the absorption coefficient of the polymer. It is well-known that shorter-wavelength NIR bands have lower absorptivity than longer-wavelength NIR bands (20). Equation 7.1 indicates that significantly more diffuse reflectance is obtained for the stronger-absorbing wavelengths (the longer wavelengths) than for the weaker-absorbing wavelengths (the shorter wavelengths). Therefore, an increase in scattering ability (density of voids) of a RIM sample is expected to enhance the diffuse reflectance intensities of longer wavelengths greater than for shorter wavelengths. This mechanism might explain the correlation of the first principal component to sample density.

The second principal component loading spectrum (Figure 7.3, B, top) indicates a spectral trend corresponding to increasing hard block percentage in the samples. The positive peaks at 1140 nm, 1648 nm, 2124 nm, and 2156 nm correspond to aromatic CH bands in the hard block of the polymer (21). The positive NH band at 1496 nm and the carbonyl band at 1984 nm also indicate a positive correlation to hard block percentage. The most prominent negative peaks, at 1228 nm and 1732 nm, correspond to aliphatic CH groups

(18,21), which are a major component of the soft block of the polymers.

A plot of the third principal component scores versus the first principal component scores (Figure 7.4, A) indicates that the third principal component describes a variation between the two groups of polymers with the highest hard block percentage (groups A and B). The third principal component loading spectrum is shown in Figure 7.4, B. Positive aliphatic CH peaks at 1188 nm, 1228 nm, 1704 nm, and 1740 nm, and negative aromatic CH peaks at 1644 nm and 2152 nm indicate a negative correlation of this component with hard block percentage.

Additional features in the third principal component loading spectrum (Figure 7.4, B) at 1484 nm, 1548 nm, 1588 nm, 1936 nm, and 2076 nm correspond to carbonyl and NH groups (20). First overtone NH stretching bands at 1484 nm, 1548 nm, and 1588 nm are assigned on the basis of earlier assignments of IR bands in similar model polyurethanes (14,15). The sharp negative band at 1484 nm is the first overtone band of the free NH group. The sharpness of this band is indicative of non-hydrogen-bonded species (39-42). The positive bands at 1548 nm and 1588 nm correspond to hydrogen-bonded NH groups. The positive band at 2076 nm is probably a combination amide II and NH stretching band. The negative peak at 1936 nm might correspond to a free urethane carbonyl group, but the overlap of water absorbances makes interpretation of this feature very tentative (22).

Figure 7.4: First and third principal component scores (after rotation) (**A**), and the third principal component loading spectrum (**B**), from principal components analysis of NIR spectra of RIM polyurethanes in sample set **a**.

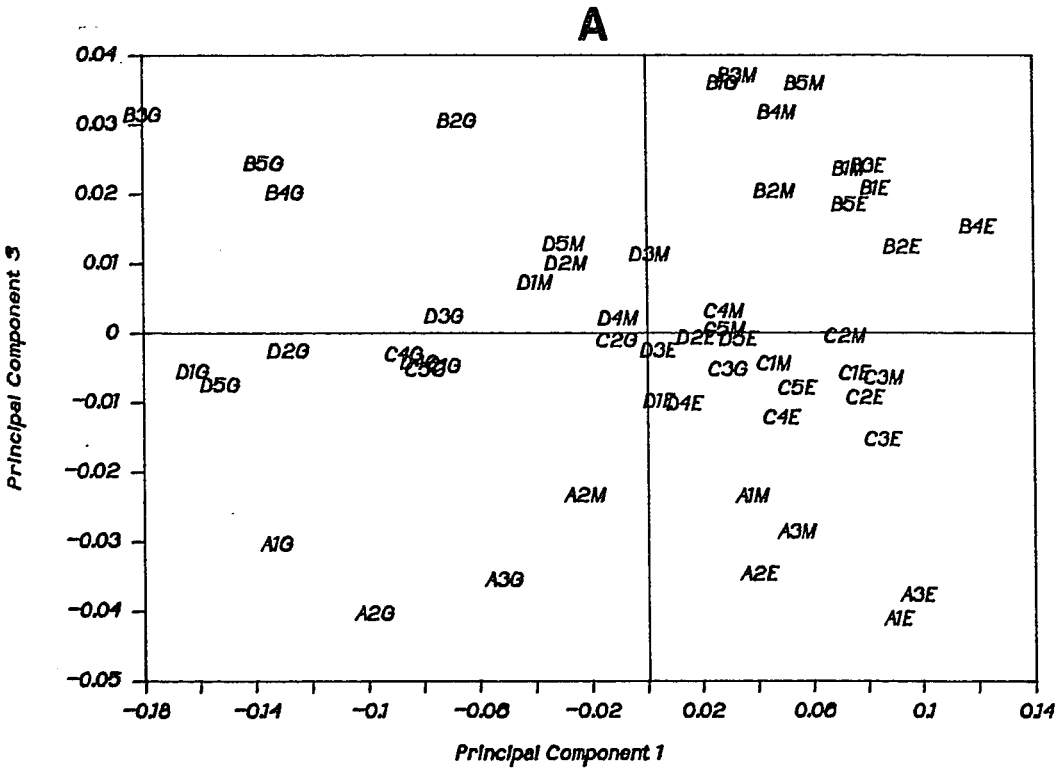
A
0.04
0.03
0.02
0.01
0
-0.01
-0.02
-0.03
-0.04
-0.05
-0.18
-0.14
-0.1
-0.06
-0.02
0.02
0.06
0.1
0.14
Principal Component 2
Principal Component 1
B3G
B2G
B5G
B4G
D5M
D2M
D1M
D3M
B3M
B5M
B4M
B2M
B5E
B4E
B2E
D3G
D4M
C4M
C2G
D3E
C2M
D2G
D1G
D5G
C3G
C1M
C5E
C2E
C3M
C4E
C3E
D4E
A2M
A1M
A3M
A1G
A3G
A2E
A3E
A2G
A1E

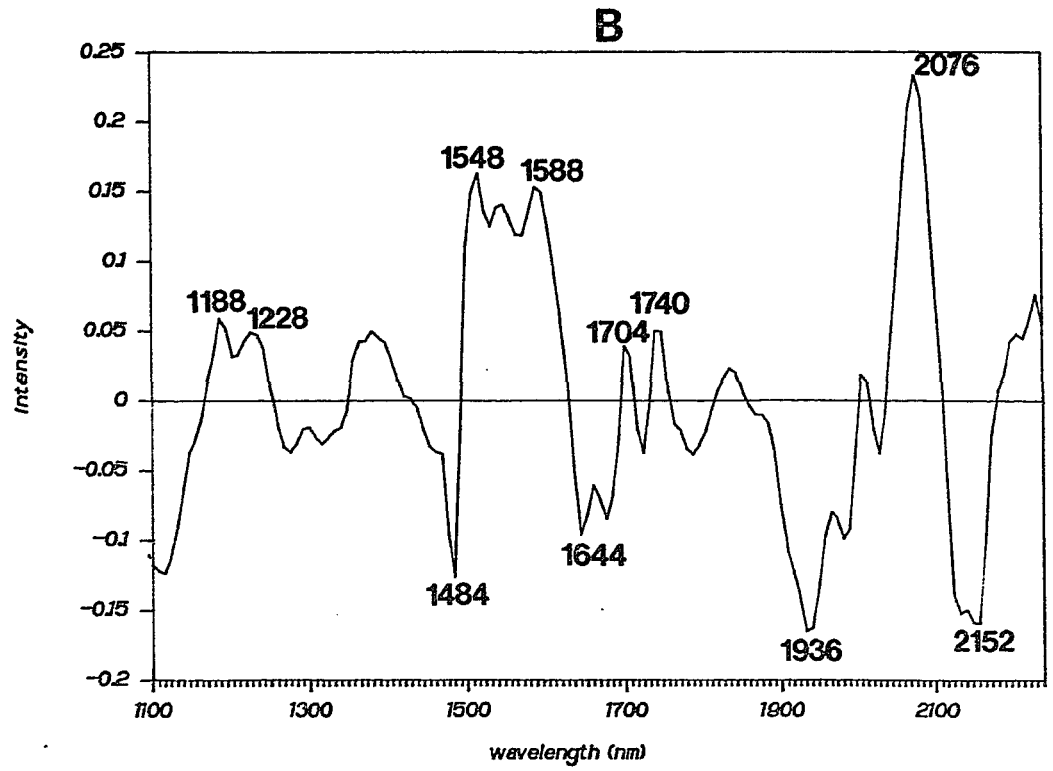
B
0.25
0.2
0.15
0.1
0.05
0
-0.05
-0.1
-0.15
-0.2
1100
1300
1500
1700
1900
2100
Intensity
wavelength (nm)
2076
1548
1588
1740
1188
1228
1704
1644
1484
1936
2152

The third principal component indicates a change in the hydrogen-bonding states of NH groups in the polymers. Although this effect probably corresponds to a change in the phase separation in the polymers, it is not certain whether is it positively or negatively correlated to phase separation. Results from the analysis of the hard block model compound for the sample set **b** samples (Figure 7.2, **D** and **E**) cannot be used to aid this interpretation, because the hard blocks used in the two sample sets are different. Detailed NIR investigations of phase separation of these polymers, or analyses of an appropriate hard block model compound for these polymers, are necessary to determine whether this principal component indicates an increase or decrease of phase separation. However, this result indicates that NIR spectroscopy can be used to monitor the effect of phase separation on the NH groups in the polymer. Earlier FT-IR investigations (14,15) could not fully characterize the effect of phase separation on NH groups, because the fundamental free NH stretching band is very weak.

The PCA results indicate that the samples in group A have a different degree of phase separation than the samples in group B. It is known that phase separation in RIM samples depends on several reaction parameters, such as catalyst concentration and reaction temperature (5-7). It is quite possible that the group A and B samples were prepared under slightly different reaction conditions. Unfortunately, no significant differences in the preparation of these samples are known, and we therefore cannot confirm this assertion.

7.3.2.2 Sample set b

Cross-validation results indicate that three principal components describe the variation in the NIR spectra of the flex modulus samples. The first principal component explains 71.7% of the spectral variation, the second principal component explains 19.7%, and the third principal component explains 3.9%. The loadings spectra for the three principal components are shown in Figure 7.5. The first principal component loading spectrum (**A**) has positive aromatic CH bands at 1142 nm and 1654 nm, positive urethane NH bands at 1494 nm and 2094 nm, a positive urethane carbonyl band at 1998 nm, and a negative aliphatic CH band at 1734 nm. These bands indicate that the first principal component is positively correlated to the hard block percentage of the polymer.

The second principal component loading spectrum (**B**) has a negative aliphatic CH peak at 1182 nm, a negative NH peak at 1494 nm, a positive NH peak at 2054 nm, and a positive aromatic CH peak at 2158 nm. This loading spectrum is almost identical to the first loading spectrum obtained from principal components analysis of the sample set a samples (Figure 7.3, **B**, bottom). In the previous section, it was determined that a loading spectrum of this type indicates a negative correlation to the density of the samples. Therefore, it can be concluded that the second principal component in this analysis is negatively correlated to density.

Figure 7.5: Principal component loadings spectra for the first (**A**), second (**B**) and third (**C**) principal components, obtained from principal components analysis of the near-infrared spectra of the 1" by 3" polyurethane samples in sample set **b**.

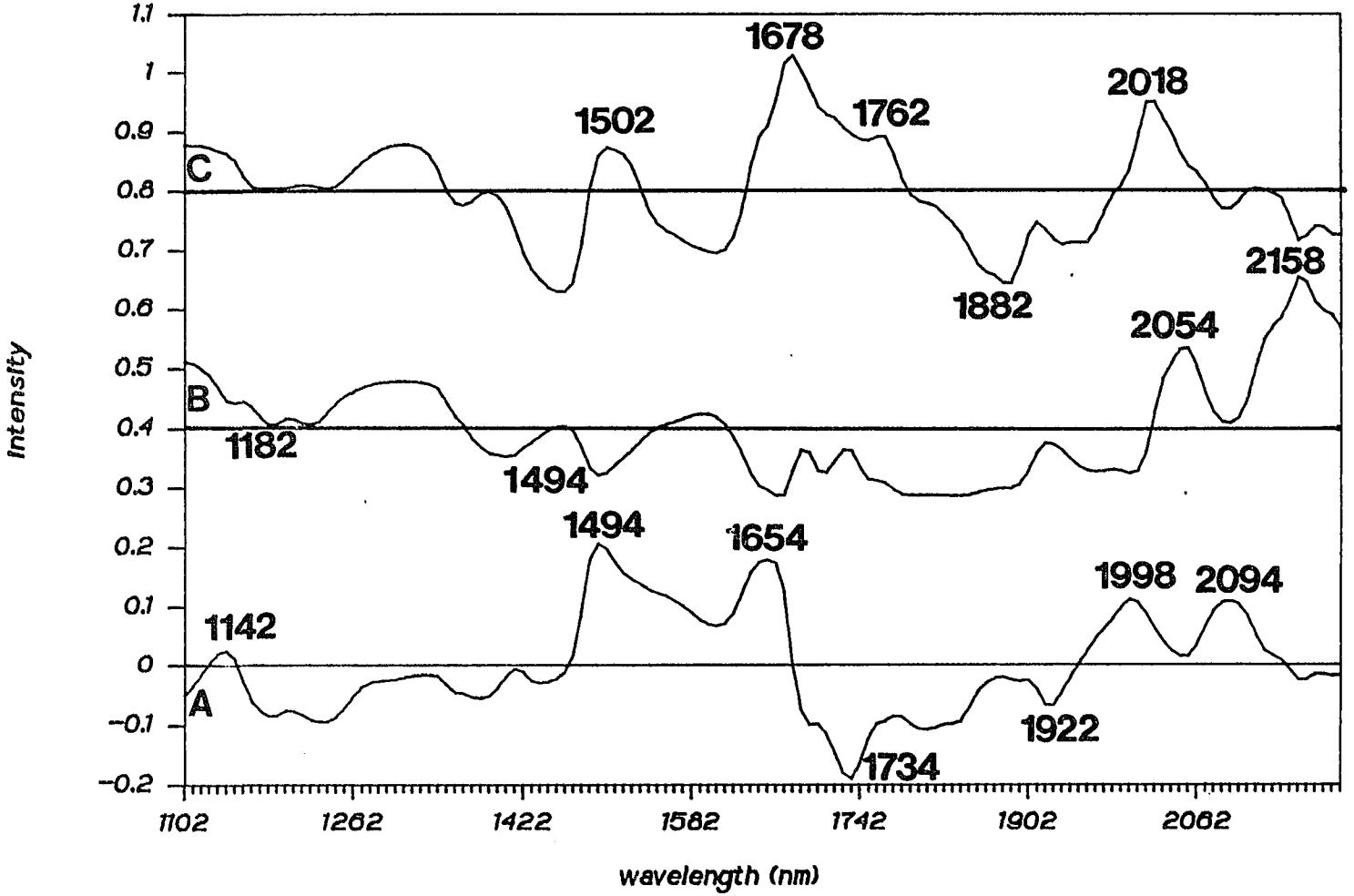
1.1
1
0.9
0.8
0.7
0.6
0.5
0.4
0.3
0.2
0.1
0
-0.1
-0.2
Intensity
C
B
A
1678
1502
1762
2018
2158
1882
2054
1182
1494
1494
1654
1998
2094
1142
1734
1922
1102
1262
1422
1582
1742
1902
2062
wavelength (nm)

The second principal component in this analysis explains a lower percentage of the spectral variation (19.7%) than the first principal component in the previous analysis (49.5%). Because the variation in other properties (such as hard block percentage) are expected to be nearly equal for the samples in set **a** and set **b**, it can be concluded that the densities of the samples in set **b** vary less than the densities of the samples in set **a**. This result suggests that the density gradients across individual plaques prepared from the large mold (3 ft. by 4 ft., as in the sample set **a** study) were larger than the density gradients across individual plaques prepared from the smaller mold (1 ft. by 1 ft., as in this study).

The two-dimensional scores plot for the first and second principal components is shown in Figure 7.6, A. The four distinct clusters of samples in the scores plot correspond to the four different hard block percentages of the samples in this analysis. The principal component 1 score increases as one moves from formulation D to formulation A. This result supports the earlier conclusion that the first principal component is positively correlated to the hard block percentage. It is also noticed that the index (indicated by the middle digit of the sample name) within each cluster is positively correlated to the principal component 1 score. This result is expected, because an increase in the index during the RIM procedure causes an increase in the hard block percentage of the finished material (Chapter 1.4.2).

Variations in the densities of the samples are represented by the principal component 2 scores. Note that the variation between

Figure 7.6: The second principal component scores plotted against the first principal component scores (**A**), and the third principal component scores plotted against the first principal component scores (**B**), obtained from principal components analysis of the near-infrared spectra of the 1" by 3" polyurethane samples in sample set **b**. Sample names are described in Table 7.1.

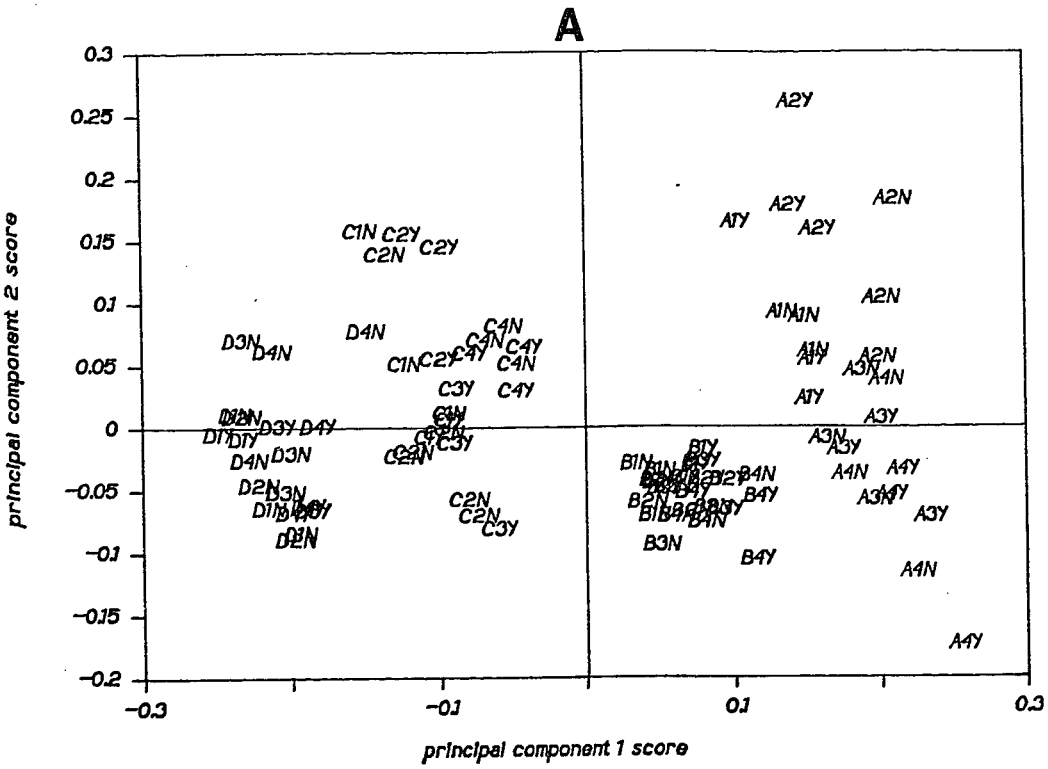
A
principal component 2 score
principal component 1 score
0.3
0.25
0.2
0.15
0.1
0.05
0
-0.05
-0.1
-0.15
-0.2
-0.3
-0.1
0.1
0.3

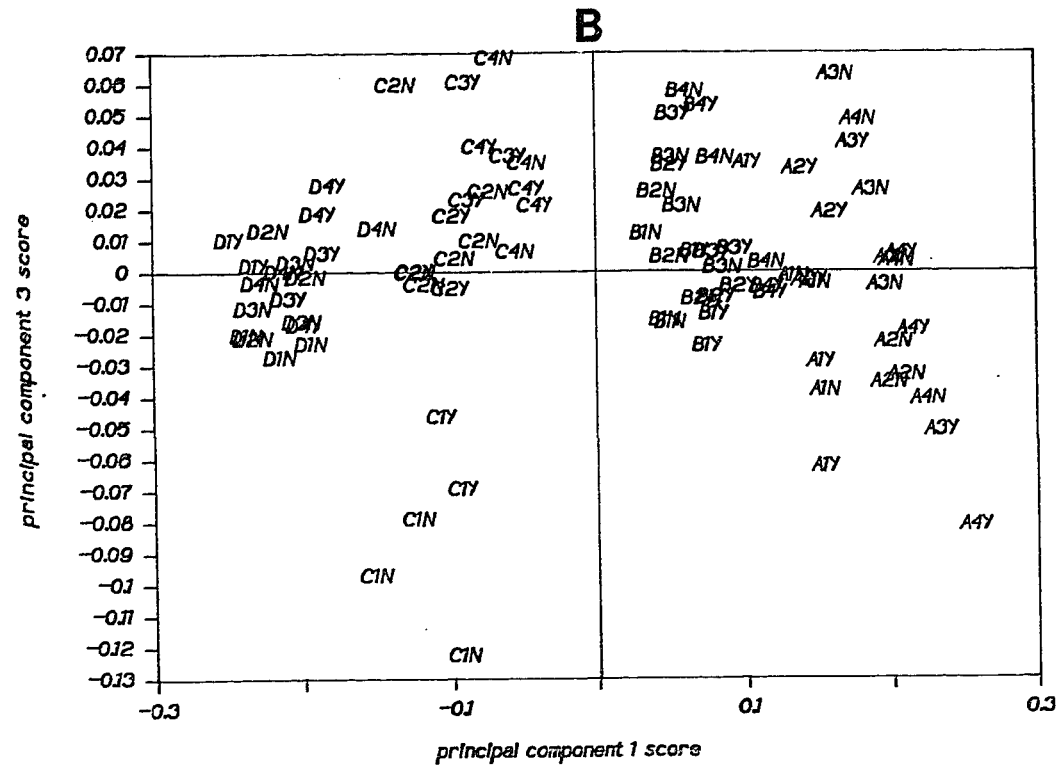
B
principal component 3 score
principal component 1 score
0.07
0.06
0.05
0.04
0.03
0.02
0.01
0
-0.01
-0.02
-0.03
-0.04
-0.05
-0.06
-0.07
-0.08
-0.09
-0.1
-0.11
-0.12
-0.13
-0.3
-0.1
0.1
0.3

the densities of the samples with formulation B is much less than the variation between the densities of the samples with formulation A. This result suggests that the densities of the samples with formulation B were more accurately controlled during the RIM procedure than the densities of the samples with formulation A.

The variation in the principal component 1 and principal component 2 scores of samples obtained from the same plaque reflects the non-homogeneities of composition and density across single RIM plaques. For example, the principal component 1 scores for the three replicate samples from plaque A3Y are significantly different. This result indicates the presence of significant compositional variations across plaque A3Y. The variation of the principal component 2 scores for the three replicate samples from plaque A2N indicate a significant density variation across plaque A2N. The variation of composition and density across single plaques might be caused by incomplete mixing during the RIM procedure.

The third principal component loading spectrum is shown in Figure 7.5, C. Positive NH bands at 1502 nm and 2018 nm, a positive aromatic CH band at 1678 nm, and a positive MDI methylene band at 1762 nm indicate positive correlations to NH content and hard block percentage. The negative isocyanate band at 1882 nm indicates a negative correlation of this principal component with the amount of unreacted isocyanate groups in the polymer.

The two-dimensional scores plot for principal components 1 and 3 is shown in Figure 7.6, B. It should be noted that samples

from plaques C1Y and C1N each have exceptionally low values of the principal component 3 score. Visual inspection of these plaques reveals the presence of many defects, which were probably the result of incomplete mixing of the reactants during the RIM procedure. If incomplete mixing did occur during the preparation of these plaques, a significant amount of unreacted isocyanate groups is expected to be present in the samples obtained from these plaques. This situation is confirmed by the low principal component 3 scores for these samples, which indicate the presence of a significant amount of unreacted isocyanate groups in the samples. The higher principal component 3 scores for the post-cured samples (C1Y) relative to the non-post-cured samples (C1N) indicate that post-curing caused reaction of some of the isocyanate groups that were present in the finished plaque. The positive correlation of the third principal component to NH content is observed because reaction of isocyanate groups results in formation of urethane NH groups. The positive correlation of the third principal component with hard block percentage is caused by the fact that the C1Y and C1N samples (which have the highest amount of unreacted isocyanate groups) coincidentally have the lowest possible hard block percentages of the samples with formulation C.

7.3.3 Calibrations of NIR Spectra to Physical Properties

7.3.3.1 Sample Set a

The results of PLS calibrations of NIR spectra to flex modulus and heat sag for sample set a samples are shown in Table 7.2. Cross validation results indicate that three factors are required for all calibrations. Prediction errors are 4.0% relative for flex modulus at 23 °C, and slightly higher for flex moduli at 38 °C (5.9%) and 70 °C (5.4%). These prediction errors are comparable to the estimated repeatability in the reference method (7.96%). However, the relative prediction error for heat sag (11.3%) is substantially higher than the estimated error in the reference method (2.26%). The lowest relative error of prediction is obtained for prediction of flex modulus at 23 °C, because this property and the NIR spectra of the samples are measured at the same temperature. Prediction errors for flex moduli at 38 °C and 70 °C and for heat sag are higher, because these properties depend on the state of the polymer at temperatures other than the temperature of NIR sampling. For prediction of the flex moduli at 38 °C and 70 °C, it would be more appropriate to use the NIR spectra of the samples measured at 38 °C and 70 °C. In addition, improved heat sag predictions could be obtained if the spectra of the polymers at 120 °C are used. Unfortunately, these approaches might not be feasible for rapid process analysis.

The first PLS loading spectrum for the calibration to flex modulus at 23 °C is shown in Figure 7.7, A. Positive aromatic CH peaks at 1140 nm, 1648 nm, and 2156 nm, a positive NH peak at 1500 nm, and negative aliphatic CH peaks at 1228 nm and 1736 nm

Figure 7.7: First PLS loading spectra for the calibration to flex modulus at 23 °C (A) and the calibration to heat sag (B), obtained from PLS calibrations prepared from sample set a.

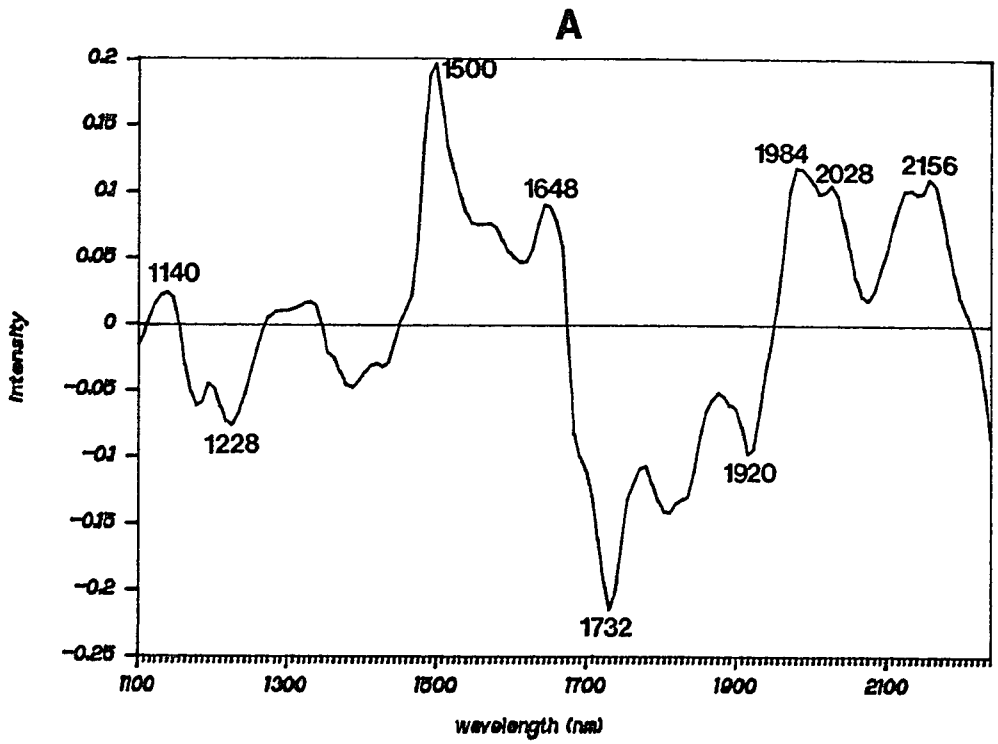
A
0.2
0.15
0.1
0.05
0
-0.05
-0.1
-0.15
-0.2
-0.25
Intensity
1140
1228
1500
1648
1732
1920
1984
2028
2156
1100
1300
1500
1700
1900
2100
wavelength (nm)

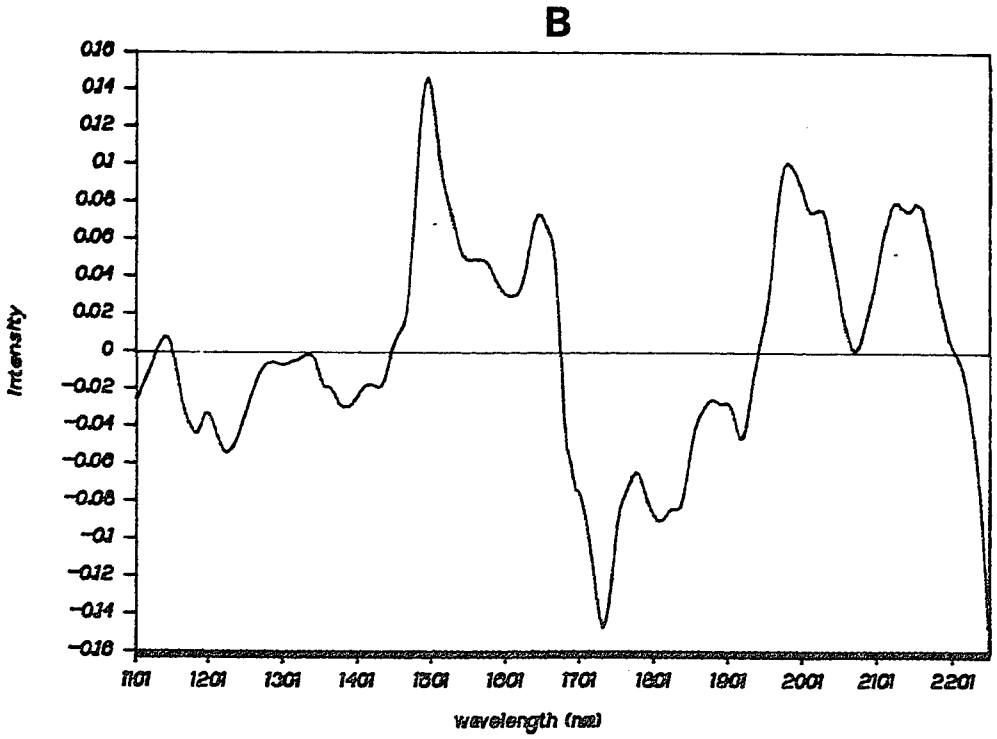
B
0.16
0.14
0.12
0.1
0.08
0.06
0.04
0.02
0
-0.02
-0.04
-0.06
-0.08
-0.1
-0.12
-0.14
-0.16
Intensity
1101
1201
1301
1401
1501
1601
1701
1801
1901
2001
2101
2201
wavelength (nm)

Table 7.2: Calibration and prediction results from PLS calibrations of NIR spectra to various physical properties of RIM polyurethanes.

Table 7.2

property (units)	Calibration SEE	Calibration range	Calibration relative error (%)	Prediction SEP	Prediction range	Prediction relative error (%)	Repeatability of reference method (%)[1]
Sample Set a:							
flex modulus, 23 °C ($\times 10^{-7}$ N/m^2)	1.26	23.7-55.0	4.0	1.23	24.6-54.2	4.0	7.96
flex modulus, 38 °C ($\times 10^{-7}$ N/m^2)	1.68	19.0-45.3	6.4	1.36	19.4-42.6	5.9	7.96
flex modulus, 70 °C ($\times 10^{-7}$ N/m^2)	0.83	14.2-31.0	5.0	0.79	14.4-29.0	5.4	7.96
heat sag (cm)	0.32	0.71-3.81	10.3	0.28	0.97-3.48	11.3	2.26
Sample Set b:							
flex modulus, 23 °C ($\times 10^{-7}$ N/m^2)	3.2	4.0-47.5	7.5	3.7	4.1-46.2	8.9	7.96
heat sag (cm)	0.36	1.19-4.24	12.0	0.43	1.32-3.66	18.6	2.26

1 : repeatability values expressed as percentage of the mean; these values are obtained from within-lab replicate measurement of several samples (see Reference 31 for flex modulus, Reference 32 for heat sag)

are observed. This result indicates that the modulus at 23 °C is positively correlated to hard block percentage. The positive band at 1984 nm corresponds to a hydrogen-bonded urethane carbonyl group, the negative band at 1920 nm might correspond to a free carbonyl group, and the positive band at 2028 nm corresponds to a free urea carbonyl group. An earlier study (22) showed that the phase separation of a very similar polymer system involves a decrease in the amount of free urea carbonyl groups, an increase in the amount of free urethane carbonyl groups, and a decrease in the amount of hydrogen-bonded urethane carbonyl groups. Therefore, the first PLS loading spectrum might indicate a negative correlation of flex modulus with the degree of phase separation in the polymer. It is also possible that the negative band at 1920 nm is a water band. If this is the case, the loading spectrum indicates a negative correlation of flex modulus to moisture content of the polymer.

The first PLS loading spectrum for the calibration to heat sag is shown in Figure 7.7, **B**. This plot is almost identical to the first PLS loading spectrum for the flex modulus calibration (Figure 7.7, **A**). As a result, it can be tentatively concluded that heat sag is positively correlated to hard block percentage.

The positive correlation of heat sag to hard block percentage can be explained by a "compression set" mechanism. A compression set measurement, which is similar to a heat sag measurement, involves the compression of a sample for approximately 24 hours at an elevated temperature, and removal of the load to allow the

sample to recover (43). During the hot compression, breaking and reforming of hydrogen bonds in the hard segment blocks can occur. The new hydrogen bonds are in equilibrium with the compressed state, and serve to retain the compressed state against recovery of the polymer. At the temperature of the heat sag measurement (120 °C, kT = 0.78 kcal/mole) substantial breaking of the N-H..O=C hydrogen bonds in the hard blocks (with a hydrogen bond strength of approximately 3.5 Kcal/mole, as found in dimers of caprolactam, reference (41)) is possible. If a hydrogen bond breaking and reforming mechanism is an accurate model for heat sag, it is expected that this property is proportional to the number of possible hydrogen bond pairs (or the hard block percentage) in the polymer.

7.3.3.2 Sample Set b

The results of PLS calibrations for flex modulus at 23 °C and heat sag of the sample set **b** samples are shown in Table 7.2. Three PLS factors were used for both calibrations. The relative error of prediction for flex modulus at 23 °C (8.9%) is comparable to the estimated precision of the reference method (7.96%) (32), but the relative error of prediction for heat sag (18.6%) is substantially higher than the estimated precision of the reference method (2.26%) (33). As mentioned earlier, the error for the heat sag calibration is higher because the heat sag depends on the state of the polymer at

an elevated temperature, which is difficult to determine from the spectrum of the polymer at room temperature.

Table 7.2 also indicates that the calibration and prediction errors for flex modulus at 23 °C of the sample set **b** samples are much higher than the corresponding errors for flex modulus at 23 °C of the sample set **a** samples. The source of this discrepancy is indicated by observation of the PLS calibration curves for the flex modulus at 23 °C (Figure 7.8) derived from sample set **a** (**A**) and sample set **b** (**B**). The major difference between these two calibration curves is the presence of large deviations in the sample set **b** calibration curve (**B**) for samples with very high or very low flex moduli. This result might indicate systematic errors in the reference flex modulus measurement for samples with very high or very low flex moduli, or a non-linear relationship between NIR spectral absorbances and flex modulus of the sample set **b** samples. The lack of this effect for the high flex modulus samples in the sample set **a** calibration curve (**A**) indicates that systematic errors in the reference measurement for high flex modulus samples are not present. As a result, the apparent curvature in the sample set **b** calibration curve (**B**) is probably caused by a non-linear relationship between NIR absorbances and flex modulus. The lack of such curvature in the sample set **a** calibration curve (**A**) might be caused by the fact that the samples in sample set **a** are in a "linear" region, where the relationship between NIR absorbances and flex modulus is approximately linear.

Figure 7.8: Calibration curves for the PLS calibration of near-infrared spectra to flex modulus at 23 °C, derived from the polyurethane samples in sample set **a** (A) and sample set **b** (B).

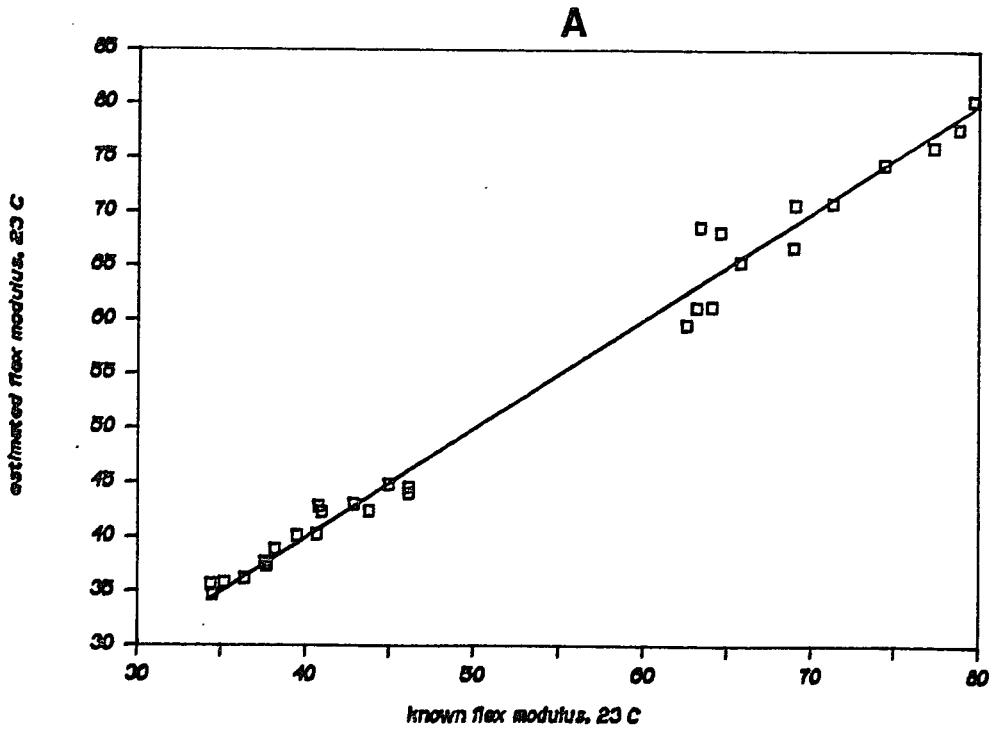
A
estimated flex modulus, 23 C
known flex modulus, 23 C
85
80
75
70
65
60
55
50
45
40
35
30
30
40
50
60
70
80

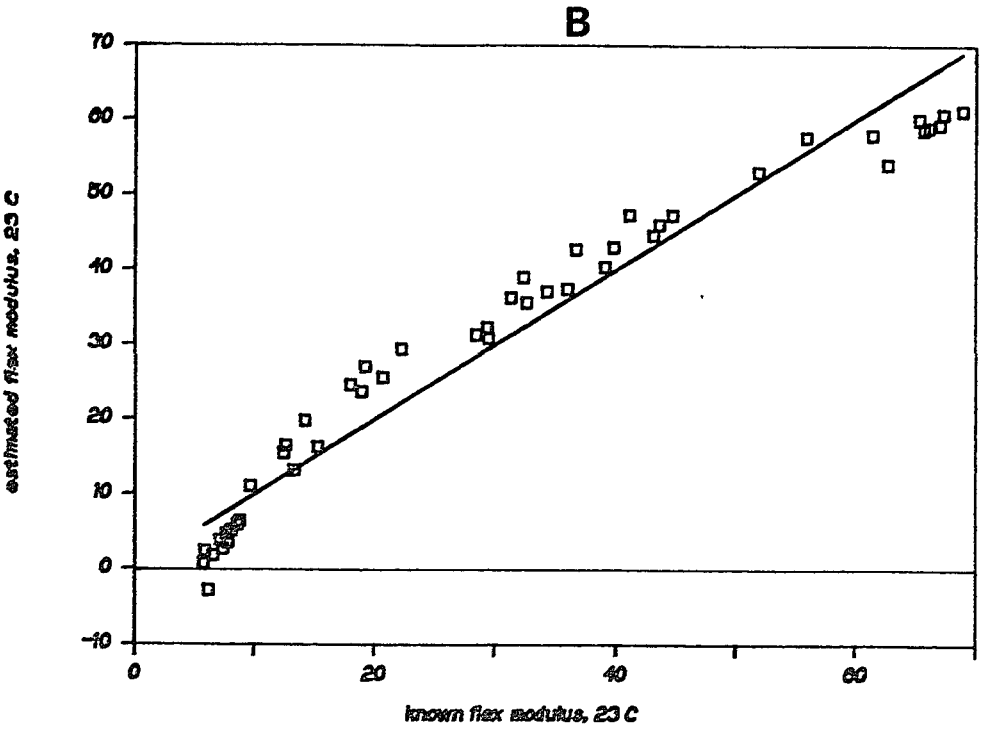
B
estimated flex modulus, 23 C
known flex modulus, 23 C
70
60
50
40
30
20
10
0
-10
0
20
40
60

The first PLS loading spectrum for the calibration to flex modulus (Figure 7.9, **A**) has positive aromatic CH bands (1142 nm and 1654 nm), positive NH bands (1494 nm and 1998 nm) and negative aliphatic CH bands (1230 nm and 1734 nm). This result indicates that the flex modulus is positively correlated to the hard block percentage. The negative band at 1922 nm might correspond to the free urethane carbonyl group or to moisture in the polymer (22). Although other factors are expected to influence the flex modulus, these factors cannot be easily identified from the first PLS loading spectrum.

The first PLS loading spectrum for the calibration to heat sag (Figure 7.9, **B**) is almost an exact inversion of the first PLS loading spectrum for the flex modulus calibration. Therefore, this result indicates a negative correlation of heat sag with hard block percentage for the sample set **b** samples. It should be noted that this result is exactly opposite to the result obtained from the PLS calibration obtained from the sample set **a** samples (Figure 7.7, **B**). This discrepancy might indicate fundamental differences in the molecular heat sag mechanism for the two different polymer systems used in sample sets **a** and **b**. However, it is also possible that different intercorellations of chemical properties of the polymers in the two sample sets caused this difference. If the heat sag is primarily affected by a chemical property that has a weak effect in the NIR spectrum, the observed spectral correlations to heat sag will have features that are directly corellated to that chemical property

Figure 7.9: First PLS loading spectra for the calibration to flex modulus at 23 °C(A) and the calibration to heat sag (B), obtained from PLS calibrations derived from sample set **b** samples.

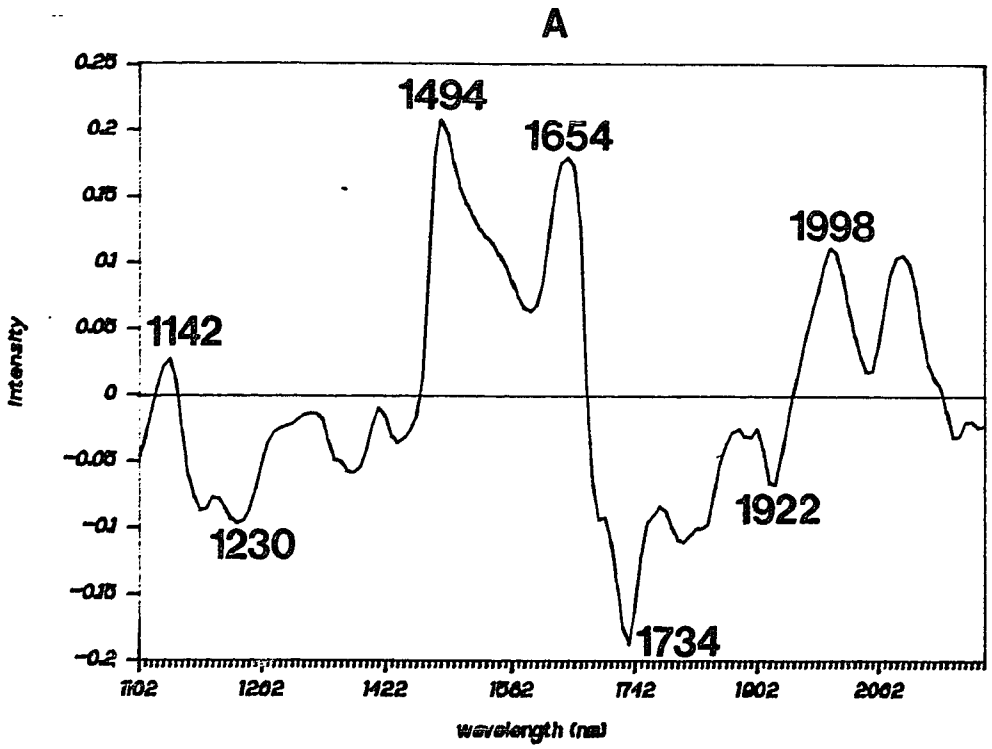
A
1494
1654
1998
1142
1230
1922
1734
Intensity
wavelength (nm)

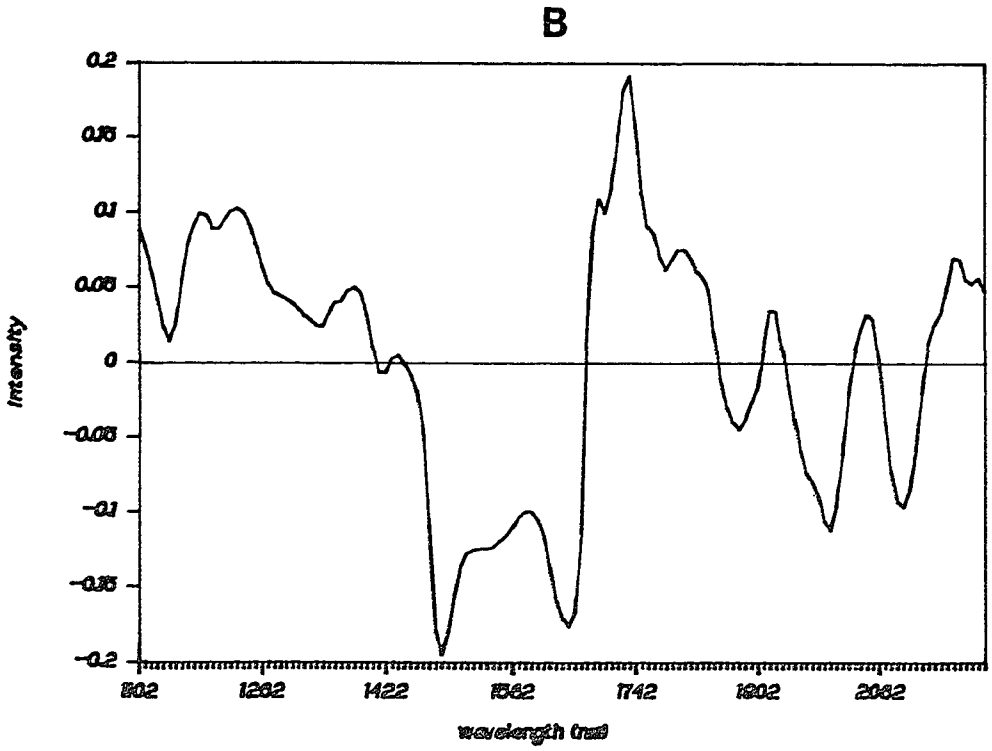
B
Intensity
wavelength (nm)

(which are weak) and features of other chemical properties, such as hard block percentage, that are coincidentally corellated to that property (which are much stronger). It is possible that the intercorellation between the chemical property that influences heat sag and the hard block percentage of the polymers is different for the two studies.

7.3.4 Moisture Effect

Figure 7.10, **A** shows the spectra of sample A2E (in sample set **a**) before drying (**a**), after drying at 120 °C for 90 min. (**b**), and after 20 additional hours at room temperature in the open atmosphere (**c**). The heating procedure (**a** to **b**) caused a decrease in the absorbance of the first overtone OH band at 1430 nm and the combination OH band at 1922 nm. These bands have been previously assigned to water absorbances (20). Subsequent exposure of the sample to the atmosphere (**b** to **c**) allowed the dried polymer to absorb moisture from the air, which caused an increase in the intensities of these moisture bands.

The absorbance at 1572 nm behaves in the same way as the moisture bands. As mentioned previously, this absorbance is in the region of first overtone stretching bands of NH groups that are hydrogen bonded. The behavior of this absorbance with respect to

Figure 7.10: **A**: Near-infrared diffuse reflectance spectrum of RIM sample A2E (in sample set **a**) as received (**a**), after 1.5 hours drying at 120 °C (**b**), and after 20 additional hours exposed to the atmosphere at room temperature (**c**); **B**: absorbance at three different near-infrared wavelengths versus the mass of the sample during the moisture study.

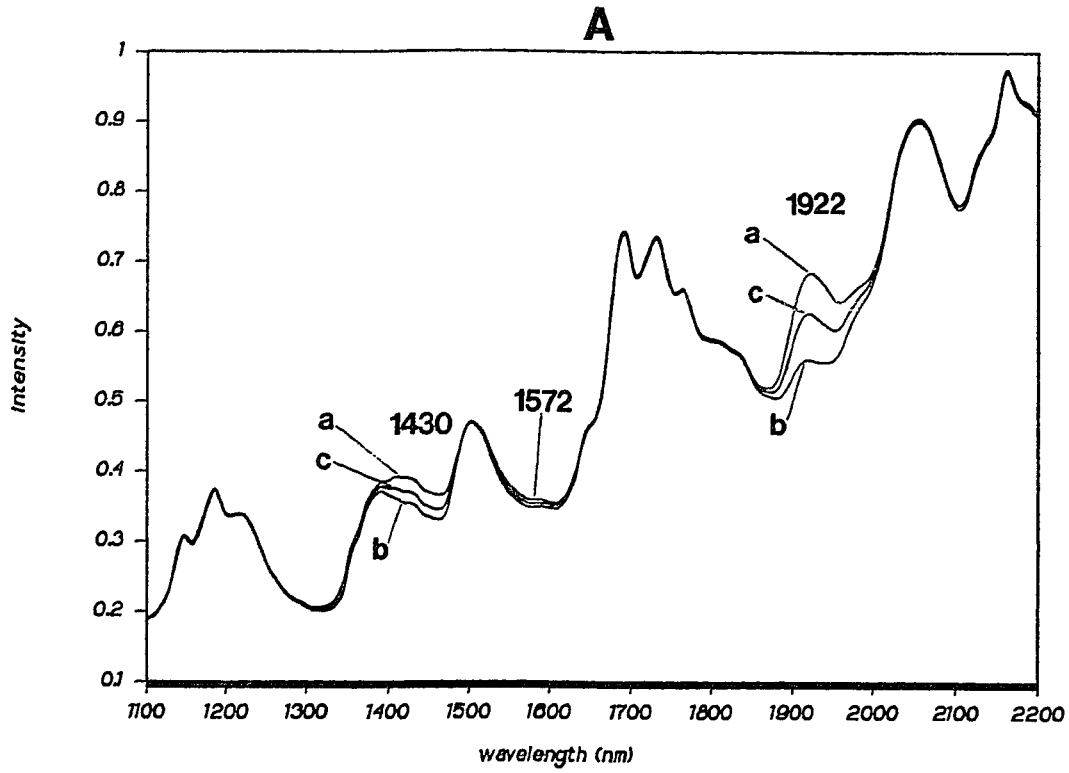
A
1
0.9
0.8
0.7
0.6
0.5
0.4
0.3
0.2
0.1
Intensity
1100
1200
1300
1400
1500
1600
1700
1800
1900
2000
2100
2200
wavelength (nm)
1922
a
c
b
1572
1430
a
c
b

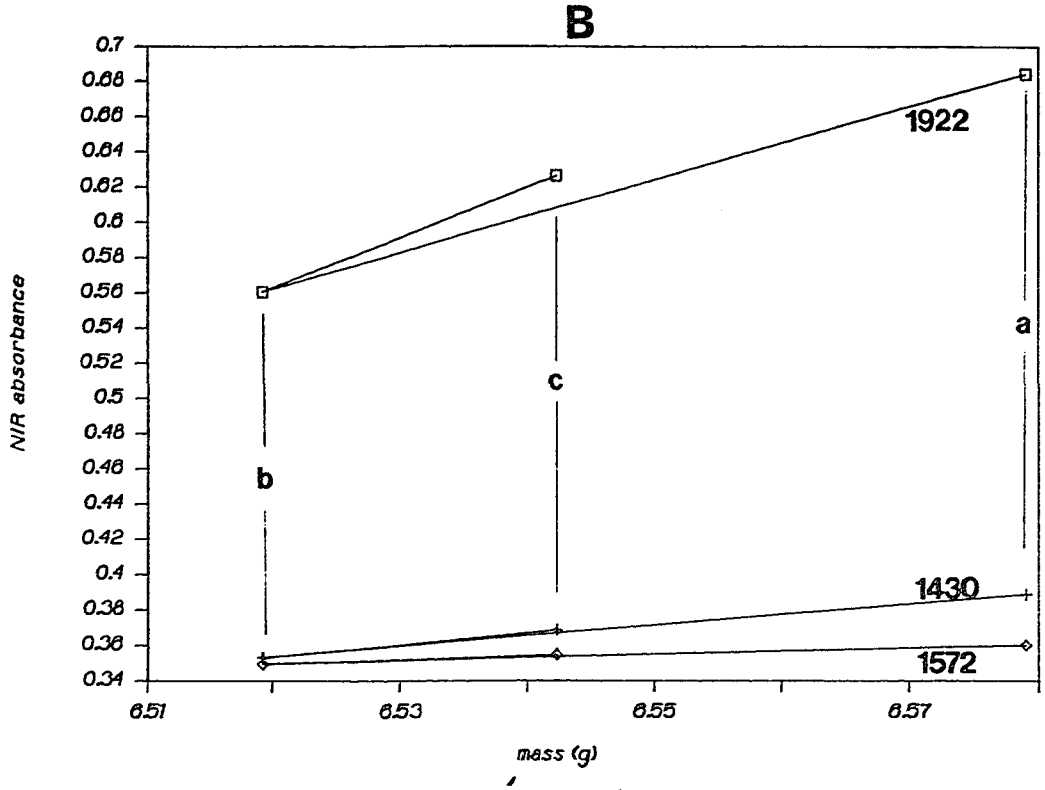
B
0.7
0.68
0.66
0.64
0.62
0.6
0.58
0.56
0.54
0.52
0.5
0.48
0.46
0.44
0.42
0.4
0.38
0.36
0.34
NIR absorbance
6.51
6.53
6.55
6.57
mass (g)
1922
a
c
b
1430
1572

moisture content suggests that it is a band for a NH-water hydrogen-bonded complex in the polymer.

The moisture bands at 1430 nm and 1922 nm, and the NH-water complex band at 1572 nm can be used to determine moisture content in the polymer. Figure 7.10, **B** shows the absorbance of these three bands versus the total mass of polymer weighed after each spectrum was taken. It is assumed that the only mass changes in the polymer during this experiment were from moisture loss or gain. The correlations between each of the three absorbances and moisture content (correlation coefficients = 0.998 for 1430 nm, 0.992 for 1572 nm, and 0.986 for 1922 nm) are very high.

The correlation to moisture is lowest for the 1922 nm absorbance. This result is probably caused by interference of the moisture absorbance at this wavelength with the free urethane carbonyl absorbance at 1916 nm (22) (Figure 7.2, **E**). Phase separation, which (for the diamine-extended polymers used in sample set **a**) is accompanied by an increase in the intensity of the free urethane carbonyl band, might occur during the drying procedure. If this is the case, the decrease in water absorbance during the drying step (**a** to **b**, in Figure 7.10, **B**) is partially offset by the increase in the absorbance of the free urethane carbonyl band. The moisture regaining step (**b** to **c**) involves a larger slope in the absorbance versus mass curve, because no offsetting effect of phase separation occurs.

7.4 Conclusion

Near infrared spectroscopy can provide rapid and accurate predictions of flex modulus and heat sag in RIM polyurethanes. Accurate determinations are possible because NIR spectroscopy can detect changes in composition, density and phase separation, which affect physical properties. It was found that NIR spectra of RIM polyurethanes at room temperature can be used to predict physical properties of the materials at elevated temperatures. Moisture in the polymer can be monitored by OH bands from moisture, or by an NH stretching overtone band for a NH-water hydrogen-bonded complex.

7.5 Notes to Chapter 7

(1) Macosko, C.W., *RIM, Fundamentals of Reaction Injection Molding*; Hanser Publishers: Munich, 1989.

(2) *Modern Plastics*, **1987**, *64(10A)*, p. 122

(3) Chen, Z.S., Yang, W.P., Macosko, C.W., *Rubber Chem. and Technol.*, **1988**, *61*, 86.

(4) Blackwell, J., Quay, J.R., Turner, R.B., *Poly. Eng., and Sci.*, **1983**, *23*, 816.

(5) Camargo, R.E., Macosko, C.W., Tirrell, M.V., Wellinghoff, S.T., *Polymer*, **1985**, *26*, 1145.

(6) Camargo, R.E., Macosko, C.W., Tirrell, M.V., Wellinghoff, S.T., *Poly. Eng. and Sci.*, **1982**, *22*, 719.

(7) Yang, W.P., Macosko, C.W., *Makromol. Chem., Macromol. Symp.*, **1989**, *25*, 23.

(8) Smith, S.A., Galbraith, C.J., Cartmell, M.J., Moore, M.L., Brown, R.K., *Polyurethanes World Congress*, 1987, 74.

(9) Provder, T., *J. of Coatings Technol.*, **1989**, *61*, 33.

(10) Hiemenz, P.C., *Polymer Chemistry*, Marcell Dekker: New York, 1984.

(11) Camargo, R.E., Macosko, C.W., Tirrell, M.V., Wellinghoff, S.T., *Polymer Comm.*, **1983**, *24*, 314.

(12) Harthcock, M.A., *Polymer*, **1989**, *30*, 1234.

(13) Drushel, H.V., *CRC Crit. Rev. in Anal. Chem.*, **1970**, *1*, 161.

(14) Lee, H.S., Hsu, S.L., *Macromolecules*, **1989**, *22*, 1100.

(15) Pollack, S.K., Shen, D.Y., Hsu, S.L., Wang, Q., Stidham, H.D., *Macromolecules*, **1989**, *22*, 551.

(16) Blackwell, J., Lee, C.P., *J. Poly Sci., Poly. Phys. Ed.*, **1984**, *22*, 759.

(17) Weyer, L.G., *Appl. Spectrosc. Rev.*, **1985**, *21*, 1.

(18) Miller, C.E., *Appl. Spectrosc.*, **1989**, *43(8)*, 1435.

(19) Miller, C.E., Eichinger, B.E., "Determination of Crystallinity and Morphology of Fibrous and Bulk Poly(ethylene terephthalate) by NIR Diffuse Reflectance Spectroscopy", *Appl. Spectrosc.*, **1990**, *44(3)*, in press.

(20) Murray, I., Williams, P.C., in *Near-infrared Technology in the Agricultrual and Food Industries*, American Association of Cereal Chemists: St. Paul, MN, 1987, chapter 2.

(21) Miller, C.E., Edelman, P.G., Ratner, B.D., *Appl. Spectrosc.*, **1990**, in press.

(22) Miller, C.E., Edelman, P.G., Ratner, B.D., Eichinger, B.E., "Near-infrared Spectroscopic Analysis of Polyether(urethaneurea) Block Copolymers, II. Phase Separation", *Appl. Spectrosc.*, **1990**, in press.

(23) Martens, H., Naes, T., in *Near-infrared Technology in the Agricultrual and Food Industries*, American Association of Cereal Chemists: St. Paul, MN, 1987, chapter 4.

(24) Jolliffe, I.T., *Principal Component Analysis*, Springer-Verlag: New York, 1986.

(25) Sharaf, M.A., Illman, D.L., Kowalski, B.R., *Chemometrics*, John Wiley and Sons: New York, 1986.

(26) Beebe, K., Kowalski, B.R., *Anal. Chem.*, **1987**, *59*, 1007A.

(27) Geladi, P., Kowalski, B.R., *Anal. Chim. Acta.*, **1986**, *185*, 1.

(28) Haaland, D.M., Easterling, R.G., Vopicka, D.A., *Appl. Spectrosc.*, **1985**, *39*, 73.

(29) Ilari, J.L., Martens, H., Isaksson, T., *Appl Spectrosc.*, **1988**, *42*, 722.

(30) Geladi, P., MacDougall, D., Martens, H., *Appl Spectrosc.*, **1985**, *39*, 491.

(31) Yeo, P., Honigs, D.E., Appl. Spectrosc., **1988**, *42*, 1128.

(32) ASTM Method D790-86, *1989 Annual Book of ASTM Standards*, ASTM : Philadelphia PA, **1989**, volume *08.01*, p.280.

(33) ASTM Method D3769-85, *1989 Annual Book of ASTM Standards*, ASTM : Philadelphia PA, **1989**, volume *09.02*, p.370.

(34) Veltkamp, D., PCA Modeling Program, Version 1.0 (IBM), Center for Process Analytical Chemistry, BG-10, Seattle WA, 98195, 1989.

(35) Veltkamp, D., Kowalski, B.R., *PLS-2 Block Modeling, Version 1.9 (IBM)*, Center for Process Analytical Chemistry, BG-10, Seattle WA 98195, 1986.

(36) Born, L., Hespe, H., Crone, J., Wolf., K.H., *Colloid and Polymer Sci.*, **1982**, *260*, 819.

(37) Birth, G.S., Hecht, H.G., in *Near-infrared Technology in the Agricultrual and Food Industries*, American Association of Cereal Chemists: St. Paul, MN, 1987, chapter 1.

(38) Kortum, G., *Reflectance Spectroscopy*, Springer-Verlag: New York, 1969, chapter 2, p. 23.

(39) Davies, A.M.C., Miller, C.E., *Appl. Spectrosc.*, **1988**, *42*, 703.

(40) Pimental, G., McClellan, A.L., *The Hydrogen Bond*, W.H. Freeman, San Fransisco, 1960.

(41) Schuster, P., Zundel, G., Sandorfy, C., *The Hydrogen Bond, II. Structure and Spectroscopy*, North-Holland Publ. Co.: New York, 1976.

(42) Miller, C.E., Honigs, D.E., *Spectroscopy*, **1989**, *4*, 44.

(43) Saunders, J.H., Frisch, K.C., *Polyurethanes, Chemistry and Technology, Part I: Chemistry*, Wiley-Interscience: New York, 1962, pp. 329 - 337.

Chapter 8

Determination of Compression and Thermal Properties of Rigid Polyurethane Foams by Near-infrared Diffuse Reflectance Spectroscopy

8.1 Introduction to Chapter 8

Rigid polyurethane foams are commonly used as insulation and packaging material (1). The performance of a foam depends greatly on its compression and thermal properties. As a result, it is necessary to make physical property determinations in order to assess the quality of a foam for a specific application. Physical testing methods, such as compression and thermal conductivity (2) tests, directly measure the physical properties of foams. However, these methods are usually destructive, subject to high variability, and require substantial sampling times. In many situations, a faster, non-destructive analytical method is desired.

Near-infrared (NIR) diffuse reflectance spectroscopy has been used to rapidly and non-destructively sample materials that are similar to rigid foams with respect to optical properties (3-6). In this work, the ability of near-infrared (NIR) diffuse reflectance spectroscopy to determine compression and thermal properties of rigid polyurethane foams is demonstrated. Principal Components Analysis (PCA) (7) of the NIR spectra of the foams is used to indicate differences between the spectra of foams that were prepared from different formulations. In addition, Partial Least Squares (PLS) (4,8-

10) calibrations of NIR spectra to compression modulus, compression strength, deformation at failure, and K-factor (thermal conductivity) are done.

8.2 Experimental

Two separate sets of rigid polyurethane foams were obtained from ICI Polyurethanes: 1) 26 samples that are tested for compression properties (see Table 8.1) and 2) 27 samples that are tested for K-factor, or thermal conductivity. The K-factor tested samples had K-factor values ranging from 0.158 to 0.202 Btu-in/^{o}F-hr-ft^{2}. All samples were prepared from pure or polymeric 4,4'-diphenylmethane diisocyanate (MDI) and a variety of different polyols and chain-extenders. The compression-tested samples were prepared from one of, or a combination of, three different polyols: a PET-based polyol, an aliphatic-based polyol, and an amine-based polyol. All of the foams contained small amounts of catalysts and surfactants. Each sample originally consisted of a large (approximately 1 ft. x 1 ft. x 3/4 in.) block, from which smaller blocks were cut for physical testing and NIR sampling.

Compression measurements (ASTM Method D1621-73) (11) were performed in triplicate, from three 2" x 2" blocks of each sample. A Universal Testing Machine (Instron) was used for compression testing. Three 1 in. x 1 in. blocks, which were cut adjacent to the blocks used for compression testing, were used for

Table 8.1: List of physical properties of rigid polyurethane foam samples that were tested with compression measurements. Intercorrelations of physical properties are also shown.

Table 8.1

Average values from Compression Test

sample number	modulus (P.S.I)	strength (P.S.I)	deformation (%)
1	639	33.29	6.7
2	429	20.06	7.95
3	737	35.07	6.14
4	454	20.29	7.77
5	317	15.86	10
6	510	22.14	7.04
7	500	20.84	6.07
8	642	31.85	6.49
9	368	19.38	10
10	720	34.98	6.52
11	681	32.87	6.31
12	631	31.38	7.51
13	538	25.73	6.9
14	546	22.45	6.96
15	396	17.82	10
16	462	18.94	8.67
17	565	23.26	5.43
18	547	26.17	6.3
19	502	21.85	6.84
20	376	19.37	8.68
21	433	20.01	9.24
22	382	17.55	10
23	392	18.5	10
24	664	34.9	6.94
25	199	12.67	10
26	544	21.53	5.48

Correlation coefficients for intercorrelation of physical properties:

	modulus	strength
strength	0.974	1
deformation	-0.802	-0.664

NIR analysis. A stress versus deformation curve for a biaxial compression (perpendicular to the direction of elongation of voids in the foam, see Chapter 1.4.1) was obtained for each compression test sample. Three physical properties were obtained from this curve: 1) the compression modulus, 2) compression strength, and 3) percent deformation at failure. Samples that did not fail at 10% deformation were assigned a value of 10% deformation. For each property, the average of the three values obtained from triplicate tests were used for correlation to NIR spectra.

K-factor measurements (ASTM Method C518-85) (12) were performed on a K-matic heat flow meter (Holometrix). A single K-factor measurement was made from a 1 ft. x 1 ft. block of each sample. A smaller 2 in. x 2 in. block, which was cut adjacent to the sample used for the K-factor measurement, was used for NIR analysis.

In order to avoid errors caused by aging effects in the foams, NIR and physical testing methods were performed within several days of each other. The estimated error for each of the compression-measured properties were determined as the pooled standard deviation of triplicate measurements of the property for all samples. The estimated error in the K-factor measurement was obtained from reference (2).

NIR diffuse reflectance spectra of the rigid foams were obtained with a Technicon InfraAlyzer 500C grating instrument (Chapter 1.2.4.2). The spectral range was 1100 nm to 2500 nm (in 2

nm increments), the nominal resolution was 10 nm, and the wavelength accuracy was 1 nm. Rigid foam blocks were placed on a sampling stage and covered with a quartz plate for NIR analysis. Each scan lasted approximately 2 minutes. Two replicate NIR scans for each block were obtained by sampling two opposite faces of the block.

Pre-analysis treatment of NIR spectra consisted of three steps: 1) averaging over samples, 2) averaging over wavelengths, and 3) correcting for scattering effects. For the K-factor-tested samples, duplicate spectra were averaged and adjacent wavelengths were averaged (resulting in 351 wavelength points for 27 spectra). For the compression-tested samples, three sets of duplicate spectra from the three blocks of each sample were averaged. Every other wavelength point, starting at 1102 nm, was removed, and every adjacent two wavelengths of those remaining were averaged (resulting in 176 wavelength points for 26 spectra). In all cases, Multiplicative Scatter Correction (MSC) (13) was used to correct the spectra for scattering effects after sample and wavelength averaging.

Principal Components Analysis (PCA) (7) of the spectra of the 26 compression-tested foam samples was performed with the UNSCRAMBLER software package (CAMO A/S, Trondheim, Norway). All spectra were mean-centered for PCA analysis. Partial Least Squares (PLS) (4,8-10) calibration of NIR spectra to thermal and compression properties was performed with the UNSCRAMBLER software package. For each PLS analysis, the original samples were

split into calibration and prediction sets. PLS calibrations were constructed using the calibration set, and the calibrations were then used to predict the physical properties of the samples in the prediction set. Mean-centered spectra were used for all PCA and PLS analyses.

PLS calibration errors were expressed using the Standard Error of Estimate (SEE) value (Chapter 1.5.2.3.2, Equation 1.16). Prediction errors were expressed using the Standard Error of Prediction (SEP) value (Chapter 1.5.2.3.2, Equation 1.17).

The method of cross-validation (7,10) was used to determine the optimal number of NIR spectral factors for PCA and PLS analyses. The cross-validation procedure involves the removal of some of the samples in the calibration set, construction of a PCA or PLS model with the remaining samples, and subsequent prediction of the spectra (in the case of PCA) or physical properties (in the case of PLS) of the removed samples by the model. The optimal number of PCA or PLS factors is the number of factors in the model at which prediction errors for the removed samples are minimized.

8.3 Results and Discussion

8.3.1 NIR Spectra of Rigid Foams

The NIR diffuse reflectance spectra of two rigid foams are shown in Figure 8.1. These spectra have highly-overlapped bands

Figure 8.1: Near-infrared diffuse reflectance spectra of sample 1 (A) and sample 2 (B), that were subsequently tested with compression measurements.

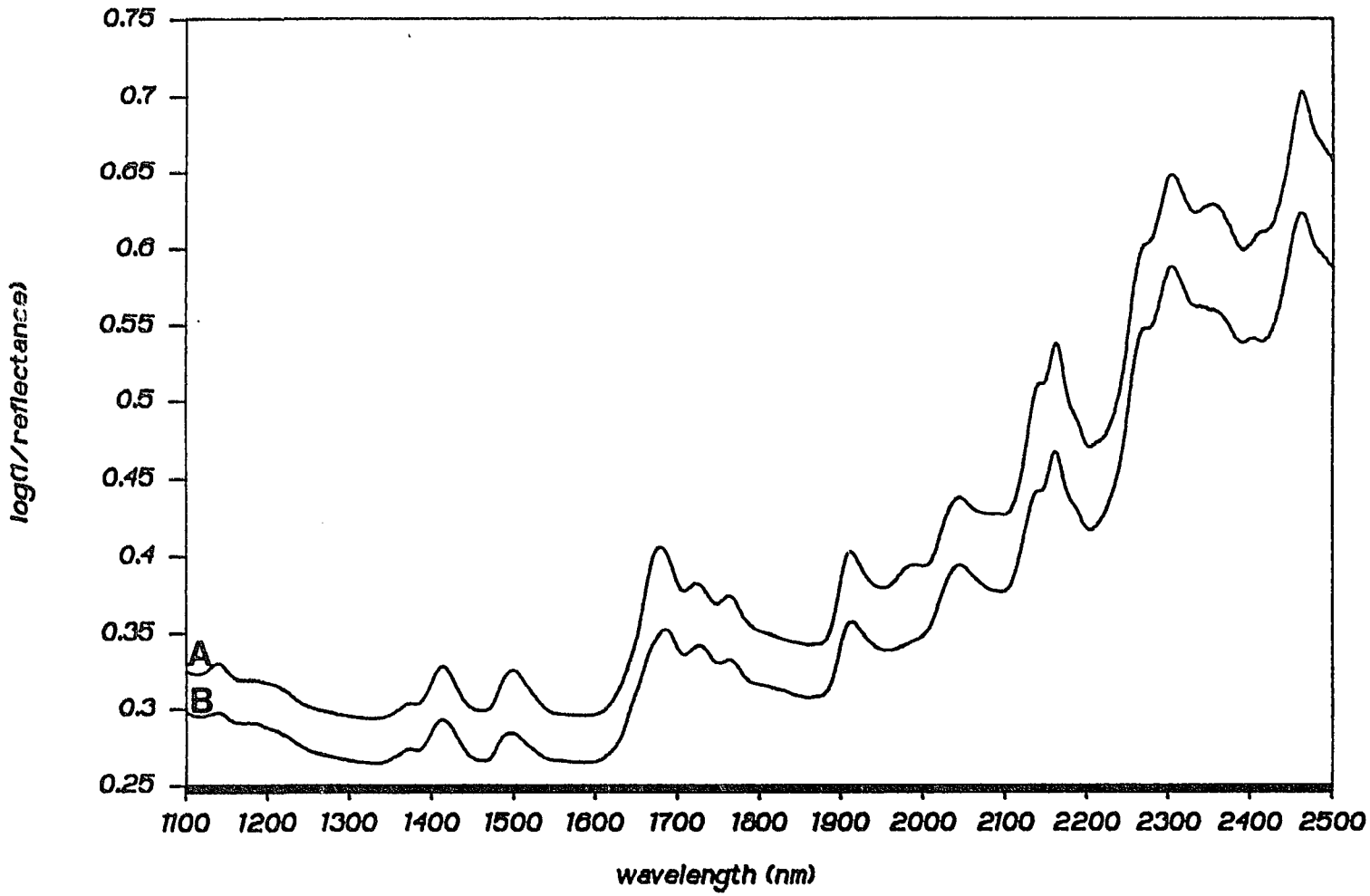
0.75
0.7
0.65
0.6
0.55
0.5
0.45
0.4
0.35
0.3
0.25
log(1/reflectance)
A
B
1100
1200
1300
1400
1500
1600
1700
1800
1900
2000
2100
2200
2300
2400
2500
wavelength (nm)

from CH, NH, and C=O groups in the samples. Bands in the regions 1100 nm to 1250 nm, 1600 nm to 1800 nm, and 2150 nm to 2500 nm are from various aromatic and aliphatic CH groups. NH absorbances are found at approximately 1500 nm and 2050 nm, and C=O absorbances are in the region 1900 nm to 2100 nm. More specific assignments of NIR peaks can be made by reference to earlier NIR analyses of polymers (14-16).

The differences in the two spectra in Figure 8.1 originate from chemical and physical differences in the foam samples. The difference in baseline offset of the two spectra is a result of physical differences, or scattering differences, of the two samples. The differences in peak shape or relative peak amplitudes, such as those observed at approximately 1650 to 1750 nm, 1980 to 2050 nm, and 2250 to 2350 nm in Figure 8.1, arise from differences in the chemistry of the samples. In this analysis, the method of Multiplicative Scatter Correction (MSC) is used to minimize the scattering effects and leave only the chemical effects to be used for calibration purposes.

8.3.2 Principal Components Analysis of Compression-tested Foams

Cross-validation results indicate that three components of variation exist in the NIR spectra of the compression-tested foams. Table 8.2 shows the percentage of explained spectral variance for

Table 8.2: Results of principal components analysis of NIR spectra of rigid polyurethane foams that were subsequently compression-tested.

Table 8.2

Explained Spectral Variance:

number of principal components in model	percentage of spectral variation explained
1	52.6
2	73.1
3	86.7

Observed Sample Clusters:

cluster number	samples in cluster	polyol component(s) corresponding to cluster
I	1,3,8,10,11,12, 13,18,24	aliphatic-based polyol
II	5,9,21,23,25	PET-based polyol
III	7,15,20,26	PET-based and amine-based polyol
IV	2,4,6,14,16,17, 19,22	PET-based and aliphatic-based polyol

PCA models that have 1, 2, and 3 principal components. It should be noted that a significant amount of spectral variation (13.3%) is not explained by the three principal component model. The unexplained variance can be caused by the presence of minor components in the foams, such as catalysts and surfactants, the presence of reaction by-products in the foams, or inadequate removal of scattering effects in the spectra. It is more likely, however, that this unexplained variance corresponds to the spectral noise level relative to the spectral variance from chemical differences.

Figure 8.2, A, which shows a representation of the 26 samples in the space defined by the first and second principal components, indicates the relationship between the spectra of the different foam samples. The most striking feature of this plot is the presence of 4 well-defined clusters of samples. Furthermore, it is known that each of these clusters corresponds to a specific polyol component in the foams. Each cluster is assigned a cluster number of I to IV. Table 8.2 lists the samples that belong to the different clusters, and the polyol component that corresponds to the different clusters.

In order to quantitate the degree of clustering of samples in the three-dimensional PCA score space, several Euclidean distances in the space are calculated. For this analysis, distances along each principal component axis are defined as the principal component score divided by the square root of the eigenvalue of that principal component. As a result, all three principal components have equal weight. Distances between the mean points of different clusters are

Figure 8.2: Representation of the NIR spectra of compression-tested samples in the two-dimensional spaces defined by the first and second principal component scores (A), and the first and third principal component scores (B). In plot A, sample clusters are labeled I, II, III, and IV. In plot B, only cluster III is identified.

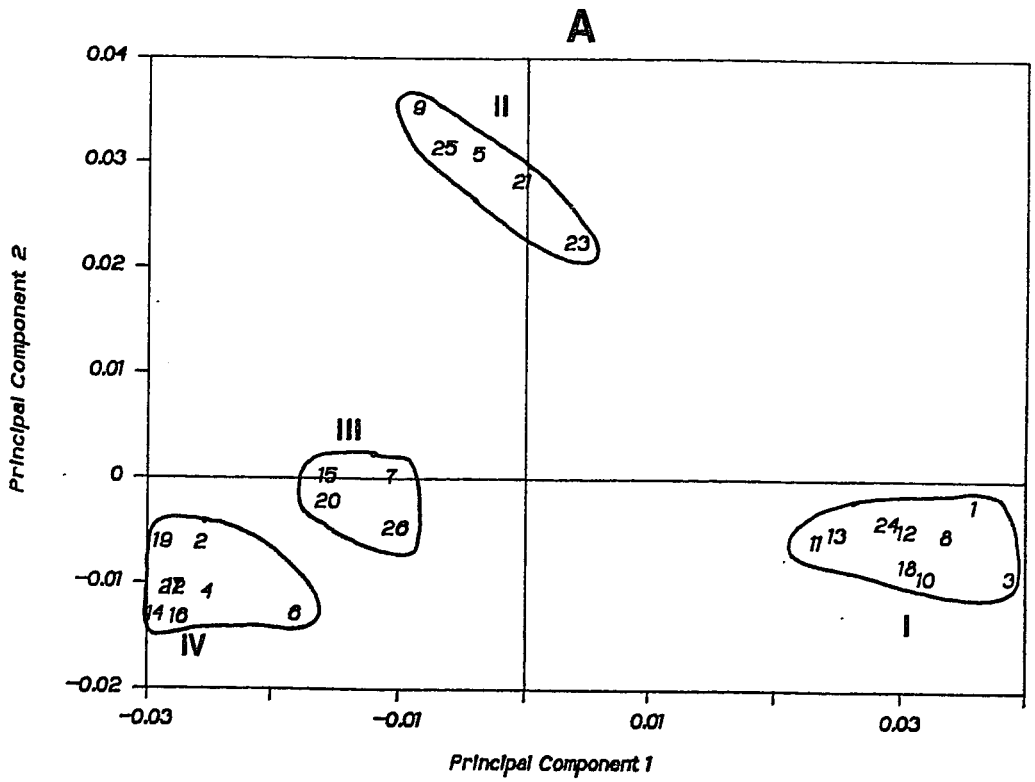
A
0.04
0.03
0.02
0.01
0
−0.01
−0.02
−0.03
−0.01
0.01
0.03
Principal Component 2
Principal Component 1
II
III
IV
I
9
25
5
21
23
15
7
20
26
19
2
22
4
14
16
6
1
11
13
24
12
8
18
10
3

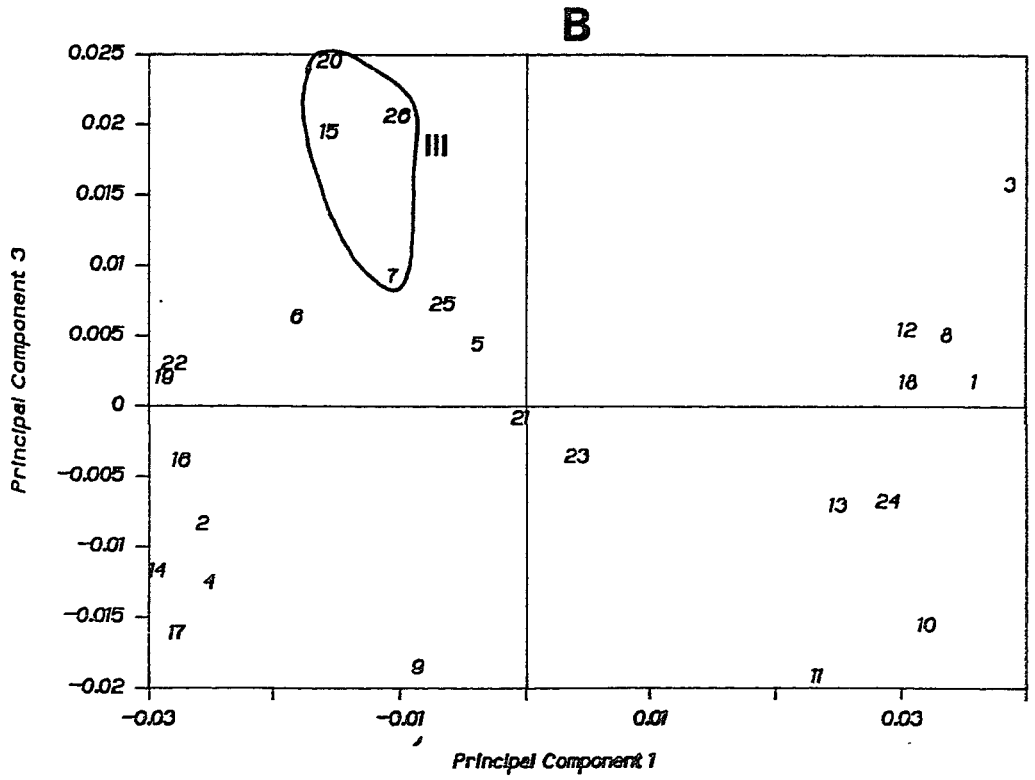
B
0.025
0.02
0.015
0.01
0.005
0
−0.005
−0.01
−0.015
−0.02
−0.03
−0.01
0.01
0.03
Principal Component 3
Principal Component 1
III
20
26
15
7
6
25
5
22
19
21
16
23
2
14
4
17
9
11
13
24
10
12
8
18
1
3

compared to average deviations of individual points from their corresponding mean cluster point. The results of this analysis are shown in Table 8.3. All inter-cluster distances are much larger than the intra-cluster deviations. This result suggests that the clusters are well-defined.

The identities of the polyol components corresponding to the different clusters can be confirmed by observation of the PCA loading spectra. Figure 8.3 shows the loading spectra for the first (A) and second (B) principal components. Assignment of positive and negative bands in the loading spectra are aided by previous NIR analyses of poly(ether urethaneurea) copolymer (14), poly(ethylene terephthalate) (15), and ethylene-propylene-diene terpolymer (16). Positive peaks in the first principal component loading spectrum at 1142, 1674, 2142, and 2166 nm correspond to aromatic CH bands of the MDI group. In addition, positive peaks are observed at 1910 nm and 1978 nm (from C=O groups) and at 1502 nm (from NH groups). These results suggest that the first principal component is positively correlated to the fraction of MDI and urethane groups in the sample.

Negative peaks at 1646, 2118, and 2446 nm in the first principal component loading spectrum (Figure 8.3,A) correspond to the aromatic CH vibrations of poly(ethylene terephthalate) (PET) (15). Other negative bands at 2262 and 2390 nm are from the ethylene groups in the ethylene glycol part of PET. These results indicate that the first principal component is negatively correlated to the fraction of PET-based polyol in the foams.

Table 8.3: Weighted euclidean distances between different sample clusters, and variations within each sample cluster in 3-dimensional PCA score space.

Table 8.3

Distances between mean points of clusters:

	Cluster I	Cluster II	Cluster III
Cluster II	0.543		
Cluster III	0.496	0.541	
Cluster IV	0.469	0.560	0.423

Average deviation of individual points from mean point of cluster:

Cluster I: 0.141

Cluster II: 0.141

Cluster III: 0.088

Cluster IV: 0.113

Figure 8.3: Principal component loading spectra of the first (A), second (B), and third (C) principal components, obtained from principal components analysis of rigid foam samples that were subsequently compression-tested.

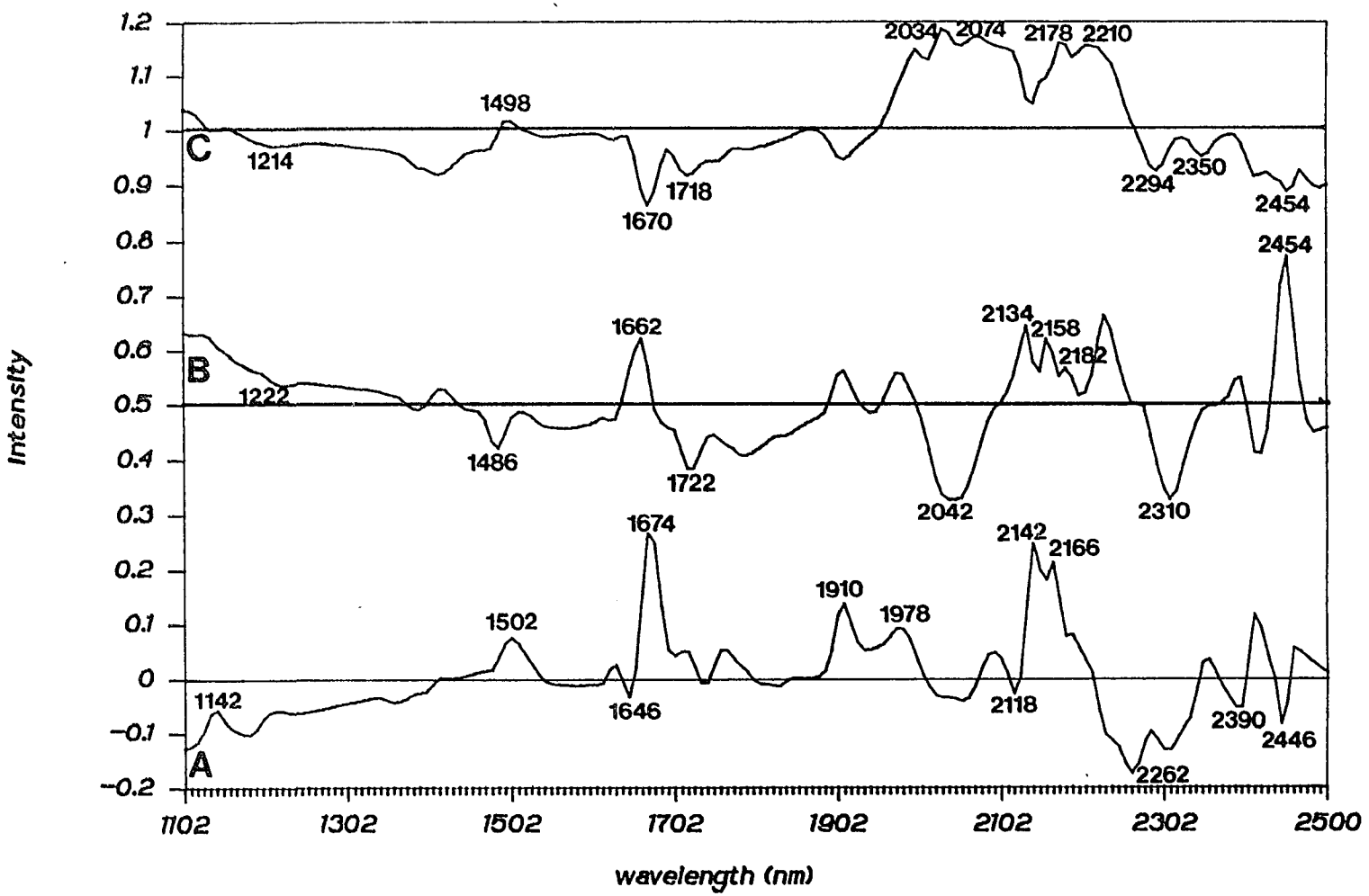
1.2
1.1
1
0.9
0.8
0.7
0.6
0.5
0.4
0.3
0.2
0.1
0
−0.1
−0.2
Intensity
C
1214
1498
1670
1718
2034
2074
2178
2210
2294
2350
2454
B
1222
1486
1662
1722
2042
2134
2158
2182
2310
2454
A
1142
1502
1646
1674
1910
1978
2118
2142
2166
2262
2390
2446
1102
1302
1502
1702
1902
2102
2302
2500
wavelength (nm)

Positive bands in the second principal component loading spectrum (Figure 8.3, B) at 1662, 2134, 2158, 2182, and 2454 nm are from aromatic CH groups in PET. Negative bands at 1486 nm and 2042 nm correspond to NH vibrations in the urethane groups of the polymers. Other negative bands at 1222, 1722 and 2310 nm are probably from ethylene groups in the polyol component of the polymer. These results indicate that the second principal component is positively correlated to the amount of PET-based polyol in the polymers and negatively correlated to the amount of aliphatic-based polyol and the urethane groups in the polymers.

The third principal component explains a small, but significant amount of variation in the spectra of the compression-tested foams. The third principal component loading spectrum, shown in Figure 8.3, C, has positive peaks in the NH and C=O regions (1498, 2034 and 2074 nm) and negative bands in the ethylene CH regions (1214, 1718, 2294, and 2350 nm). The negative peaks at 1670 and 2454 nm probably correspond to aromatic CH vibrations in PET, and the positive peaks at 2178 and 2210 nm probably correspond to aromatic CH vibrations in the MDI group. These results indicate that the third principal component is positively correlated the MDI and NH content of the polymers. Table 8.4 shows the summary of functional group correlations for the three principal components.

The PCA results indicate that the samples in cluster I, which have the highest values of the first principal component score and negative values of the second principal component score, must have

Table 8.4: Functional groups in the rigid polyurethane foams that are positively and negatively correlated to each principal component (obtained from Principal Components Analysis of NIR spectra of rigid polyurethane foam samples).

Table 8.4

Functional Groups in the Polymers

Principal Component	Positive Correlation	Negative Correlation
1	MDI, urethane	PET
2	PET	urethane, ethylene (aliphatic C-H)
3	MDI, NH, carbonyl	PET, ethylene

the highest urethane content and lowest PET content. These results are consistent with the fact that the samples in cluster I contain an aliphatic-based polyol. Furthermore, the observation that these samples have the highest urethane content is consistent with the observation that they have the highest compression moduli (1) (consult Tables 8.1 and 8.2).

The samples in clusters II, III and IV have negative values of the first principal component score, which indicates that these samples each contain a PET-based polyol. The samples in cluster IV also have negative values of the principal component 2 score, which indicates that they also contain an aliphatic-based polyol. These results are consistent with the known correlations of polyol components to the different clusters of samples (Table 8.2).

Figure 8.2, **B** shows the representation of the foam samples in the space defined by principal components 1 and 3. The only samples that are affected by the 3rd principal component are the samples in cluster III. The samples in the other clusters have principal component 3 score values that are distributed about zero. If this result is combined with functional groups correlations of the third principal component (Table 8.4), it can be concluded that the samples in cluster III have significantly more NH content than the other samples. This result is consistent with the fact that these samples contain an amine-based polyol component, because an amine-based polyol would produce urea groups (with 2 NH bonds

each) instead of urethane groups (with one NH bond each) upon reaction with isocyanate.

8.3.3 PLS Calibrations for Compression Properties

The results of PLS calibrations to compression modulus, compression strength, and percent deformation are shown in Table 8.5. The cross-validation results suggest the use of only two spectral factors for calibration to these properties. These results might appear contradictory to the PCA results, which indicate that three sources of spectral variation are present. However, the cross-validation results are a better indicator of the optimal number of spectral factors for calibration to a specific property.

The calibration SEE values and prediction SEP values for the two-factor PLS calibrations are shown in Table 8.5. Estimated errors in the physical measurement of compression properties are also shown. These results indicate that NIR spectroscopy can be used to predict compression modulus within 63.6 P.S.I., compression strength within 2.63 P.S.I., deformation at failure within 1.44% and K-factor within 0.0089 Btu-in/^{o}F-hr-ft^{2}. The modulus and strength calibrations are the most accurate, in terms of relative calibration and prediction error. However, the standard error of calibration and prediction for each property is only slightly greater than, or even less than, the estimated error in the physical measurement. This

Table 8.5: Calibration and prediction errors of PLS calibrations of NIR spectra to various physical properties of rigid polyurethane foams.

Table 8.5

physical property (units)	error of physical measurement	SEE	relative calibration error (%)	SEP	relative prediction error (%)	number of PLS factors used[c]
Compression modulus (P.S.I.)	50.3[a]	53.2	9.89	63.6	20.3	2
Compression strength (P.S.I.)	1.84[a]	1.95	8.71	2.63	17.2	2
Deformation at failure (%)	1.29[a]	0.88	19.3	1.44	39.0	2
K-factor (Btu-in/^{o}F-hr-ft^{2})	0.013[b]	0.0095	21.6	0.0089	26.2	2

a determined as pooled standard deviation of triplicate measurements

b obtained from Reference 2

c determined by cross-validation

result suggests that errors in the physical measurements are the major source of calibration and prediction errors.

The first PLS loading spectrum for the compression modulus calibration, shown in Figure 8.4, A, indicates the NIR spectral features that are positively and negatively correlated to the compression modulus of the foams. Positive features at 1674 nm and 2142 nm are from aromatic CH vibrations in the MDI group. The positive band at 1502 nm corresponds to the NH group and the positive bands at 1910 nm and 1982 nm correspond to the carbonyl group. These results indicate that modulus increases with increasing fraction of urethane and MDI groups in the foam. Positive ethylene bands at 1718 nm and 1762 nm indicate a positive correlation between modulus and ethylene content. The negative features are dominated by PET bands (1646, 2118, 2262, and 2450 nm). The positive ethylene bands and negative PET bands indicate that, for a given fraction of MDI groups in the polymer, the foams with the aliphatic polyol component have a higher modulus than the foams with the PET-based polyol components. Because the three compression properties are highly intercorrelated (see Table 8.1), first PLS loading spectra for strength and deformation have very similar features. The functional group correlations for strength are the same as those for compression modulus, and the correlations for deformation are exactly opposite to those for compression modulus.

Figure 8.4: First PLS loading spectra for the correlation of NIR spectra to compression modulus (**A**) and K-factor (**B**) of rigid polyurethane foams.

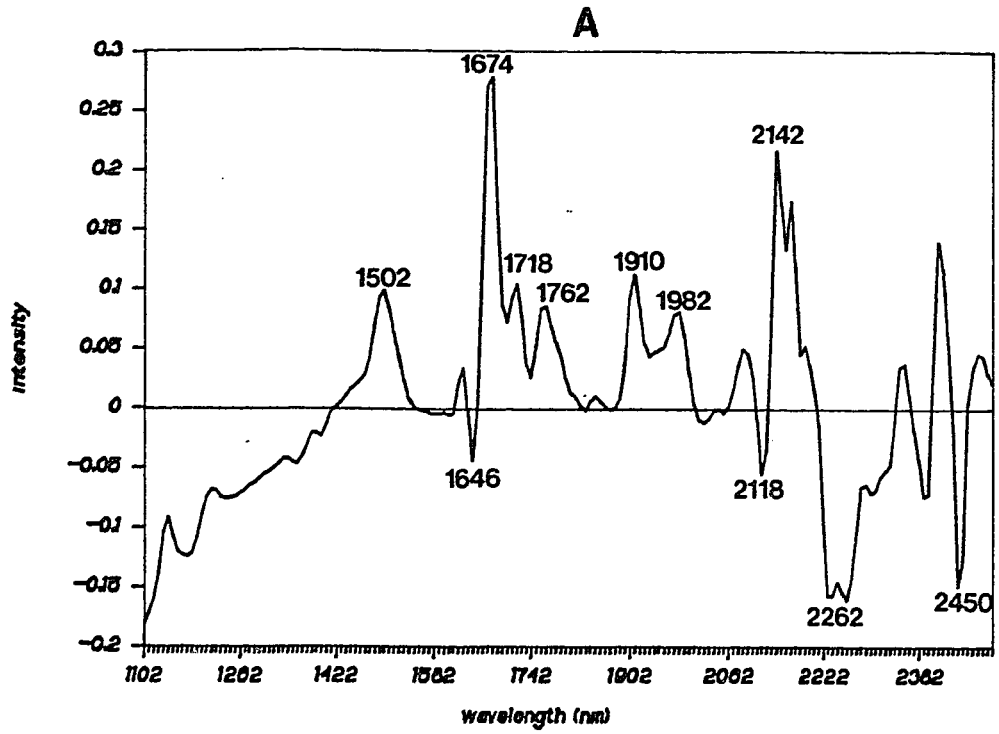
A
1674
2142
1718
1910
1502
1762
1982
1646
2118
2262
2450
0.3
0.25
0.2
0.15
0.1
0.05
0
-0.05
-0.1
-0.15
-0.2
Intensity
1102
1262
1422
1582
1742
1902
2062
2222
2382
wavelength (nm)

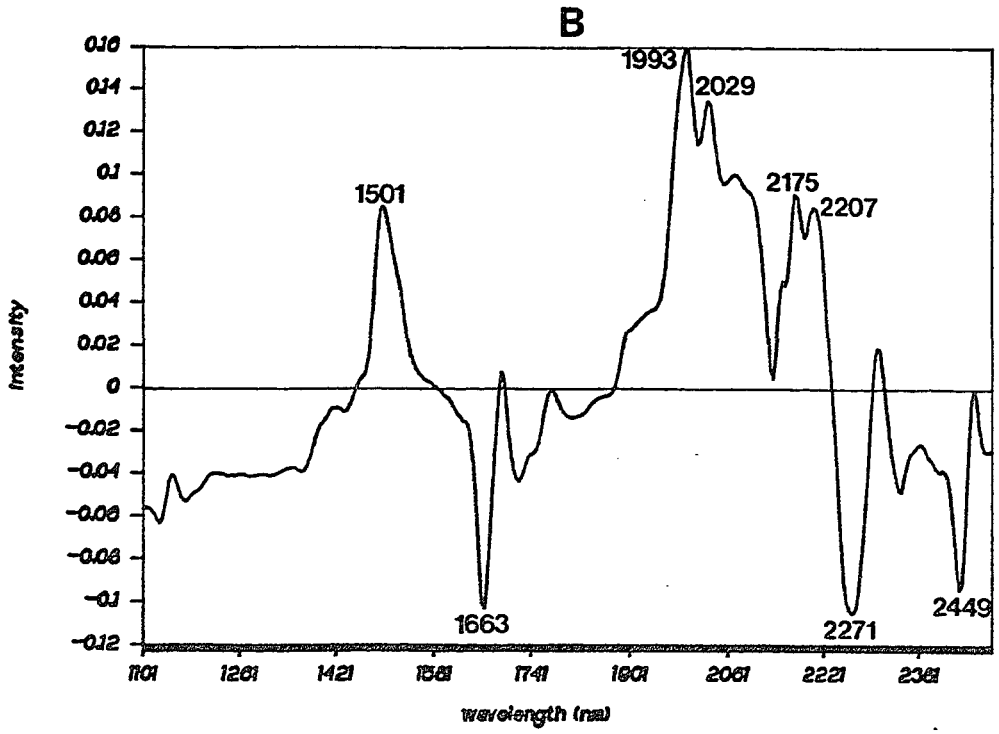
B
1993
2029
1501
2175
2207
1663
2271
2449
0.16
0.14
0.12
0.1
0.08
0.06
0.04
0.02
0
-0.02
-0.04
-0.06
-0.08
-0.1
-0.12
Intensity
1101
1261
1421
1581
1741
1901
2061
2221
2381
wavelength (nm)

8.3.4 PLS Calibration for K-factor

The results for the PLS calibration to K-factor are shown in Table 8.5. Cross-validation results indicate that two spectral factors are necessary for the calibration. Although the relative calibration and prediction errors are large, the absolute SEE and SEP values are lower than the estimated error of the physical K-factor measurement (2). As a result, the error in the physical measurement is probably the main contributor to the calibration and prediction errors.

The first PLS loading spectrum for the calibration to K-factor is shown in Figure 8.4, **B**. Positive bands at 1501, 1993 and 2029 nm correspond to urethane NH and carbonyl absorbances. The negative peaks at 1663 nm and 2449 nm correspond to the terphthalic acid group in PET, and the negative peak at 2271 nm coresponds to the ethylene glycol group in PET. These results suggest that the thermal conductivity of the foams is positively correlated to the fraction of urethane groups and negatively correlated to the PET content of these foams.

8.4 Conclusion

This study demonstrates the ability of NIR diffuse reflectance spectroscopy to perform rapid chemical characterizations of rigid polyurethane foams. The chemical information provided by NIR spectroscopy enables discrimination between foams that were

prepared from different polymeric formulations. In addition, accurate NIR determinations of compression and thermal properties of rigid foams are possible.

It is important to note that the formulation (or polyol component) was the major source of variation of the foam samples used in this work. As a result, the studies in this work indicate the effect of formulation on the spectra and properties of rigid foams. An additional study that uses foams of the same formulation, but with different compositions (or relative percentage of MDI and polyol in the polymer) could be used to determine the effects of composition and other factors on the NIR spectra and physical properties of rigid foams.

8.5 Notes to Chapter 8

(1) Frisch, K.C., Reegen, S.L., *Advances in Urethane Science and Technology*; Technomic, Stamford CT, (1971).

(2) Smith, S.A., Galbraith, C.J., Cartmell, M.J., Moore, M.L., Brown, R.K., *Polyurethanes World Congress* **1987**, *Sept. 29 - Oct. 2*, 1987, 74.

(3) Stark, E. Luchter, K., Margoshes, M., *Appl. Spectrosc. Rev.*, **1986**, *22*, 335.

(4) Williams, P., Norris, K., *Near-infrared Technology in the Agricultural and Food Industries*; American Association of Cereal Chemists: St. Paul MN (1987).

(5) Weyer, L.G., *Appl. Spectrosc. Rev.*, **1985**, *21*, 1.

(6) Miller, C.E., Yin, T-K., *J Mat. Sci. Lett.*, **1989**, *8*, 467.

(7) Joliffe, I.T., *Principal Components Analysis*, Springer-Verlag, N.Y., (1986).

(8) Beebe, K., Kowalski, B.R., *Anal. Chem.*, **1987**, *59*, 1007A.

(9) Geladi, P., Kowalski, B.R., *Anal. Chim. Acta.*, **1986**, *185*, 1.

(10) Haaland, D.M., Thomas, E.V., *Anal. Chem.*, **1988**, *60*, 1202.

(11) ASTM Method D1621-73, *1989 Annual Book of ASTM Standards*, ASTM: Philadelphia, **1989**, volume *08.02*, p. 11.

(12) ASTM Method C518-85, *1988 Annual Book of ASTM Standards*, ASTM: Philadelphia, **1988**, volume *04.06*, p. 151.

(13) Geladi, P., MacDougall, D., Martens, H., *Appl. Spectrosc.*, **1985**, *39*, 491.

(14) Miller, C.E., Edelman, P.G., Ratner, B.D., "Near-infrared Spectroscopic Analysis of Polyether(urethaneurea) Block Copolymers, I. Bulk Composition", *Appl. Spectrosc.*, **1990**, in press.

(15) Miller, C.E., Eichinger, B.E., "Determination of Crystallinity and Morphology of Fibrous and Bulk Poly(ethylene terephthalate) by NIR Diffuse Reflectance Spectroscopy", *Appl. Spectrosc.*, **1990**, *44(3)*, in press.

(16) Miller, C.E., *Appl. Spectrosc.*, **1989**, *43(8)*, 1435.

Bibliography

Alaki, Y., Yoshimoto, T., Dnanari, M, Takenchi, M., *Rubber Chem. and Tech.*, **1973**, *46*, 350.

Ambrose, E.J., Elliot, A., *Proc. Roy. Soc. (London)*, **1951**, *208A*, 75.

Angel, S.M., Katz, L.F., Archibald, D.D., Lin, L.T., Honigs, D.E., *Appl. Spectrosc.*, **1988**, *42*, 1327-1331.

Archibald, D.D., Lin, L.T., Honigs D.E., *Appl. Spectrosc.*, **1988**, *42*, 1558.

Archibald, D.D., Miller, C.E., Lin, L.T., Honigs, D.E., *Appl Spectrosc.*, **1988**, *42(8)*, 1549.

ASTM Committee D-2 and API Research Project 44, *Physical Constants of Hydrocarbons C_1 to C_{10}*; ASTM: Philadelphia PA, 1971; pp. 2, 14.

ASTM Method C518-85, *1988 Annual Book of ASTM Standards*, ASTM: Philadelphia, **1988**, volume *04.06*, p. 151.

ASTM Method D790-86, *1989 Annual Book of ASTM Standards*, ASTM: Philadelphia PA, **1989**, volume *08.01*, p.280.

ASTM Method D1621-73, *1989 Annual Book of ASTM Standards*, ASTM: Philadelphia, **1989**, volume *08.02*, p. 11.

ASTM Method D3769-85, *1989 Annual Book of ASTM Standards*, ASTM: Philadelphia PA, **1989**, volume *09.02*, p.370.

Baranwal, K.C., Lindsay, G.A., *Rubber Chem. Tech.*, **1972**, *45*, 1334.

Basch, A., Wasserman T., Lewin, M., *J. Poly. Sci.*, **1974**, *12*, 1143.

Beebe, K., Kowalski, B.R., *Anal. Chem.*, **1987**, *59*, 1007A.

Bergin, F.J., Shurvell, H.F., *Appl. Spectrosc.*, **1989**, *43*, 516.

Binder, J.L., *Anal. Chem.*, **1954**, *26*, 1877.

Blackwell, J., Lee, C-D., *J. Poly. Sci., Poly. Phys.*, **1984**, *22*, 759.

Blackwell, J., Nagarajan, M.R., *Polymer*, **1981**, *22*, 202.

Blackwell, J., Quay, J.R., Turner, R.B., *Poly. Eng., and Sci.*, **1983**, *23*, 816.

Bly, R.M., Kiener, P.E., Fries, B.A., *Anal. Chem.*, **1966**, *38*, 217.

Born, L., Hespe, H., Crone, J., Wolf., K.H., *Colloid and Polymer Sci.*, **1982**, *260*, 819.

Bovey, F.A., *High Resolution NMR of Macromolecules*, Academic Press: N.Y., 1972.

Brimmer, P.J., doctoral dissertation, University of California, Riverside, 1987.

Brown, C.W., Obremski, R.J., *Appl. Spec. Rev.*, **1984**, *20*, 373.

Brown, D.L., Weissert, J.T., Bhakuni, R.S., Rogowski, G.S., *U.S. Patent 4,654,253*, March 31, 1987.

Buback, M., Vogele, H., Winkels, H., *Makromol. Chem., Macromol. Symp.*, **1986**, *5*, 69.

Buchanan, B.R., doctoral dissertation, University of Washington, Seattle WA, 1987.

Buchat, R. K., Richard, A. J., *J. Chem. Thermodyn.*, **1975**, *7*, 271.

Burnshlegl, E., Bonart, R., *Colloid and Poly. Sci.*, **1980**, *258*, 319.

Calvert, P.D., Tormey, E.S., Pober, R.L., *Am. Ceram. Soc. Bull.*, **1986**, *65*, 669.

Camargo, R.E., Macosko, C.W., Tirrell, M.V., Wellinghoff, S.T., *Poly. Eng. and Sci.*, **1982**, *22*, 719.

Camargo, R.E., Macosko, C.W., Tirrell, M.V., Wellinghoff, S.T., *Polymer Comm.*, **1983**, *24*, 314.

Camargo, R.E., Macosko, C.W., Tirrell, M.V., Wellinghoff, S.T., *Polymer*, **1985**, *26*, 1145.

Cannon, C.G., *Mikrochim. Acta*, **1955**, *2-3*, 555.

Chen, Z.S., Yang, W.P., Macosko, C.W., *Rubber Chem. and Technol.*, **1988**, *61*, 86.

Claque, A.D.H., vanBroekhoven, J.A.M., Blaavin, R.P., *Macromolecules*, **1974**, *7*, 348.

Colthup, N.B., Daly, L.H., Wiberly, S.E., *Introduction to Infrared and Raman Spectroscopy, 2nd edition*, Academic: N.Y., 1975.

Crandall, E.W., *J. Appl. Poly. Sci.*, **1975**, *19*, 897.

D'Esposito, L., Koenig, J.L., *J. Poly. Sci., Phys. Ed.*, **1976**, *14*, 1731.

Daubeny, R.P., Bunn, C.W., Brown, C.J., *Proc. Roy, Soc. A*, **1954**, *226*, 531.

Davies, A.M.C, Rutland, S.G., *Spectrochim. Acta*, **1988**, *45A*, 1143.

Davies, A.M.C., Grant, A., Gavrel, G.M., Steeper, R.V., *Analyst*, **1985**, *110*, 643.

Davies, A.M.C., Miller, C.E., *Appl. Spectrosc.*, **1988**, *42*, 703.

Drushel, H.V., *CRC Crit. Rev. in Anal. Chem.*, **1970**, *1*, 161.

Drushel, H.V., Iddings, F.A., *Anal. Chem.*, **1963**, *35*, 28.

Durbetaki, A.J., Miles, C.M., *Anal. Chem.*, **1965**, *37*, 1231.

Edelman, P.G., Ratner, B.D., unpublished results, 1988.

Eichinger, B.E., Flory, P.J., *Trans. Faraday Soc.*, **1968**, *64*, 2035.

Elliot, E., *Proc. Roy. Soc. (London)*, **1951**, *211A*, 490.

Ellis, J.W., Bath, J., *J. Chem. Phys.*, **1938**, *6*, 723.

Evans, A., Hibbard, R.R., Powell, A.S., *Anal. Chem.*, **1951**, *23*, 1604.

Fakirov, S., Fischer E.W., Hoffmann, R., Schmidt, G.F., *Polymer*, **1977**, *18*, 1121.

Farrow, G., Ward, I.M., *Polymer*, **1960**, *1*, 330.

Fina, L.J., Koenig, J.L., *Macromolecules*, **1984**, *17*, 2572.

Fischer, E.W., *Polymer J.*, **1985**, *17*, 397.

Flory, P.J., *Principles of Polymer Chemistry*, Cornell Univ. Press: Ithaca NY, 1953.

Fontana, B.J., Thomas, J.R., *J. Phys. Chem.*, **1961**, *65*, 480.

Frisch, K.C., Reegen, S.L., *Advances in Urethane Science and Technology*; Technomic, Stamford CT, (1971).

Geladi, P., Kowalski, B.R., *Anal. Chim. Acta*, **1986**, *185*, 1.

Geladi, P., MacDougall, D., Martens, H., *Appl Spectrosc.*, **1985**, *39*, 491.

Ghosh, S., Rodgers, J.E., *Text. Res. J.*, **1985**, *55*, 556.

Gilbert, M., Briggs, J.E., Omana, W., *Br. Poly. J.*, **1979**, *11*, 81.

Glatt, L., Ellis, J.W., *J. Chem. Phys.*, **1951**, *19*, 459.

Glatt, L., Webber, D.S., Seaman, C., Ellis, J.W., *J. Chem. Phys.*, **1950**, *18*, 413.

Goddu, R.F., *Anal. Chem.*, **1957**, *29*, 1790.

Goddu, R.F., Delker, D.A., *Anal. Chem.*, **1958**, *30*, 2009.

Goddu, R.F., Delker, D.A., *Anal. Chem.*, **1960**, *32*, 140.

Groeninckx, G., Reynaers, H., Berghmans, H., Smets, G., *J. Poly. Sci., Phys. Ed.*, **1980**, *18*, 1311.

Groeninckx, G., Reynaers, H., *J. Poly. Sci., Phys. Ed.*, **1980**, *18*, 1325.

Gupta, V.B., Kumar, S., *J. Appl. Poly. Sci.*, **1981**, *26*, 1865.

Haaland, D.M., Easterling, R.G., Vopicka, D.A., *Appl. Spectrosc.*, **1985**, *39*, 73.

Haaland, D.M., Thomas, E.V., *Anal. Chem.*, **1988**, *60*, 1202.

Harthcock, M.A., *Polymer*, **1989**, *30*, 1234.

Hecht, H.G., in *Modern Aspects of Reflectance Spectroscopy, Symposium Proceedings*, Plenum Press: N.Y., 1968, pp. 1-26.

Hecht, K.T., Wood, D.L., *Proc. Roy. Soc. London*, **1956**, *235*, 174.

Heuvel, H.M., Huisman, R., *J. Appl. Poly. Sci.*, **1985**, *30*, 3069.

Hiemenz, P.C., *Polymer Chemistry*, Marcell Dekker: New York, 1984.

Hill, L.G., Hedren, A.M., Myers, G.E., Koutsky, J.A., *J. Appl. Polym. Sci.*, **1984**, *29*, 2749.

Holman, R.J., Edmondson, P.R., *Anal. Chem.*, **1956**, *28*, 1533.

Honigs, D.E., *Anal. Instr.*, **1985**, *16*, 1.

Honigs, D.E., doctoral dissertation, Indiana University, Bloomington, IN, 1984.

Honigs, D.E., Hirschfeld, T.B., Hieftje, G.M., *Anal. Chem*, **1985**, *57*, 443.

Ilari, J.L, Martens, H., Isaksson, T., *Appl. Spectrosc.*, **1988**, *42*, 722.

International Data Series, Selected Data for Mixtures, Ser. A, **1973**, 100.

International Data Series, Selected Data for Mixtures, Ser. A, **1975**, 186.

International Data Series, Selected Data for Mixtures, Ser. A, **1975**, 188.

International Data Series, Selected Data for Mixtures, Ser. A, **1976**, 55.

Ito, E., Yamamoto, K., Kobayashi, Y., Hatakeyama, T., *Polymer*, **1978**, *19*, 39.

Jolliffe, I.T., *Principal Component Analysis*, Springer-Verlag: New York, 1986.

Kamlet, M.J., Abboud, J.M., Abraham, M.H., Taft, R.W., *J. Org. Chem.*, **1983**, *48*, 2877.

Kaye, W., *Spectrochimica Acta*, **1954**, *6*, 257.

Kelly, J.J., Barlow, C.H., Jinguji, T.M., Callis, J.B., *Anal. Chem.*, **1989**, *61*, 313.

Kirkham, M.C., *J. Appl. Poly. Sci.*, **1973**, *17*, 1101.

Koenig, J.L., *Chemical Microstructures of Polymer Chains*, John Wiley and Sons: New York, 1970.

Korn, M., Killmann E., Eisenlauer, J., *J. Colloid and Interface Sci.*, **1980**, *76*, 7.

Kortum, G., Braun, W., Herzog, G., *Angew. Chem.*, **1963**, *2(7)*, 333.

Kortum, G., *Reflectance Spectroscopy*, Springer-Verlag: New York, 1969.

Kubelka, P., Munk, F., *Z. Tech. Phys.*, **1931**, *12*, 593.

Ladd, M.F.C., Palmer, R.A., *Structure Determination by X-ray Diffraction*, Plenum Press: N.Y., 1977.

Lee, H.S., Hsu, S.L., *Macromolecules*, **1989**, *22*, 1100.

Lee, H.S., Wang, Y-K., MacKnight, W.J., Hsu, S.L., *Macromolecules*, **1988**, *21*, 270.

LeFevre, R.J.W., Parkins, G.M., Roper, R., *Aust. J. Chem.*, **1959**, *13*, 169.

Lelah, M.D., Cooper, S.L., *Polyurethanes in Medicine*, (CRC press, Boca Raton FL, 1986).

Lin, S-B, Koenig, J.L., *J. Poly Sci, Poly. Phys. Ed.*, **1982**, *20*, 2277.

Lin, S-B, Koenig, J.L., *J. Poly Sci, Poly. Phys. Ed.*, **1983**, *21*, 2365.

Liu, L.B., Sumita, M., Miyasaka, K., *Macromolecules*, **1988**, *21*, 3424.

Macosko, C.W., *Plast. Eng.*, **1983**, *39(4)*, 21.

Macosko, C.W., *RIM, Fundamentals of Reaction Injection Molding*, Hanser Publishers: Munich, 1989.

Mandelkern, L., *Crystallization of Polymers*, McGraw-Hill: New York, 1964.

Mark, H., *Anal. Chem.*, **1986**, *58*, 2814.

Mark, J.E., Erman, B., *Rubberlke Elasticity, A Molecular Primer*, John Wiley and Sons: N.Y., 1988.

Martens, H., Naes, T., *Trends Anal. Chem.*, **1984**, *3(8)*, 204.

McClure, W.F., in *Near-infrared Technology in the Agricultural and Food Industries*, Williams, P, Norris, K., Eds., American Association of Cereal Chemists: St. Paul MN, 1987, Chapter 5.

Melveger, A.J., *J. Poly. Sci., A-2*, **1972**, *10*, 317.

Miller, C.E., "Analysis of Reaction-Injection-Molded Polyurethanes by NIR Diffuse Reflectance Spectroscopy", unpublished work, 1989.

Miller, C.E., *Appl. Spectrosc.*, **1989**, *43(8)*, 1435.

Miller, C.E., Edelman, P.G., Ratner, B.D., Eichinger, B.E., "Near-infrared Spectroscopic Analysis of Polyether(urethaneurea) Block Copolymers, II. Phase Separation", *Appl. Spectrosc.*, **1990**, in press.

Miller, C.E., Edelman, P.G., Ratner, B.D., "Near-infrared Spectroscopic Analysis of Polyether(urethaneurea) Block Copolymers, I. Bulk Composition", *Appl. Spectrosc.*, **1990**, in press.

Miller, C.E., Eichinger, B.E., "Analysis of RIM Polyurethanes by Near-infrared Diffuse Reflectance Spectroscopy", unpublished work, 1989.

Miller, C.E., Eichinger, B.E., "Determination of Compression and Thermal Properties of Rigid Polyurethane Foams by NIR Diffuse Reflectance Spectroscopy", *Appl. Spectrosc.*, submitted 1989.

Miller, C.E., Eichinger, B.E., "Determination of Crystallinity and Morphology of Fibrous and Bulk Poly(ethylene terephthalate) by NIR Diffuse Reflectance Spectroscopy", *Appl. Spectrosc.*, **1990**, *44(3)*, in press.

Miller, C.E., Eichinger, B.E., Gurley, T.W., Hermiller, J.G., "Determination of Microstructure and Composition of Butadiene and Styrene-butadiene polymers by NIR Spectroscopy", *Anal. Chem.*, submitted 1989.

Miller, C.E., Honigs, D.E., *Spectroscopy*, **1989**, *4*, 44.

Miller, C.E., Naes, T., "A Path Length Correction Method for Near-infrared Spectroscopy", *Appl. Spectrosc.*, submitted 1989.

Miller, C.E., Yin, T-K., *J Mat. Sci. Lett.*, **1989**, *8*, 467.

Modern Plastics, **1987**, *64(10A)*.

Morton, M., *Rubber Technology*, Robert E. Kreiger Co.: Malabar FL, 1981.

Naes, T., Irgens, C., Martens, H., *Appl. Statist.*, **1986**, *35*, 195.

Norris, K., Williams, P.C., *Cereal Foods World*, **1979**, *24*, 459.

Odian, G., *Principles of Polymerization, 2nd edition*, Wiley and Sons: N.Y., 1970.

Palys, L.H., Phillips, P.J., *J. Poly. Sci., Phys. Ed.*, **1980**, *18*, 829.

Pimental, G., McClellan, A.L., *The Hydrogen Bond*, W.H. Freeman: San Fransisco, 1960.

Pollack, S.K., Shen, D.Y., Hsu, S.L., Wang, Q., Stidham, H.D., *Macromolecules*, **1989**, *22*, 551.

Porter, M.D., *Anal. Chem.*, **1988**, *60*, 1143A.

Provder, T., *J. of Coatings Technol.*, **1989**, *61*, 33.

Reisch, M.S., *Chem. and Eng. News*, **1989**, *67(36)*, 21.

Renyuan, Q., Xigao, J., *Scientia Sinica*, **1982**, *25*, 137.

Roberts, R.C., *Polymer*, **1969**, *10*, 117.

Sadler, D.M., Gilmer, G.H., *Polymer*, **1984**, *25*, 1446.

Samuels, R.T, *Structured Polymer Properties*, Wiley-Interscience: N.Y., 1974.

Saunders, J.H., Frisch, K.C., *Polyurethanes, Chemistry and Technology, Part I: Chemistry*, Wiley-Interscience: N.Y., 1962.

Schmidt, P.G., *J. Poly. Sci., A*, **1963**, *1*, 1271.

Schuster, P., Zundel, G., Sandorfy, C., *The Hydrogen Bond, II. Structure and Spectroscopy*, North-Holland Publ. Co.: New York, 1976.

Seasholtz, M.B., Archibald, D.D., Lorber, A., Kowalski, B.R., *Appl. Spectrosc.*, **1989**, *43*, 1067.

Seymour, R.B., Carraher, C.E., *Structure-Property Relationships in Polymers*, Plenum Press: N.Y., 1984.

Sharaf, M.A., Illman, D.L., Kowalski, B.R., *Chemometrics*, John Wiley and Sons: New York,1986.

Shih, C.K., Cluff, E.F., *J. Appl. Polym. Sci.*, **1977**, *21*, 2885.

Smith, S.A., Galbraith, C.J., Cartmell, M.J., Moore, M.L., Brown, R.K., *Polyurethanes World Congress* **1987**, *Sept. 29 - Oct. 2*, 1987, 74.

Stark, E., Luchter, K., Margoshes, M., *Appl. Spectrosc. Rev.*, **1986**, *22(4)*, 335.

Stokr, J., Schneider, B., Doskocilova, D., Lovy, J., Sedlacek, P., *Polymer*, **1982**, *23*, 714.

Sung, C.S.P., Hu, C.B., Wu, C.S., *Macromolecules*, **1980**, *13*, 111.

Sung, C.S.P., Smith, T.W., Sung, N.H., *Macromolecules*, **1980**, *13*, 117.

Sverdlov, L.M., Kovner, M.A., Krainov, E.P., *Vibrational Spectra of Polyatomic Molecules*, John Wiley and Sons: N.Y., 1974.

Takeuchi, T., Tsuge, S., Sugimura, Y., *Anal. Chem.*, **1969**, *41*, 184.

Tenge, B., Buchanan, B.R., Honigs, D.E., *Appl. Spectrosc.*, **1987**, *41*, 779.

Tenge, B.J., doctoral dissertation, University of Washington, Seattle, WA, 1989.

Thompson, R.E., Butler, G.B., *J. Poly. Sci. Poly. Chem Ed.*, **1978**, *16*, 1367.

Veltkamp, D., Kowalski, B.R., Center for Process Analytical Chemistry, BG-10, Seattle WA 98195, *PLS-2 Block Modeling, Version 1.9 (IBM)*, 1986.

Veltkamp, D., PCA Modeling Program, Version 1.0 (IBM), Center for Process Analytical Chemistry, BG-10, Seattle WA, 98195, 1989.

Ward, I.M., *Chem. Ind. (London)*, **1957**, *1957*, 905.

Ward, I.M., in *Advances in Polymer Science*, Springer-Verlag: Berlin, 1985.

Weidner, V.R., Barnes, P.Y., Eckerle, K.L., *NBS Journal of Research*, **1986**, in press

Wendlandt, W.W., *Thermal Analysis*, Wiley: N.Y., 1986.

Wetzel, D.L., *Anal. Chem.*, **1983**, *55(12)*, 1165A.

Weyer, L.G., *Appl. Spectrosc. Rev.*, **1985**, *21*, 1.

Williams, A.D., Flory, P.J., *J. Poly. Sci., A-2*, **1967**, *5*, 417.

Williams, P., Norris, K., *Near-infrared Technology in the Agricultural and Food Industries*, American Association of Cereal Chemists: St. Paul MN, 1987.

Wilson, E.B., Decius, J.C., Cross, P.C., *Molecular Vibrations*, McGraw-Hill: N.Y., 1955.

Yang, W.P., Macosko, C.W., *Makromol. Chem., Macromol. Symp.*, **1989**, *25*, 23.

Yau, W.W., *Gel Permeation Chromatography*, Wiley-Interscience: N.Y., 1979.

Yeo, P., Honigs, D.E., *Appl. Spectrosc.*, **1988**, *42*, 1128.

Yin, T-K, Eichinger, B.E., Aksay, I.A., "Lubricating Polymers for Powder Compaction" in *Proceedings of First International Conference on Ceramic Powder Processing Science*, Orlando FL, 1987.

Yoon, D-Y., Flory, P.J., *Faraday Discuss. Chem. Soc.*, **1979**, *68*, 288.

Yoon, S.C., Ratner, B.D., *Macromolecules*, **1986**, *19*, 1068.

Yoon, S.C., Ratner, B.D., *Macromolecules*, **1988**, *21*, 2392.

Yoon, S.C., Ratner, B.D., *Macromolecules*, **1988**, *21*, 2401.

Zachmann, H.G., *Poly. Eng. and Sci.*, **1979**, *19*, 966.

Zbinden, R., *Infrared Spectroscopy of High Polymers*, Academic: N.Y., 1964.

Zerbi, G., *Appl. Spectrosc. Rev.*, **1968**, *2*, 193.

Appendix A

Analysis of Reaction Injection Molded Polyurethanes by NIR-FT-Raman Spectroscopy

A.1 Introduction to Appendix A

Polyurethane block copolymers made by Reaction Injection Molding (RIM) (1) are used predominantly for automotive applications (2). The studies in Chapter 7 demonstrated the ability of near infrared diffuse reflectance spectroscopy to rapidly analyze RIM polyurethanes. However, NIR-FT-Raman spectroscopy also has potential as a rapid analysis technique (4-6). For the analysis of polymeric materials, NIR-FT-Raman (with 1064.1 nm excitation) usually avoids the fluorescence difficulties that are commonly experienced with conventional Raman spectroscopy (typically 488 nm or 514.5 nm excitation). Excellent frequency precision is another feature of NIR-FT-Raman that ought to be important for quantitative studies. In this work, the method of NIR-FT-Raman is applied to the determination of flex moduli of the diamine-extended RIM polyurethanes used in Chapter 7, sample set **a**. The results of this work are compared to results of the NIR diffuse reflectance analysis of these polymers.

A.2 Experimental

The samples used in this study are the 1" by 3" diamine-extended RIM polyurethanes that were designated as sample set a in Chapter 7 (3). Non-destructive flex modulus measurements at 23 °C (ASTM method D-790-86) (7) were performed as discussed in Chapter 7.2.3. A single flex modulus measurement was performed for each sample.

Raman sampling was performed after physical testing of the samples. The spectrometer was a Perkin-Elmer Model 1800 FT-IR that was modified as described in an earlier report (8). The spectra were obtained with 6 cm^{-1} nominal resolution and data was collected every 2 cm^{-1} over the spectral range from 9500 cm^{-1} to 6500 cm^{-1}. This spectral range corresponds to Raman shifts of -102.4 cm^{-1} to 3297.6 cm^{-1}. The 180° sampling geometry was similar to that described previously (12), except that the spot diameter at the sample was 2.5 mm. About 750 mW of 1064 nm light was incident on the samples. Each spectrum is a result of 6 minutes of signal averaging. The Rayleigh scattering peak (0 cm^{-1}) was used to monitor the overall scattering intensities of the samples. A single Raman spectrum was obtained from each sample.

For each spectrum, every intensity point was normalized with respect to the intensity of the Rayleigh scattering peak. The intensity of the Rayleigh scattering peak, scaled so that its variance over all samples is equal to the average variance of intensities in the

Raman spectra, was used as an additional variable (called the scattering variable) for this analysis. Every three consecutive intensity points were averaged, and spectral regions with no appreciable Raman intensity were removed. These manipulations resulted in spectra covering Raman shifts of 301.6 cm^{-1} to 1897.6 cm^{-1}, and 2503.6 cm^{-1} to 2997.6 cm^{-1} in 6 cm^{-1} increments.

Three seperate calibrations for flex modulus at 23 °C were prepared, using three different sets of spectral variables: 1. normalized Raman spectra only, 2. normalized Raman spectra with the scattering variable and 3. the scattering variable only. The method of Partial Least Squares (PLS) was used for the multivariate analyses (that use data sets 1. and 2.) and a univariate least squares calibration was used for the analysis that used data set 3..

For all calibration analyses, calibration and prediction sets were designated in the same way as in Chapter 7. The method of cross-validation (Chapter 1.5.2.3.1) was used to determine the optimal number of spectral factors for the PLS calibrations. Calibration error is indicated by the Standard Error of Estimate (SEE) (Equation 1.16), and prediction error is indicated by the Standard Error of Prediction (SEP) (Equation 1.17). Relative errors were calculated as the standard error divided by the range of flex moduli of the samples used in the analysis.

A.3 Results

The NIR-FT-Raman spectra of two RIM polyurethanes are shown in Figure A.1. No significant fluorescence is observed in these spectra. Tentative assignments of the bands are made from reference to earlier Raman analyses of n-hexane (9), para-substituted benzenes (10), and urea-formaldehyde resins (11). Bands at 2974 cm^{-1} (CH_3 stretch), 2936 cm^{-1} and 2876 cm^{-1} (CH_2 stretch), and 1456 cm^{-1} (CH_2 bend) originate from the poly(ethylene oxide) and poly(propylene oxide) units in the soft block of the polymers. The other bands are from vibrations of aromatic and urea groups in the hard block of the polymers. Bands at 640 cm^{-1}, 900 cm^{-1}, 1184 cm^{-1}, and 1617 cm^{-1} are from benzene ring modes, the band at 1712 cm^{-1} is a carbonyl stretching band, and the band at 1523 cm^{-1} is an amide I band. The 1318 cm^{-1} band might be a N-C-N stretching band, and the 1258 cm^{-1} band might arise from the penta-substituted benzene ring in the DETDA chain extender in the hard block of the polymer (see Figure 7.1,A).

The differences in relative band amplitudes in the NIR-FT-Raman spectra (for example the relative amplitude of the 1617 cm-1 and 2936 cm-1 bands in Figure A.1), are a result of differences in the composition of the polymers. It is also observed that the overall intensity, indicated by the Rayleigh scattering band at 0 cm^{-1}, is slightly greater for spectrum B than for spectrum A. Visual observation of the RIM samples revealed that the overall scattering intensity is proportional to the concentration of nitrogen voids in the sample (Chapter 1.4.1), and is therefore inversely proportional to the

Figure A.1: NIR-FT-Raman spectra of two different RIM polyurethanes, collected with 1064 nm excitation (100 cycles).

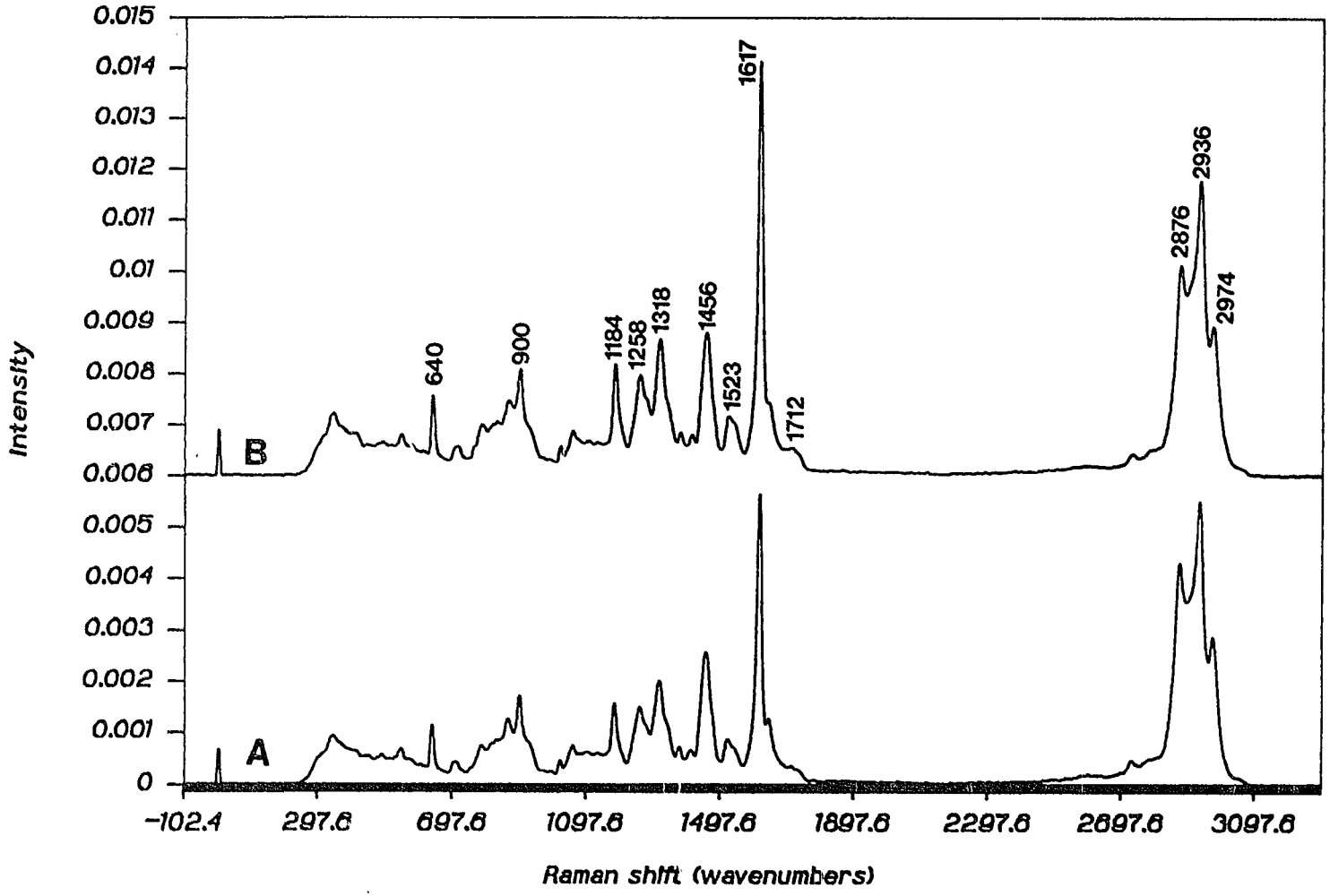
0.015
0.014
0.013
0.012
0.011
0.01
0.009
0.008
0.007
0.006
0.005
0.004
0.003
0.002
0.001
0
Intensity
B
A
640
900
1184
1258
1318
1456
1523
1617
1712
2876
2936
2974
-102.4
297.6
697.6
1097.6
1497.6
1897.6
2297.6
2697.6
3097.6
Raman shift (wavenumbers)

density of the sample (Chapter 7.3.2). Because the density of a RIM material greatly affects its modulus, the overall scattering intensity observed in the Raman spectrum (indicated by the scattering variable) is expected to be important for the determination of flex modulus.

The PLS cross-validation results are shown in the second column of Table A.1. They indicate that two factors are necessary for the PLS calibration that uses the Raman spectra alone, and three factors are necessary for the calibration that uses Raman spectra with the scattering variable. Two important results are obtained from this observation: 1) the scattering variable adds information not present in the Raman spectra, and 2) a third factor (in addition to density and composition) is influencing the Raman spectra. As mentioned earlier, the information supplied by the scattering variable is probably the sample density. The additional factor influencing the Raman spectra might be phase separation, which involves the self-association (or hydrogen-bonding) of hard blocks in the polymer (12,13). It is possible that differences in phase separation in the polymers can be detected by shifts in the amide, carbonyl, and aromatic ring bands in the spectra. However, more detailed studies are necessary to identify the Raman spectral features that indicate phase separation.

The PLS calibration and prediction results are also shown in Table A.1. Results are improved if the scattering variable is added to the Raman data. However, prediction from the scattering variable

Table A.1: Calibration and prediction results for PLS calibrations of three different sets of Raman spectral variables to flex modulus (at 23 °C) of RIM polyurethanes.

Table A.1

data used	number of PLS factors	Calibration SEE[1]	Calibration relative error (%)	Prediction SEP[1]	Prediction relative error (%)
Normalized NIR-Raman spectra	2	3.4	10.9	2.5	8.4
Normalized NIR-Raman spectra, with scattering variable	3	2.1	6.6	1.7	5.8
scattering variable only	-	10.8	34.5	11.0	37.4

[1] : SEE and SEP values are in units of 10^{-7} N/m^2

alone gives poor results. These results suggest that both the scattering variable, which primarily indicates sample density, and the Raman spectrum, which contains information about composition and phase separation, are necessary to accurately predict the flex modulus of a sample.

As mentioned earlier, NIR diffuse reflectance spectroscopy (3) was also used to determine physical properties of the polymers used in this work. The smallest relative prediction error (of flex modulus at 23 °C) for the NIR-FT-Raman method (5.8%) is slightly greater than the smallest relative prediction error for the NIR diffuse reflectance method (4.0%) (Table 7.2). Although this result suggests that NIR diffuse reflectance spectroscopy is a better method for analysis of RIM polyurethanes, other factors must be considered. NIR-FT-Raman spectra contain much different information than NIR diffuse reflectance spectra. For example, the effect of phase separation on the NIR diffuse reflectance spectrum (3,14) is expected to be much greater than the effect on the NIR-FT-Raman spectrum, because C=O and N-H bands in the Raman spectrum are very weak. However, NIR-FT-Raman spectroscopy is expected to provide better information about polymer backbone vibrations (15).

It should be clear that the most suitable spectroscopic technique for polymer analysis is strongly dependent on the composition of the polymer and the properties of interest. Near-infrared spectroscopy is effective if strong perturbations of NH, OH, or CH bonds in the polymer, such as those caused by hydrogen-

bonding interactions, affect the property of interest. Raman analysis will be superior when sampling of non-polar bonds provides information about the properties of interest.

In terms of instrumentation, NIR-FT-Raman is significantly more costly and poses a greater potential hazard to personnel. Moreover, heating of the sample is more likely in Raman spectroscopy, and this might result in sampling error or sample damage. However, complete NIR-FT-Raman spectra can be obtained over optical fibers (5), whereas the collection of complete NIR spectra over fiber optics is prevented by substantial absorption of light in the optical fiber (16).

A.4 Notes to Appendix A

(1) Macosko, C.W., *RIM, Fundamentals of Reaction Injection Molding*, Hanser Publishers: Munich, 1989.

(2) *Modern Plastics*, **1987**, *64(10A)*, p. 122.

(3) Miller, C.E., Eichinger, B.E., "Analysis of RIM Polyurethanes by Near-infrared Diffuse Reflectance Spectroscopy", unpublished work, 1989.

(4) Bergin, F.J., Shurvell, H.F., *Appl. Spectrosc.*, **1989**, *43*, 516.

(5) Archibald, D.D., Lin, L.T., Honigs D.E., *Appl. Spectrosc.*, **1988**, *42*, 1558.

(6) Seasholtz, M.B., Archibald, D.D., Lorber, A., Kowalski, B.R., *Appl. Spectrosc.*, **1989**, *43*, 1067.

(7) ASTM method D790-86, *1989 Annual Book of ASTM Standards*, **1989**, volume *08.01*, ASTM: Philadelphia, p. 280.

(8) Angel, S.M., Katz, L.F., Archibald, D.D., Lin, L.T., Honigs, D.E., *Appl. Spectrosc.*, **1988**, *42*, 1327-1331.

(9) Sverdlov, L.M., Kovner, M.A., Krainov, E.P., *Vibrational Spectra of Polyatomic Molecules*, John Wiley and Sons: New York, 1974, pp. 194-195.

(10) ibid., p. 341.

(11) Hill, L.G., Hedren, A.M., Myers, G.E., Koutsky, J.A., *J. Appl. Polym. Sci.*, **1984**, *29*, 2749.

(12) Lee, H.S., Hsu, S.L., *Macromolecules*, **1989**, *22*, 1100.

(13) Lee, H.S., Wang, Y-K., MacKnight, W.J., Hsu, S.L., *Macromolecules*, **1988**, *21*, 270.

(14) Miller, C.E., Edelman, P.G., Ratner, B.D., Eichinger, B.E., "Near-infrared Spectroscopic Analysis of Polyether(urethaneurea) Block Copolymers, II. Phase Separation", *Appl. Spectrosc.*, **1990**, in press.

(15) Koenig, J.L., *Chemical Microstructures of Polymer Chains*, John Wiley and Sons: New York, 1970.

(16) Tenge, B., Buchanan, B.R., Honigs, D.E., *Appl. Spectrosc.*, **1987**, *41*, 779.

Appendix B

A Path Length Correction Method for Near Infrared Spectroscopy

B.1 Introduction to Appendix B

Near-infrared (NIR) spectroscopy has been used to rapidly and accurately determine important properties of agricultural products (1-3) and polymeric materials (3-5). The sampling ease of NIR methods makes them particularly appealing for rapid analysis. However, a major difficulty with NIR methods is the presence of additive and multiplicative effects in the spectra. These effects arise from variations in the particle size and path length (or thickness) of the samples. Additive effects, which are baseline offset variations, can be reduced by the use of first or second derivative spectra. Multiplicative effects, caused by variation in sample thickness or particle size, can be removed if the path lengths of the samples are known. However, the path lengths of samples are seldom known, especially in situations where rapid analyses of relatively unprepared samples are done. In this situation, it is difficult to distinguish between multiplicative path length effects and chemical variation effects in the spectra. It is important to determine the multiplicative path length effect in a spectrum, because removal of this effect results in more accurate determinations of analyte concentrations from the spectrum.

The method of Multiplicative Scatter Correction (MSC) (6-8) has been used to reduce multiplicative path length effects in NIR diffuse reflectance and transmission spectra. This method generally improves the prediction ability of NIR spectra when the spectral variability from chemical variation is small. However, the spectral variability from chemical variation can be very large in some situations. For example, variations in the composition of poly(urethaneurea) block copolymers (9) and EPDM terpolymers (5) causes very large changes in the NIR spectra of these materials. In these situations, the MSC method is expected to make approximate, but not accurate corrections for multiplicative path length effects.

This chapter presents a multiplicative correction method, called Path Length Correction with Chemical Modeling (PLC-MC), which can be used when spectral variablility from chemical variation is large. This method involves Principal Components Analysis (PCA) modeling of chemical variations in the NIR spectra of samples that have differences in chemical composition but no differences in multiplicative path length effects. This model can then be used to estimate the multiplicative path length effect of a future sample from its NIR spectrum.

B.2 Theory

B.2.1 PCA Modeling:

A NIR spectral response matrix **X** (*m* by *n*) contains the spectra of *m* standards at *n* wavelengths. It is assumed that there are no additive or multiplicative path length variations in the spectra, and that all chemical variations in the samples are represented. Data compression of **X** is done by PCA (Chapter 1.5.1):

$$\mathbf{X} = \mathbf{1}_n\bar{\mathbf{x}} + \mathbf{T}\mathbf{P}^t + \mathbf{E} \qquad \text{(B.1)}$$

where $\mathbf{1}_n$ is a column vector of ones with *n* elements, $\bar{\mathbf{x}}$ is the average spectrum of the *m* spectra in **X**, **T** is a *m* by *f* matrix of PCA scores (where *f* is the number of principal components needed to explain the variance in **X**), and **P** is a *n* by *f* matrix of PCA loadings. The matrix **E** contains the spectral variations that are not modeled by the PCA procedure. The optimal number of factors (*f*) is usually determined by cross validation.

All of the spectra in **X** can be represented in *n*-dimensional space, in which each dimension corresponds to a single wavelength response in the NIR spectrum. However, PCA results indicate that these spectra can be located in an *f*-dimensional subspace. For instance, in the case of *f*=2, the spectra lie on a plane in the *n*-dimensional space. In addition, the spectra defined by $\mathbf{T}\mathbf{P}^t$, which are the PCA estimates of the mean centered spectra, must lie on a plane that passes through the origin. Figure B.1 shows a geometrical representation of the spectra. The planes containing the PCA-

Figure B.1: Representation of plane spanning $\mathbf{1}_n\bar{\mathbf{x}} + \mathbf{TP}^t$, plane spanning $\mathbf{TP}^t$, mean spectrum ($\bar{\mathbf{x}}$), prediction spectrum ($\mathbf{x}_p$), and prediction spectrum corrected by the PLC-MC method ($\hat{a}\mathbf{x}_p$) in 3-dimensional space.

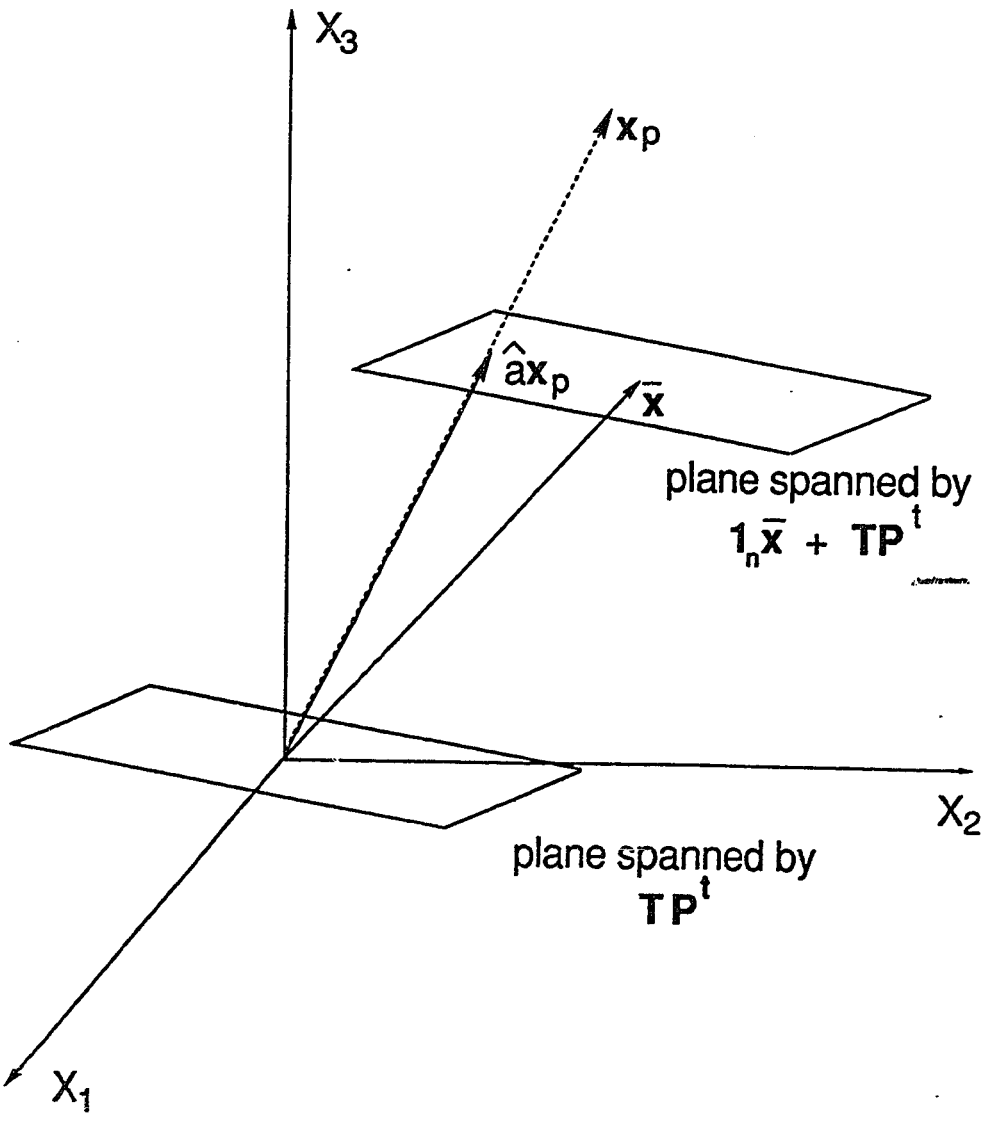
X_3
$\mathbf{x}_p$
$\hat{a}\mathbf{x}_p$
$\bar{\mathbf{x}}$
plane spanned by
$\mathbf{1}_n\bar{\mathbf{x}} + \mathbf{TP}^t$
X_2
plane spanned by
$\mathbf{TP}^t$
X_1

modeled spectra ($\mathbf{1}_n\bar{\mathbf{x}} + \mathbf{TP}^t$) and PCA-modeled mean-centered spectra ($\mathbf{TP}^t$) are also shown.

B.2.2 Path Length Correction

In many situations, it is desired that a calibration that was constructed from standards with identical path lengths can be used to predict the concentrations of a prediction sample that has an unknown path length. For example, the NIR spectra of polymer films with identical thicknesses are used to construct a calibration for a specific property, and it is desired that this calibration can be used to predict the property of a film of unknown thickness from its NIR spectrum. In this situation, a PCA model (Equation B.1) can be constructed from the spectra of the calibration standards. A prediction spectrum ($\mathbf{x}_p$) with a path length different than the path length of the standards used to develop the PCA model, is simply a multiple of a spectrum that is modeled by the PCA model:

$$a\mathbf{x}_p = \bar{\mathbf{x}} + \mathbf{t}_p\mathbf{P}^t + \mathbf{e} \qquad \text{(B.2)}$$

where $\mathbf{t}_p$ contains the principal component scores of the spectrum of a sample that has the path length of the standards and the same composition as the future sample, $a = 1/a^*$, where a^* is the path length of the future sample relative to the standard path length. In geometrical terms, a multiple of $\mathbf{x}_p$ ($a\mathbf{x}_p$) is in the plane spanned by

$\bar{x} + TP^t$ (see Figure B.1). The vector e represents the lack of fit to the multiplicative model. Rearrangement of Equation B.2 yields:

$$x_p = a^*\bar{x} + t_p^* P^t + e^* \qquad (B.3)$$

where $t_p^* = t_p/a$ and $e^* = e/a$. Because x_p, P and $\bar{x}$ are known, estimates of the parameters a* and t_p^* ($\hat{a}^*$ and $\hat{t}_p^*$) can be obtained by least-squares regression. The path length corrected spectrum (x_c) can then be calculated:

$$x_c = \hat{a}x_p = (1/\hat{a}^*)x_p \qquad (B.4)$$

B.2.3 Comparison with Multiplicative Scatter Correction

The MSC correction method is easier to use than the principal component-based method, because standards with identical path lengths are not required. However, it can be shown that the MSC method is not as accurate as the PLC-MC correction when spectral variability from chemical variations are large. If no additive offset effects are present in the spectra, the MSC model is given by Equation B.5 (8):

$$a_m x_p = \bar{x} + e \qquad (B.5)$$

where a_m is the MSC multiplicative constant. Because $\mathbf{x}_p$ and $\bar{\mathbf{x}}$ are known, the multiplicative constant (a_m) can be determined by least-squares regression.

When the MSC model (Equation B.5) is compared to the PLC-MC model (Equation B.2), it is found that the MSC model lacks the $\mathbf{t}_p\mathbf{P}^t$ contribution that accounts for spectral variability from chemical variations. Therefore, it is expected that the error in the MSC method increases as the difference between the chemistry of the prediction sample and the chemistry of the average sample (which is equal to $\mathbf{t}_p\mathbf{P}^t$) increases.

Differences between MSC and PLC-MC correction methods can also be observed geometrically (Figure B.2). The MSC solution is given by Equation B.6:

$$a_m = \frac{|\bar{x}|}{|\text{proj}_{\bar{x}}\, x_p|} \qquad \text{(B.6)}$$

From observation of Figure B.2, it is clear that the MSC-corrected spectrum $a_m x_p$ is not in the plane spanned by $\bar{\mathbf{x}} + \mathbf{TP}^t$, and is therefore not properly normalized to the path length of the standards. It is also apparent that the error in the MSC correction increases in magnitude as the chemical variation between the prediction spectrum and the mean spectrum (or the angle between x_p and $\bar{x}$) increases.

Figure B.2: A prediction spectrum ($\mathbf{x}_p$), the prediction spectrum corrected by the MSC method ($\hat{a}_m \mathbf{x}_p$), and the prediction spectrum corrected by the PLC-MC method ($\hat{a}\mathbf{x}_{\bar{p}}$) in 3-dimensional space.

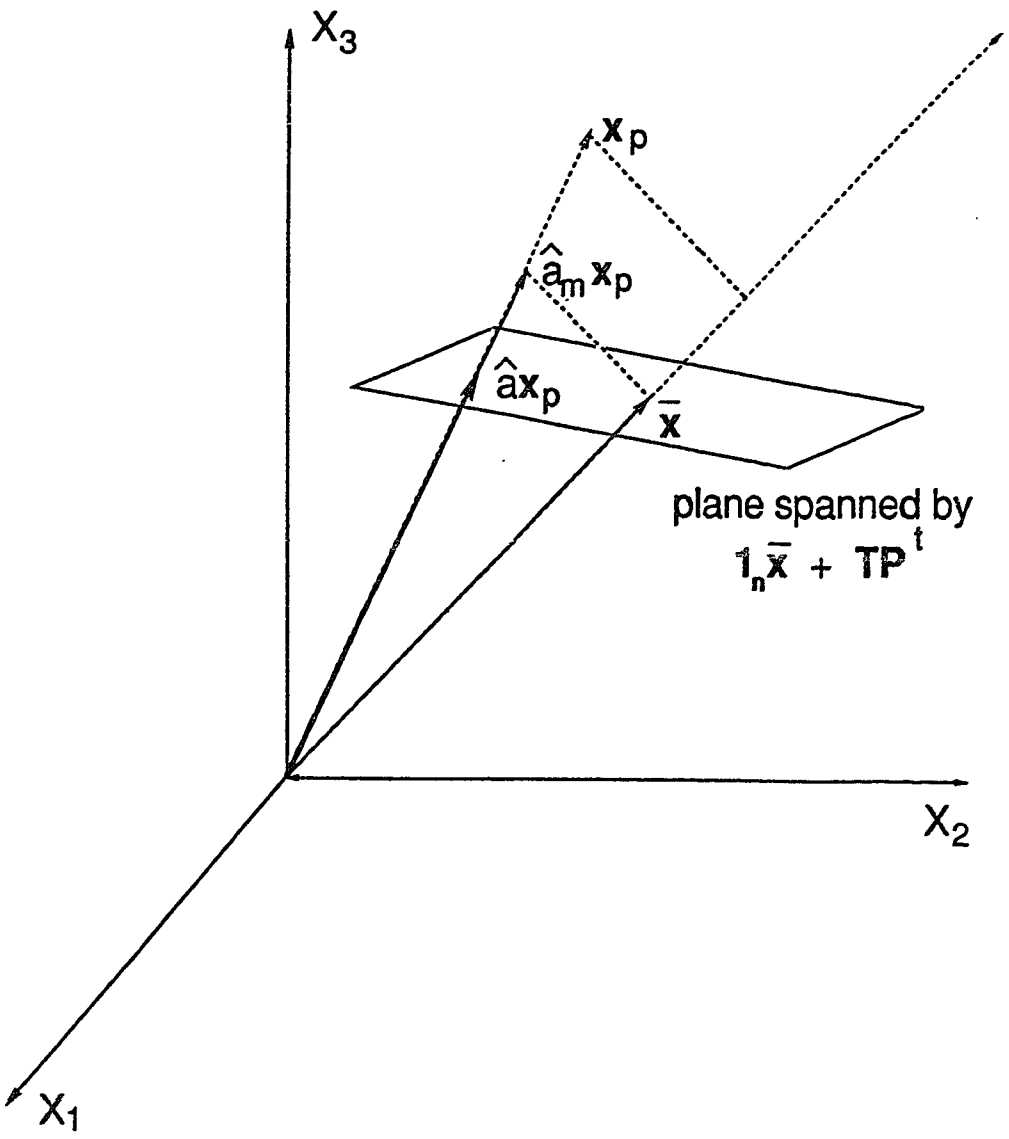
X_3
x_p
$\hat{a}_m x_p$
$\hat{a}x_p$
$\bar{x}$
plane spanned by
$1_n\bar{x} + TP^t$
X_2
X_1

B.3 Experimental

The samples used in this work were the 23 poly(butadiene) polymers (Goodyear Tire and Rubber Co., Akron OH) that were used for the studies in Chapter 4. These samples have varying amounts of three structural isomers: cis-1,4, trans-1,4, and 1,2 butadiene (12) (Figure 1.3). The concentrations of the three isomers in each sample were determined by ^{13}C NMR spectroscopy of the sample dissolved in $CDCl_3$. Acquisition and pre-analysis treatment of NIR spectra were done as described in Chapter 4.2. The second derivative spectra in region II (1570 nm to 1850 nm) of the samples dissolved (1% w/v) in CCl_4 were used for this study.

The samples were split into a calibration set and prediction set (as in Chapter 4). The spectra of the samples in the calibration set remained normalized with respect to path length. However, the absorbances at every wavelength in each prediction spectrum were multiplied by a path length factor of .6, .8, 1, 1.2 or 1.4, in order to simulate the presence of varying path lengths for the prediction samples.

All PCA and PLS models were made using the Unscrambler software package (CAMO A/S, P.O. Box 28893, N-7001, Trondheim, Norway). Three PLS calibrations (13,14) for the three analytes in the polymers were constructed from both the original and MSC-corrected calibration spectra using the Unscrambler software package (CAMO A/S, P.O. Box 28893, N-7001 Trondheim, Norway). Spectra were

mean-centered before each PLS calibration. Cross-validation was used to determine the optimal number of PLS factors for each calibration. It was found that two factors were required for each calibration. A PCA model, for use in the PLC-MC correction method, was constructed from the original calibration spectra. PLS calibrations constructed from uncorrected calibration spectra were used to predict analyte concentrations from both uncorrected prediction spectra and PLC-MC-corrected prediction spectra. The PLS calibrations constructed from MSC-corrected calibration spectra were used to predict analyte concentrations from MSC-corrected prediction spectra. The MSC reference spectrum was chosen as the average spectrum of the calibration set (obtained by averaging the absorbances over all calibration samples at each wavelength). For all PLS predictions, the prediction error is expressed as the Standard Error of Prediction (SEP) (Chapter 1.5.2.3.2, Equation 1.17).

The MSC and PLC-MC methods also provide estimates of the arbitrarily-assigned path lengths for each prediction sample. The standard errors of the predicted path lengths are determined in the same way as the errors in the analyte concentrations (as in Equation 1.17).

B.4 Results and Discussion

Figure 4.1, A (in Chapter 4), which shows the estimated spectra of the three pure analytes (1,2 butadiene, 1,4-cis butadiene and 1,4-

trans butadiene) in the samples, indicates that the pure analyte spectra are very different. Because the ranges of analyte concentrations for the samples used in this analysis are very large (82.7 % mass for 1,2 butadiene, 90.8 % mass for 1,4-cis butadiene and 73.1 % mass for 1,4-trans butadiene), the spectral variablility from chemical variations is very large for this analysis.

The results of PLS predictions that use original, MSC-corrected, and PLC-MC-corrected spectra are shown in Table B.1. In addition, the errors of the predicted path lengths obtained from the MSC and PLC-MC methods are given. Both the MSC and PLC-MC methods provide good approximations of the path lengths of the prediction samples. As a result, the use of either correction method improves prediction results relative to the results for uncorrected spectra. However, the PLC-MC method predicts the path lengths of the prediction samples more accurately than the MSC method. As a result, significantly better predictions of analyte concentrations are obtained with spectra that are corrected with the PLC-MC method than with spectra corrected with MSC.

The errors in the PLC-MC correction method arise from several sources: 1) noise in the calibration and prediction spectra, 2) lack of fit of prediction spectra to the multiplicative model (Equation B.2), and 3) differences in the actual path lengths of the PCA standards. Lack of fit of the prediction spectrum to the multiplicative model can be detected by observation of the residual of the prediction spectrum (e_p):

Table B.1: Errors of MSC and PLC-MC predicted path lengths, and errors of PLS predictions of analyte concentrations that use uncorrected, MSC-corrected and PLC-MC-corrected prediction spectra.

TABLE B.1

Prediction Errors (SEP)

Path Length Correction Used	path length[1]	1,2 butadiene (% mass)	1,4-cis butadiene (% mass)	1,4-trans butadiene (% mass)
none	-----	8.12	5.48	5.94
MSC	0.058	1.37	1.43	0.71
PLC-MC	0.013	0.68	0.91	0.78

[1] as predicted by the MSC or PLC-MC method, range of path lengths = 0.6 to 1.4

$$e_p = x_p - \hat{a}*\bar{x} - \hat{t}_p*P^t \qquad (B.7)$$

If the elements of e_p are significantly large relative to spectral noise, then the prediction spectrum x_p is an outlier, and cannot be used for analysis. One possible cause for a lack of fit to the multiplicative model is the presence of isolated non-linearities in the spectrum. This error can be minimized by avoiding the use of highly-absorbing prediction samples that can cause isolated non-linear absorbances from stray light effects. If the use of highly-absorbing samples cannot be avoided, it is possible to remove non-linear spectral regions from the spectra before analysis. Error source 3), which is specific to the PLC-MC method, must be minimized by careful sample preparation and reproducibility of NIR sampling methods for the PCA standards.

The MSC method does not require a PCA model, and is therefore easier to use than the PLC-MC method. However, the large chemical variations in the spectra used in this study caused the MSC model (Equation B.5) to be inaccurate. As a result, large errors of MSC-determined path lengths of prediction samples and significant errors of PLS predictions of analyte concentrations from MSC-corrected spectra are observed (Table B.1). It is clear that there is a tradeoff between the MSC and PLC-MC correction methods. The PLC-MC method performs accurate path length corrections, regardless of the magnitude of spectral variability from chemical variations, if

carefully-prepared standards can be made. If the preparation of such standards is impractical, and the chemical variations in the spectra are small, the MSC method can be used effectively.

Several experimental techniques can be used to produce standards with identical path lengths for use in the PLC-MC correction. For powdery materials, samples can be sieved to the same particle size or ground to a very fine powder (to make spectral variations from particle size differences very small). For solutions, samples with identical dilution ratios can be analyzed in the same, fixed path length cuvette. For non-scattering bulk materials (such as bulk polymers), films of reproducible thickness (from 0.1 to 10 mm thick) can be prepared by pressing or solution casting. In all cases, reproducibility of NIR sampling procedures, such as sample placement and settings of instrumental parameters, is essential.

It should be emphasized that the described PLC-MC correction method is unable to account for additive (or baseline offset) variations in the spectra. These variations can be minimized before analysis by the use of first or second derivative spectra. Nevertheless, modifications of the PLC-MC correction method, to account for both additive and multiplicative effects, are currently being investigated.

B.5 Conclusion

This analysis has demonstrated the usefulness of the Path Length Correction with Chemical Modeling (PLC-MC) method for quantitative NIR analysis. If a series of calibration standards with equal path lengths are available, and spectral responses at all wavelengths are linear with path length, accurate predictions from the spectra of future samples with unknown path lengths can be made. This procedure might be particularly appealing for analyses that require rapid sampling of unprepared materials with unknown path lengths.

B.6 Notes to Appendix B

(1) Williams, P., Norris, K., *Near-infrared Technology in the Agricultural and Food Industries*; American Association of Cereal Chemists: St. Paul MN, 1987.

(2) Norris, K., Williams, P.C., *Cereal Foods World*, **1979**, *24*, 459.

(3) Stark, E., Luchter, K., Margoshes, M., *Appl. Spectrosc. Rev.*, **1986**, *22*, 335.

(4) Weyer, L.G., *Appl. Spectrosc. Rev.*, **1986**, *22*, 335.

(5) Miller, C.E., *Appl. Spectrosc.*, **1989**, *43(8)*, 1435.

(6) Geladi, P., MacDougall, D., Martens, H., *Appl. Spectrosc.*, **1985**, *39*, 491.

(7) Ilari, J.L, Martens, H., Isaksson, T., *Appl. Spectrosc.*, **1988**, *42*, 722.

(8) Naes, T., Irgens, C., Martens, H., *Appl. Statist.*, **1986**, *35*, 195.

(9) Miller, C.E., Eichinger, B.E., "Determination of Crystallinity and Morphology of Fibrous and Bulk Poly(ethylene terephthalate) by NIR Diffuse Reflectance Spectroscopy", *Appl. Spectrosc.*, **1990**, *44(3)*, in press.

(10) Jolliffe, I.T., *Principal Components Analysis*, Springer-Verlag: New York, 1986.

(11) Sharaf, M.A., Illman, D.L., Kowalski, B.R., *Chemometrics*, John Wiley and Sons: New York,1986.

(12) Miller, C.E., Eichinger, B.E., Gurley, T.W., Hermiller, J.G., "Determination of Microstructure and Composition of Butadiene and Styrene-butadiene polymers by NIR Spectroscopy", *Anal. Chem.*, submitted 1989.

(13) Beebe, K., Kowalski, B.R., *Anal. Chem.*, **1987**, *59*, 1007A.

(14) Haaland, D.M., Thomas, E.V., *Anal. Chem.*, **1988**, *60*, 1202.

Vita

Charles Edward Miller was born on February 13, 1963, in Rochester, New York. He graduated from Greece Athena High School (Rochester, New York) in 1981. In September of 1981, he enrolled at the State University of New York at Binghamton, where he started his undergraduate studies. In February of 1983, he transferred to Oberlin College, as a chemistry major. His first research project at Oberlin, under the direction of Prof. Norman C. Craig, involved organic synthesis and low-temperature vibrational spectroscopy. His senior thesis research, under the direction of Prof. Robert Q. Thompson, was the investigation of valving options and enzymatically-active reactors for flow injection analysis. As a result of his accomplishments in the thesis research and in oral and written examinations, he received the distinction of "high honors in chemistry" upon graduation. In addition, he was inducted as a member of Phi Beta Kappa in 1984 and Sigma Xi in 1985. He received his Bachelor of Arts degree from Oberlin in June 1985.

In the summer of 1985, Charles worked as a research intern at the Procter and Gamble Company in Cincinnati, Ohio, where he investigated the use of near-infrared spectroscopy and multivariate statistics for the analysis of processed and unprocessed foods. In the fall of 1985, he entered the graduate program in the Analytical division of the Department of Chemistry at the University of Washington. In the spring of 1986, he joined the research group of

Dr. David E. Honigs, and pursued research on various applications of near-infrared spectroscopy.

In January 1988, recently after it was announced that Dr. Honigs would transfer to an industrial position, Charles transferred to the research group of Prof. B. E. Eichinger. As a student in Prof. Eichinger's group, he researched the application of near-infrared spectroscopy to polymer analysis. In the summer of 1988, he worked as a research intern at the Goodyear Tire and Rubber Company, and developed near-infrared analysis methods for rubbers and polyesters. In later studies at the University of Washington, he developed near-infrared analysis applications for several additional polymer systems. He completed his doctoral studies in December 1989. In March 1990, he will receive the 1990 Tomas Hirschfeld Award in Near-infrared Analysis at the Pittsburgh Conference in New York City.